CHARLES UNIVERSITY IN PRAGUE

FACULTY OF SCIENCE

Ph.D. study program: Molecular and Cellular Biology, Genetics and Virology

Mgr. Vojtěch Žíla

Mouse polyomavirus: The role of cell cytoskeleton in virus endosomal trafficking and properties of the minor capsid proteins

Myší polyomavirus: Role buněčného cytoskeletu v endozomálním transportu viru a vlastnosti minoritních kapsidových proteinů

Ph.D. Thesis

Supervisor: doc. RNDr. Jitka Forstová, CSc.

Prague 2014

STATEMENT

This is to declare that I did not use this Ph.D. Thesis to acquire another academic degree. Further, I worked on the Ph.D. Thesis independently, under the supervision of Jitka Forstová, Associate Professor.

In Prague, 17. 7. 2014 

Signature

ACKNOWLEDGMENT

First and foremost I want to thank my supervisor Jitka Forstová for the opportunity to study and work in her laboratory. I appreciate all her contributions of time, ideas, and funding to make my study productive and stimulating. Besides my supervisor, I am very grateful to all people who have been contributing to my work, in particular to Jitka Štokrová who introduced me generously to the methods of electron microscopy. I would also like to acknowledge everyone in our laboratory who gave me a support and encouraged me during the study. Finally, I want to thank my family for their endless support and patience, and I would like to dedicate this thesis to memory of my sister Petra Hirschová (1965 – 2009). I hope she would have been proud.

This work was kindly supported by the Grant Agency of the Czech Republic (Project P302/13-26115S), by the Ministry of Education, Youth and Sports of the Czech Republic (Projects 1M0508, MSM0021620858, LC545 and SVV-2014-260081), by the Grant Agency of the Charles University in Prague (Project no. 156307), by the Charles University in Prague (Project UNCE 204013) and by the project BIOCEV – Biotechnology and Biomedicine Centre of the Academy of Sciences and Charles University (CZ.1.05/1.1.00/02.0109), from the European Regional Development Fund.

ABSTRACT

Mouse polyomavirus (MPyV) is a non-enveloped DNA tumor virus, which replicates in the host cell nucleus. MPyV enters cells by receptor-mediated endocytosis and its subsequent transport towards the nucleus requires acidic environment of endosomes and intact microtubules, which are important for virus delivery to endoplasmic reticulum (ER). In ER, capsid disassembly and uncoating of viral genome take place. The mechanism of subsequent translocation of viral genome from ER into nucleoplasm is still only poorly understood process with predicted involvement of cellular factors and viral minor capsid proteins VP2 and VP3. Once the genome appears in the nucleus, early viral antigens are produced and mediate suitable environment for replication of viral genomes. After replication of viral DNA and morphogenesis of virions, virus progeny is released from the cells during its lysis. The research presented in the first part of thesis focused on intracellular transport of MPyV and involvement of cytoskeletal networks during virus delivery to the ER. In particular, we investigated still unclear role of microtubules during virus trafficking in endosomes, and involvement of microtubular motors. We found that MPyV trafficking leading to productive infection does not require the function of kinesin-1 and kinesin-2, but depends on functional dynein-mediated transport along microtubules. Dynein was shown to mediate translocation of virions from peripheral often multicaveolar-like compartments to the early and late endosomes, and further virus trafficking to the ER. Despite microtubules were also found to mediate virus transport to recycling endosomes, these compartments were showed to be dispensable for productive infection. In the second part, research focused on properties of the minor capsid proteins VP2 and VP3. Minor capsid proteins were showed to be indispensable for delivery of viral genome into the nucleus. The affinity of both minor proteins to artificial membranes and ability of VP2 protein to perforate these membranes were demonstrated. These finding thus suggest that the internal minor capsid proteins, exposed after capsid disassembly in the ER, might contribute to translocation of viral genome from ER to nucleoplasm. We prepared fusion variants of minor capsid proteins by linking them to enhanced green fluorescent protein (EGFP) and tested them during their individual expression in the absence of other MPyV gene products. Our biochemical studies proved each of the minor proteins to be a very potent inducer of apoptosis. Confocal and immunoelectron microscopy analyses showed ability of both minor proteins to interact with and damage the intracellular membranes, suggesting the mechanism of their cytotoxicity. Nevertheless, further analysis of apoptotic markers and cell death kinetics in cells transfected with MPyV genome mutated in both VP2 and VP3 translation start codons revealed that the minor proteins are only moderate contributors to apoptotic processes during infection and dispensable for cell destruction at the end of the virus replication cycle. These results thus indicate the role of the minor capsid proteins preferentially during virus entry and delivery of viral genome into the cell nucleus.

ABSTRAKT

Myší polyomavirus (MPyV) je neobalený tumorogení DNA virus, replikující se v jádře hostitelské buňky. Do buněk vstupuje endocytózou zprostředkovanou receptorem a jeho následný transport k jádru je závislý na kyselém prostředí endozomů a vláknech mikrotubulů, potřebných pro dopravení virionů do endoplazmatického retikula (ER). V ER dochází k disociaci virové kapsidy a rozbalení genomu viru. Mechanizmus, kterým je virový genom následně dopraven do nukleoplazmy není doposud objasněn, ale předpokládá se, že se ho kromě buněčných faktorů účastní také virové minoritní kapsidové proteiny VP2 a VP3. Po dopravení genomu do jádra dochází k produkci časných virových antigenů, které navozují vhodné prostřední pro replikaci viru. Po replikaci virové DNA a morfogenezi virionů, virové potomstvo opouští buňku během její lyze. Výzkum této disertační práce se ve své první části zaměřil na vnitrobuněčný transport MPyV a zapojení cytoskeletárních sítí během dopravy viru do ER. Zejména byl zacílen na stále nejasnou roli mikrotubulů během transportu viru v endozómech a na roli asociovaných mikrotubulárních motorů, která v případě MPyV nebyla doposud testována. Náš výzkum ukázal, že transport MPyV vedoucí k produktivní infekci nevyžaduje funkci kinesinu-1 či kinesinu-2, ale je závislý na transportu zprostředkovaném mikrotubulární motorem dyneinem. Funkce dyneinu se ukázala potřebná pro efektivní translokaci virionů z periferie buněk, často z kompartmentů připomínajících multikaveolární komplexy, do časných a pozdních endozómů a dále pro dopravení virionů do ER. I přesto, že na mikrotubulech závisel i transport viru do recyklujících endozómů, tyto kompartmenty se neukázaly jako potřebné pro produktivní infekci. Ve své druhé části se výzkum zaměřil na studium vlastností minoritních kapsidových proteinů VP2 a VP3. Minoritní kapsidové proteiny jsou nepostradatelné pro dopravení virového genomu do jádra. U obou minoritních proteinů byla demonstrována afinita k arteficielním membránám, a u proteinu VP2 schopnost tyto membrány perforovat. Tyto výzkumy tak naznačují, že interní minoritní strukturní proteiny, exponované po disociaci kapsidy v ER, mohou přispívat k translokaci virového genomu z ER do nukleoplazmy. My jsme připravili fúzní varianty minoritních kapsidových proteinů s fluorescenčním proteinen EGFP, pro jejich individuální expresi v savčích buňkách bez přítomnosti ostatních genových produktů MPyV. Biochemické analýzy ukázaly, že minoritní proteiny MPyV jsou cytotoxické a že jsou silnými induktory apoptotických procesů. Konfokální a immuno-elektronová mikroskopie ukázala schopnost obou minoritních proteinů interagovat s vnitrobuněčnými membránami a poškozovat je, což naznačuje mechanizmus zodpovědný za jejich cytotoxicitu. Nicméně, analýza apoptotických markerů a kinetiky smrti buněk transfekovaných genomem MPyV divokého typu či genomem mutovaným v iniciačních kodónech pro translaci VP2 a VP3 ukázala, že minoritní proteiny významně nepřispívají k indukci apoptotických procesů během infekce, a že jsou zcela postradatelné pro destrukci buňky na konci replikačního cyklu viru. Tyto výsledky tak indikují preferenční roli minoritních kapsidových proteinů během vstupu viru do buněk a dopravení virového genomu do jádra.

CONTENT

1. PREFACE

Based on World Health Organization (WHO), approximately 20% of cancer deaths in low- and middle-income countries are caused by viral infections such as those of hepatitis B and C viruses and human papillomaviruses. Hepatitis B and C viruses, human papillomaviruses, human T-cell lymphotropic virus and herpesviruses, such as Epstein-Barr virus and Kaposi's associated Sarcoma Herpesvirus, contribute to 10 – 15% of the cancers worldwide [1]. Polyomaviruses are small non-enveloped DNA viruses replicating in the cell nucleus. Members of *Polyomaviridae* family, Simian virus 40 (SV40) and Mouse polyomavirus (MPyV), encode very strong oncoproteins which can promote tumors in animal models [2]. Tumorogenic character of polyomaviral infection was showed to be connected with cell tropism and with the ability of different polyomavirus strains to bind specific receptors at plasma membrane [3-5]. Despite of their strong transformation and tumorogenic ability, polyomaviruses were considered to be no dangerous for human, because of lack of conclusive evidence that either of the known polyomaviruses directly causes or acts as a cofactor in human cancer development. Instead, human JC virus (JCV) was identified as the etiological agent of the fatal disease, progressive multifocal leukoencephalopathy [6], and human BK virus (BKV) was found to cause hemorrhagic cystitis in bone marrow recipients, ureteric stenosis and BKV nephropathy in immunosupressed patients [7-9]. However, there are growing evidences implicating human, as well as simian polyomaviruses in various types of human tumors [10,11]. Not long time ago, a new human polyomavirus, Merkel cell polyomavirus (MCV) was found associated with Merkel Cell carcinoma (MCC), a rare but aggressive skin cancer [12]. Bovine polyomaviruses (together with bovine papillomaviruses) were suggested to be possible cause of colorectal cancer [13], killing at the present time approximately 600.000 people per year worldwide (WHO). The emerging role of polyomaviruses as opportunistic pathogens in immunocompromised patients as well as in human tumors has raised importance of better understanding to individual steps of polyomavirus infection.

In our laboratory, we use MPyV as a model polyomavirus. Very important aspect of MPyV infection is the mechanism of virus entry to cells and delivery of viral genome into the nucleus. In comparison to other viruses, trafficking of polyomaviruses seems to be unique and very complicated process, with multiple endocytic pathways suggested to be utilized by polyomaviral capsid to reach the cell nucleus [14-21].

Identification of productive and non-productive endocytic pathways as well as involvement of cellular factors such as cell cytoskeleton are thus crucial for understanding of polyomavirus endocytic trafficking. Another important question is the role of the minor capsid proteins during virus replication cycle. Internal minor capsid proteins of MPyV are essential for delivery for genome into the nucleus [22], and they have ability to interact with and perforate artificial membranes [23]. These findings suggest involvement of the minor capsid proteins in early stages of infection when polyomaviral genome has to cross nuclear membrane to reach the nucleoplasm, but as well as during release of virus progeny during host cell lysis at the late stages of virus replication cycle.

This PhD thesis summarizes and discusses results of author's contribution to the complex research project on the MPyV, focused on i) the role of cell cytoskeleton in trafficking of MPyV towards the nucleus and ii) the cytotoxic properties of the MPyV minor capsid proteins and their ability to interact with intracellular membranes.

2. LITERATURE OVERVIEW

2.1. REPLICATION CYCLE OF POLYOMAVIRUSES

Polyomaviruses have a broad range of possible hosts in which they may replicate, like a birds, rodents, rabbits and primates including humans. The first discovered polyomavirus was MPyV, isolated from the extracts of leukemic mice by Ludwik Gross in 1953 [24]. SV40, discovered in 1960 as a contaminant of poliovirus vaccine (prepared using Rhesus monkey kidney cells) induces cytopathic effects and vacuole formation in monkey cells [25]. The first identified human polyomaviruses were BKV and JCV, both isolated from immunosupressed patients in 1971. JCV was isolated from human fetal brain cultures inoculated with extracts made from the brain of a patient with progressive multifocal leukoencephalopathy [6]. BKV was isolated from VERO (African green monkey kidney) cells inoculated with urine of a renal transplant recipient [26]. Till now, a number of additional human polyomaviruses has been discovered, including important discovery of MCV whose genome was identified in samples of human MCC by Feng et al [12].

Productive infection of polyomaviruses includes several steps, which can be divided onto early and late phase of infection (schematically in Figure 2.1). During the early phase, virions bind to receptor at the surface of susceptible cells, enter the cells and deliver viral DNA genomes into the host cell nucleus. Time interval of genome delivery into the nucleus is not precisely known, but it is estimated to take several hours. Attachment of virions to the cell surface and their internalization was showed to be finished up to 45 minutes for most virus particles [27]. Capsid proteins were observed accumulated around the nucleus approximately from 3 hours post-infection [19,21]. However, kinetics of entry, trafficking and genome delivery to nucleus might differ among polyomaviruses or may reflect particular cell type. Main aspects of early stages of polyomaviral infection are described in chapters 2.3 – 2.5.

Genome of polyomaviruses (Figure 2.2) is organized into the early and late region, separated by the regulatory sequence, which contains early and late promoters, transcription enhancer and origin (Ori) of replication. After viral genome appearance in the nucleus, expression of viral antigens occurs from the early region, encoding genes for early T (Tumor) antigens: large T (LT) antigen (100 kDa) and small T (ST) antigen (22 kDa). Some rodent polyomaviruses, including MPyV, encode also middle T (MT) antigen (55 kDa). Individual T-antigens are synthesized from monocistronic mRNA molecules, produced by alternative splicing from the early synthesized mRNA

precursor. For MPyV, expression of early antigens was detected already between 6 – 8 hours post-infection and amount of early antigen still raised throughout virus replication cycle [28]. Chen and Fluck [28] also showed that early phase of MPyV replication cycle (cell entry + early expression) lasted at least 12 hours until infected cells progressed to S phase of cell cycle.

Activities of T-antigens are responsible for immortalization and transformation of polyomavirus-infected cells. T-antigens alter the infected cell in order to provide a suitable environment for replication of viral genomes. This includes S phase induction, which is necessary for virus replication and for massive production of viral antigens. LT antigen was shown to bind oncosupressor pRb (Retinoblastoma protein) and inactivate its function. The protein is responsible for block of S phase induction during G0 and G1 phase of cell cycle, through the inhibition of E2F transcription factor. Interaction of LT with pRb thus causes the entry of cell cycle into the S phase of DNA synthesis (reviewed in [29]). Events causing cell immortalization normally trigger the activation of p53 protein, promoting apoptosis in virus infected cells, limiting thus virus replication and tumor formation [30]. However, T-antigens evolved to be able to bind and inactivate p53. In the case of SV40, LT antigen is responsible for inactivation of p53 functions, causing thus transformation of infected cells. In case of MPyV, LT immortalizes cells, but the major oncogene, responsible for cell transformation, is MT antigen. MT does not interact with p53 directly but modulates p53 function via interaction with Src family kinases and their constitutive activation (reviewed in [31]). Tumorogenic character of polyomaviral infection is connected with cell tropism and ability of different polyomavirus strains to bind specific receptors at plasma membrane. Receptors utilized by polyomaviruses for cell entry are present not only on the surface of permissive cells, but also of other cell types, which are non-permissive or semi-permissive for polyomaviral infection. In such cells, productive infection cannot be established, but cells might be immortalized or transformed if the viral genome is delivered to nucleus and expression of early T-antigens occurs [3-5,32].

The late stages of polyomaviral replication cycle start during the first S phase (approximately 16 hours post-infection) by replication of viral genomes in the host cell nucleus [28]. Replication is accomplished through the interaction of viral genome with multimeric complex of the LT antigen and LT-recruited cellular DNA replication proteins [33,34]. LT is multifunctional protein, which recognizes and binds to specific sequence in Ori, and then creates hexameric structures which posses ATPse [35],

helicase [36] and topoisomerase I [37] activity, necessary for melting and unwinding of DNA strands. For regulation of LT enzymatic activities and its interactions with host cell its post-translational phosporylation proteins is required (reviewed in [38]). LT has number of other post-translational modifications, whose significance is still not known, such as glycosylation [39], acetylation [40], adenylation [41], poly(ADP)-ribosylation [41] and N-terminal acetylation [41]. LT antigen has a J domain (homologous with J domain of *Escherichia coli* DnaJ chaperone) at the amino terminus, and LT with mutations in the J domain is frequently defective in DNA replication (J domain at N-terminus is common for all polyomavirus T antigens, and for each T antigen, J-domain mutants are defective in some aspect of T-antigen function) [42,43].

Replication of polyomavirus genome is accompanied by expression of late structural proteins, the major capsid protein, VP1 (45 kDa), and the minor capsid proteins, VP2 (35 kDa) and VP3 (23 kDa). Some mammalian polyomaviruses encode additional late non-structural protein known as agnoprotein (3.7 – 17.6 kDa), with function in regulation of gene expression, viral DNA replication, and virus morphogenesis and release [44]. Genes for structural proteins are encoded from the late region of viral DNA (Figure 2.2). Approximately 6 hours after first appearance of structural proteins (~ 22 hours post-infection for MPyV protein VP1), their amount becomes larger than that of early antigens [28]. Structural proteins are produced in the cytoplasm of infected cells and subsequently transported into the nucleus for assembly of virions. VP1 protein contains nuclear localization sequence (NLS) on its N-terminus, while the minor proteins possess NLS at their C-terminus [45,46]. Studies suggested that structural proteins are transported into the nucleus as an capsid "subunits" – complexes of VP1 pentamers with incorporated VP2 or VP3 proteins [47-49].

Appearance of new copies of viral genome and sufficient amounts of structural proteins lead to virus morphogenesis. Assembly of virions occurs at specific intranuclear sites, which have been termed ''virus factories'' (Figure 2.3). Candidate sites for polyomavirus assembly initiation are PML-NBs, since replication of polyomaviruses has been localized adjacent to PML-NBs [17,28–30], and in association with cellular DNA damage-related proteins [31,32]. The mechanism of virion assembly is still only poorly understood. It was supposed that polyomavirus morphogenesis is a gradual process when structural proteins condense with viral chromatin to create virions [50,51]. Protein VP1 binds to DNA non-specifically (in chapter 2.2) and has the ability to self-assemble into capsid-like structures – virus-like particles (VLPs). Neither DNA,

nor the minor structural proteins or post-translational modifications of VP1, are needed for VLPs formation [52]. How the capsid protein subunits specifically identify the viral genome is unknown. In the regulatory region of SV40 genome, *cis*-acting DNA sequence has been identified, which was suggested to serve as an encapsidation iniciation signal. The mammalian transcription factor, Sp1, was proposed to recruit the structural proteins to the viral minichromosome [53,54]. However, recent study did not confirm the existence of encapsidation sequence in MPyV genome and as the primary factor determining selection of DNA for encapsidation was suggested to be concentration of viral DNA at the site of virion formation [55]. On the other hand, other specific sequences near the viral Ori along with the J-domain of LT antigen might have important functions in assembly of virions [43,56-59].

Newly formed virus progeny accumulated in the host cell nucleus is released from the cell during its lysis in the end of virus replication cycle. The exit of virions occurs approximately 48 hours post-infection, when also cytopathic effect is apparent among infected cell population [28]. The mechanism of cell death induction is still unknown, but necrotic processes apparently play a crucial role [60]. Study on SV40 suggested that for lysis of SV40-infected cell is responsible late viral protein VP4 (15 kDa) [61]. VP4 is not present in viral particles and is produced exclusively in the very late phase of SV40 infection (~24 hours after start of expression of late structural proteins). Authors of this study observed oligomerization of VP4 with minor structural protein VP3, followed by binding of oligomers to the plasma membrane causing its perforation. These observations indicate induction of cell death by VP4 protein. For polyomaviruses which do not produce VP4, such as MPyV, the role of the minor capsid proteins, VP2 and VP3, was suggested instead, since *in vitro* studies revealed oligomerization of MPyV minor capsid proteins on membranes of isolated microsomes and their subsequent perforation [23]. Interestingly, although the cell lysis is generally accepted way of exit of polyomaviruses, study of Sanjuan et al. [62] demonstrated that at late stages of infection, MPyV virions interact with the free end and the lateral sides of microtubules, VP1 protein was observed to co-immunoprecipitate with tubulin and importantly, depolymerization of microtubular network was observed to prevent MPyV migration from the nucleus to the cell surface. These results suggest that some portion of virions might be released in more gentle way yet prior to host cell destruction.

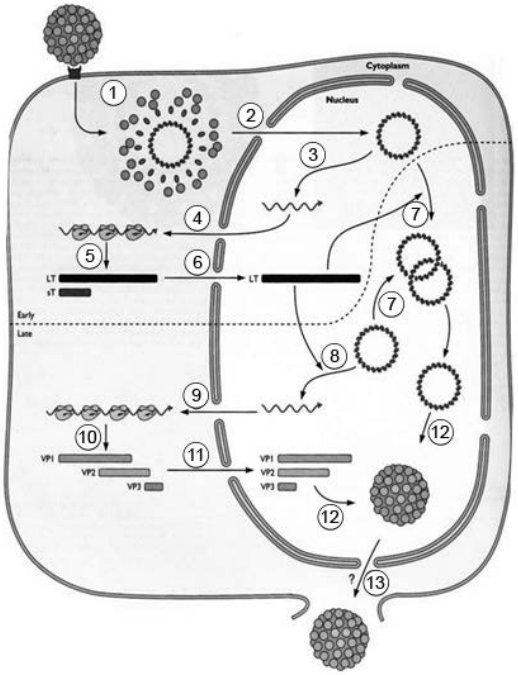

Figure 2.1 Replication cycle of polyomaviruses. (1) Attachment, internalization and trafficking of virions towards the cell nucleus; **(2)** Uncoating of viral genome and its import into the nuclei; **(3)** Early genes expression; **(4)** Translation of early mRNAs; **(5)** Production of early T antigens; **(6)** Transport of LT antigen to the nucleus; **(7)** Replication of viral genome; **(8)** Late gene expression; **(9)** Translation of late mRNAs; **(10)** Production of late structural antigens; **(11)** Transport of structural proteins to the nucleus; **(12)** Assembly of virions **(13)** Exit of virus progeny from cells. Reproduced from Fields Virology, 4th edition [63].

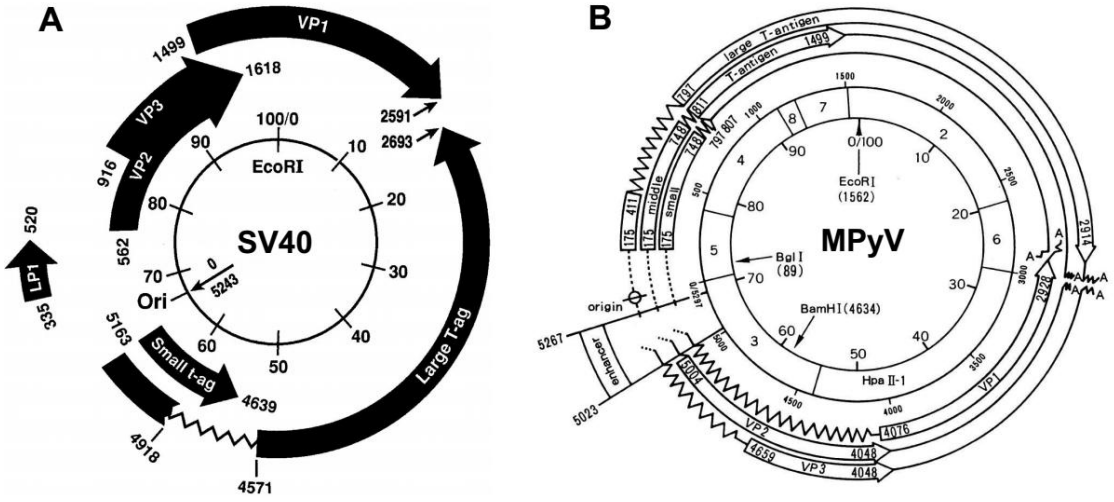

Figure 2.2 Genetic map of SV40 and MPyV genome. **(A)** The circular SV40 DNA genome (5.243 kbp) is represented, with the unique *Eco*RI site shown at map unit 100/0. Nucleotide numbers based on reference strain SV40-776 begin and end at the Ori of viral DNA replication (map unit 0/5243). The open reading frames that encode viral proteins are indicated. Arrowheads point in the direction of transcription; the beginning and end of each open reading frame are indicated by nucleotide numbers. The early T-antigens of SV40, large T antigen and small t antigen, are shown on the right, and the late structural proteins VP1, VP2 and VP3 are shown on the left. The beginning and end of each open reading frame are indicated by nucleotide numbers. Reproduced from Butel and Lednicky [64]. **(B)** The circular MPyV DNA genome (5.297 kbp) is represented with a various landmarks included: an inner circle with the position of useful restriction endonuclease sites (*Hpa*II [*Msp*I] and its eight fragments and the unique *Eco*RI, *Bgl*I, and *Bam*HI sites); nucleotide position markers every 500 nucleotides; the Ori; the enhancer region, which controls the expression of both early and late transcripts; the three early mRNAs and their proteins: large, middle and small T-antigen; and the three late mRNAs and their three late structural (VP) proteins. Reproduced from Wirth et al [65].

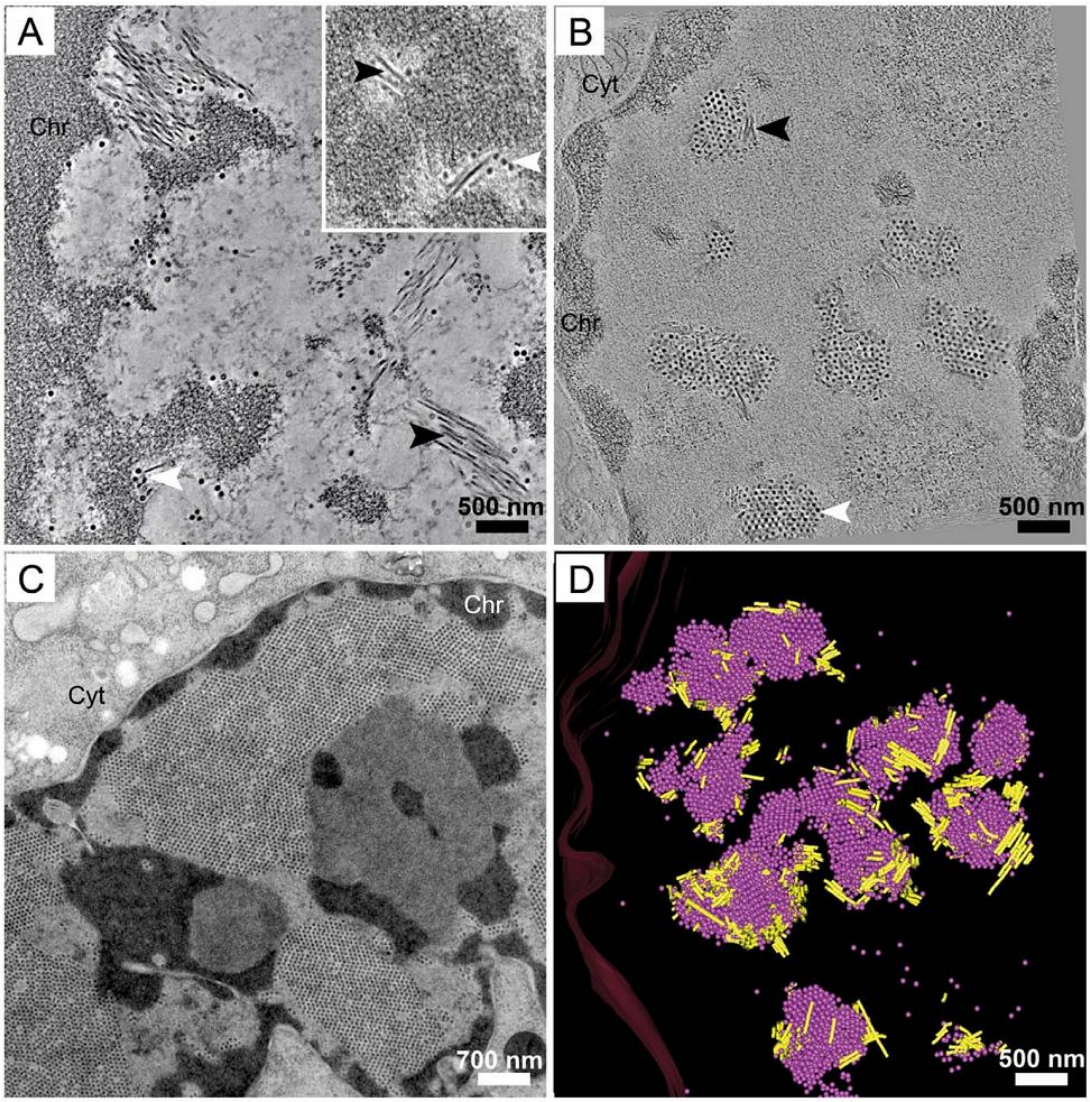

Figure 2.3 Progression of MPyV nuclear assembly. Images from dual-axis tomograms of high pressure frozen, Epon-embedded, 300 nm thick sections of 3T3 cells infected with MPyV (MOI of 10–20 pfu/cell) and harvested at 32 hpi. **(A)** Tubular structures (black arrowhead) are present in the periphery of the condensed chromatin adjacent to occasional virions (white arrowhead). **(B)** A 1 nm section extracted from a 262 montage over six serial sections (1.8mm thick) of a 3T3 nucleus in which the interchromatin space is partially filled with virion clusters and each cluster is associated with tubular structures. As infection proceeds, the number of virus clusters (white arrowhead) increases while the tubular structures (black arrowhead) are less prominent. **(C)** Late in infection virions fill the entire interchromatin space and tubular structures are not seen. **(D)** 3-D model of the 262 montage over six serial sections (each 300 nm thick) of a PyV-infected 3T3 nucleus. The model represents 1.8mm thick section of the nucleus showing the connections between virion clusters and tubular structures. An image extracted from the tomogram is shown in (B). Pink spheres, full virions; yellow cylinders, tubular structures. Chr, host condensed chromatin; Cyt, cytoplasm. Reproduced from Erickson et al [66].

2.2. VIRION STRUCTURE

Polyomaviruses have a small size virion, with a diameter of 40 – 45 nm. The architecture of non-enveloped polyomavirus particles (Figure 2.4) is known from X-ray crystal structures of SV40 and MPyV virions [67-69]. Their capsids are formed by 72 pentamers of the major structural protein, VP1, arranged in an icosahedral lattice (T = 7), from which 12 and 60 pentamers are pentavalently and hexavalently coordinated, respectively. Interpentameric connections are mediated by the N- and C-termini of VP1 monomers, which emanate from the bottom of the pentamer. C-terminal "arms" of VP1 monomers invade structures of neighboring pentamers, where they interact with the N-terminal extension of the invaded VP1 monomer. These interactions are stabilized by calcium ions. In contrast to other tested polyomaviruses, the capsid of SV40 is stabilized also by interpentameric disulfide bonds covalently linking the C-terminal arms to neighboring pentamers.

The central cavity of each VP1 pentamer contains one of the minor structural protein, VP2 or VP3 [70]. The internal minor capsid proteins overlap in sequence and VP3 protein sequence is entirely included in C-terminal part of VP2 (Figure 2.5A). The C-terminus of VP2/VP3 inserts into the axial cavity of the VP1 pentamer in hairpin-like manner, where it is strongly anchored by tight hydrophobic interactions across three VP1 monomers. On the other hand, the larger N-terminal part of the minor proteins appears to have significant flexibility (Figure 2.5B,C) [71].

The shell of structural proteins encloses viral minichromosome, composed of genomic circular double-stranded DNA (~ 5.3 kbp), which is wrapped around histone octamers (H2A, H2B, H3 and H4). Whole complex is composed of ~20 nucleosomes and is formed into chromatin-like structure [72-74]. Individual VP1 pentamers are expected to interact with the minichromosome. VP1 of SV40 has been shown to bind non-specifically the DNA [75], and the sequence of non-specific DNA binding domain has been identified also in VP1 protein of MPyV [76]. Concerning DNA binding activity of the minor capsid proteins, VP2 and VP3 of MPyV do not bind DNA [77], whereas minor structural proteins of primate and most human polyomaviruses (e.g. BKV and JCV) have additional amino acids in their C-terminus that are responsible for nonspecific DNA-binding activity [78]. Interestingly, human MCV does not have VP3 minor capsid protein, and DNA-binding domain is probably missing in VP2 protein sequence, similar to VP2 of MPyV [79].

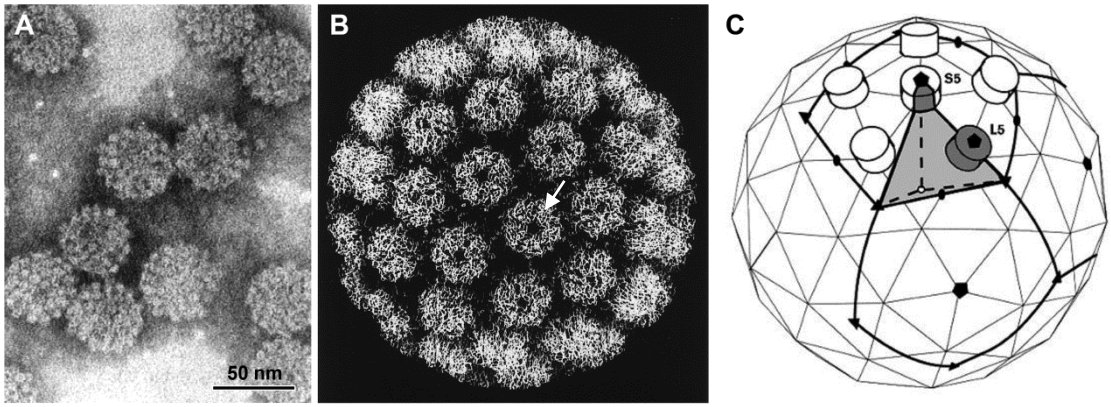

Figure 2.4 Architecture of polyomaviral capsid. (A) Purified MPyV virions visualized by electron microscopy (negative staining; by Liebl D., 2000). **(B)** Computer graphic representation of the structure of the SV40 virion. The shell is made up of 72 pentamers of VP1. Twelve of these lie on icosahedral fivefold axes (arrohead) and are surrounded by five other pentamers. The remaining 60 pentamers, such as the ones near the center of this diagram (arrow), are surrounded by six other pentamers. The pentamers are linked together by extended C-terminal arms of VP1 molecules of the subunits. Reproduced from Fields Virology, 4th edition [63]. **(C)** Schematic representation of the T=7d icosahedral lattice of SV40. The six VP1 pentamers that project from the virion surface and make up the crystallographic asymmetric unit of the space group I23 are represented by small disks. One pentamer is centered at a strict icosahedral 5-fold symmetry axis (S5); the remaining five pentamers have only local 5-fold symmetry (L5). Axis S5 is valid for the entire particle, whereas axis L5 is only valid for the invariant (core) part of the pentamer centered on it. The icosahedral asymmetric unit (one-fifth of the crystallographic asymmetric unit) is shown shaded. It is a pyramidal volume, with its apex at the origin (white sphere) and with its edges defined by adjacent 5-fold, 3-fold, and 2-fold axes. The Patterson asymmetric unit is half this volume. Also outlined is the asymmetric unit of space group I222 (bold lines) that was used for computational purposes and contains 3×6=18 pentamers (one-quarter of the virion) in the asymmetric unit. I222 is a subgroup of the true SV40 space group, I23. Reproduced from Yan et al 1996 [80].

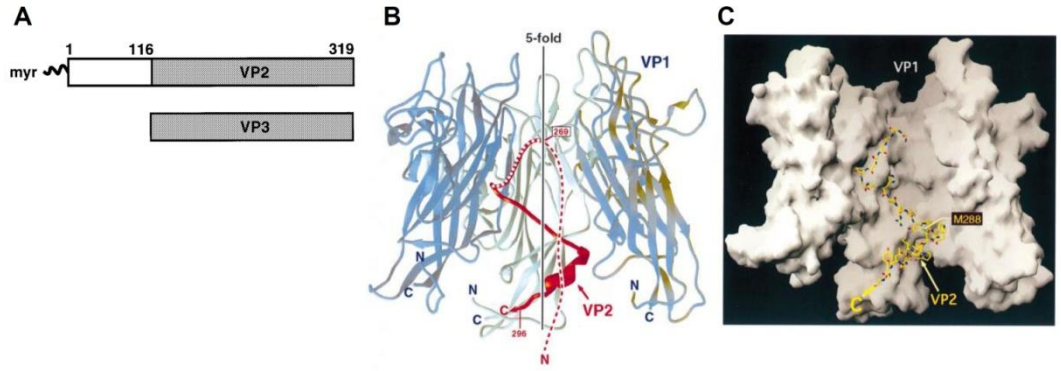

Figure 2.5 Structure of the VP1-VP2 complex. (A) Linear alignment of polyomavirus VP2 and VP3, showing the extent of a common C-terminal segment and the N-terminal VP2-unique region. **(B)** Cutaway view, showing VP2 in red and the three VP1 monomers that form contacts with VP2 in green (middle) and blue (left and right). The two remaining VP1 monomers that lie above the plane of the paper are not shown. Dotted line at the top of VP2 indicates that the electron density in that region does not allow us to model side chains. Residues N-terminal to this dotted line of VP2 are not visible in our electron density map and are shown as dashed line. **(C)** Surface representation of the complex shown in (B). The surface of the VP1 pentamer shows various grooves, protrusions and ridges, and the VP2 chain aligns very well with these features. Reproduced from Chen et al 1998 [71].

2.3. ENTRY OF POLYOMAVIRUSES INTO HOST CELLS

Non-enveloped polyomaviruses enter the cells by receptor-mediated endocytosis. The entry process of polyoma particles consists of several subsequent steps: (i) the attachment of virus capsids to the specific receptor at the surface of susceptible cells, (ii) receptor-triggered activation of signaling pathways inducing the clustering of lipids and remodeling of cortical actin beneath plasma membrane, (iii) receptor-mediated endocytosis of virions. Receptors are required for polyomavirus entry, but they also direct virions on endocytic pathway leading to productive infection [81,82]. Thus, only virions whose entry was mediated by their specific receptor(s) have a chance to deliver their genomes into the nucleus and establish productive infection.

The essential component of polyomavirus receptor is the sialic acid (SA) residue, which is recognized by the major structural protein, VP1 [32,83]. Most polyomaviruses were found to use gangliosides as their specific receptors. Gangliosides are glycosphingolipids consisting of ceramide backbone embedded in the plasma membrane and with three or more esterified sugars located extracellularly, one of these being SA (*N*-acetylneuraminic acid; NeuNAc). Structural studies showed that polyomaviruses bind strongly SA moiety in ganglioside structure by the shallow groove of several loops of VP1 protein, which are exposed at the capsid surface [69,84]. The character of the engagement of VP1 protein to SA residues predestines the specificity of interaction between polyomaviruses and gangliosides. MPyV, SV40, BKV and JCV utilize GD1a and GT1b, GM1, GD1b and GT1b, and GT1b gangliosides, respectively [85-87]. Recently discovered MCV was shown to recognize terminal α2,3-linked and α2,8-linked SA of GT1b ganglioside [88]. Structure of the ganglioside receptors utilized by polyomaviruses is present in Figure 2.6. Not only gangliosides were showed to be utilized by polyomaviruses. JCV in glial cells was showed to recognize α2,6-linked SA of N-linked glycoproteins or α2,6-linked SA in structure of serotonin receptor 5HT2aR [85,89]. Recently, SV40 in GM95 mouse melanoma cells (deficient in all glycosphingolipids [90]), was showed to utilize integrins as specific receptors [91]. Heavily glycosylated integrins carrying terminal SA residues have been considered as possible co-receptors for MPyV, since specific recognition sequence for binding of integrins was found in VP1 but also in VP2 minor capsid proteins of MPyV [92]. Caruso et al. [92] proposed model, where interaction of virions with ganglioside receptors induces conformation change in virus capsid structure, allowing subsequent

interaction with integrin co-receptor (Figure 2.7). Specific receptors and possible co-receptors of polyomaviruses are presented in Table 2.1.

Polyomavirus	Receptor	Co-receptor	References
MPyV	Terminal α2,3-linked sialic acid on GD1a and GT1b	Integrin α4β1	Tsai et al 2003 [87]; Stehle & Harrison 1996 [84]; Caruso et al 2003 [92]; Caruso et al 2007 [93]
SV40	GM1 ganglioside Integrin α2 and β1 (GM95 cells)	Class I MHC	Tsai et al 2003 [87]; Breau et al 1992 [94]; Atwood & Norkin 1989 [95]; Stergiou et al 2013 [91]
BKV	α2,8-linked disialic acid on GD1b and GT1b	Unknown glycoprotein	Low et al 2006 [86]; Dugan et al 2005 [96]
JCV	Terminal α2,3-linked sialic acid on GT1b	Serotonin receptor 5HT2aR; Terminal α2,6-linked sialic acid on an unknown glycoprotein	Komagome et al 2002 [85]; Elphick et al 2004 [89]; Dugan et al 2008 [97]; Liu et al 1998 [98]
MCV	Terminal α2,3-linked sialic acid and α2,8-linked disialic acid on GT1b		Erickson et al 2009 [88]

Table 2.1 Summary of receptors and co-receptors of polyomaviruses. Reproduced from Taube et al 2010 [99]; table was updated for latest results.

Attachment of polyomaviruses to receptors is followed by endocytosis of virions into the cell. Most polyomaviruses utilize caveolae- and clathrin-independent endocytosis for entry, being internalized via tightly-fitting invaginations into smooth endocytic vesicles (Figure 2.8) [21,100,101]. However, for instance, JCV utilizes clathrin-coated pits for entry [102]. Gangliosides are receptors typically associated with lipid rafts, dynamic microdomains at the plasma membrane with the role in signal transduction and cholesterol trafficking [103,104]. Studies showed that infection of SV40, BKV and MPyV is sensitive for disruption of lipid rafts by cholesterol depletion (using treatment of infected cells with methyl-β-cyclodextrin). In some cell types, entering virions massively co-localized with caveolin-1, protein abundantly present in subpopulation of lipid raft microdomains [16,18,20,21,105,106]. These results thus leaded to conclusion that these polyomaviruses utilize raft-associated caveolar endocytosis for entry [16,20,105]. Typically, SV40 was reported as representative virus entering the cells via caveolar invaginations. Besides observed co-localization of SV40 virions with caveolin-1, SV40 infection in CV-1 cells was showed to be inhibited by expression of dominant-negative mutant of caveolin-1 and also by dominant negative

mutant of dynamin [20,106]. Transient recruitment of dynamin II on SV40-containing vesicles was also observed [106]. Dynamins are large GTPases involved in the final stage of scission of transport vesicles from the plasma membrane and dynamin II is known to be involved in the internalization of caveolae [107,108]. However, expression of dominant-negative mutant of dynamin II did not affect SV40 infection in caveolin-1-deficient (Cav-1 -/-) human hepatoma 7 cells [109] and dynamin inhibitor dynasor did not affect internalization of SV40 in (Cav-1 -/-) mouse embryonic cells (MEF) [110]. These results indicate that SV40 utilizes caveolar endocytosis only in some cell types. For MPyV, involvement of dynamin II was not tested, but MPyV was showed to enter both, permissive 3T6 cells [21] and caveolin-1-deficient Jurkat cells [18], using tight invaginations, and dominant-negative mutant of caveolin-1 did not affect MPyV infectivity [18].

A recent study presented model of polyomavirus internalization process by inducing membrane curvature itself from the extracellular side of the membrane through multivalent binding of VP1 pentamers to cell surface gangliosides [110]. Authors of this study suggested that VP1 pentamers of polyomaviruses serve as nanoscale devices for membrane mechanical processes leading to the coat-independent formation of endocytic membrane invaginations. Membrane scission forming polyomavirus-containing endocytic vesicle was shown to be dependent on signal transduction and active cellular fusion factors [106,111,112]. Other factors suggested to be involved during scission are: actin cytoskeleton, cholesterol and tyrosine kinases signalization [110].

Effective endocytic uptake of polyomaviruses requires remodeling of cortical actin beneath the plasma membrane. Studies performed on MPyV showed association of virions with actin rich areas at the surface of cells, and uptake and penetration of MPyV virions into cells were showed to be accompanied by disorganization of actin stress fibers (Figure 2.9A) [21]. Infectivity of MPyV was found to be significantly increased in the presence of actin destabilizing drugs (e.g. latrunculin A, cytochalasin B – added to cells prior to virus addition) [113,114], whereas actin stabilizing drug (jasplakinolide – applied by the same way) decreased uptake and infectivity of MPyV [113]. These results suggest that MPyV infection induces destabilization and remodeling of cortical actin meshwork, which apparently represents a physical barrier for the entering virions, and whose dynamic state is important for virus efficient internalization. Transient disorganization of actin stress fibers was observed also during SV40 infection (Figure 2.9B). However, SV40 infectivity was showed to be remarkably

inhibited by actin destabilizing and stabilizing drugs [106,110], indicating that SV40 requires dynamic as well as intact actin cytoskeleton for its entry to cells.

The participation of microtubular network in polyomavirus entry was not observed, and neither the internalization of MPyV nor SV40 was affected by microtubule disrupting compounds [15,113].

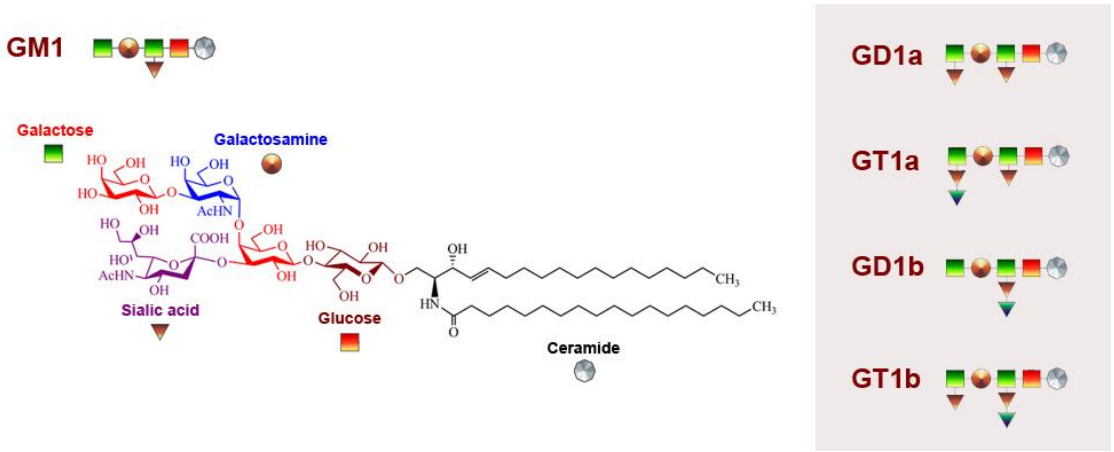

Figure 2.6 Structure of the gangliosides utilized by polyomaviruses for entry. Structure of ganglioside receptor of the SV40 (GM1), MPyV (GD1a and GT1b), BKV (GD1b and GT1b), JCV (GT1b) and MCV (GT1b) is shown. Modified from Hossain et al 2012 [115].

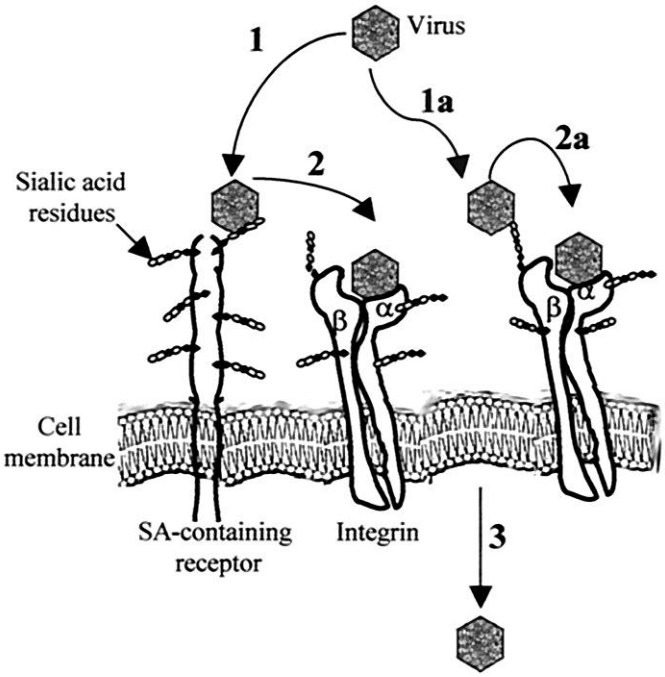

Figure 2.7 Proposed model for the early interaction of MPyV with host cells. First, MPyV interacts with SA-containing cell receptors (**step 1**). This initial interaction is a prerequisite for subsequent proper recognition of the α4β1 integrin (**step 2**), either to promote a conformational change of the MPyV capsid, rendering the LDV motif more accessible to the integrin molecule, or to bring it in closer proximity to the integrin. This second interaction may facilitate the entry of the virus into the cells (**step 3**). Considering that both α4 and β1 integrin subunits are heavily glycosylated, carrying, in particular, terminal SA residues, integrins may themselves be a component of the SA-containing receptor molecules for MPyV (**steps 1a** and **2a**). Reproduced from Caruso et al 2003 [92].

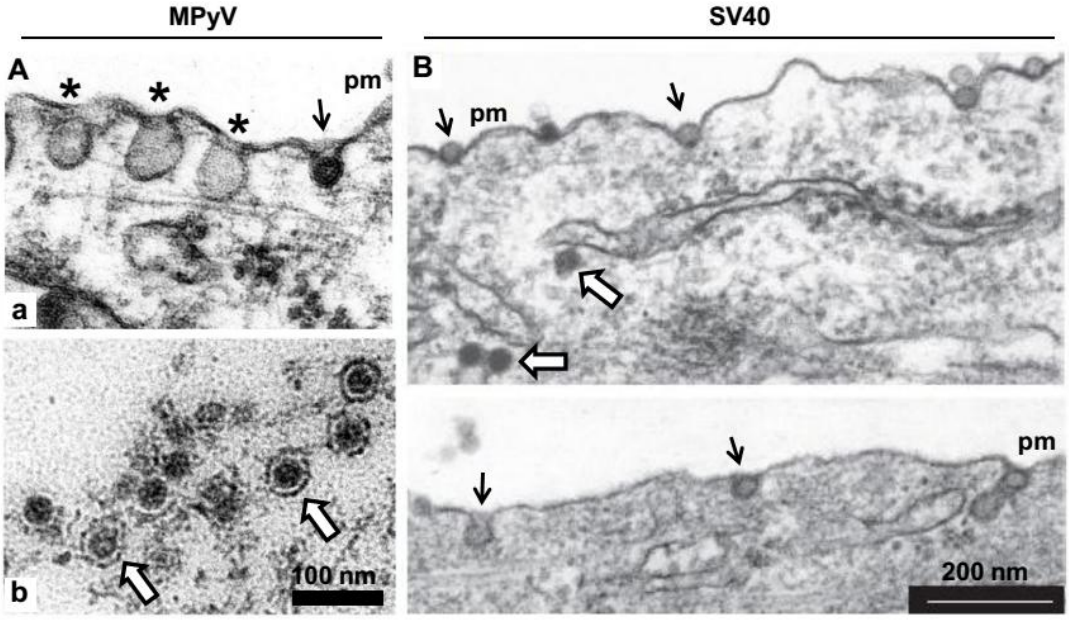

Figure 2.8 Internalization of MPyV and SV40. MPyV **(A)** and SV40 **(B)** virions enter the cells via tight invaginations enclosing virions (black arrows), independently of flask shape caveolar invaginations (asterisks). Virions are internalized into smooth, tightly-fitting endocytic vesicles (white arrows). Electron micrographs of NIH 3T6 cells at 20 min p.i. with MPyV (**Aa** and **Ab**) and electron micrographs of CV-1 cells that were incubated for 7 min with SV40 (B) are shown. Pm, plasma membrane. Panel A is modified from Richerova et al 2001 [21], panel B is modified from Ewers et al 2010 [110].

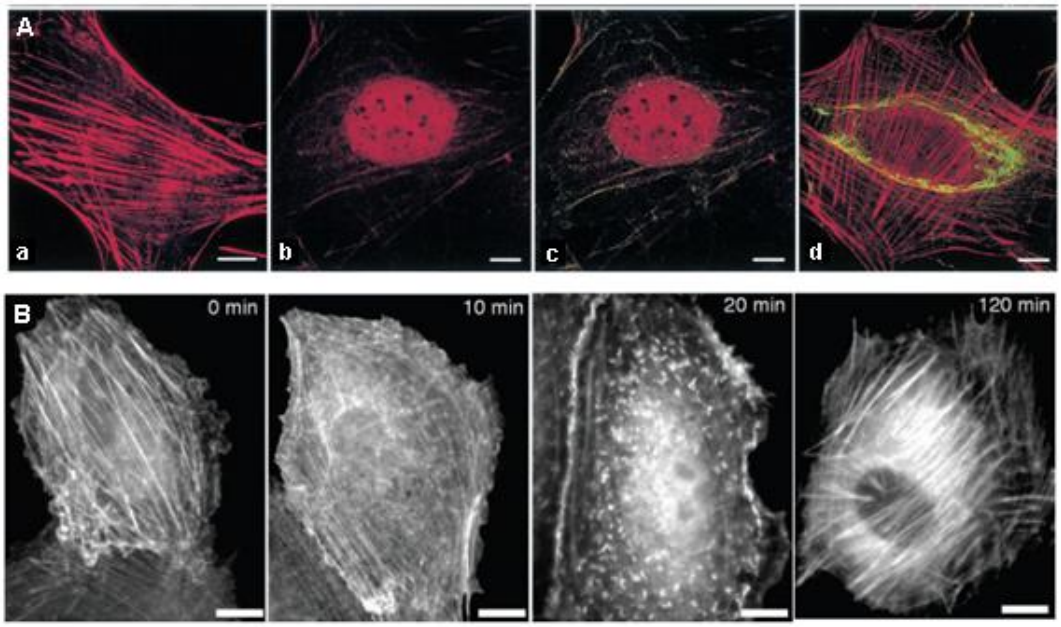

Figure 2.9 Transient disorganization of actin stress fibers during uptake and penetration of MPyV and SV40. (**A**) 3T6 cells infected with MPyV VP1 pseudoparticles fixed 20 min p.i. (**b** and **c**) or 3 hrs p.i. (**d**) visualized by confocal microscopy. (**a**) Control, mock-infected, cells fixed 20 min p.i. Staining was done with the rabbit anti-MPyV VP1 serum followed by the Alexa Fluor 488-goat anti-rabbit IgG antibody (green) and with phalloidin conjugated with rhodamine (red). Bars, 10 μm. (**B**) CV-1 cells expressing GFP-β-actin with bound SV40, show that initially most GFP-β-actin is present in stress fibers. Then, actin foci appear and, subsequently, actin tails. The number and intensity of stress fibers are correspondingly reduced (20 min p.i.). After further incubation, actin tails disappear and stress fibers reappear (120 min). Scale bars, 10 μm. Panel A is reproduced from Richerova et al 2001 [21], panel B is reproduced from Pelkmans et al 2002 [106].

2.4. TRAFFICKING TOWARDS THE NUCLEUS

Like other viruses replicating in the nucleus, internalized polyomaviruses have to deliver their genomes into the host cell nucleus for replication. Nevertheless, the way how polyomaviruses approach the nucleus is unique among viruses. Many viruses (enveloped or non-enveloped) usually exit the endosomal system in acidic endosomes by penetration of their capsids or nucleocores (genome in complex with structural proteins) into the cytosol. Acidic environment in endosomes was showed to cause activation or exposition of viral proteins mediating the fusion of viral envelope with endosomal membrane, or, in case of non-enveloped viruses, perforation of endosomal membrane. As a result, capsids or nucleocores translocate through the endosomal membrane and their transport continues in cytosol (reviewed in [116]). However, polyomaviruses seem not to escape endosomal system, but still enclosed in membraneous compartments, they are transported to the ER. In ER, lumenal enzymes (oxidoreductases, disulfide isomerases) facilitate disassembly of virus capsid and partial uncoating of viral genome [117-120].

Regardless the mode of entry, infectious trafficking of polyomaviruses towards the ER was showed to be regulated by Rab5 and Rab7 GTPases, mediating virus transport to the early (sorting) endosomes and their subsequent maturation [15,81,121,122]. For MPyV, pathway via early and recycling endosomes to the ER was also postulated [18,19]. Despite polyomaviruses do not leave endosomal system in acidic endosomes, latest studies showed that temporal capsid presence in low pH of late endosomes is essential for their infectivity [15,18,121,122]. Study on MPyV showed that low pH causes specific re-arrangement of polyomavirus capsid, and these structural changes were suggested to be important for subsequent capsid disassembly in the ER and for virus transfer through the ER membranes into the nucleus [81,121]. Infection of SV40 was believed to be low pH-independent and virus transport through the intracellular compartments called “caveosomes” (described as pH neutral organelles positive for caveolin-1 [20]) was reported [14,20,106]. However, the model of caveosomes was revisited and cavosomes were identified as late endosomes or lysosomes modified by overexpression of caveolin-1 [15,123]. Later, productive transport of SV40 was shown to be also dependent on low pH, and SV40 virions were detected in late endosomal compartments [15].

From mature acidic late endosomes or endolysosomes, polyomaviruses are transported to the ER [15,81,121,122]. This transport was described to be directed by ganglioside receptor and thus probably only virions attached to their specific ganglioside receptor might reach the ER [81,82], while the rest ends up in degradative lysosomes [15,81,82]. Although temporal presence in acidic enviromnemt of endosomes is essential for polyomaviruses, it is still not clear where polyomaviruses leave the endosomal system and whether the pH of matured endosomes or even endolysosomes (pH 4.5 – 5.5) is not too low for polyomavirus-receptor interaction stability. The environment of early and premature late endosomes is mildly acidic (pH 6.0 – 6.5) and transport through these compartments is regulated by both, Rab5 and Rab7 GTPases, and thus possibility of direct transport from early or premature endosomes to the ER cannot be also excluded. Importance of early endosomes in relation to requirement of polyomavirus infection for low pH was indeed demostrated for MPyV. In cells where endosomal pH was elevated by treatement with ammonium chloride (NH_4Cl; penetrates into endosomes and increases endosomal pH) or Bafilomycin A1 (a specific inhibitor of vacuolar H^+ ATPase), MPyV infection was blocked and virions were retained in early endosomes [18].

Studies focused on trafficking of SV40 [112,124,125], BKV [86,121] and MPyV (in GD1a-supplemented rat C6 cells) [16], revealed that infection of these viruses is sensitive to treatment with brefeldin A (BFA), a compound disrupting vesicular transport within the Golgi complex and from the Golgi complex to the ER. These observations indicate that polyomaviruses are transported from endosomes to ER via passage through the Golgi complex. Similar pathway was described for some bacterial toxins, such as Cholera or Shiga toxin (reviewed in [126]). However, in contrast to these toxins, direct observation of polyomaviral capsids within the Golgi complex or *trans*-Golgi cisternae is missing. There is also study demonstrating that MPyV virions bypass Golgi complex during their transport to the ER [19]. Moreover, it was showed that BFA induces the tubulation of endosomes and inhibits cargo transport from early endosomes to endolysosomes [127,128]. Treatment with BFA has thus more complex impact on endosomal system of cells and observed sensitivity of polyomaviral infection to BFA does not necessarily point to Golgi-ER retrograde transport. Since maturation of endosomes and their fusion with lysosomes is dependent on intact microtubular network [129-132]), Engel et al [15] used treatment with microtubule disrupting drug nocodazole, to divide trafficking of SV40 into two phases: early events including virus

transfer via early endosomes and its delivery to premature late endosomes and later events, including virus transition to matured late endosomes and endolysosomes, or eventually virus delivery to ER. When authors investigated effect of BFA during early and late phase of virus trafficking, they found that presence of BFA affected processes both before and after the nocodazole block, supporting the involvement Golgi complex in trafficking of SV40.

Cytoplasmic trafficking of any cargo, whether "naked" or enclosed in vesicles or endosomes, requires functional cell cytoskeleton to reach specific sub-compartments of the cell. Productive infection of all polyomaviruses depends on intact microtubular network and microtubule depolymerizing drugs such as nocodazole or colcemid block their infectivity [14-16,20,62,113,114,121,133-135]. Microtubules and microtubule-associated motors are essential for the function and spatio-temporal organization of the endosomal system. Opposing forces provided by dynein and kinesins are responsible for the oscillatory motion of endosomes along microtubules and they are required for endosome trafficking towards the nucleus, plasma membrane or vesicular transport between other membrane compartments [136]. Interestingly, despite the polyomaviral infection rely on intact microtubules, trafficking of SV40, BKV and JCV was shown to be independent on dynein motor function [14,134]. Authors proposed the involvement of a different member of the dynein family whose function is independent of dynactin complex [14]. Another possibility that the viral proteins interact directly with microtubules for transport was also suggested [14]. However, recently published RNA interference screen, revealed dependence of SV40 infection on dynein motor function in HeLa cells [15].

Despite the productive trafficking of SV40 in human hepatoma 7 or human glial cells rely completely on intact microtubules [14,109], in CV-1 (African green monkey kidney) cells, infection of SV40 was remarkably reduced by the presence of actin binding drugs in CV-1 cells [106,110]. In these cells, SV40 was shown to induce recruitment of actin nucleation on virus-carrying vesicles in form of actin comet tails and use it for its transport from the plasma membrane. Study of Engel et al [15] showed that transport of SV40 to early and pre-mature late endosomes was unaffected by disruption of microtubular network. These results indicate that actin dynamics is involved in very early steps of SV40 trafficking in CV-1 cells, mediating virus transport from the plasma membrane to premature endosomes, whereas microtubules are required later, for virus delivery from mature endosomes to the ER. The utilization of actin

dynamics for transport was proposed also for BKV in primary human RPTE (renal proximal tubule epithelial) cells [121], but also for MPyV in ganglioside GD1a-supplemented rat C6 cells, which are naturally non-permissive for MPyV infection [16]. In GD1a-supplemented C6 cells, MPyV was showed to utilize actin cytoskeleton for delivery to caveolin-1-rich compartments, which were suggested to be “caveosomes”, whereas microtubules were required for subsequent virus trafficking to the ER [16]. Since caveosomes were identified to be an arftifacts of caveolin-1 overexpression [15,123], the involvement of actin cytoskeleton and microtubular network in MPyV endosomal trafficking still remains unclear. These findings thus suggest the ability of polyomaviruses to subvert actin cytoskeleton for their intracellular transport in some cell types.

For the summary, schematic model of infectious entry and trafficking of SV40 in CV-1 cells is presented in Figure 2.10.

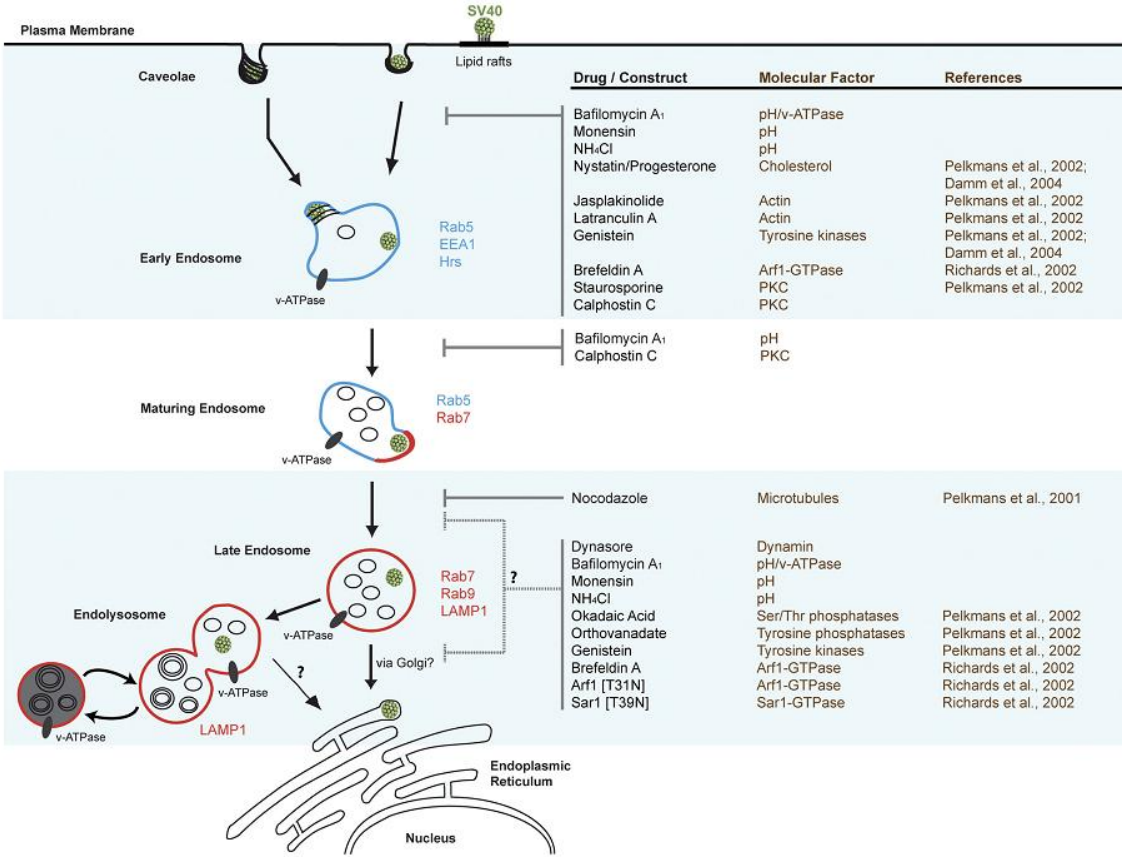

Figure 2.10 Model of infectious SV40 entry into CV-1 cells. SV40 binds to its receptor (GM1), partitions into lipid rafts, and induces internalization from the plasma membrane either by a caveola-mediated or a caveolin-1-independent, lipid raft-dependent endocytosis mechanism. The virus is transported to Rab5-, EEA1-, and Hrs-positive EEs. When these endosomes acquire Rab7, SV40 associates with the Rab7-positive domains. Through endosome maturation, viruses become lumenal components of LAMP1-, Rab9-, and Rab7-positive LEs and eventually endolysosomes. The vacuolar ATPase (v-ATPase) is responsible for the acidification of endosomes and lysosomes. Acidification is required for SV40 internalization and subsequent transport steps. Virus transport to the ER occurs from the late compartments of the endocytic pathway by an unknown mechanism either directly or, less likely, via the Golgi complex. Early and late events in the entry pathway can be blocked by various inhibitors and other perturbants. Reproduced from Engel et al 2011 [15].

2.5. IMPORT OF POLYOMAVIRAL GENOME INTO THE NUCLEUS

Viruses which replicate in the nucleus have to smuggle their genomes through the barrier of nuclear envelope (NE) to deliver them into the nucleoplasm. Most of these viruses exploit the nuclear pore complexes (NPCs) as entry gateway. To overcome size limitation of material which might penetrate through the pore (upper limit in particle diameter for transport through the NPC is 39 nm), viral capsids usually undergo partial or complete disassembly, and then, genomes in association with structural proteins (containing NLS in their sequence) enter the nucleus (reviewed in [137]). Only capsid of hepatitis B virus (HBV) or capsids of parvoviruses are small enough (18 – 20 nm in diameter) to be theoretically able to passage NPCs as intact. Despite of that, mature (DNA-containing) capsids of HBV have been shown to dock at the NPC and to enter into the basket where they disassemble, and only viral genomes were released into the nucleoplasm [138]. However, capsids of parvoviruses were indeed detected in the nucleus where they are supposed to be delivered through the NPCs, or eventually, via capsid-induced ruptures in NE [139-141]. It is important to note here, that observation of parvovirus translocation through the NE was not reported yet, and conditions or cellular factors allowing uncoating of viral genome in nucleoplasm are not known.

Despite the years of extensive study, the mechanism utilized by polyomaviruses for delivery of their genomes into the nucleus remains obscure. Regardless of the multiplicity of infection, only a few virions are able to deliver their genomic DNA into the cell nucleus [19]. Currently, two possible ways for viral genome delivery to the cell nucleus have been proposed: either partially disassembled virions are translocated from the ER to cytosol and then imported into the nucleus via NPCs, or, alternatively, genome is translocated directly from ER to nucleoplasm by penetration through the membranes of NE. Findings published so far favor the possibility of genome translocation to the nucleus via cytosol and NPCs. When the effects of ER-associated processes and factors on SV40 infection and penetration through the ER were analyzed, SV40 was showed to utilize thiol-disulfide oxidoreductases, ERp57 and PDI, as well as the retrotranslocation proteins Derlin-1 and Sel1L, indicating that virus requires the protein folding machinery for viral genome uncoating and after it, exploites the ER-associated degradation (ERAD) machinery presumably to escape from the ER lumen into the cytosol [119]. The quality control machinery in the ER was shown to be exploited also by MPyV, when ER-resident protein, Derlin-2, a factor implicated in the

removal of misfolded proteins from the ER for cytosolic degradation, was required by MPyV to establish infection [142]. Moreover, recently reported RNA interference screen identified four different DNAJ molecular co-chaperones and BiP (GRP78) protein as Hsp70 partner of DNAJB11, whose knockdown markedly inhibited SV40 exit from the ER [143]. Interestingly, despite conformation changes in the structures of polyomavirus capsid occurring in the ER, SV40 capsids were showed to cross the ER membrane as a large intact particles consisting of all structural proteins (VP1, VP2 and VP3) and viral genome, potentially through either a protein-conducting channel or the lipid bilayer [144].

Involvement of the internal minor capsid proteins is expected during the import of polyomaviral DNA into the nucleus. It has been shown that mutated MPyV virions lacking either VP2 or VP3 lost their infectivity, indicative of defects in the early stages of infection [22]. Study of Rainey-Barger et al [23], described three trans-membrane domains in MPyV minor proteins sequence: domain 1 was identified is the unique part of VP2, domain 2 was located at the N-terminus of common part of VP2/3, and amphipatic α-helix at the C-terminus of VP2/3 was marked as domain 3 (Figure 2.11). These authors further performed *in vitro* experiments which showed that structural protein VP2 is exposed in the ERp29 oxidoreductase-activated viral particles and is able to binds to, integrates into, and perforates the physiologically relevant ER membrane. Minor protein, VP3 (lacking domain 1), was shown to be able to bind to and integrate into the membrane, but it was not sufficient for membrane perforation [23]. These findings suggest involvement of the minor capsid proteins in delivery of viral genome from ER into the nucleus.

Similarly, mutated SV40 virions lacking VP2 and VP3 were showed to be poorly or non-infectious as a result of the failure to deliver viral DNA into the cell nucleus [145,146]. VP2 and VP3 of SV40 were demonstrated to integrate into the ER membrane and integration was prevented by association of the minor proteins with VP1 pentamers. VP1 thus probably regulates the function of VP2 and VP3 by directing their localization between the particle and the ER membrane [147]. In the summary, these observations suggest that after polyomavirus capsid disassembly within the ER lumen, the minor capsid proteins oligomerize and integrate into the ER membrane, potentially creating a pore that aids in viral DNA transport out of the ER to the cytosol or directly to nucleoplasm (Figure 2.12).

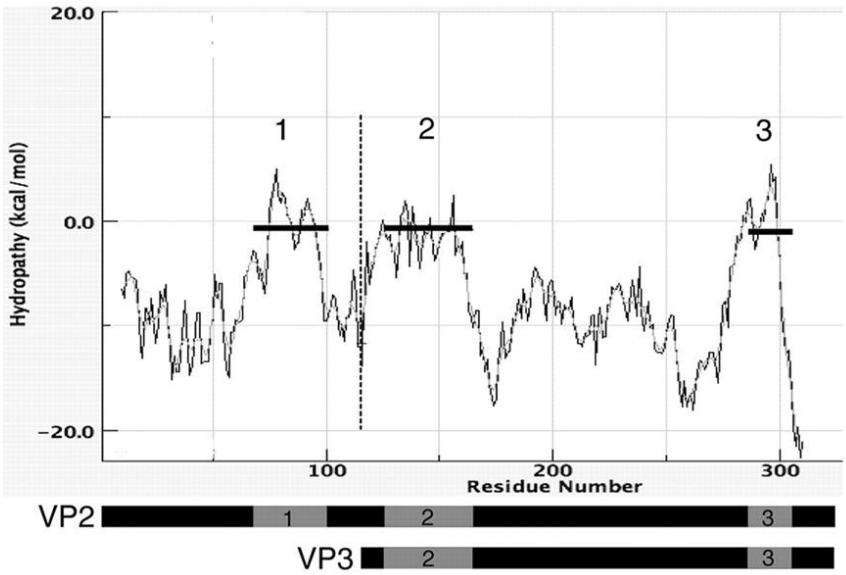

Figure 2.11 Hydropathy plot of VP2 and VP3. The hydropathy plot of VP2 and the overlapping VP3 was determined by entering the VP2 amino acid sequence into the Membrane Protein Explorer[3.0] program. Each predicted transmembrane domain is indicated by a horizontal line and numbered. The portion of the plot to the right of the dotted vertical line corresponds to VP3 (residues 116 to 319), while the portion of the plot to the left of the dotted vertical line indicates the portion unique to VP2 (residues 1 to 115). Reproduced from Rainey-Barger et al 2007 [23].

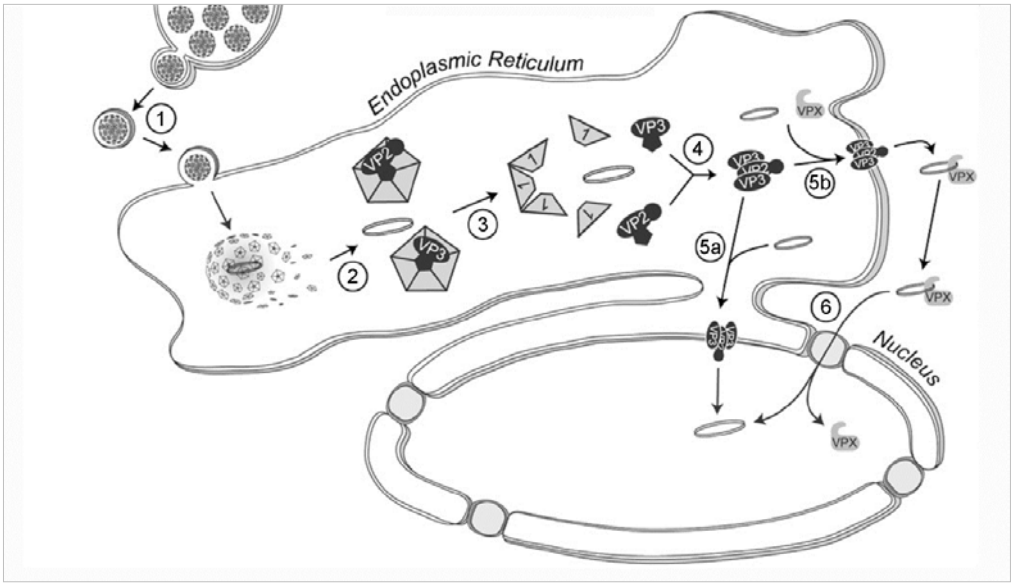

Figure 2.12 Model for SV40 entry and penetration of the ER membrane. (1) SV40 particles bud from acidic endosomes and traffic to the ER. (2) Once inside the ER, the capsid is proposed to disassemble with the aid of ER-resident molecular chaperones liberating the genome and VP1 pentamers associated with VP2 and VP3. (3) Further dissociation of the VP1 pentamers releases the bound VP2 and VP3. (4) VP2 and VP3 oligomerize and insert into the ER membrane to form a multimeric complex that aids in transporting the genome across the ER membrane. (5a) The VP2 and VP3 complex integrates in the contiguous nuclear and ER membrane to directly transport the genome into the nucleus. (5b) The VP2 and VP3 complex integrates away from the nuclear boundary, transporting the genome into the cytoplasm, (9) where one of the structural proteins, ‘‘VPX,’’ utilizes its nuclear localization sequence and DNA-binding domains to traffic the genome into the nucleus. Modified from Daniels et al 2006 [147].

3. AIMS OF STUDIES

- **To specify involvement of cell cytoskeleton in the endocytic trafficking of MPyV.**
    - To detect association of MPyV virions with cytoskeleton during their transport in living cells.
    - To elucidate dynamics of MPyV cytoplasmic trafficking.
    - To examine role of microtubular motor dynein, kinesin-1 and kinesin-2 in MPyV productive trafficking.
    - To determine involvement of cell cytoskeleton in transport of MPyV from the plasma membrane to endosomes.
    - To reveal whether the transfer via recycling endosomes represents an alternative pathway along microtubules for delivery of MPyV to the ER.

- **To characterize cytotoxic properties of the minor capsid proteins, VP2 and VP3, in the absence of other MPyV gene products.**

    - To establish the system for the efficient expression of the minor capsid proteins in mammalian cells, using fusion variants of VP2 or VP3 with EGFP.
    - To examine interactions of the minor capsid proteins fusion variants with cell sub-structures.
    - To determine cytotoxicity of the minor capsid proteins fusion variants.
    - To elucidate mechanism of cell death induction by the minor capsid proteins.
    - To reveal importance of the minor capsid proteins for host cell lysis in the end of virus replication cycle.

4. MATERIALS AND METHODS

4.1 **Cell line cultivation and transfection**

Swiss albino mouse fibroblasts 3T6 and mouse NIH 3T3 fibroblasts (both purchased from American Type Culture Collection) were grown at 37^{o}C and 5% CO_2 in complete Dulbecco's Modified Eagle's Medium (DMEM) (Sigma-Aldrich, St Louis, MO, USA) supplemented with 10% fetal bovine serum (FBS) (Sigma-Aldrich) and GlutaMAX-I (Gibco, Life Technologies). All transfections were performed by electroporation using Amaxa kits (Lonza, Basel, Switzerland). Briefly, cells were seeded 24 h before the procedure and then, 4 x 10^6 cells were transfected with 6 μg of plasmid DNA, using program T-030 (for 3T6 cells) or U-030 (for 3T3 cells). Transfected cells were incubated (15 min) in RPMI medium (Sigma-Aldrich) supplemented with 5% FBS and then seeded on coverslips (or directly to wells) in 24-well plate.

4.2 **DNA constructs**

- pEGFP-α-tubulin (Clontech) – plasmid for expression of human α-tubulin (cat. 6117-1).
- pEGFP-β-actin (Clontech) – plasmid for expression of human β-actin (cat. 6116-1).
- pDynamitin-EGFP-N1 – plasmid for expression of EGFP-fused dynamitin [148]. Construct was kindly provided by Beate Sodeik (MHH Institute of Virology, Hannover, Germany).
- pRFP-KHCct and pRFP-DTC – plasmid for production of RFP-tagged dominant-negative kinesin-1 via expression of C-terminal fragment of kinesin-1 heavy chain (KHCct) and control RFP-DTC-expressing vector [149,150]. Constructs were kindly provided by Victoria J. Allan (University of Manchester, Manchester, United Kingdom).
- pEGFP-KIF3A-HL and pEGFP-KAP3-CT – plasmids for expression of EGFP-fused dominant-negative KIF3A subunits (motorless) or dominant-negative KAP3 accessory subunit (C-terminus only) of kinesin-2 [151,152]. Constructs were kindly provided by Trina A. Schroer (The John Hopkins University, Baltimore, MD, USA).

- pEGFP-Rab11 WT, pEGFP-Rab11 DN and pEGFP-Rab11 CA – plasmids for expression of EGFP-fused wild-type, dominant-negative (S25N) and constitutively active (Q70L) mutant of Rab11 GTPase, respectively [153]. Constructs were kindly provided by Marino Zerial (Max Planck Institute, Dresden, Germany).
- pEGFP-Rab7 WT, pEGFP-Rab7 DN and pEGFP-Rab7 CA – plasmids for expression of EGFP-fused wild-type, dominant-negative (T22N) and constitutively active (Q67L) mutant of Rab7 GTPase, respectively [154]. Constructs were kindly provided by Cecilia Bucci (The University of Salento, Lecce, Italy).
- pEGFP-Rab5 WT – plasmid for expression of EGFP-fused wild-type version of Rab5 GTPase [155]. Construct was kindly provided by Philip D. Stahl (Washington University School of Medicine).
- pEGFP-N1 (Clontech) – plasmid for expression of EGFP, used as a control plasmid for the infection assays evaluating the efficiency of MPyV infection.
- pMJG – plasmid containing the entire genome of MPyV A3 strain, opened and inserted into the bacterial plasmid pMJ1 (a 2.266-base-pair derivative of pAT153 plasmid) in the unique *Eco*RI site [156]. Construct was kindly provided by Nina Krauzewicz.
- pCGVP1/2/3 and pCGVP1 – plasmids containing the late region genome of MPyV (or alternative late region mutated in the start codons of VP2 and VP3 genes) under the CMV promoter. Constructs were prepared by Hana Španielová.
- pSVL-VP2 – plasmid for expression of VP2 protein of MPyV (A3 strain), constructed using pSVL plasmid (Pharmacia, Uppsala, Sweden) with SV40 promoter. Construct was kindly provided by Lucie Klímová.
- pLNHX-VP3 – plasmid for expression of VP3 protein of MPyV (A3 strain), constructed using pLNHX plasmid (Clontech, CA, USA) with *Drosophila hsp70* promoter. Construct was kindly provided by Zuzana Kečkešová.
- pVP3-Leader-C2 – plasmid for expression of VP3 of MPyV (A3 strain), constructed using pEGFP-C2 plasmid (Clontech) by replacing the CMV IE promoter and *EGFP* gene with the *VP3* gene under control of the MPyV late promoter. Construct was kindly provided by Lucie Klímová.
- pVP2-EGFP and pVP3-EGFP – plasmids for expression of minor structural proteins, VP2 or VP3, of MPyV (A3 strain) fused with EGFP at C-terminus of

minor proteins, constructed using pEGFP-N1 vector (Clontech). Constructs were prepared by Evžen Bouřa.

- pEGFP-tVP3 – plasmid for expression of truncated VP3 (with a deletion of the first 101 amino acids at the N-terminus) of MPyV (A3 strain) fused with EGFP at N-terminus of tVP3, constructed using pEGFP-C2 vector (Clontech). Construct was prepared by Evžen Bouřa.
- pVP2-FLAG and pVP3-FLAG – plasmids for expression of minor structural proteins, VP2 or VP3, of MPyV (A3 strain) fused with FLAG epitope at their C-termini, constructed using pCMV-FLAG-5a plasmid (Sigma-Aldrich). Constructs were prepared by Evžen Bouřa.
- pMJMA – plasmid for production of MPyV lacking minor structural proteins VP2 and VP3. Plasmid was constructed using the plasmids previously published [156]: pMJA has a deletion in the VP3 start codon and pMJM has a mutation in the VP2 start codon. pMJMA was prepared from pMJM by exchanging the WT *VP3* gene with the mutated *VP3* gene cleaved from pMJA. Construct was prepared by Hana Španielová.

DNA constructs prepared by author for the study of Huerfano et al [157]:

- pEGFP-VP2 and pEGFP-VP3 – plasmids for production of VP2 or VP3, fused with EGFP at their N-termini. Plasmids were prepared by the insertion of amplified sequences into the pEGFP-C2 plasmid (Clontech) using *Bgl*II and *Eco*RI cloning sites. Sequences encoding VP2 and VP3 were amplified by PCR using the pMJG plasmid, which contains the entire genome of MPyV (A3 strain).

    - Primers (synthetized by KRD [Invitrogen] company):
      VP2 forward (*Bgl*II):
      5’ CAGAC AGA TCT TG GGA GCC GCA CTG AC 3’
      VP2 backward (*Eco*RI):
      5’ CAGAC GAA TTC TTA GAG ACG CCG CTT TTT C 3’
      VP3 forward (*Bgl*II):
      5’ CAGAC AGA TCT TG GCG TTG ATA CCA TGG C 3’
      VP3 bacward (*Eco*RI):
      5’ CAGAC GAA TTC TTA GAG ACG CCG CTT TTT C 3’

- ptVP3-EGFP – plasmid for production of truncated VP3 (tVP3; with a deletion of the first 101 amino acids at the N-terminus) fused with EGFP (at C-terminus of tVP3). Plasmid was prepared by the insertion of amplified sequence into the pEGFP–N1 plasmid (Clontech) using *Bgl*II and *Sal*I cloning sites. Sequence encoding tVP3 was amplified by PCR using the pMJG plasmid, which contains the entire genome of MPyV (A3 strain).

    - Primers (synthetized by KRD [Invitrogen] company)
      tVP3 forward (*Bgl*II):
      5' CAGAC AGA TCT ATG AGC TCA GGG TAC TCA TCA C 3'
      tVP3 reverse (*Sal*I):
      5' CAGAC GTC GAC TT GAG ACG CCG CTT TTT CTT TTG 3'

4.3 **Stable cell lines**

- 3T6-actin-EGFP and 3T6-tubulin-EGFP – 3T6 fibroblasts stably expressing EGFP tagged α-tubulin and β-actin, respectively. For stable expression of EGFP-tubulin and EGFP-actin, cells were transfected with pEGFP-human α-Tub vector and with pEGFP-human β-actin vector, respectively (both purchased from Clontech). Cell lines were established by sub-cloning and maintained upon G418 (Sigma-Aldrich) antibiotic selection in DMEM culture medium supplemented with 10% FBS and 4mM L-glutamine (Gibco). *De novo* cell lines were prepared by David Liebl.

4.4 **Virus**

The A3 strain of MPyV (large-plaque strain) was isolated from infected WME (whole mouse embryo) or 3T6 fibroblasts according to Türler and Beard [158] and purified to homogeneity by CsCl and sucrose gradient ultracentrifugation. The quality of preparation was confirmed by Coomassie blue-stained sodium dodecyl sulfate-acrylamide gel electrophoresis and electron microscopy (negative staining). For microscopy of living cells, virions were labeled with the red fluorescent marker Alexa Fluor 546 carboxylic acid succinimidyl ester (Molecular Probes, Life Technologies) as described in Liebl et al [18]. Briefly, purified virus was dialyzed in 0.1 M carbonate buffer (pH 8.3) and 1 mg of the virus with 0.1 mg of the fluorescent reagent was incubated for 1 h at room temperature (RT). Separation of the conjugate from un-reacted labelling reagent was made by extensive dialysis and subsequent purification of

the virus on 10 – 40 % sucrose gradient. The virus was aliquoted and stored at -20°C before use. The optimal degree of labelling (virus: fluorescent marker ratio) was assessed and improved not to affect virus natural infectiveness: Alexa Flour 546 pre-stained virus was used to infect cells and after fixation, co-immunolabeling with anti-VP1 antibody was performed, followed by green Alexa Fluor 488 secondary antibody. Co-localization of red and green signals proved that all viral particles were conjugated with red Alexa Fluor 546 dye while the VP1 immuno-epitope remained available for anti-VP1 antibody binding. Viral titers were determined by plaque assays and particle numbers by hemagluttination assays. For infections, MPyV was used at indicated multiplicities of infection (MOIs).

4.5 **Virus tracking**

For live microscopy, cells were grown in glass-bottom dishes (MatTek, Ashland, MA, USA) in phenol red-free DMEM culture medium supplemented with 10% FBS. Glass-bottom dishes were then mounted into a CO_2-supplemented chamber, maintained at 37°C. To avoid rapid temperature changes and microtubule depolymerization at 4°C, all procedures were performed at 37°C with pre-warmed media and solutions. The fluorescently labeled virus was diluted in serum-free culture medium and added to cells at MOI of 10^2 to 10^3 particles per cell. Unbound virus was gently washed away after 20 min and complete culture medium was added. Cytoplasmic transport was monitored by time-lapse live imaging using a Leica TCS SP2 AOBS confocal microscope equipped with an Argon laser (458, 476, 488, 496, 514 nm; 10 mW) and a HeNe laser (543, 594 nm; 1 mW). Cells were examined with a 1.2 N.A. water immersion objective (60x). To minimize the possibility of tracking of not yet internalized virions attached to the cell surface, a complete z-scanning of the cell starting from the apical until the basal cell membrane was performed. After this step, the objective focus was fixed on the middle plane of the cell, and only virions moving in the internal area of the cell corresponding to the cytosol were tracked. According to the specific signal to noise ratio and EGFP level of expression, we applied different sampling frequencies (ΔT = 3 – 6 s). Sequential scanning between channels was used to separate fluorescence emission from different fluorochromes and to completely eliminate bleed through channels. EGFP-tubulin-expressing cells were alternatively examined with an Olympus IX81 CellR microscope equipped with an MT20 illumination system and a 63× oil-immersion objective, using Tx Red and GFP filter cube set. Video sequences and images were

processed by Image J software (NIH, Bethesda, MD, USA) and Adobe Photoshop (Adobe Systems, San Jose CA, USA), respectively. Velocities and trajectories were calculated by 'particle tracking' plug-ins for Image J software (NIH) and data were processed with Excel software (Microsoft Corporation).

4.6 **Live imaging of cells expressing EGFP-fused minor protein variants**

Cell membranes of cells transiently expressing EGFP-fused variants of MPyV minor capsid proteins were labeled by incubation with 1,6-diphenylhexatriene (10 μM in culture medium) for 30 min at 37°C. Cells in glass-bottom dishes (MatTek) were placed into CO_2-supplemented chamber, maintained at 37°C, and live images were taken. Confocal microscopy of living cells was performed using a Leica TCS SP2 AOBS confocal microscope. To determine the distribution and intensities of markers, cell section images were analyzed using 'RGB Profiler' plug-in for Image J software (NIH).

4.7 **Immunofluorescence staining**

For fixed-cell staining, cells were fixed with 4% formaldehyde in PBS (20 min) and permeabilized with 0.5% Triton X-100 in PBS (5 min). Alternatively, to follow the virus localization in EGFP-Rab7-positive compartments, we fixed cells with 4% formaldehyde plus 0.05% glutaraldehyde in PBS (60 min) as combined fixative was shown to sufficiently preserve the fragile structures of late endosomes for immunofluorescence analysis [154,159]. After washing in PBS, cells were incubated with 0.25% bovine serum albumin and 0.25% porcine skin gelatin in PBS. Immunostaining with primary and secondary antibody was carried out for 1 h and 30 min, respectively, with extensive washing in PBS after each incubation. For testing the EGFP-fused versions of Rab11 GTPase, transferrin tagged with Alexa Fluor 647 (Molecular Probes) was used.

Live-cell labeling was performed as described in Zhou et al [160]. At indicated times (15 or 90 min) post-infection, cells were washed three times with complete Dulbecco's PBS (DPBS) at 37°C and incubated with mouse monoclonal anti-MPyV VP1 antibody for 20 min at 37°C. The cells were then washed three times with DPBS (37°C) and fixed with 4% formaldehyde in PBS (10 min). Fixed but not permeabilized cells were washed in PBS and incubated with Cy3-conjugated anti-mouse secondary antibody as described above.

4.8 **Antibodies**

The following primary antibodies were used: rat monoclonal anti-MPyV large T (LT) antigen (kindly provided by B. E. Griffin, Imperial College of Science, Technology and Medicine at St. Mary's, London, United Kingdom); mouse monoclonal anti-MPyV VP1, and mouse monoclonal IgG against the common region of MPyV VP2 and VP3 [47]; rabbit polyclonal anti-MPyV VP1 (prepared in our laboratory); rabbit polyclonal anti-caveolin-1 (Santa Cruz, CA, USA); rabbit polyclonal anti-BiP (Abcam, Cambridge, UK); rabbit polyclonal anti-BiP (Alexis, Enzo Life Sciences, Farmingdale, NY, USA); mouse monoclonal anti-α-tubulin (Exbio, Prague, Czech Republic); rabbit polyclonal anti-GFP (Abcam); rabbit polyclonal anti-GFP (Sigma-Aldrich); rabbit polyclonal anti-β-actin (Cell Signaling, Danvers, MA, USA); rabbit polyclonal anti-caspase 3, mouse monoclonal anti-cleaved PARP IgG (Asp214) and rabbit polyclonal anti-cleaved caspase 9 (all purchased from Cell Signaling, Danvers, MA, USA); rabbit polyclonal anti-β-actin (Cell Signaling); goat polyclonal anti-lamin B (Santa Cruz) and rat monoclonal anti-GRP94 (Abcam).

The following secondary antibodies were used: donkey anti-rat, donkey anti-mouse and goat anti-rabbit conjugated with Alexa Fluor 488; goat anti-rat, goat anti-rabbit and donkey anti-goat conjugated with Alexa Fluor 546; Cy3-conjugated goat anti-mouse antibody (all purchased from Molecular Probes); donkey anti-rabbit conjugated with CF633 fluorescent dye (Biotinum, CA, USA); and goat anti-rabbit and goat anti-mouse conjugated with peroxidase (Pierce).

4.9 **Infectivity assays**

To determine MPyV infectivity during the expression of fluorescently tagged versions of the proteins or fluorescent proteins alone, cells were transfected with protein encoding plasmid DNA and seeded on 13-mm glass coverslips in 24-well plates. Cells were allowed to grow for 24 or 48 h (two days for expression of kinesin-2 subunits, as they turn out slowly [151]), washed and incubated with MPyV diluted in serum-free medium at MOI of 0.3 PFU/cell, for 1 h at 37^{o}C. The infection start was measured from virus addition to cells. After virus adsorption, cells were washed to remove the unbound virus and incubated in DMEM with 10% FBS until 24 hours p.i. and fixed. Fixed cells were immunostained with antibody against MPyV early LT antigen. The efficiency of infection was determined from the percentage of LT-positive cells also expressing the fluorescently tagged protein of interest, normalized to that obtained in control cells.

To determine the reversibility of MPyV infection after nocodazole treatment, cells were pre-treated in medium with 5 μM nocodazole (Calbiochem, Merck) for 1 h at 37^{o}C and in the presence of drug infected with MPyV as above (the functional disruption of microtubules by nocodazole was confirmed in parallel samples by immunostaining with anti-α-tubulin antibody). At 7 hours p.i., the drug was washed out and the cells were incubated until 24 hours p.i., or in parallel samples, cells were incubated for additional 24 hours prior to fixation and immunostaining to prove the reversibility of the inhibition effect. Fixed cells were immunostained for the MPyV LT antigen and the cell nuclei were visualized by DAPI (4‘, 6‘-diamidino-2-phenylindole). The efficiency of infection was determined from the percentage of cells positive for LT antigen normalized to that obtained in cells infected in the absence of drug and fixed 24 hours p.i.

To determine effect of disruption of actin cytoskeleton on virus productive trafficking, cells (grown on coverslips in 24-well dishes) were pre-chilled on ice (15 min) and MPyV diluted in ice cold serum free medium was added to cells at MOI of 0.3 PFU/cell. After virus adsorption (45 min on ice, rocking), inoculum was removed and pre-warmed (37^{o}C) DMEM medium supplemented with 10% fetal bovine serum was added to cells (infection start was measured from this time). At 1 hour p.i., neutralizing anti-MPyV VP1 antibody was added to neutralize extracellular virus. After additional 30 min (1.5 hour p.i.), 0.1 μM latrunculin A (Calbiochem, Merck) was added to cells. Drug was kept for 5.5 hours (until 7 hours p.i.), then washed out and cells were further incubated until 24 hours p.i. As control, cells infected in absence of drug but treated with neutralizing antibody (added at the same time p.i.) were used. Fixed cells were immunostained for MPyV LT antigen and nuclei of cells were visualized by DAPI. The efficiency of infection was determined from the percentage of cells positive for LT antigen normalized to that obtained in control cells.

For assay quantification, coverslips were observed with an Olympus BX-60 fluorescence microscope equipped with a COHU CCD camera and images of optical fields were taken using Lucia software (Laboratory Imaging, Prague, Czech Republic). Cells were counted using the ‘cell counter‘ plug-in for Image J software (NIH).

4.10 **Internalization assay**

Cells grown on 13-mm glass coverslips in 24-well plates were incubated with MPyV labeled with Alexa Fluor 546 dye, diluted in serum-free culture medium and

added to cells at MOI of 10^3 particles per cell. After 20 min (at 37°C), cells were washed to remove unbound virus and complete DMEM medium (37°C) was added. Cells were incubated until indicated time points p.i. and fixed with 4% formaldehyde in PBS (20 min). The detection of non-internalized virions was accomplished by surface labeling of non-permabilized cells, washed in PBS and incubated with anti-MPyV VP1 antibody, followed by incubation with secondary antibody conjugated to green dye Alexa Fluor 488. The percentages of internalized virions were determined from the maximum-intensity projections of Z-stacks of confocal optical sections of the examined cells.

4.11 **Quantification of co-localization**

Cells transfected with plasmid DNA for expression of the EGFP-fused protein of interest, mock-transfected or non-transfected cells were seeded on 13-mm coverslips in 24-well plates and left to grow for 16 – 24 h. Cells at 10 – 20% of confluency were used. For co-localization analysis in the presence of cytoskeleton drugs, cells were pre-incubated in culture medium alone (control) or medium containing 5 μM nocodazole or 0.1 μM latrunculin A (Calbiochem, Merck) for 1 h (at 37°C) prior to infection (the functional disruption of microtubules or microfilaments by the drugs was confirmed in parallel samples by immunostaining with anti-α-tubulin antibody or with rhodamine-conjugated phalloidin). Cells were infected with MPyV diluted in serum-free culture medium (with or without the drug) at MOI ~ 5 x 10^2 virus particles/cell, allowing quantification of individual virions (counted approximately from 30 to 120 virions per cell). The infection start was measured from virus addition to cells. After 1 h at 37°C, the inoculum was removed, cells were washed three times to remove unbound virions, and complete DMEM medium + 10% FBS (with or without drug) was added. Cells were incubated until indicated time p.i., fixed, and immunostained for MPyV VP1 capsid protein and the second marker of interest if not fused to EGFP. The cells were examined with a Leica TCS SP2 AOBS confocal microscope using a ×63 1.4 N.A. oil immersion objective. For each examined cell, Z-sections were taken and co-localization of individual virions was determined in individual sections using the 'colocalization highlighter' plug-in for Image J software (NIH). The intensity ratio of co-localized pixels was set at 50%. The obtained image with co-localizing pixels was merged with the image with MPyV VP1 signal and co-localized and non-colocalized virions were counted.

4.12 **Evaluation of cytotoxicity**

The release of lactate dehydrogenase (LDH) occurring upon cell lysis at different time-points post-transfection of mouse fibroblasts was quantified using a CytoTox 96 cytotoxicity assay kit (Promega, Madison, WI, USA). Two 24-plate wells were processed per sample. From the first well, medium was collected while cells in the second well were treated with Triton X-100 (1 h / 37^{o}C) to be used as control of maximum LDH release. Samples collected from each well were mixed with the substrate (tetrazolium salt + diaphorase) and incubated for 30 min at RT in dark. Absorbance of samples was measured at 490 nm using a plate reader. The percentage of cytotoxicity was calculated using the formula: % cytotoxicity = Experimental LDH release (OD_{490}) / Maximum LDH release (OD_{490}). The maximum LDH release (100%) was obtained by treatment of cells with 9% Triton X-100.

To evaluate possible cytotoxic effect of temporary (5.5 h) treatment with latrunculin A, we measured the LDH concentration in the medium at infection start and at the time of infectivity evaluation (24 hours p.i.). Then, total cell numbers were determined to compare the rate of cell growth for treated and non-treated cells. Supernatants of lysates of cells were collected at indicated times p.i., mixed with the substrate (tetrazolium salt + diaphorase) and incubated (30 min / RT) in the dark. Absorbance of samples was measured at 490 nm using a plate reader as described above. OD values of maximum LDH release were used for comparison of total cell numbers for treated and non-treated samples.

4.13 **Flow cytometry analysis**

Externalization of phosphatidylserine was assessed using an Annexin V-Cy3 Apoptosis Detection Kit (Abcam), and dead cells were detected by exclusion using Hoechst 33258 (Molecular Probes). Briefly, floating and adherent cells (~ 2 x 10^5 cells) were collected, incubated (for 15 min / RT) in the dark and analysed using a flow cytometer (LSRII cytometer; BD Biosciences, San Jose, CA, USA). Data were processed using FlowJo software (Treestar, San Carlos, CA, USA).

4.14 **Quantification of caspase 3 activity**

At indicated time-points, cell lysates were prepared and tested for cleavage of amino acids sequence DEVD by caspase 3 using the CaspACE assay system, Colorimetric (Promega). Activity of caspase 3 was measured at the time-points

indicated. Incubation of cells with 1 or 2 μM actinomycin D (for 18 – 24 h) was used as a positive control of apoptosis induction.

4.15 **Electron microscopy**

Cells were washed in PBS, fixed with 3% glutaraldehyde in 0.1 M cacodylate buffer, postfixed with 1% osmium tetroxide, dehydrated through an increasing ethanol series and embedded in Agar 100 resin (Gröpl, Tulln, Austria). Sections (65 nm) were contrasted with a saturated uranyl acetate solution in water (10 min / RT), and Reynold's lead citrate (7 min / RT). Samples were observed with a JEOL JEM 1200EX electron microscope operating at 60 kV.

4.16 **Immunoelectron microscopy of cryosections**

Cells grown on Petri dishes were pre-treated (1 h / 37^{o}C) in culture medium alone or medium containing 5 μM nocodazole and in the absence or presence of the drug were infected with MPyV at MOI of 5 x 10^3 virus particles per cell for 1 h (rocking). Cells were washed and complete DMEM with 10% FBS (37^{o}C) with or without nocodazole was added. Cells were fixed with 4% formaldehyde plus 0.05% glutaraldehyde solution in 0.1M Sörensen buffer (Na_2HPO_4/NaH_2PO_4, pH 7.2). Fixed cells were gently scraped from the plate with a rubber policeman and embedded in 10% gelatin in PBS. Gelatin-embedded samples were cut into 1-mm^3 blocks and infiltrated with 2.3M sucrose overnight at 4^{o}C. Infiltrated blocks were mounted onto aluminum pins, frozen in liquid nitrogen and then sectioned at -120^{o}C with a Leica EM FC7 microtome. Ultrathin cryosections were transferred in a drop of 2.3M sucrose, 2% methylcellulose onto formwar-carbon-coated nickel grids and immunolabeled with rabbit polyclonal antibody against caveolin-1 (BD Transduction Laboratories, BD Biosciences), followed by incubation with goat anti-rabbit antibody conjugated to 10 nm gold particles (British Biocell Int.). After labeling, the sections were contrasted and embedded in a mixture of 3% aqueous uranyl acetate and 2% methylcellulose. The samples were observed with a JEM-1011 JEOL electron microscope equipped with a side mounted 2k x 2k CCD Camera (Veleta, Olympus SIS).

4.17 **Immunoelectron microscopy of plastic sections**

Cells were fixed with 3% formaldehyde and 0.1% glutaraldehyde in 0.2M Hepes buffer, pH 7.5. Pelleted cells were washed twice in Sörensen buffer, pH 7.4, dehydrated

in a series of increasing ethanol concentrations and embedded in LR-White resin (Polysciences, Inc., Warrington, PA, USA). Ultrathin sections on nickel grids were immunolabelled. Nonspecific binding was blocked with 10% normal goat serum in PBS containing 1% BSA, followed by incubation of cells with rabbit anti-GFP diluted in PBS containing 0.5% BSA and 0.1% fish gelatine (pH 7.4). After washing in PBS containing 0.1% BSA, sections were incubated with the goat anti-rabbit antibody conjugated with 5- or 10-nm-diameter gold particles (GE Healthcare, Waukesha, WI, USA) that were diluted in PBS containing 0.5% BSA and 0.1% fish gelatine (pH 8.2). Sections were washed in PBS containing 0.1% BSA, then, contrasted by staining with uranyl acetate. The samples were examined using a JEOL JEM 1200 EX electron microscope operating at 60 kV.

5. RESULTS

5.1 **Role of cell cytosketon in the trafficking of MPyV to the ER**

This chapter refers to the results published in the paper entitled, "**Involvement of microtubular network and its motors in productive endocytic trafficking of mouse polyomavirus**" by Žíla V., Difato F., Klímová L., Huerfano S., Forstová J., *PLoS ONE* 2014 9(5): e96922 (reference [161]). It also describes unpublished results concerning involvement of actin cytoskeleton during trafficking of MPyV. Most of the work was carry out by me, contribution of co-authors is described where presented. The published paper is in the attachment #1.

5.1.1 *Association of transported MPyV virions with cell cytoskeleton*

To visualize involvement of cell cytoskeleton during MPyV transport, we followed trafficking of fluorescently labeled virions at early times (up to 2 h post-infection [p.i.]), by time-lapse fluorescence microscopy in living 3T6 cells expressing either α-tubulin or β-actin fused with EGFP. Tracking experiments in cells producing EGFP-tubulin, revealed that virions were transported along microtubular tracks into the cell interior, but also back to the cell periphery in bi-directional manner (Figure 5.1A). Although the virus cargo was transported in both directions (often along an identical microtubule), the virus fluorescent signal was found accumulated around the nucleus at later times post-infection (from 3 hours p.i.) (Figure 5.1B), indicating that MPyV transport to the vicinity of the nucleus is prevalent during longer time spans of virus trafficking.

Cells producing EGFP-fused β-actin had standard morphology and lamellipodia, filopodia and membrane protrusions of intercellular contacts retained their natural dynamics (not shown). At 20 min p.i. (during virus adsorption), active movement of endosomes mediated by assemblies of dynamic EGFP-actin recruited on their membranes was observed within cytoplasm of cells (Figure 5.2A). From 30 min p.i., virions were observed to be transported in such endosomes (a vesicular structure was apparent in transmission light), propelled by one or more of assemblies of dynamic EGFP-actin, whose length was ≤ 0.5 μm (Figure 5.2B). Character of actin assemblies fitted to that described in NIH 3T3 [30] or in mouse podocytes [35], suggesting this transport as a part of regular endocytic machinery of cells. *(These experiments were realized in cooperation with Francesco Difato and Lucie Klimova)*

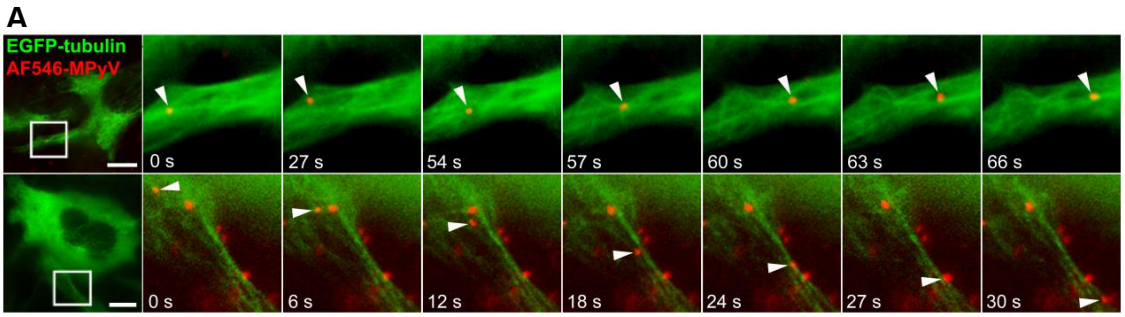

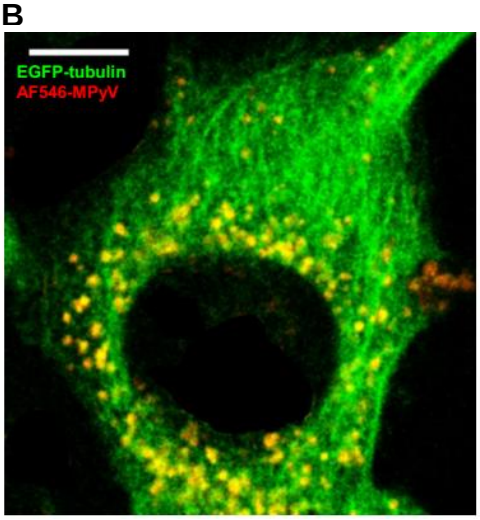

Figure 5.1 Tracking of MPyV in cells expressing EGFP-fused tubulin. 3T6 cells expressing EGFP-tubulin (green) were infected with Alexa Fluor 546-labeled MPyV (red) at 37°C and scanned with ΔT = 3 s. (A) Virions were transported to both directions: to the nuclear periphery (upper panel) and to the cell periphery (lower panel). Selected frames from two different cells at 1 hour p.i. are shown in detail. Arrowheads point to selected MPyV virions. (B) Accumulation of MPyV virions in perinuclear space at 3 h post-infection. Bars, 10 µm.

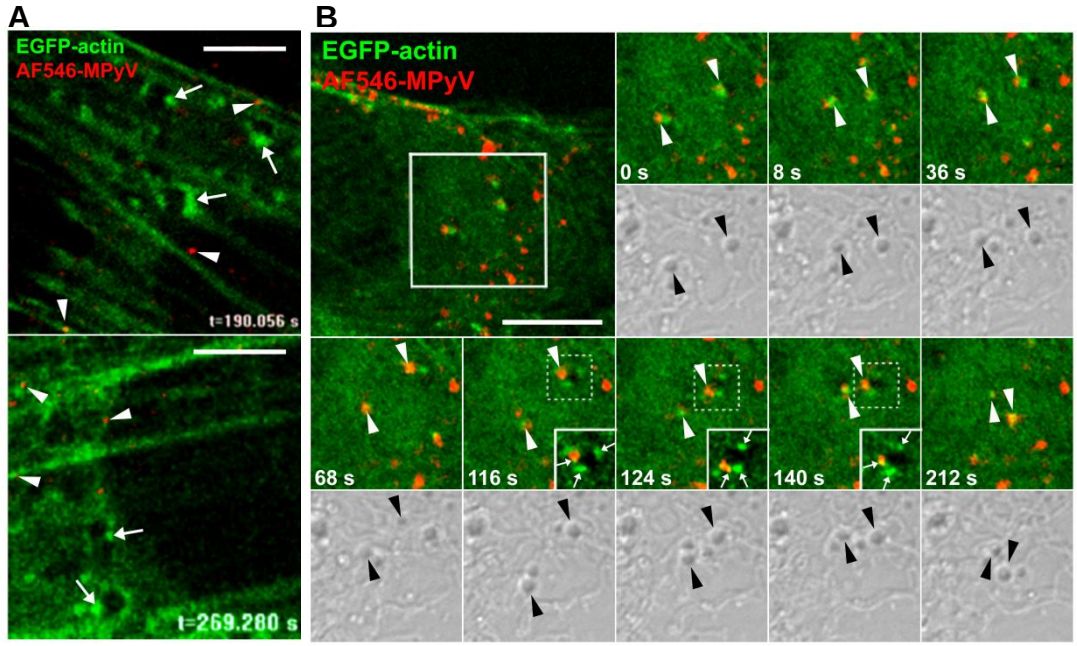

Figure 5.2 Movement of MPyV-carrying endosomes associated with dynamic actin assemblies. 3T6 cells stably expressing EGFP-fused β-actin (green) were infected with Alexa Fluor 546-labeled MPyV (red) at 37°C and scanned with ΔT = 4 s. (A) Active movement of endosomes via dynamic assemblies of EGFP-actin. In surface confocal sections of two different cells at 20 min p.i. are shown in detail. (B) Selected frames of in depth confocal section of cell at 45 min p.i. with corresponding transmission light images illustrate short-distance movement of virus-carrying endosomes associated with dynamic assemblies of EGFP-actin. White arrowheads point to MPyV virions. Arrows point to endosome-associated actin assemblies. Black arrowheads indicate MPyV-containing endosomes. Bars, 5 µm.

5.1.2 *Dynamics of MPyV intracellular transport*

To follow the dynamics of MPyV intracellular trafficking, we performed single particle tracking analysis and mapped transport trajectories of fluorescently labeled virions in living 3T6 cells by time-lapse confocal microscopy. We followed trafficking of virions from 0.5 to 3 hours p.i., as the internalization assay showed that a considerable amount of virions (~50%) is internalized after 30 min of infection and that the major part of the virus was internalized at 60 min p.i. (Figure 5.3). Virus trajectories were not clearly oriented from the cell surface towards the nucleus. Instead, they displayed the characteristics of Brownian motion with fast random switching in velocities and direction of movement (Figure 5.4A). The dynamics of virion transport was mostly saltatory – the fast forward movements were interrupted by short back-step movements or pausing at intervals (average pause duration of 40±6.5 s). Measurement of the frequency of velocity rates revealed that slow movements were most prevalent (< 0.2 μm/s) (Figure 5.4B). They can be assigned to pausing of virus-loaded vesicles on microtubule tracks before another motor was recruited (or activated), or to dynamic actin-driven motility of virus-carrying endosomes (Figure 5.2) as the velocity of vesicles/endosomes propelled by actin polymerization reaches rates around 0.2 μm/s [162-164]. During such a "stationary phase", we detected movement only in a limited range (0.5 – 1 μm). In contrast, fast, long-distance movements (up to 1.5 μm/s) were rare, with a distinct peak at 0.6 μm/s (Figure 5.4B). Measurements of fast movements (≥ 0.6 μm/s) revealed that the average length of a single continuous movement was 2.5 μm (Figure 5.4C). It corresponds to recruitment of a single microtubular motor molecule on the transported vesicle and fits well with the processivity of individual kinesin or dynein molecule-mediated transport, producing movements of approximately 1.5 μm before the motor dissociates from the microtubule [165]. Events of faster (> 0.6 μm/s) long-range transport occurred exclusively for short time intervals and the time span of the movements was characterized by peaks at 3.3 and 7.2 s (Figure 5.4D). These data indicated that dynamics of MPyV trafficking reflected an inherent microtubular motor processivity. *(This part was realized in cooperation with Francesco Difato, who, with the help of David Liebl and Jiří Janáček [both named in Acknowledgments section of the published paper], performed single particle tracking analysis)*

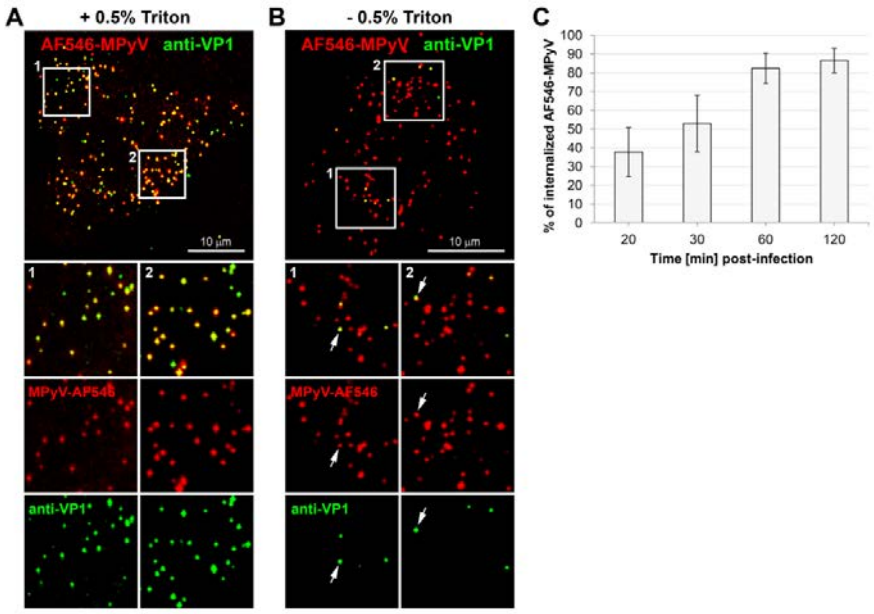

Figure 5.3 Internalization assay. 3T6 cells were incubated with MPyV, labeled with red fluorescent dye Alexa Fluor 546 (AF546-MPyV) diluted in serum-free medium (MOI of 10^3 virus particles/cell) for 20 min at 37°C. After virus adsorption, cells were washed and incubated in complete DMEM medium (37°C) until indicated times p.i. The extracellular and intracellular AF546-MPyV virions (red) were distinguished as described in Materials and Methods. (A and B) Visualization of AF546-MPyV virions (red) in permeabilized (A) and non-permeabilized (B) cells by immunostaining with anti-VP1 antibody (green). Confocal sections of cells fixed 60 min p.i. with enlarged details are shown. In panel B, arrows point to selected extracellular virions. (C) Quantification of the amount of internalized AF546-MPyV virions at 20, 30, 60 and 120 min p.i. The percentages of internalized virus were calculated from images such as shown in panel B. More than 1100 virions were evaluated for each time point. Data in the graph represent mean values ± s.d. for 10 different cells.

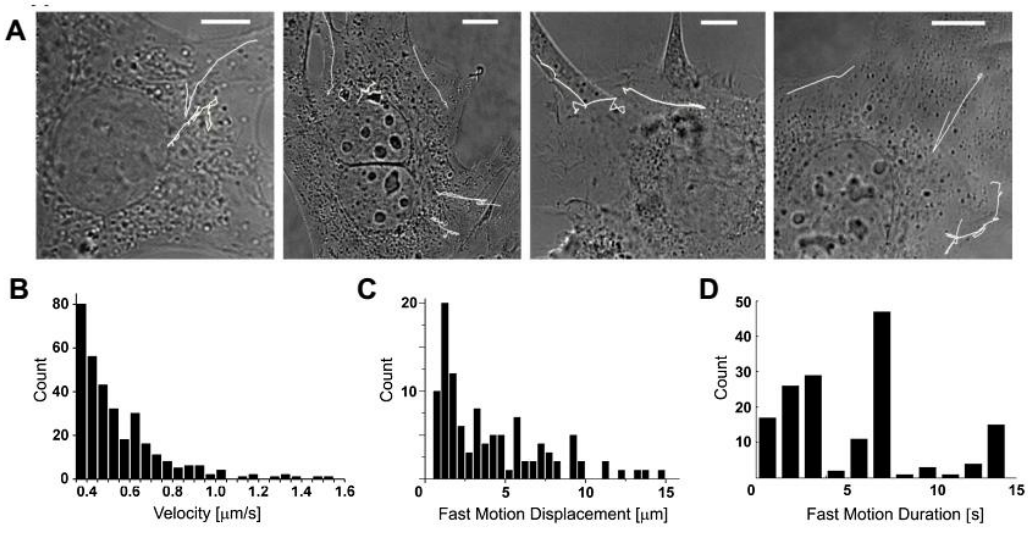

Figure 5.4 Single particle tracking analysis 3T6 cells were infected with Alexa Fluor 546-labeled MPyV at 37°C and scanned with ΔT = 6 s. (A) Complex trajectories marked in white tracking curves in four selected cells shown in transmission light. Bars, 5 µm. (B) Frequency of virion transport velocity rates, counted from more than 200 different tracking experiments in 3T6 cells, with a distinct peak at 0.6 µm/s (x-coordinate was cropped to cut off the high frequency of short-range movements at rates < 0.3 µm/s). (C) Histogram of fast movement distances counted from 109 single fast movements and sampled into 0.5 µm step intervals, with a maximum at 1.5 µm and the average distance of 2.5 µm. (D) Time span frequency of fast (≥ 0.6 µm/s) movements with maximum counts at 3.3 and 7.2 s.

5.1.3 *Role of microtubular motors in MPyV productive trafficking*

We next investigated the role of dynein, kinesin-1 and kinesin-2 motors in MPyV productive trafficking. The importance of the dynein motor for MPyV infection was tested by infectivity assays in 3T6 cells transiently overexpressing EGFP-fused dynamitin, which causes disassembly of the dynein-dynactin complex and inhibits dynein motor function [166-168]. Compared to controls (mock-transfected cells and cells expressing EGFP alone), overexpression of EGFP-dynamitin dramatically reduced the number of infected cells (more than 70% decrease) (Figure 5.5A). Confocal fluorescence microscopy performed later (5 h) post-infection in dynamitin-EGFP expressing cells, revealed that substantial amounts of virions are still localized at the cell periphery (Figure 3B, right panel), while in mock-transfected cells, the virus was accumulated predominantly in perinuclear area (Figure 5.5B, left panel). The importance of kinesin-1 and kinesin-2 motor for MPyV infection was investigated by infectivity assays in cells expressing their dominant-negative forms. The function of kinesin-1 was inhibited by overexpression of the C-terminal domain of kinesin-1 heavy chain fused with red fluorescent protein (RFP-KHCct), as the expression of C-terminal segment inhibits kinesin-1-driven microtubule activity by binding to the kinesin motor domain [149,150,169]. The kinesin-2 motor was inhibited by overexpression of EGFP-fused dominant-negative mutant of subunits of kinesin-2, motorless KIF3A subunit (EGFP-KIF3A-HL), or C-terminus of KAP3 subunit (EGFP-KAP3-CT) [151,152]. For controls, we infected mock-transfected cells, cells expressing RFP-fused form of kinesin-1 light chain (RFP-DTC) as negative control for kinesin-1 [149,150], and cells expressing EGFP alone as a control for EGFP-fused kinesin-2. Production of dominant-negative from of kinesin-1 or kinesin-2 did not reduce the virus infectivity. Moreover, a slight increase in the number of infected cells was detected when compared with controls (Figure 5.5C). Also, confocal microscopy of cells producing dominant-negative form of kinesin-1 or kinesin-2 did not reveal any significant difference in virus localization when compared to mock-transfected cells (Figure 5.5D). These data indicated that dynein motor is critical for MPyV infectivity and its perinuclar localization, while function of kinesin-1 or kinesin-2 was dispensable. *(This part was realized in cooperation with Lucie Klimova)*

Further, we investigated the involvement of dynein motor in delivery of MPyV virions to the ER. For this, we infected dynamitin-EGFP-expressing cells and fixed them 5 hours p.i. In the cells, we followed and quantified co-localization of individual

MPyV virions with the BiP (GRP78) protein as a marker of ER and compared it with that in control, mock-transfected cells. Co-localization of the VP1 signal of MPyV virions with the fluorescent signal of BiP protein was quantified from confocal images such as those shown in Figure 5.6A. The quantification revealed that inhibition of the dynein motor function by overexpression of dynamitin significantly reduced virus co-localization with BiP (by 40 – 50%) when compared to that in control cells (Figure 5.6B). We thus concluded that dynein motor function is essential for delivery of MPyV to the ER.

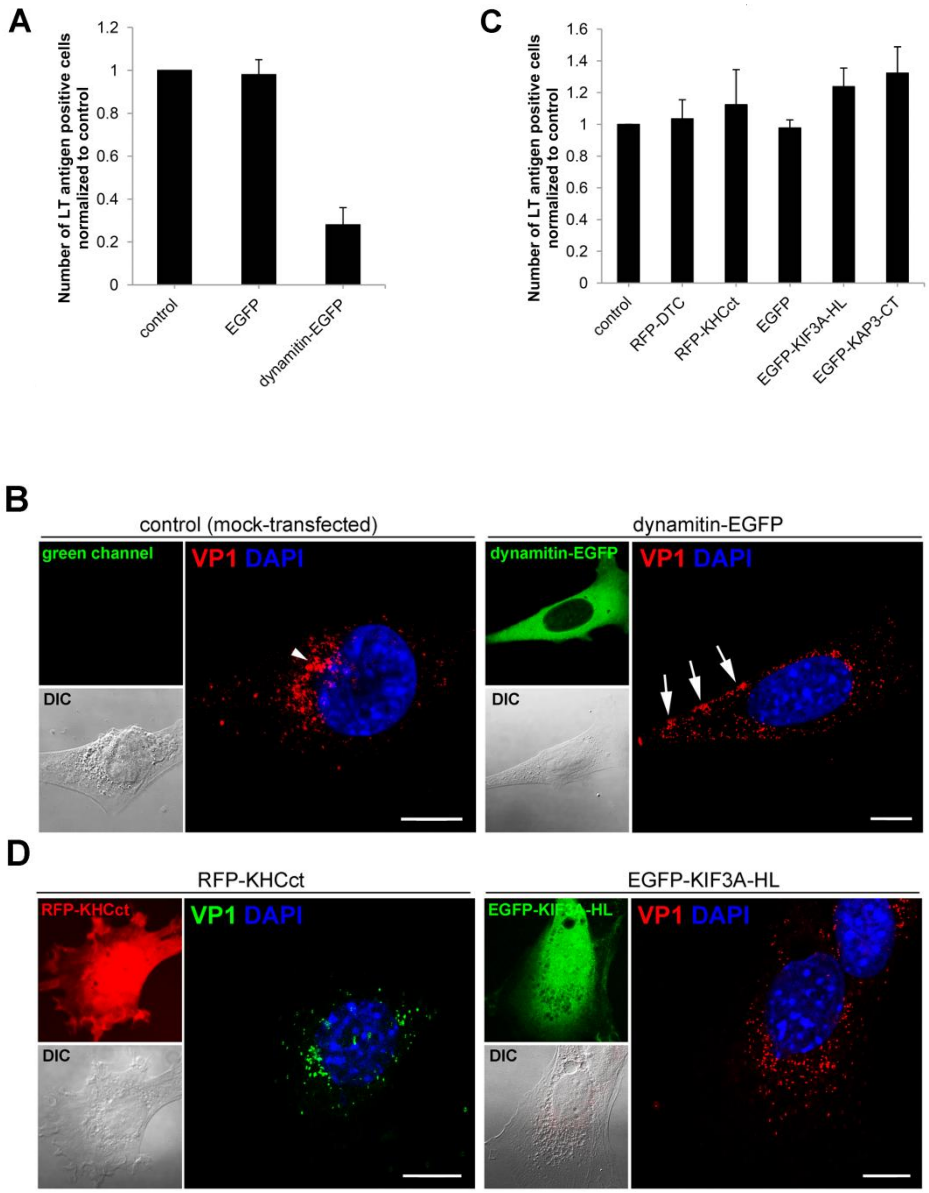

Figure 5.5 Role of microtubular motors in MPyV productive trafficking. (A and C) 3T6 cells were transfected with: (A) plasmid DNA for transient expression of EGFP (pEGFP-N1) or dynamitin-EGFP (inhibiting the dynein motor function) or (C) plasmid DNA for transient expression of RFP-DTC protein (pRFP-DTC); RFP-fused C-terminal fragment of kinesin-1 (pRFP-KHCct; inhibiting kinesin-1 motor function); EGFP (pEGFP-N1) or EGFP-fused dominant-negative subunits of kinesin-2 (pEGFP-KIF3A-HL or pEGFP-KAP3-CT). After 24 or 48 hours (two days for expression of kinesin-2 subunits, as they turn out slowly [151]), cells expressing constructs were infected with MPyV, incubated until 24 hours p.i., fixed and immunostained for MPyV LT antigen. The efficiency of infection was determined by levels (%) of LT antigen-positive cells normalized to that obtained in control, mock-transfected cells. During the experiment, more than 500 cells were counted for each sample. Data in the graphs represent mean values ± s.d. from three independent experiments. (B and D) Control, mock-transfected cells, or cells expressing dynamitin-EGFP, RFP-KHCct or EGFP-KIF3A-HL, infected with MPyV (MOI of 10^3 virus particles per cell), fixed 5 hours p.i. and immunostained for MPyV VP1 capsid protein. DNA in nuclei was stained with DAPI (blue). Confocal sections of representative cells with corresponding signal in green or red channel and differential interference contrast (DIC) images are presented (the virus localization during EGFP-KIF3A-CT expression is not presented as it was similar to that in cells expressing the -HL form of kinesin-2). Arrowhead point to the virus at nuclear periphery. Arrows point to the virions at cell periphery. Bars, 10 μm.

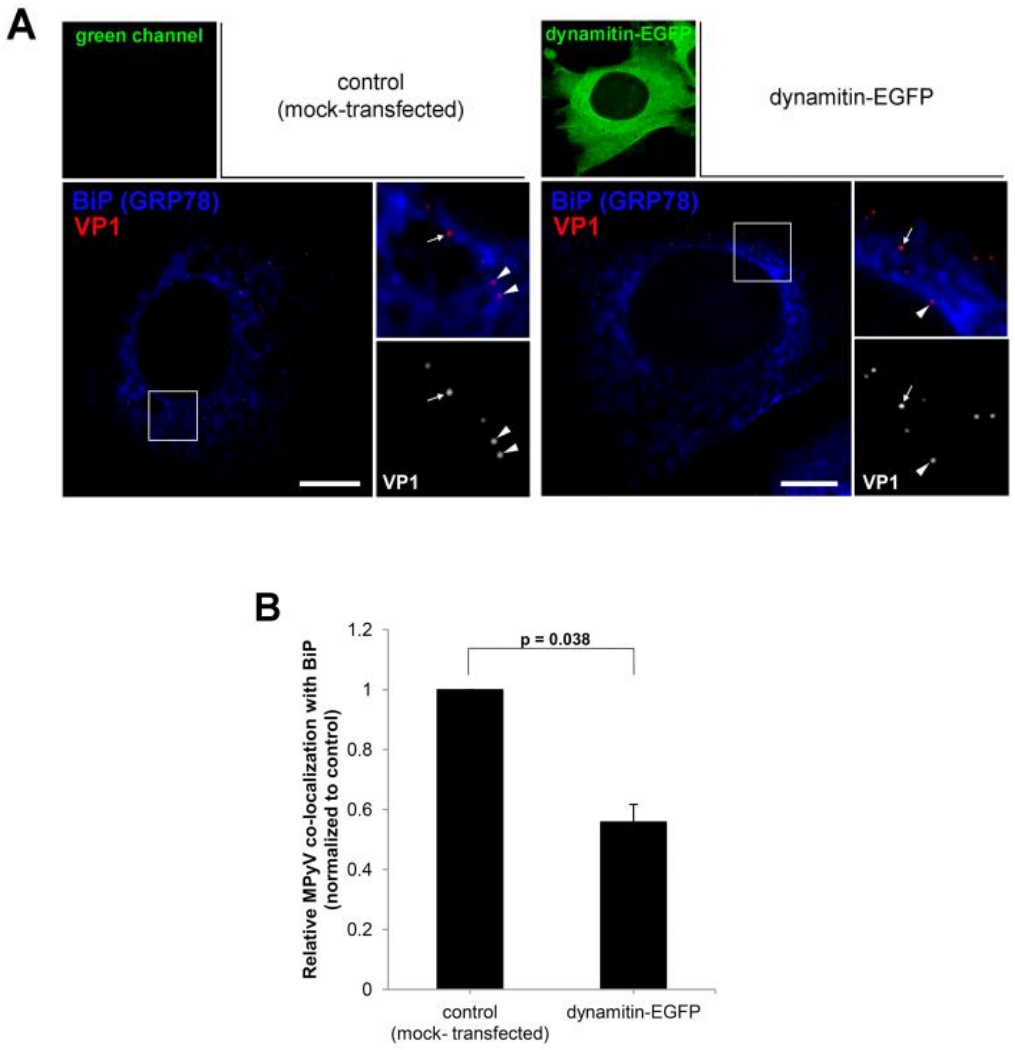

Figure 5.6 Dynein motor is required for trafficking of MPyV to the ER. 3T6 cells were transfected with plasmid DNA for expression of dynamitin-EGFP, infected with MPyV (MOI of 5 x 10^2 virus particles per cell) and fixed 5 hours p.i. Cells were immunostained for MPyV VP1 capsid protein (red) and BiP (GRP78) marker of ER (blue). (A) Confocal sections of representative control (mock-transfected) cells and dynamitin-EGFP expressing cells at 5 hours p.i. with enlarged details. Arrowheads point to selected MPyV virions co-localizing with BiP protein. Arrows point to selected MPyV that did not co-localize with BiP protein. Bars, 10 μm. (B) Quantification of co-localization of MPyV virions with BiP at 5 hours p.i. The percentage of co-localizing virions was calculated from images such as shown in panel A and levels (%) of co-localizing virions in dynamitin-expressing cells were normalized to that in control. During the experiment, more than 600 virions in at least 10 different cells were evaluated for each sample. Data in the graph represent mean values ± s.d. from three independent experiments; Student's t-test was used.

5.1.4 *Involvement of cytoskeleton in MPyV transport to endosomes*

The effect of overexpression of dynamitin-EGFP on MPyV intracellular localization (Figure 5.5B) suggested that dynein-mediated transport is required soon after virus internalization for virus trafficking from the plasma membrane. However, investigation of SV40 trafficking showed that transport of the virus to early and premature late endosomes is independent of intact microtubules and that microtubules are required later for maturation of SV40-containing late endosomes and subsequent virus delivery to the ER [15]. The same group described that SV40 utilizes actin dynamics for its transport from plasma membrane [106]. To dissect the involvement of microtubules or actin cytoskeleton in MPyV transport to individual endocytic compartments, we infected 3T6 cells (non-transfected or expressing EGFP-fused marker of interest) in the absence or presence of compounds selectively affecting the structure and dynamics of microtubules (nocodazole) or actin cytoskeleton (latrunculin A) and fixed them 5 hours p.i. In the cells, we quantified tendence in co-localization of individual MPyV virions with markers previously shown to be involved in trafficking of MPyV towards the nucleus: caveolin-1 for caveolar or other compartments functionally connected to lipid rafts, EGFP-Rab5 GTPase for early endosomes, EGFP-Rab7 GTPase for late endosomes, EGFP-Rab11 GTPase for recycling endosomes, and BiP protein as ER marker.

At 5 hours p.i. in control untreated control cells, MPyV virions co-localized with all of the tested markers (Figure 5.7A). Quantification of co-localization in control cells (Figure 5.7B, light grey bars) revealed that the highest percentage of virions co-localized with caveolin-1 (40%), but a substantial amount also co-localized with EGFP-Rab7 (27%) and small virus populations co-localized with EGFP-Rab11 (15%) and BiP (13%). Only residual (~6%) co-localization of MPyV with early endosomal marker EGFP-Rab5 was detected at 5 hours p.i. In the presence of microtubule-disrupting drug, nocodazole (Figure 5.7B, dark grey bars), virus co-localization with caveolin-1 increased by 20%, and a minor fraction of virions also co-localized with EGFP-Rab7 GTPase (13%). Only sporadic virions (~2%) co-localized with other tested markers (EGFP-Rab5, EGFP-Rab11, BiP). In contrast, in cells with actin cytoskeleton disrupted by latrunculin A (Figure 5.7B, black bars), MPyV co-localization with caveolin-1 dropped by ~50%, while its co-localization with EGFP-Rab5, EGFP-Rab7, EGFP-Rab11 and BiP increased by 30 – 50% when compared to that in untreated cells. As the presence of the virions in early endosomes was sporadic even in control cells at 5 hours

p.i., we performed co-localization analysis at 1.5 hour p.i., when a higher population of virions could be expected to localize in early endosomes. In untreated cells, a minor virus population co-localized with EGFP-Rab5 (12%) at 1.5 hour p.i. Virus co-localization with EGFP-Rab5 was markedly reduced in the presence of nocodazole, and substantially increased (by 60%) in the presence of latrunculin A (Figure 5.7C).

These data indicated that disruption of microtubules perturbed the virus presence in endosomes positive for Rab5, Rab7 and Rab11 GTPases and in the ER. Contrary to that, disruption of actin microfilaments apparently enhanced the efficiency of microtubule-mediated transport, and thus, higher percentage of virions (in comparison with control untreated cells) co-localized with all markers except caveolin-1. We concluded that dynein-mediated movement along microtubules is important already for virus transport from the plasma membrane to classical endosomes, while the actin meshwork rather represents a barrier that slows down the rate of virus transport and is connected with accumulation of the virions in caveolin-1-positive compartments.

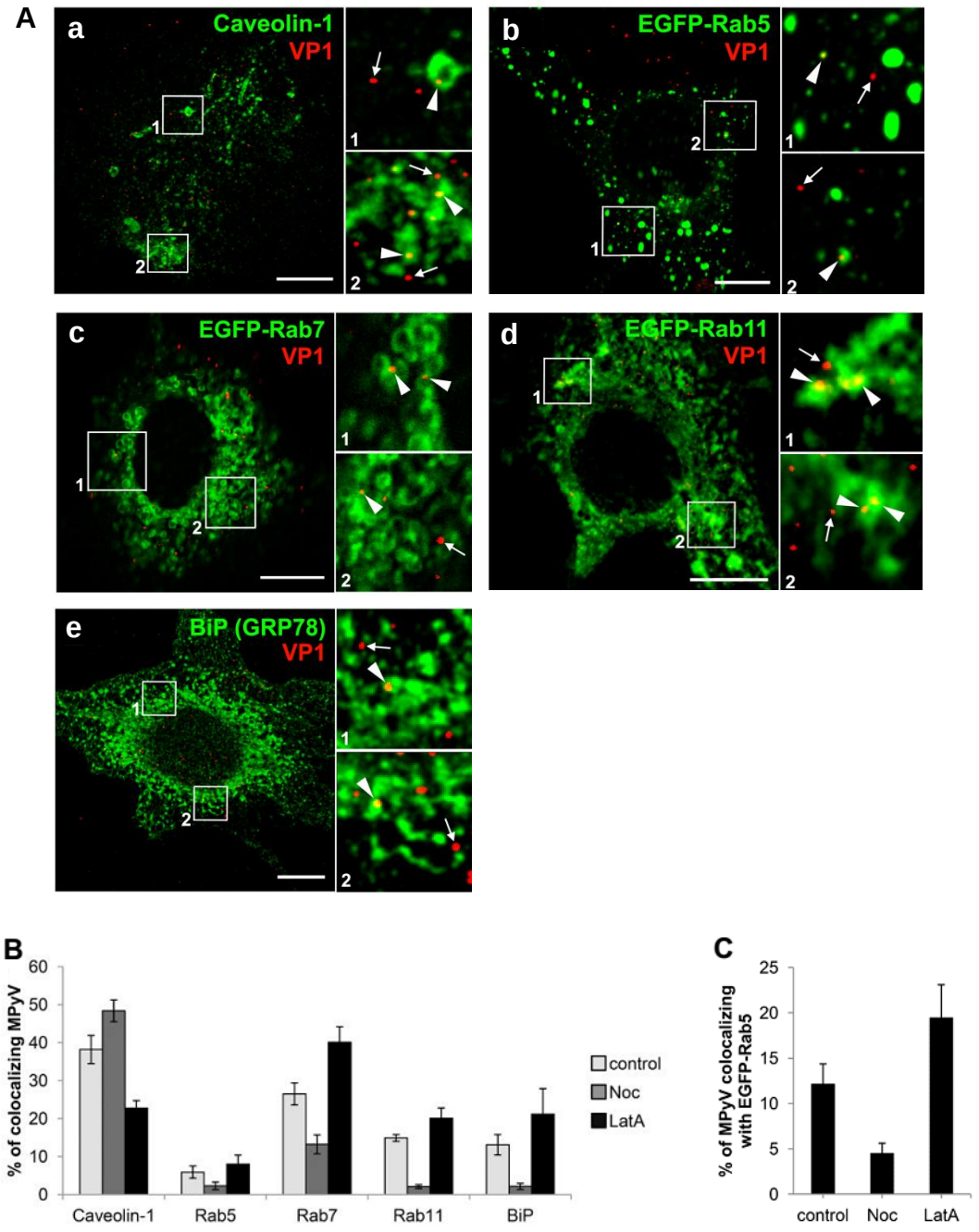

Figure 5.7 Effect of cytoskeleton-disrupting drugs on subcellular localization of MPyV. (A) Non-transfected 3T6 cells (a and e) or cells transiently expressing EGFP-tagged marker of interest (b–d) were infected with MPyV and fixed 5 hours p.i. Cells were immunostained for MPyV VP1 capsid protein (red) and for a second marker of interest (caveolin-1, BiP) if not fused with EGFP (green). Confocal sections of cells with enlarged details are shown. Arrowheads point to selected MPyV virions co-localized with the marker of interest. Arrows point to selected MPyV that did not co-localize with the marker of interest. Bars, 10 μm. (B) Quantification of co-localization of MPyV virions with indicated markers at 5 hours p.i. in non-treated cells (control) or cells pre-treated (1 h) and infected in the presence of nocodazole (Noc) or latrunculin A (LatA). (C) Quantification of co-localization of MPyV virions with EGFP-Rab5 at 1.5 hours p.i., in control, Noc- or LatA-treated cells. The percentage of co-localizing virions was calculated from images such as those showed in Aa–Ae. During the experiment, more than 600 virions in at least 10 different cells were evaluated for each sample. Data in the graph represent mean values ± s.d. from three independent experiments.

5.1.5 *Localization of MPyV in the absence of microtubules*

We found that only a minor subpopulation of the virus appeared in Rab7-positive endosomes of nocodazole-treated cells, while a substantial amount of virions was located within structures positive for caveolin-1. The presence of microtubule disrupting drug, nocodazole, increased virus co-localization with caveolin-1 by 20% when compared to control untreated cells (Figure 5B). To identify caveolin-1-positive compartments where MPyV virions appear in absence of intact microtubules, we perfomed immunogold labeling of caveolin-1 on thawed cryosections of the cells fixed 5 h post-infection in presence of nocodazole. Immunoelectron microscopy (IEM) revealed that most virions were located at the cell periphery in tightly-fitting endocytic vesicles (~ 60 nm in diameter), often also positive for caveolin-1. These virus-carrying vesicles were found connected to flask-shape caveolae-like "empty" structures (70 – 100 nm in diameter), but also to other virus-carrying vesicles, creating caveolin-1-positive membrane clusters of irregular shape (Figure 5.8A) whose morphology resembled multicaveolar complexes [170,171]. Only individual virions were found in late endosomal multivesicular bodies (MVBs), which were occasionally also positive for caveolin-1, and in caveolin-1-free endosomes (Figure 5.8B). These endosomal structures probably represented early or pre-mature late endosomes, since maturation of endosomes and their fusion with lysosomes is dependent on intact microtubular network and dynein motor function [129-132]. Contrary to that, in non-treated cells, 5 hours p.i., the accumulation of MPyV in caveolin-1-positive clusters was not apparent. Instead, virions were found accumulated within caveolin-1-negative, but also within caveolin-1-positive MVBs or within caveolin-1-negative multilamellar bodies (Figure 5.9), suggesting that a high percentage of MPyV virions co-localizing with caveolin-1 in untreated cells (Figure 5.7B) was largely made up of virus present within late endosomal structures. These data demonstrated that in a situation when microtubular transport is not available, most virions persist at the cell periphery within endocytic vesicles or within multicaveolar-like clusters.

Since previous studies provided evidence that internalization of MPyV is caveolae-independent [17,18,21,101,113], we further tested whether presence of nocodazole did not affected the way of virus internalization. We first performed live-cell labeling at 15 or 90 min p.i of untreated or nocodazole-pretreated cells using anti-MPyV VP1 primary antibody, to visualize non-internalized virions (see Materials and Methods, chapter 4.7). For both, untreated or nocodazole-pretreated cells,

immunostaining at 15 min p.i. revealed abundant presence of MPyV virions attached to the cell surface, whereas at 90 min p.i., only residual presence of virus attached at the surface of cells was detected (Figure 5.10A). Further, we followed the way of MPyV internalization in the presence of nocodazole by immunoelectron microscopy. We found that virions were internalized independently of caveolar invaginations into tightly-fitting endocytic vesicles (Figure 5.10B, panels a and b) and that the presence of caveolin-1 on virus-carrying vesicles is caused by virus uptake via caveolin-1-rich domains at the plasma membrane (Figure 5.10B, panel c). In addition, we tested the impact of temporary absence of a functional microtubular network on virus infectivity. We pre-treated (1 h prior to infection) and infected cells with MPyV in the presence of nocodazole. We found that more than 70% inhibition of MPyV infection in the cells kept with the drug until 7 hours p.i. could be efficiently restored by the drug washout and by prolonged time of incubation (for additional 24 hours) before cell fixation and screening (Figure 5.10C). Together, these data showed that virus uptake is not prevented in presence of nocodazole, but most of MPyV virions persist at the cell periphery within endocytic vesicles or within multicaveolar-like clusters, where they are inaccessible for surface labeling with antibody. Our results indicate that the presence of virions in these structures does not affect their ability to infect cells and that with accessibility to microtubular network the virions continue in their trafficking to the endosomes and further to ER.

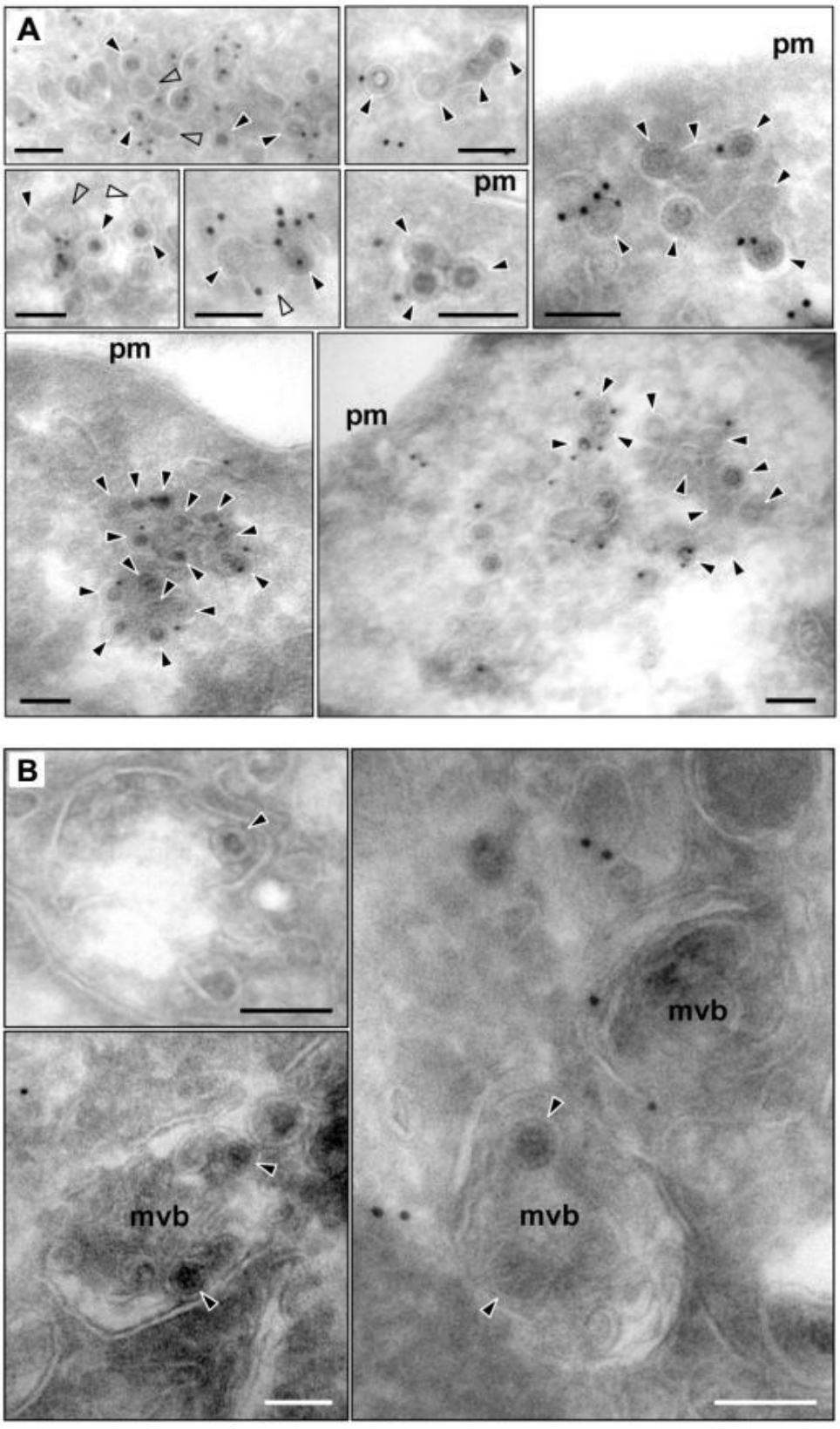

Figure 5.8 Localization of MPyV in nocodazole-treated cells. 3T6 cells were pre-treated (1 h) with nocodazole, infected with MPyV in the presence of the drug and fixed 5 hours p.i. (A and B) Immunolabeling of thawed cryosections of cells with anti-caveolin-1 antibody, followed by immunolabeling with secondary antibody conjugated with 10 nm gold particles (seen as darkly stained dots). Arrowheads point to selected virions. Empty arrowheads point to flask-shape "empty" caveolar structures. Bars, 100 nm. Pm, plasma membrane; MVBs, multivesicular bodies.

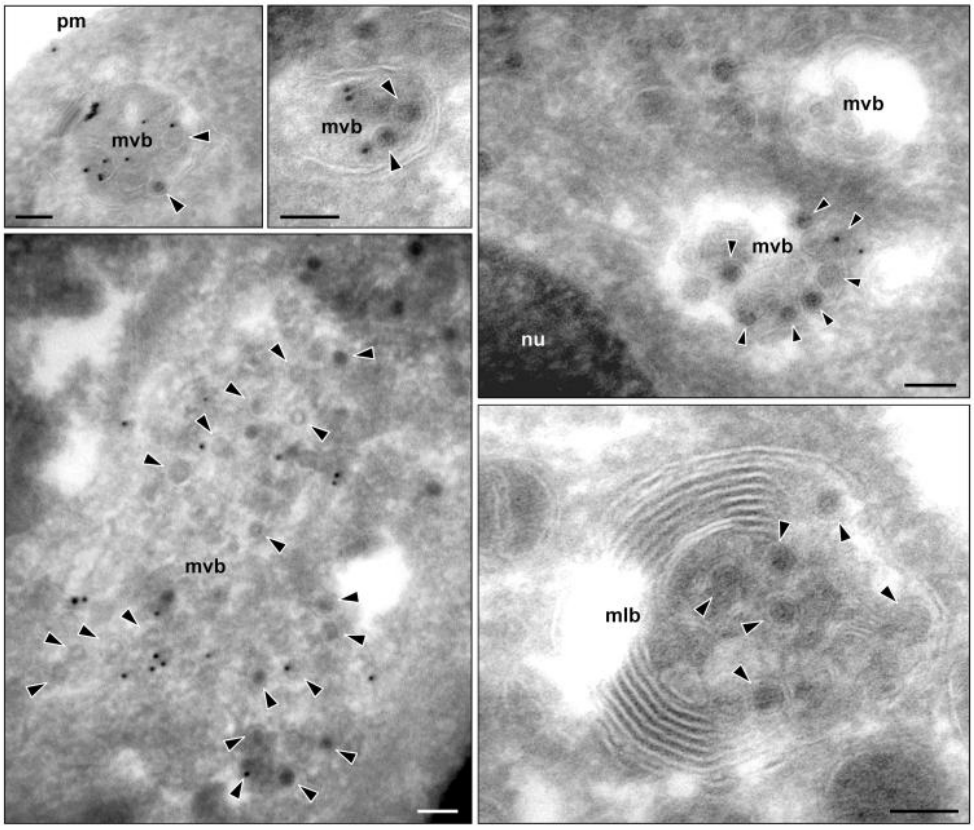

Figure 5.9 Immunoelectron microscopy of 3T6 cells 5 h post-infection with MPyV. Thawed cryosections were immunolabeled with anti-caveolin-1 antibody followed by incubation with secondary antibody conjugated with 10 nm gold particles. Arrowheads point to selected virions. Bars, 100 nm. Pm, plasma membrane; MVBs, multivesicular bodies; MLB, multilamellar body; Nu, nucleus.

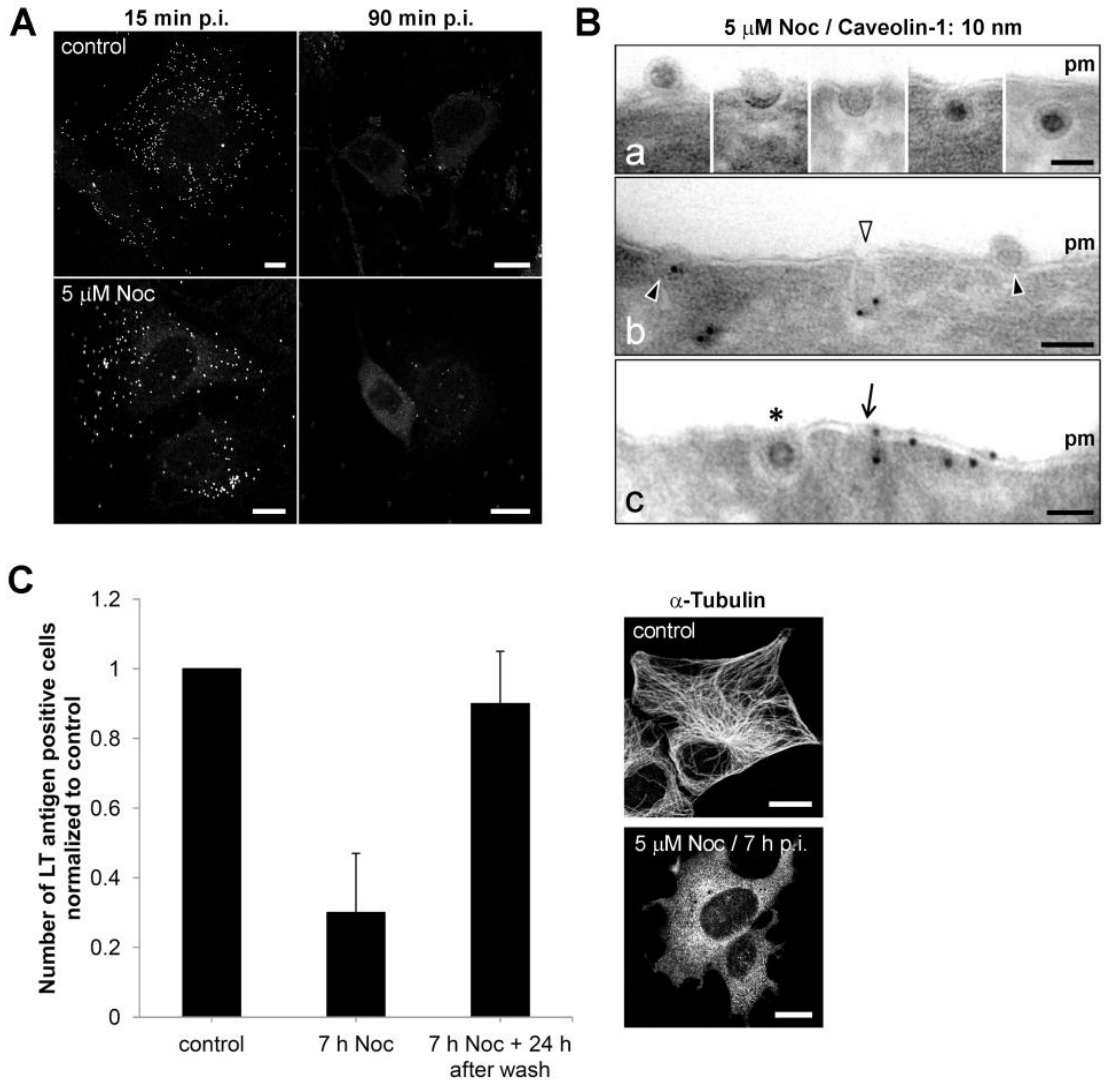

Figure 5.10 Internalization and infectivity of MPyV in nocodazole-treated cells. (A) 3T6 cells were pre-treated (1 h / 37°C) in culture medium alone or in medium supplemented with nocodazole and then incubated with MPyV for 15 or 90 min (at 37°C), also in the presence or absence of the drug. After that, immunofluorescence analysis was performed using an anti-MPyV VP1 antibody added to live cells, followed by fixation and immunostaining with secondary antibody. Confocal sections of representative cells are shown. Bars, 10 μm. (B) Immunolabeling of thawed cryosections of cells pre-treated and infected with MPyV in the presence of nocodazole. Cells were immunolabeled with anti-caveolin-1 antibody, followed by immunolabeling with secondary antibody conjugated with 10 nm gold particles. Black arrowheads point to selected virions. Empty arrowhead points to caveolar invagination. Asterisk indicates virion internalizing into an invagination lacking caveolin-1. Arrow points to virion internalizing via plasma membrane region enriched for caveolin-1. Pm, plasma membrane. Bars, 50 nm. (C) 3T6 cells were pre-treated (1 h) with nocodazole and infected with MPyV. The drug was washed out at 7 hours p.i. and cells were further incubated until 24 hours p.i. (middle bar) or for additional 24 hours after washing (right bar). As a control, cells were infected in the absence of the drug and fixed 24 hours p.i. Cells were immunostained for MPyV LT antigen and the efficiency of infection was determined by the levels of LT antigen-positive cells, normalized to that in control. During the experiment, at least 500 cells of each sample were counted. Data in the graph represent mean values ± s.d. from three independent experiments. Immunofluorescent staining of microtubules (anti-α-tubulin antibody; panel on the right) shows the morphology of microtubular network at the time of washing (7 hours p.i.) in control or nocodazole-treated cells. Bars, 10 μm.

5.1.6 *Importance of recycling endosomes for MPyV infection*

Co-localization analysis revealed that MPyV transport to recycling endosomes is dependent on intact microtubules (Figure 5.7B). To investigate whether MPyV infection depends on the virus transfer through the recycling endosomes, we followed the virus infectivity in 3T6 cells transiently expressing EGFP-fused WT, DN or constitutively active (CA) mutant of Rab11 GTPase. As an additional control, we tested the virus infectivity during transient expression of analogous mutants of Rab7 GTPase, since the dependence of MPyV infection on late endosomes was proved using DN mutant of Rab7 GTPase in NIH 3T3 cells [81]. Infection assays revealed that neither expression of EGFP-fused WT nor any mutant version of Rab11 GTPase affected the virus infectivity (Figure 5.11A). On the other hand, the expression of EGFP-fused DN version of Rab7 substantially reduced virus infectivity in comparison to the WT or CA Rab7 version (Figure 5.11B). Functional expression of Rab11 constructs was verified by intracellular distribution of fluorescently tagged transferrin in cells expressing EGFP-tagged versions of Rab11 GTPase. In accordance with report of Ren et al [172] and Hölttä-Vuori et al [173], cytoplasmic localization of WT and CA version of EGFP-Rab11 was concentrated in the juxtanuclear region corresponding to the pericentriolar recycling compartment and most of the transferrin was accumulated in these structures. On the other hand, DN Rab11 was dispersed in the cytoplasm or created thinner tubular perinuclear elements, but presence of transferrin in these structures was diminished (Figure 5.12). These data indicate that virus transport along microtubules to the Rab11-positive recycling compartments is dispensable for MPyV infection. *(This part was realized in cooperation with Sandra Huerfano)*

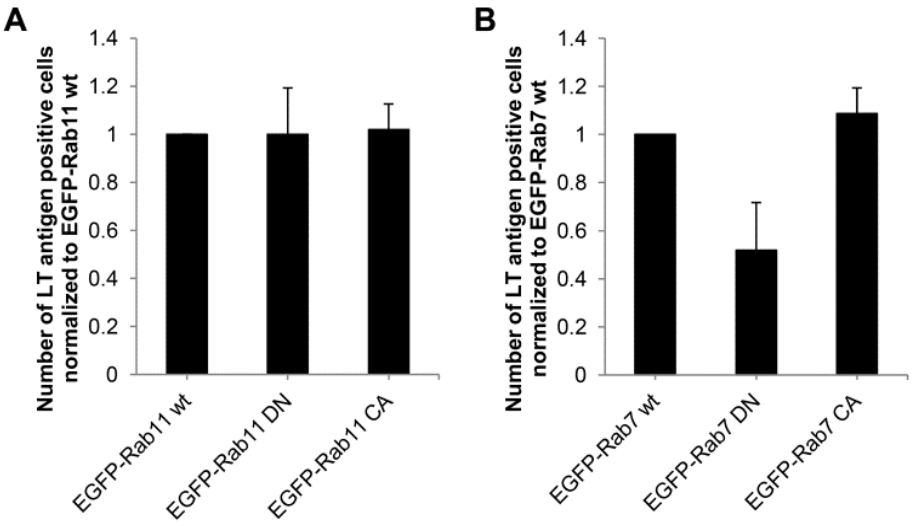

Figure 5.11 Requirement of Rab11 and Rab7 GTPase for MPyV infection in 3T6 fibroblasts. Cells were transfected with plasmid DNA for transient expression of (A) EGFP-fused WT, DN or CA version of Rab11 GTPase, or (B) EGFP-fused WT, DN or CA version of EGFP-Rab7 GTPase. After 24 hours, cells were infected with MPyV, incubated until 24 hours p.i., fixed and immunostained for MPyV LT antigen. The efficiency of infection was determined by the levels of LT antigen-positive cells from that expressing EGFP-fused version of the Rab11 or Rab7 GTPase normalized to that obtained in cells expressing its wild-type version. During the experiment, more than 500 cells were counted for each sample or control. Data in the graph represent mean values ± s.d. from three independent experiments.

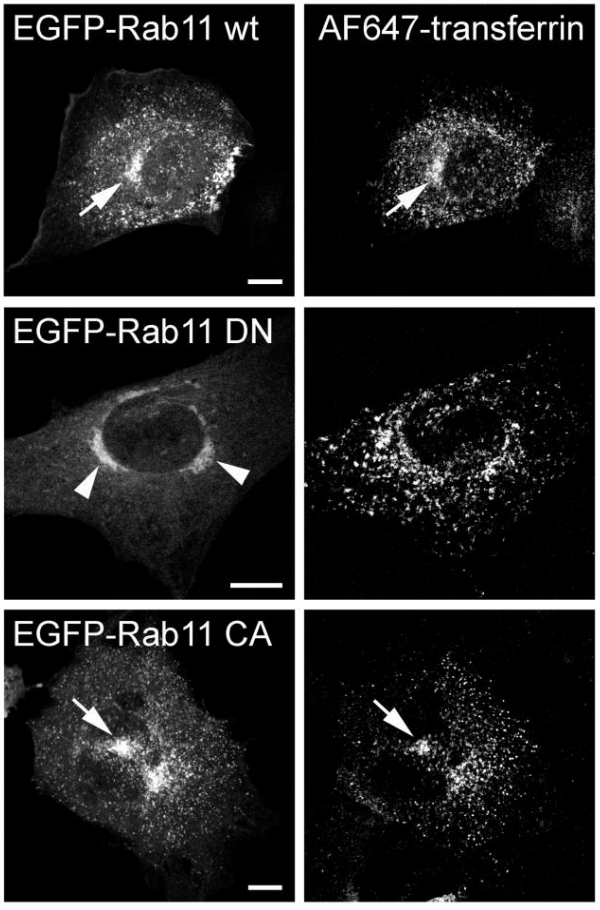

Figure 5.12 Intracellular distribution of fluorescently tagged transferrin during expression of Rab11 GTPase mutants. 3T6 cells expressing EGFP-fused WT, DN or CA version of Rab11 were incubated for 5 min (pulse) at 37°C with 25 μg/ml Alexa Fluor 647-transferrin. Cells were further incubated for 30 min (chase) at 37°C in serum-containing medium, fixed and processed for fluorescence microscopy. Confocal sections showing representative distribution of transferrin in the cells are presented. Arrows point to places of concentrated transferrin. Arrowheads point to tubular perinuclear elements of Rab11 DN. Bars, 10 μm.

5.1.7 *Role of actin microfilaments in MPyV productive trafficking*

Our co-localization analysis suggested that actin meshwork represents rather a barrier for virus endocytic transport and is connected with accumulation of the virions in caveolin-1-positive compartments (Figure 5.7B). However, while in naturally permissive cells, actin disrupting drugs (added prior to infection) enhanced infectivity of MPyV [113,114], latrunculin A (applied in the same way) strongly reduced MPyV infection in ganglioside GD1a-supplemented rat C6 cells [16]. Thus, to verify results of co-localization analysis, we tested the effect of depolymerization of actin microfilaments on productive transport of MPyV. We performed infectivity assays in 3T6 cells where actin disrupting drug latrunculin A was added to cells after virus uptake and neutralization of extracellular virions by MPyV-neutralizing antibody. Addition of the drug after neutralization of non-internalized virus allowed us to exclude previously reported effect of actin disrupting drugs on MPyV uptake by cells [27,113]. The infection assays revealed that depolymerization of actin microfilaments by latrunculin A enhanced the infectivity of MPyV by ~40%, when compared to control (non-treated) cells (Figure 5.13A). To evaluate possible cytotoxic effect of latrunculin A during its temporary presence (5.5 hours), we measured concentration of LDH (released from dead cells) in the medium at infection start and at time of infectivity evaluation (24 hours p.i.). Further, we determined total cell numbers to compare the rate of cell growth of treated and non-treated cells. The percentage of cytotoxicity for treated and non-treated cells was lower than 2%. Further we used maximum LDH values as indicator of total cell numbers (see Materials and Methods, chapter 4.12). The increase of cell population measured 24 hours p.i. was similar (~2-fold amount of cells than at beginning of infection) for both, control or latrunculin A-treated cells (Figure 5.13B), indicating that presence of latrunculin A was no toxic for cells and did not influence the cells growth. Together these data demonstrated that productive transport of MPyV is more efficient upon depolymerization of actin microfilaments. *(This part was realized in cooperation with Sandra Huerfano)*

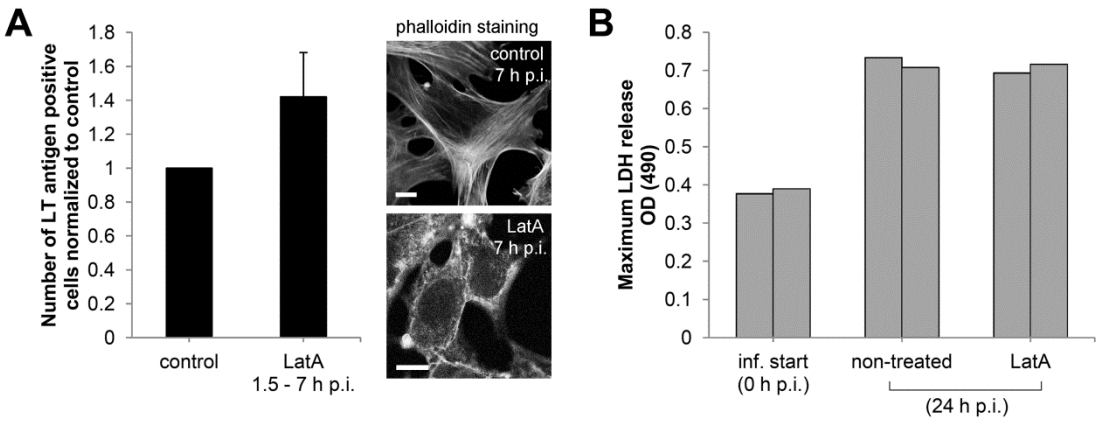

Figure 5.13 Disruption of actin microfilaments enhanced productive transport of MPyV. (A) 3T6 cells were infected with MPyV (MOI of 2 PFU/cell). At 1 hour p.i., neutralizing anti-MPyV VP1 antibody was added to cells to neutralize extracellular virions. At 1.5 hour p.i., latrunculin A (LatA) was added to cells to depolymerize actin microfilaments. LatA was kept with cells until 7 hours p.i., drug was then washed out and cells were further incubated prior fixation at 24 hours p.i. Fixed cells were immunostained for MPyV LT antigen and the efficiency of infection was determined by the levels of LT antigen-positive cells normalized to that obtained in the control cells - infected in absence of drug but treated with neutralizing antibody added at the same time (1.5 hour) post-infection. During the experiment, at least 1000 cells of each sample were counted. Data in graph represent mean values ± s.d. from three independent experiments. Immunofluorescent staining (panels on the right) of actin microfilaments (by rhodamine-coupled phalloidine) shows the morphology of actin cytoskeleton at the time of washing (7 hours p.i.) in control or LatA-treated cells. (B) Measurement of maximum LDH release as indicator of total cell numbers of 3T6 cells at beginning of infection (0 hours p.i.) and 24 h post-infection without LatA (non-treated) or with LatA added from 1.5 to 7 hours p.i. Values of two independent experiments are presented.

5.2 **Cytotoxic properties of MPyV minor capsid proteins VP2 and VP3**

This chapter refers to the results published in the paper entitled, "**Minor capsid proteins of mouse polyomavirus are inducers of apoptosis when produced individually but are only moderate contributors to cell death during the late phase of viral infection"** by Huerfano S., Žíla V., Bouřa E., Španielová H., Štokrová J., Forstová J., *FEBS J*. 2010 277(5): 1270-1283 (reference [157]). I contributed to most parts of the work, including expression plasmids preparation, confocal fluorescent microscopy of fixed and living cells, electron and immunoelectron microscopic analyses and cytotoxicity assays (for FLAG-fused constructs). The published paper is in the attachment #2.

5.2.1 *Individual expression of the minor capsid proteins in mammalian cells*

To study of properties of MPyV minor capsid proteins, we expressed the minor proteins individualy in mouse NIH 3T3 cells and tested effects of their overproduction in the absence of other MPyV's gene products, the tumor antigens and the major capsid protein, VP1. Our previous attempts for expression of proteins VP2 or VP3 in mammalian cells were unsatisfactory, when only very low percentage of transfected cells (<1%) produced VP2 or VP3 (Bouřa E., Kečkéšová Z., unpublished results). Therefore, we prepared DNA constructs for expression of these proteins fused with EGFP in their C- or N-termini. We also prepared plasmids for expression of N- and C-EGFP fusion variants of VP3 truncated at its N-terminus. Truncated VP3 (tVP3) corresponds to the C-terminal part of VP2 (216 – 319 AA) that includes only the C-terminal hydrophobic domain (described by Rainey-Barger et al [23]). The expression of EGFP-fused variants of the minor structural proteins was efficient in 3T3 fibroblasts and oscillated between 50 – 70% of transfected cells. *(I contributed by preparation and characterization of plasmids for production of EGFP-VP2, EGFP-VP3 and tVP3-EGFP protein variants, as described in Materials and Methods)*

5.2.2 *Intracellular localization of overproduced minor capsid proteins*

To test whether fusion variants of the minor structural proteins possess character of their wild-type versions, we first compared distribution of the fusion versions of proteins in transfected 3T3 cells with that of WT version (expressed from plasmids – pSVL-VP2, pLNHX-VP3, pVP3-Leader-C2). Confocal microscopy analysis revealed

that WT VP2 and VP3 exhibited, besides nuclear localization, evident affinity for the NE and ER membranes (Figure 5.14A,B, upper panels). While localization pattern observed for the minor proteins fused with EGFP at their C-terminus (VP3-EGFP and VP2-EGFP) was similar to WTs, variants of the minor proteins fused with EGFP at their N-terminus (EGFP-VP2 and EGFP-VP3), as well as both fusion variants of tVP3 had substantially lower or no affinity to these membranes (Figures 5.14 A,B, lower panels and 5.15). As control, we examined also distribution of VP2 and VP3 fused at their C-terminus with the eight AA-long FLAG sequence (VP2-FLAG and VP3-FLAG). For FLAG-fused minor proteins, we observed comparable location to that observed for WT VP2 and VP3 or for VP2-EGFP, VP3-EGFP fusion variants (Figure 5.14C). In addition, we performed live imaging of cells producing EGFP-fused variants and followed mutual localization of the cytoplasmic fractions of fusion proteins with intracellular membranes (stained by 1,6-diphenylhexatriene). Consistently with results obtained with fixed cells, only VP2-EGFP and VP3-EGFP exhibited strong co-localization with intracellular membranes, while proteins fused with EGFP at their N-terminus were predominantly nuclear (Figure 5.16, upper and middle panel). Cytoplasmic subpopulation of both fusion variants of tVP3 also did not co-localize with membranes convincingly (Fig. 5.16, bottom panel). Together, these data indicated that C-terminal fusion preserved properties of WT forms of the minor structural proteins, and revealed their affinity of transiently produced minor proteins to intracellular membranes, including NE.

Localization of the minor capsid proteins observed in fixed and living cells was verified by quantification of different cell phenotypes with respect to intracellular distribution of EGFP-fused protein variants. Quantification revealed three main phenotype groups with a fused protein located i) almost exclusively in the nucleus, ii) in both nucleus and cytoplasm, or iii) almost exclusively in the cytoplasm. Figure 5.17 presents representative patterns for individual EGFP-fused variants with the percentage of cells belonging to each phenotype group. Data showed that VP2-EGFP variant was located predominantly in the cell cytoplasm (84% of cells). In large amounts (56%) of these cells, it co-localized with the ER. In contrast, inversed, EGFP-VP2 variant was present almost exclusively in the cell nucleus (98% of cells). Similarly, VP3-EGFP protein exhibited much higher affinity to ER membranes and NE (42% of cells). In some cells (17%), the VP3-EGFP signal formed “rings” where protein co-localized with the nuclear envelope. The variant EGFP-VP3 variant was found predominantly in the

nucleus (69% of cells). One of two version of truncated VP3 (tVP3-EGFP) was localized predominantly in the nucleus (68%). Both fusion variants of tVP3, had substantially lower affinity, or no affinity to membranes. *(This part was realized in cooperation with Sandra Huerfano)*

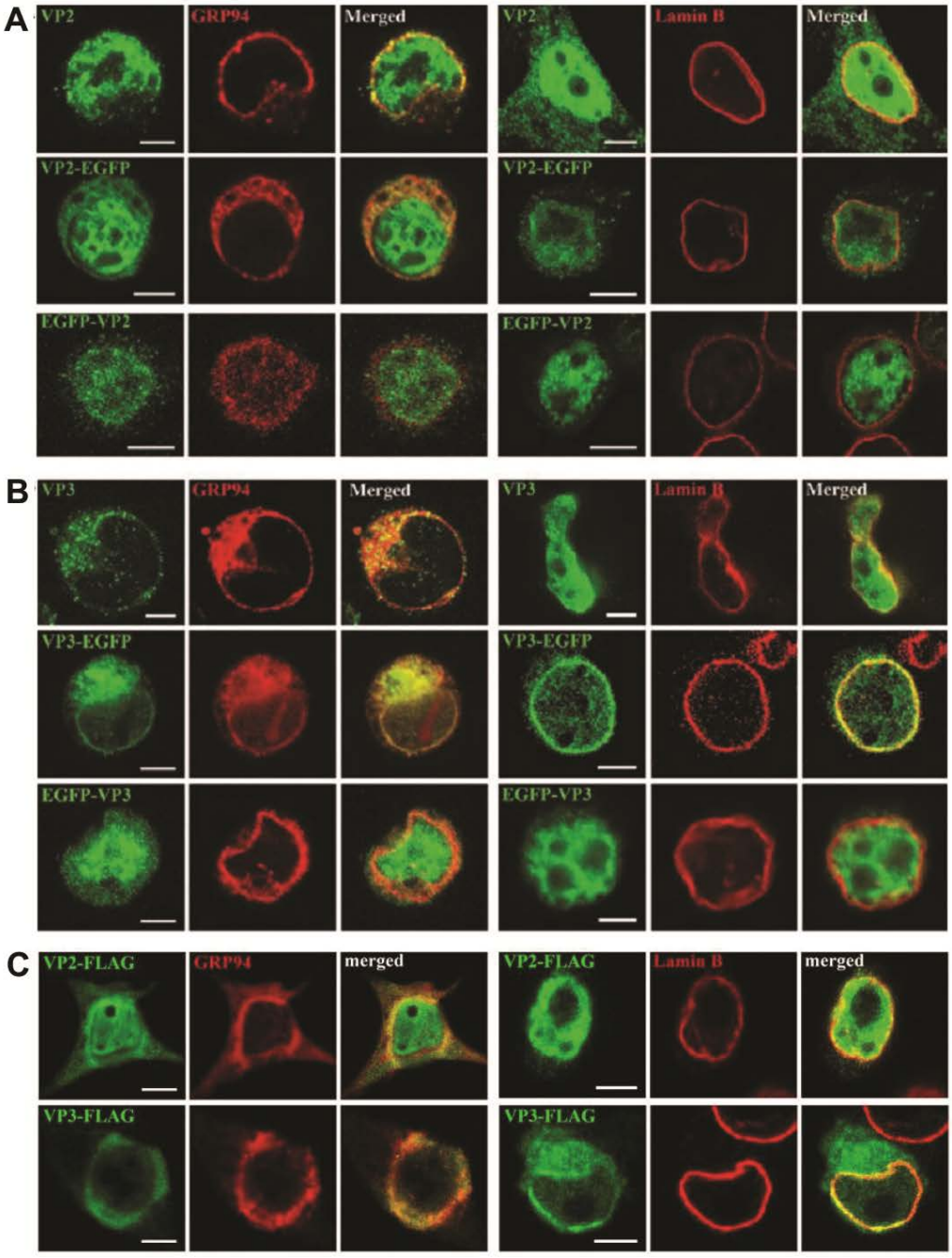

Figure 5.14 Localization of VP2 and VP3 minor proteins and their fusion variants in transfected cells. 3T6 cells were transfected with plasmids for expression of wild-type VP2 or VP3, or minor proteins fused with EGFP on its C- (VP2-EGFP, VP3-EGFP) or N-terminus (EGFP-VP2, EGFP-VP3), or control minor protein varients fused with FLAG epitope on its C-terminus (VP2-FLAG, VP3-FLAG). (A-B) Selected confocal microscopy sections of cells fixed at 4 hours post-transfection. Cells were immunostained with antibody against the GRP94 ER marker, or with lamin B (red). Signal of EGFP- or FLAG-fused minor proteins was enhanced by staining with anti-MPyV VP2⁄3 IgG (green). Bars, 5 μm.

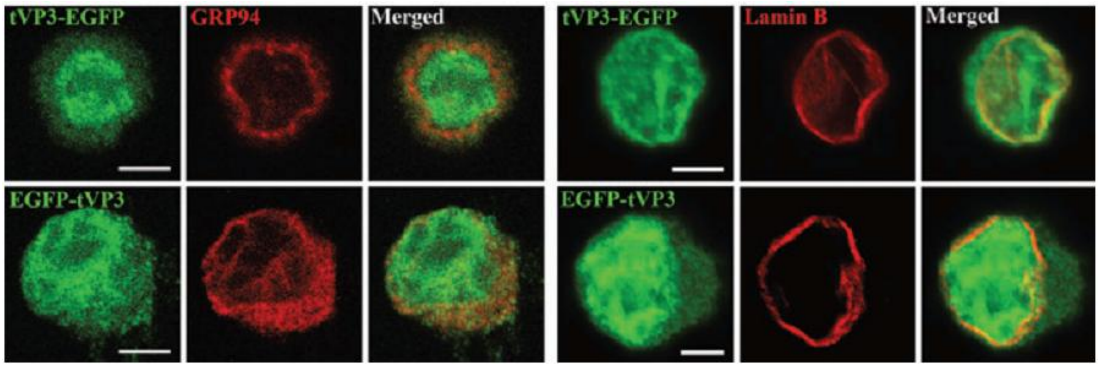

Figure 5.15 Localization of EGFP fusion variants of truncated VP3 (tVP3) in transfected cells. 3T3 cells were transfected with plasmids for expression of tVP3, fused with EGFP on its C- (tVP3-EGFP) or N-terminus (EGFP-tVP3). (A) Selected confocal microscopy sections of cells fixed at 4 hours post-transfection. Cells were immunostained with antibody against the GRP94 ER marker, or with lamin B (red). Signal of EGFP-fused tVP3 proteins was enhanced by staining with anti-MPyV VP2⁄3 IgG (green). Bars, 5 μm.

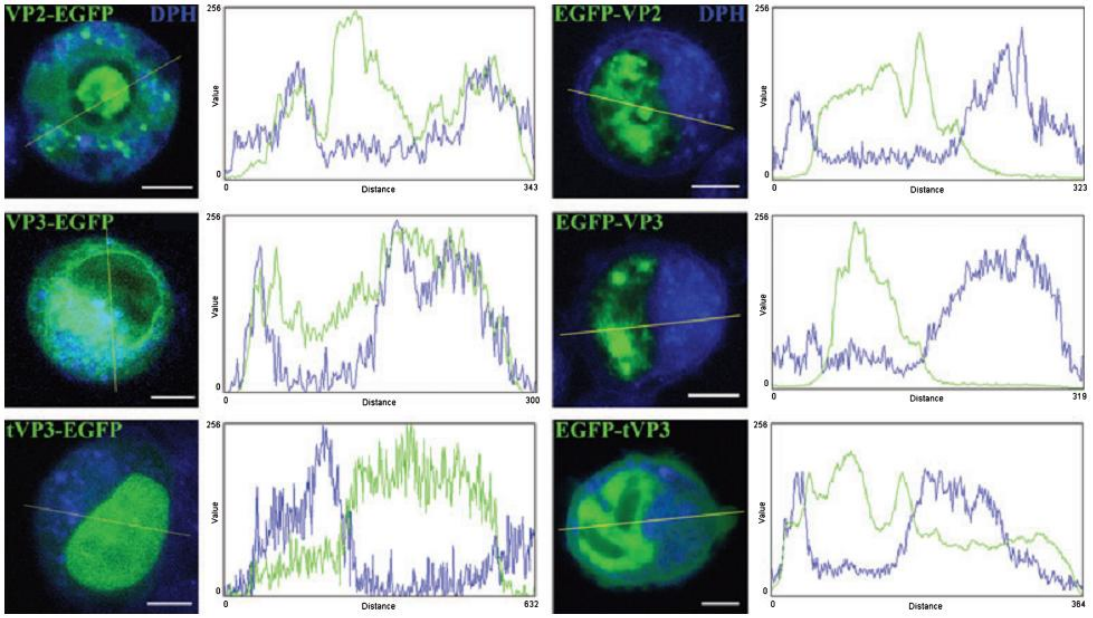

Figure 5.16 Localization of EGFP fused variants of VP2, VP3 or tVP3 in living 3T3 cells. Selected confocal microscopy sections of living cells observed 4 - 5 hours post-transfection. Membranes were stained with DHP (blue), EGFP fusion variants of the minor structural proteins (green). Profiles of signal intensities in line selection of shown cell sections are presented. Bars 5 μm.

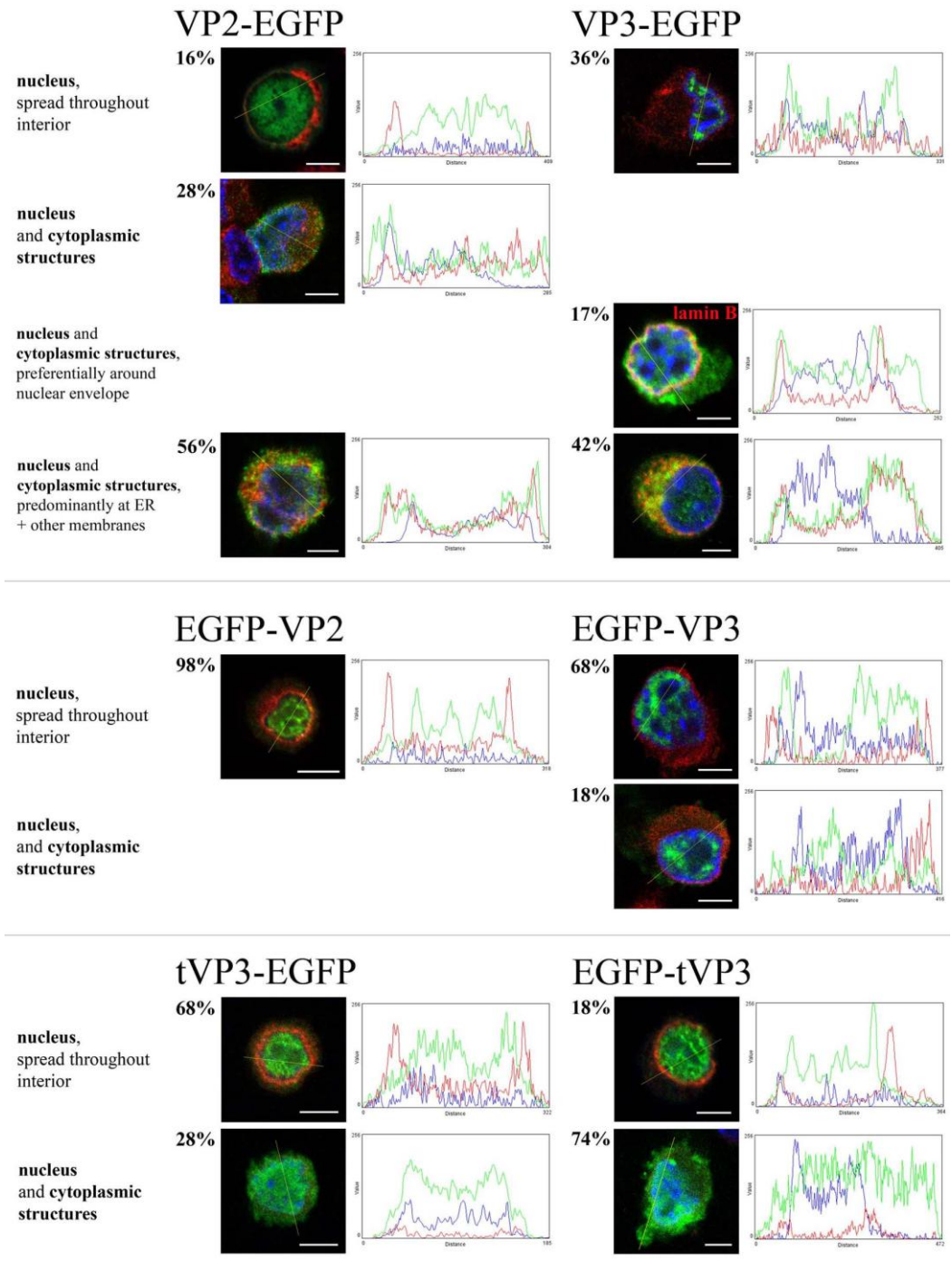

Figure 5.17 Localization of VP2 and VP3 and tVP3 fusion variants in transfected 3T3 cells. Distribution of fused minor capsid proteins was followed in selected confocal microscopy sections. At least 50 different cells were examined for each fusion variant. Representative distribution patterns are presented. Cells were fixed and stained (4 hours post-transfection) in red with an antibody against endoplasmic reticulum markers, GRP 94 or GRP 78 (not indicated), or against lamin B (indicated in the picture). The signal of EGFP-fused VP2 or VP3 was enhanced with anti-VP2/3 antibody (green). Nucleus (DNA) was stained by DAPI (blue). Profiles of signal intensities in line selection of cell sections are presented. Bars 5 µm.

5.2.3 *Cytotoxicity of overproduced minor capsid proteins*

Despite the transient expression of the individual minor structural protein VP2 or VP3 in permissive NIH 3T3 fibroblasts was not efficient, few obtained positive cells exhibited remarkable morphology alterations and died usually between 8 – 18 hours post-transfection, suggesting that the minor capsid proteins are toxic for mammalian cells (Bouřa E., Kečkéšová Z., unpublished results). These preliminary results prompted us to test the toxicity of VP2, VP3 and tVP3 fused with EGFP at selected times post-transfection by measuring concentration of LDH, released from dead cell into the culture medium (Figure 5.18A). Cytotoxicity assays revealed that only expression of VP2-EGFP and VP3-EGFP was highly toxic for cells, whereas inverted fusion proteins, EGFP-VP2 and EGFP-VP3 exhibited much lower cytotoxicity and EGFP-fused tVP3 variants did not cause cell death during the period tested (24 hours post-transfection). Cytotoxicity of VP2-EGFP and VP3-EGFP was detected as early as 7 hours post-transfection. As a control, we measured cytotoxicity of VP2-FLAG and VP3-FLAG (the same oriented fusion) and found it to be comparable with that of VP2-EGFP or VP3-EGFP (Figure 5.18B). These results supported our confocal microscopy analyses which suggested that the minor proteins variants with EGFP fused at their C-terminus possess properties similar to those of natural VP2 and VP3. Data proved that presence of the minor structural proteins is strongly toxic for cells and that deletion of half of VP3 sequences (including hydrophobic domain 2) from its N-terminus suppressed (at least during the period evaluated) the ability to kill cells. *(Cytotoxicity assays were realized in cooperation with Sandra Huerfano)*

As the above results revealed, VP2-EGFP and VP3-EGFP represent fusion variants exhibiting intracellular distribution (Figure 5.14 and 5.16) and cytotoxicity (Figure 5.18) of their WT counterparts, we further examined the association of VP2-EGFP and VP3-EGFP with cellular substructures using immunoelectron microscopy (IEM). As control, we examined cells producing EGFP alone. IEM analysis of cells at 4 h post-tranfection revealed presence of VP2-EGFP and VP3-EGFP on membranes of swollen ER and on damaged mitochondria. VP3-EGFP could be seen also associated with the nuclear membrane, often between the inner and outer layer (Figure 5.19). We thus concluded that interaction of VP2 or VP3 with ER and/or with other intracellular membranes causing their damage is responsible for cytotoxicity of the minor capsid proteins.

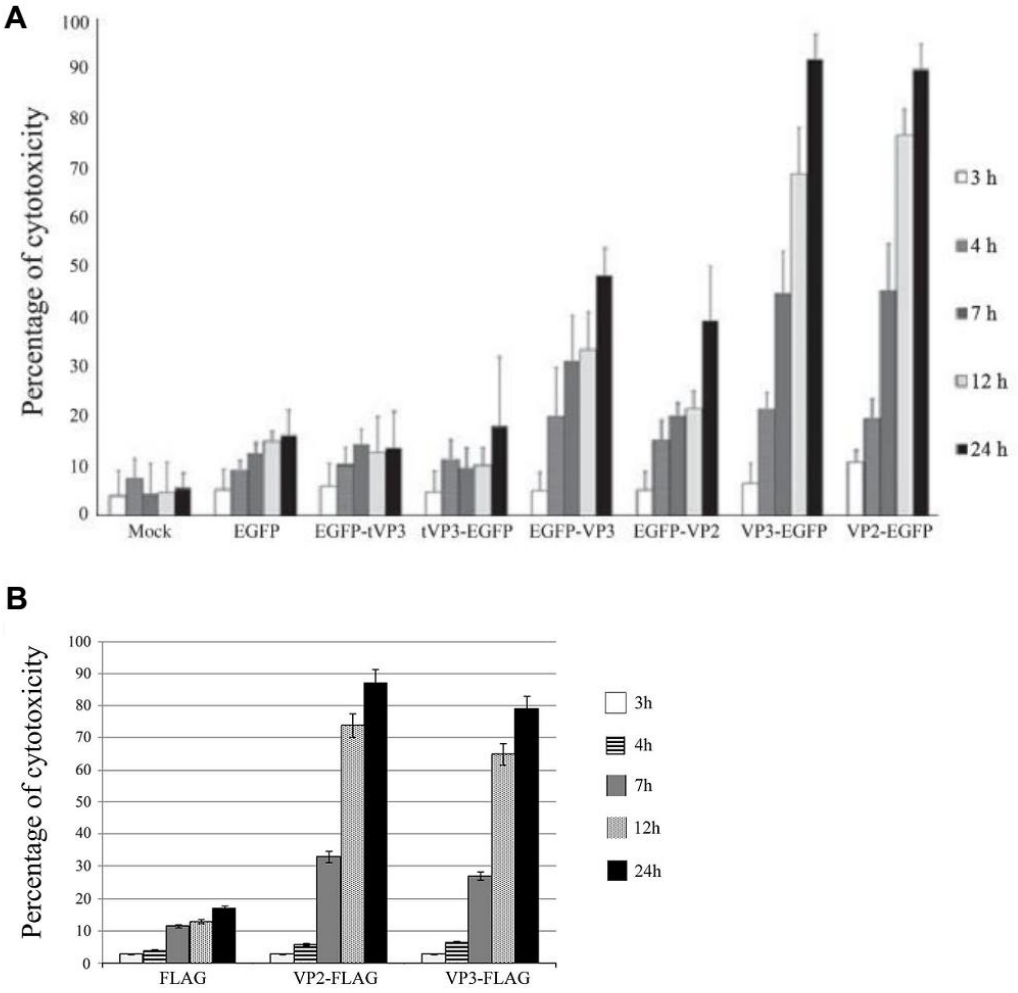

Figure 5.18 Cytotoxicity of VP2 or VP3 fusion proteins. Cytotoxicity of individual EGFP- (A) or FLAG-fused (B) minor structural protein variants transiently expressed in 3T3 cells was followed by measuring of LDH leakage from transfected cells into the medium at the indicated times post-transfection. Presented values are relative to that of LDH release obtained by treatment of cells with 9% Triton X-100 (=100%). Data represent mean values measuring duplicates of three independent experiments. Mock-transfected (A) or FLAG only producing cells (B) were used as controls.

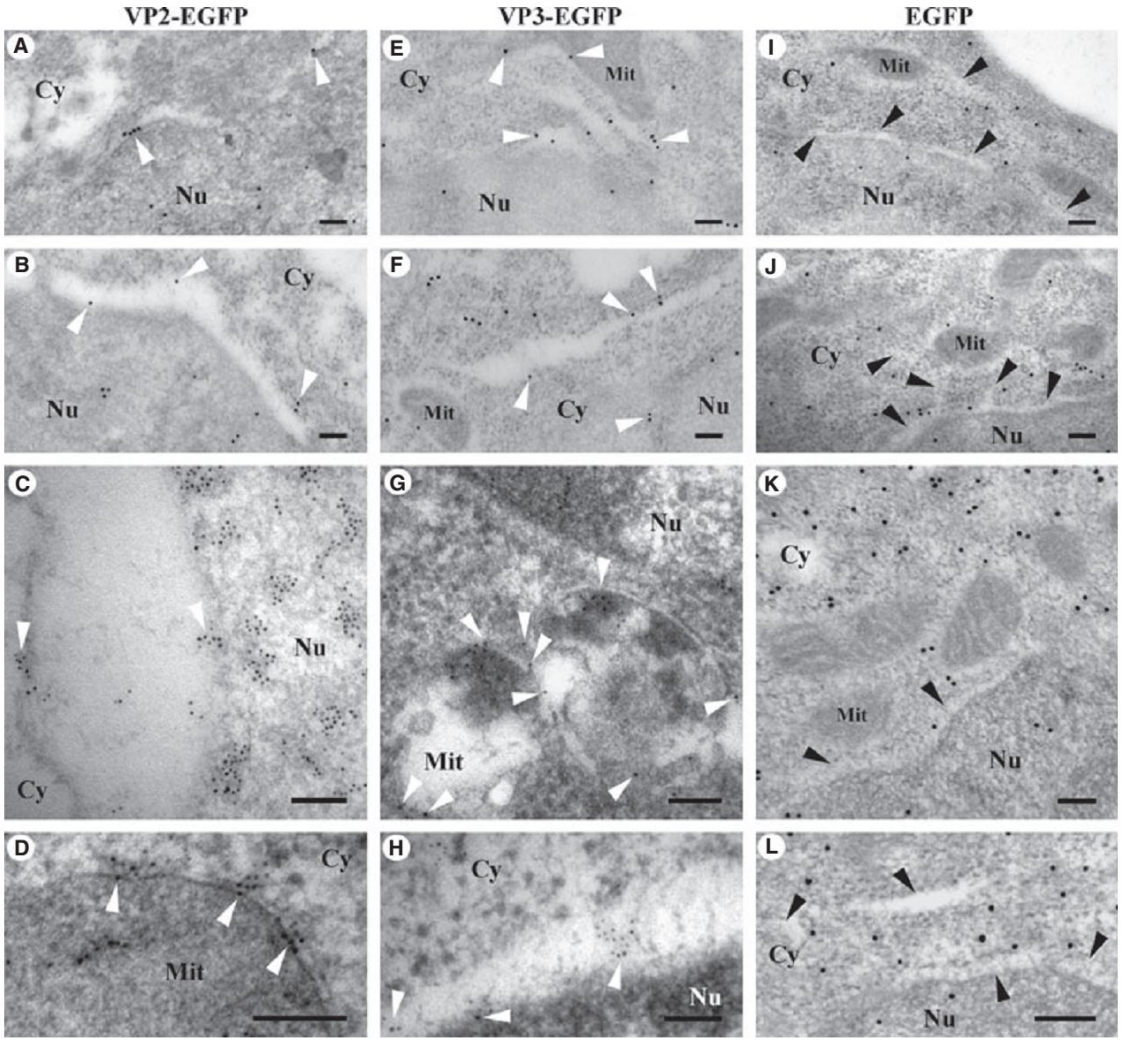

Figure 5.19 Immunoelectron microscopy on ultrathin sections of cells expressing VP2-EGFP, VP3-EGFP or EGFP alone. 3T3 cells were fixed 5 hours post-transfection. Fused minor capsid proteins were detected by incubation of cell sections with anti-GFP antibody followed by incubation with the secondary antibody conjugated with 10 nm gold particles (a, b, e, f, i - l) or 5 nm gold particles (c, d, g, h). Selected gold particles indicated by white arrowheads. Black arrowheads indicate ER cisternae on sections of cells expressing EGFP only. Bars 100 nm.

5.2.4 *Mechanism of cell death induced by the minor capsid proteins*

Further, we examined the character of cell death induced during the expression of VP2 or VP3 protein. Morphology analysis of cells producing their toxic fusion variants (VP2-EGFP, VP3-EGFP) by transmission electron microscopy at 5 hours post-transfection, revealed cells with typical caspase-dependent apoptotic condensed chromatin features among the floating cells collected from the medium (Figure 5.20), in agreement with loss of adherence, a known feature of apoptotic cells [174].

To assess the contribution of apoptosis to toxicity, we further followed specific apoptotic markers in cells transienlty expressing VP2 or VP3. First, we evaluated cleavage of effector caspase 3 and one of its substrates, poly(ADP-ribose) polymerase (PARP) by Western blotting. We detected cleavage of caspase 3 (indicating activation) as well as cleavage of PARP, as soon as 5 hours post-transfection in cells transfected with either of plasmids encoding VP2 or VP3 or tVP3, fused with EGFP either at the C- or N-terminus. Only expression of EGFP alone did not induce caspase 3 nor PARP cleavage (Figure 5.21A). However, quantification of caspase 3 activity in lysates of cells tranfected with individual constructs revealed that VP2-EGFP or VP3-EGFP protein (collected 4 hours post-transfection) induced remarkably high caspase 3 activity, comparable with activity found in cells treated with 2 μM actinomycin D (specific inductor of apoptosis). In cells producing VP2-EGFP and VP3-EGFP proteins (collected 4 hours post-transfection) remarkably high caspase 3 activity was found, whereas in cells producing EGFP-VP2, EGFP-VP3, or either fusions of tVP3, activity of caspase 3 was markedly lower (Figure 5.21B). These observations were confirmed by analysis of exposure of phosphatidylserine in the outer leaflet of the plasma membrane of cells producing fusion variants of VP2 or VP3. While significant subpopulations of cells exhibiting phosphatidylserine exposure during production of VP2-EGFP (23.9%) or VP3-EGFP (23.0%) was detected, only minor population (between 1% and 6%) was found in cells producing EGFP-VP2, EGFP-VP3, EGFP-tVP3 or tVP3-EGFP (Table 5.1). All these data indicated that MPyV minor proteins, VP2 or VP3, are very potent inductors of apoptosis when produced individually in mammalian cells. *(Biochemical analysis of apoptotic markers in cells expressing minor structural proteins was performed by Sandra Huerfano)*

Altogether, the subcellular localization of the VP2-EGFP and VP3-EGFP (Figure 5.14, 5.16), presence of the minor proteins at damaged membranes of ER, mitochondria or NE (Figure 5.19) and the fact that apoptosis is induced quickly (as soon

as production of the proteins could be detected) (Figure 5.18) suggest that the main actions of VP2 or VP3 leading to apoptosis is their interaction with intracellular membranes causing their damage.

	% of annexing positive cells
MOCK	3.49
EGFP	1.74
Actinomycin D	**32.2**
VP2-EGFP	**23.9**
VP3-EGFP	**23.0**
tVP3-EGFP	0.9
EGFP-VP2	5.93
EGFP-VP3	4.67
EGFP-tVP3	3.89

Table 5.1 Detection of phosphatidylserine exposition in cells expressing EGFP-fused MPyV structural minor capsid proteins. 3T3 cells cells were transfected with plasmids encoding either individual EGFP fused variants of the minor proteins, or control Mock-transfected cells, cells treated by actinomycin D (ActD) and cells expressing EGFP alone. Exposure of phosphatidylserine was detected by FACS analysis 5 hours post-transfection (see Materials and Methods).

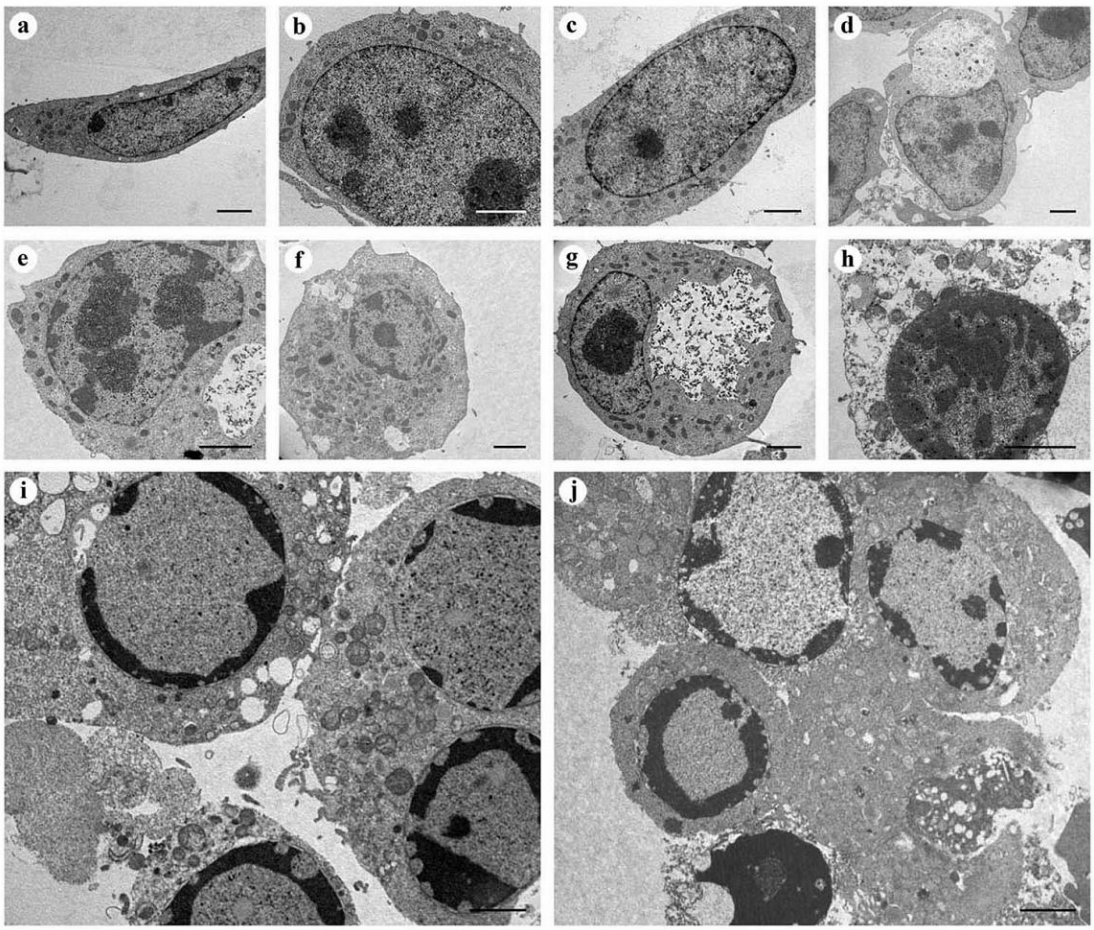

Figure 5.20 Apoptotic morphology of cells producing MPyV minor capsid proteins, VP2 or VP3. Cells were fixed 5 hours post-transfection. Electron microscopy of ultrathin sections of control, non-transfected 3T3 cells (a and b) and cells producing EGFP only (c-h) or VP2-EGFP (i), or VP3-EGFP (j). Cells attached to the plate (a-d) or floating in the medium (e-j). Bars, 2 µm.

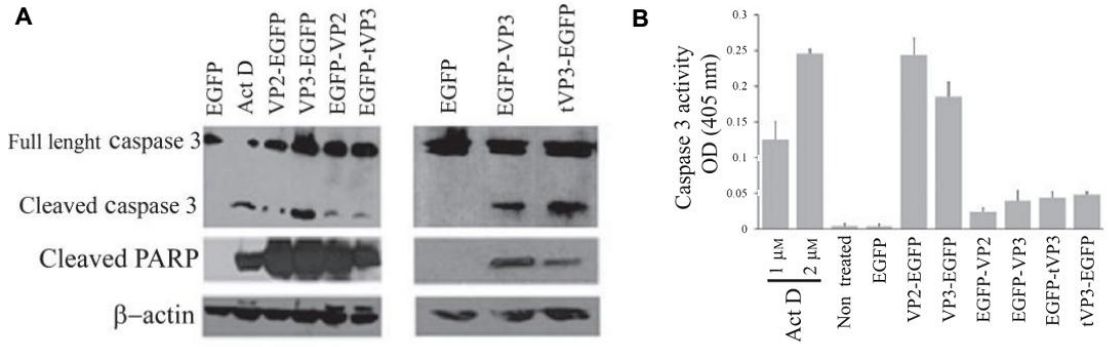

Figure 5.21 Detection of apoptosis in cells expressing EGFP-fused MPyV structural minor capsid proteins. Lysates of 3T3 cells transfected with plasmids encoding either individual EGFP fused variants of the minor proteins, EGFP only, mock-transfected cells, cells treated by actinomycin D (Act D), or untreated cells. (**A**) Cleavage of caspase 3 and PARP in lysates of cells collected 5 hours post-transfection. Western blot analysis using anti-caspase 3 (recognising full and cleaved forms), or anti-cleaved PARP antibody. An antibody against β-actin was used as a control for loaded samples. (**B**) Measurements of caspase 3 activities in cell lysates (4 hours post-transfection) by the CaspACE colorimetry assay system.

5.2.5 *Contribution of the minor proteins to lysis of MPyV-infected cells*

Observed cytotoxicity of VP2 and VP3 and their ability to induce apoptosis, prompted us to test the involvement of the minor proteins in apoptosis induction during infection and their role in lysis of infected cells in the end of virus replication cycle. For this, we first followed induction of apoptotic markers (phosphatidylserine exposure, caspase 3 activation and PARP processing) in cells transfected with WT MPyV genome and genome mutated in translation start codons of both VP2 and VP3. The analysis was perfomed in late stages (34 – 40 hours post-transfection), of the first virus replication cycle, since the virions lacking either VP2 or VP3 are practically non-infectious [22]. We found that apoptotic population measured by annexin V (detection of phosphatidylserine exposure) was similar for cells transfected with WT and mutated MPyV (Figure 5.22A). Also, although the activity of caspase 3 and PARP processing were significantly higher in the WT-transfected cells, substantial levels of both apoptotic markers were present in cells transfected by the mutant (Figure 5.22B,C). When we further followed the cytotoxicity (by measurement of LDH release) during the first viral cycle, we found that replication of both WT and mutant MPyV resulted in cell destruction within 48 hours post-transfection (Figure 5.22D). Together, these data indicated that VP2 and VP3 are only moderate contributors to apoptosis induction during the virus infection and are dispensable for cell death in the end of virus lytic cycle. *(This part was realized by Sandra Huerfano)*

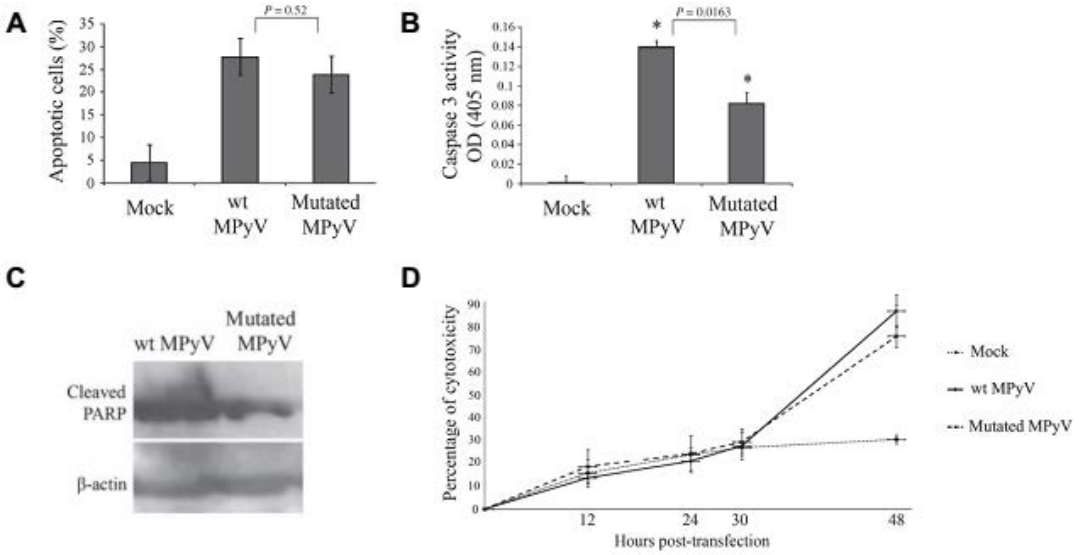

Figure 5.22 Detection of apoptotic markers and cell destruction in cells transfected with WT or mutated (in VP2 and VP3 ATG codons) MPyV genome. (**A**) Exposure of phosphatidylserine (Annexin V-positive cells) 34 hours post-transfection by FACS analysis. Mean values of three experiments are presented. (**B**) Caspase-3 activity 40 hours post-transfection by the CaspACE colorimetry assay. Mean values of three experiments are presented. (**C**) Western blot showing PARP cleavage (using antibody specific for cleavaged PARP) in lysates of cells 40 hours post-transfection. (**D**) Burst of 3T6 cells transfected with WT or mutated genomes (LDH release) related to those obtained by treatment of cells with Triton X-100 (= 100%). Data represent the mean of three independent experiments. Mock-transfected cell lysates were used as a negative control.

6. DISCUSSION

This section discusses the research focused on: (i) the dynamics of intracellular transport of MPyV virions towards the nucleus and relevance of virus movements along microtubules for its productive infection; (ii) the cytotoxic properties of MPyV minor structural proteins, VP2 and VP3, studied in the absence of other virus components as well as during the late phase of virus replication cycle.

6.1 **Role of cell cytosketon in the trafficking of MPyV to the ER**

A current model of MPyV trafficking from the host cell membrane towards the cell nucleus assumes that virions enter cells by internalization into smooth endocytic vesicles, often positive for caveolin-1. Internalized virions are subsequently transported to the early and late endosomes and further to the ER where disassembly of virus capsid take place prior to viral genome translocation into the nucleus [16,18,19,21,81]. Concerning involvement of cell cytoskeleton in trafficking of MPyV to the ER, some reported observations [16] suggest that it resembles situation described for SV40. SV40 was showed to utilize the actin dynamics for its transport from the plasma membrane to early and premature late endosomes, while microtubules were showed to mediate subsequent virus transport from mature endosomes to the ER [15,106]. Interestingly, until recent observation of dependence of SV40 infection on dynein microtubular motor in HeLa cells [15], productive trafficking of polyomaviruses was considered to be independent on dynein motor function [14,134]. Possible role of other microtubular motors involved in endosomal transport, such as kinesin-1 or kinesin-2, has not yet been investigated for any polyomavirus. Here, we present evidence that dynein motor mediates all the critical steps of MPyV trafficking, including i) efficient virus transport from the plasma membrane to endosomes of classical endocytic pathways, ii) maturation of MPyV-carrying endosomes, and iii) subsequent virus delivery to the ER. In addition, we demonstrated that MPyV transport to recycling endosomes is microtubule-dependent, but is not required for virus productive infection.

Virus tracking experiments in living cells expressing EGFP-tubulin, revealed bi-directional movement of virions along microtubules, indicating involvement of both, dynein and kinesins during MPyV endocytic trafficking. Single particle tracking analysis demonstrated that dynamics of MPyV virion transport is mostly salutatory. Measurement of fast forward movements of MPyV corresponded to recruitment of a

single microtubular motor molecule on the transported vesicle and fits well with the processivity of individual kinesin or dynein molecule-mediated transport [165]. However, slow short-range movements (up to 0.2 μm/s) or pausing at intervals were most prevalent. Besides pausing of virus-loaded vesicles on microtubule tracks, slow virus motility might be assigned also to actin-driven motility of virus-carrying endosomes which reaches similar velocity rates [162-164]. Indeed, the association of slowly moved MPyV-loaded endosomes with assemblies of dynamic actin recruited at their membranes was detected in EGFP-actin-expressing cells. Observation of MPyV endosomal trafficking along microtubules at the same times post-infection as virion-loaded endosomes propulsion by actin patches, suggest that microtubules and microfilaments are involved simultaneously (including the presence of different types of specific molecular motors on virion-carrying vesicles) or, alternatively, after short-distance movement at the cell periphery (driven by actin polymerization) vesicles can recruit a minus end microtubule-associated motor to reach the proximity of the nucleus (or MTOC). Similar mode of transport was described for influenza virions: the initial actin-driven motion of virus-loaded endosomes has been followed by dynein-dependent transport to the perinuclear space [175].

Our further investigation revealed that dynein is critical for MPyV infection, perinuclear sorting and virus delivery to ER. Previous studies that focused on the role of microtubular network in trafficking of polyomaviruses reported that perturbation of the dynein motor function did not lead to significant inhibition of JCV, SV40 or BKV infection [14,134]. Authors suggested involvement of a different member of the dynein family whose function is independent of dynactin complex, or that the viral proteins can interact directly with microtubules for transport [14]. However, Engel et al [15] recently published RNA interference screen in HeLa cells that revealed the dependence of SV40 infection on dynein motor at least in this cell line, in accordance with our results. Neither the kinesin-1 nor kinesin-2 function was required for MPyV infection or virus perinuclear location. It has been found that kinesin-2 is required for normal steady-state localization of late endosomes. However, authors of this study showed that the uptake and trafficking of molecules through the conventional endocytic pathway was unaffected by inhibition of kinesin-2 [151]. Our results thus imply that this might be true also for cargo trafficking via early endosomes whose motility requires kinesin-1 [176], since transfer via both, early and late endosomes is important for MPyV [18,81].

Nevertheless, the role of microtubules during transport of MPyV in endosomes is still not clear. There is one study on MPyV [16], suggesting that actin cytoskeleton is involved in delivery of MPyV virions from the plasma membrane to endosomes, similarly to SV40 [15,106]. Transport of SV40 to early and premature late endosomes was independent of intact microtubules. They were required later for maturation of SV40-carrying late endosomes and subsequent virus delivery to the ER [15]. The same group reported previously that vesicles carrying SV40 virions recruit actin in the form of actin comet tails and use it for their transport from the plasma membrane [106]. However, our results from 3T6 cells infected in the absence or presence of compounds selectively affecting the structure and dynamics of microtubules (nocodazole) or actin cytoskeleton (latrunculin A), indicate that dynein-mediated transport along microtubules is important already for effective trafficking of MPyV from the plasma membrane to endosomes, while the actin meshwork rather slows down the rate of virus endocytic transport and is connected with accumulation of the virions in caveolin-1-positive compartments. Correspondingly, our infectivity assay showed that addition of latrunculin A during virus transport increases its infectivity (Figure 5.13), in agreement with others who tested effect of actin disrupting drug on MPyV infection in naturally permissive cells [113,156]. We might speculate that enhaced productive trafficking of MPyV in the presence of actin disrupting drugs is caused by more efficient transport along microtubules without a barrier of microfilaments in cell cytosol, or, by better accesibility of virus-loaded endosomes to dynein motor molecules without presence of the dynamic actin polymerizing on their membranes. We also cannot exclude the possibility that dynamic actin directs virions on non-productive pathways.

In the presence of nocodazole, most MPyV virions was found accumulated at the periphery of cells within endocytic vesicles often connected to flask-shape caveolae-like empty structures, or within membrane clusters heavily labeled for caveolin-1. Morphology of virion-containing clusters strikingly resembled multicaveolar complexes described previously [170,171]. However, we showed that virions entered the cells independently of flask-shaped caveolae, similarly as in untreated cells [18,21,101]. We also showed that enrichment of virus-containing vesicles for caveolin-1 is caused by virus internalization via caveolin-1-rich domains at plasma membrane. Recently, formation of multicaveolar complexes was shown to occur along actin microfilaments from individual caveolae domains physically linked to the microfilament structure [177], This is in agreement with our observation of reduced co-localizition of MPyV

with caveolin-1 in the presence of actin-disrupting latrunculin A. We thus hypothesized that during internalization of MPyV via caveolin-rich domains at the plasma membrane, invaginating virions might be, due to the presence of caveolins, organized along actin microfilaments similarly to caveolar domains. No apparent difference in detection of virions at the plasma membrane of nocodazole-treated or non-treated cells indicate that these clusters are intracellular or that they are connected to the cell surface by very narrow invaginations. Almost complete reversibility of inhibition of virus infection by nocodazole after its washout suggests that microtubules and dynein motor mediate the link for MPyV between these multicaveolar-like structures and acidic endosomes. Several studies have reported caveolin-1 or caveolae trafficking into early endosomes [178] and, under specific conditions, also into MVBs and endolysosomal compartments [123,170,179]. Nevertheless, our results indicate that the presence of MPyV virions in multicaveolar-like complexes is dispensable for virus infection and rather decreases and/or delays productive trafficking of the MPyV virions.

In previous reports we showed that substantial portion of MPyV VP1 capsid protein appeared in Rab11-positive recycling endosomes of 3T6 cells [18,19]. Here, we showed that transport of MPyV to Rab11-positive endosomes was dependent on intact microtubules, consistently with the finding that Rab11 together with the dynein motor mediate transport to the endosomal-recycling compartments [180]. However, virus infectivity in cells expressing EGFP-fused wild-type, dominant-negative or constitutively active mutant of Rab11 GTPase showed that Rab11-positive recycling compartments are dispensable for MPyV. The appearance of MPyV in these compartments may thus be connected with recycling of the virus material back to the plasma membrane, as slow sorting of the VP1 signal from the perinuclear region to the cell periphery was observed in the interval 6 – 24 hours post-infection (Stancikova-Pappova M., unpublished results).

Our future investigation will focus on the involvement of actin cytoskeleton during trafficking of MPyV, since our results might suggest possible defence role of actin dynamics agains incoming MPyV virions. Further effort will focus also on still unclear mechanism of translocation of MPyV virions from acidic endosomes to the ER, and finally, from where and by what mechanism MPyV genome translocate into the nucleoplasm.

6.2 **Cytotoxic properties of MPyV minor capsid proteins VP2 and VP3**

Minor structural proteins, VP2 and VP3, are essential for MPyV infection. Our previous analysis showed that MPyV lacking minor structural proteins, VP2 or VP3, fails to deliver its genome into the nucleus [22], suggesting possible function(s) of the minor capsid proteins during virus entry, uncoating and/or delivery of the virus genomes into the cell nucleus. Study of Rainey-Barger et al [23], described three trans-membrane domains in the minor capsid proteins sequence: domain 1, identified in the unique part of VP2; domain 2, located at N-terminus of common part of VP2/3; and domain 3, composed of α-helix at C-terminus of VP2/3 (see Figure 2.11). Authors also presented *in vitro* experiments, which showed that protein VP2 was able to binds to, integrate into, and perforate the physiologically relevant ER membranes, while VP3 was able to integrate to membranes, but was not sufficient for membrane perforation. These findings suggest that after capsid disassembly within the ER lumen, the minor capsid proteins integrate into the ER membrane, potentially creating a pore that aids in viral DNA transport out of the ER to the cytosol or directly to nucleoplasm. These results also suggest a different involvement of the minor proteins based on their trans-membrane domains. Here, we investigated properties of the minor structural proteins in the absence of other gene products of MPyV (the tumor antigens and the major capsid protein VP1). We found that both minor structural proteins are highly toxic for cells and both associate with damaged intracellular membranes. Cytotoxicity of the minor proteins was showed to be result of induction of apoptosis. Only truncated version of VP3 protein, containing only C-terminal α-helix (marked as domain 3 by Rainey-Barger et al [23]) has no apparent affinity to membrane and was low or not toxic for cells. However, despite of cytotoxicity of VP2 and VP3, and their strong ability to induce apoptosis, the proteins were found only as moderate contributors to apoptosis in MPyV infected cells and were dispensable for lysis of host cells in the end of virus replication cycle.

To follow cellular responses to production of VP2 or VP3, in the absence of other MPyV gene products, we prepared DNA constructs for expression of minor proteins fused with EGFP attached to either their C- or N-terminus. We also prepared VP3 truncated at its N-terminus (tVP3), corresponding to C-terminal part of VP2/3 (216 – 319 AA). This fragment contained only the C-terminal hydrophobic domain (marked as domain 3 by Rainey-Barger et al [23]). Intracellular distribution of the fusion variants revealed that minor proteins fused with EGFP (or FLAG) at their C-terminus exhibited

strong affinity for the intracellular membranes, particularly for membranes of NE and ER, similarly to that observed for their WT versions. Surprisingly, although VP2 contains the entire VP3 sequence and possesses another trans-membrane domain in its unique region (domain 1) [23] and myristyl at its N-terminal glycine [181], it did not seem to have higher affinity for intracellular membranes than VP3. On the other hand, the minor proteins fused with EGFP at their N-terminus, as well as both, fusion variants of tVP3 were targeted preferentially into the cell nucleus and had substantially lower or no affinity to intracellular membranes. These results are consistent with the fact that C-terminal tagging of proteins is in general preferable to N-terminal tagging, in that the corresponding proteins usually resemble their wild-type versions [182].

When we followed toxicity of fusions versions of VP2, VP3 and tVP3 during their transient expression, we observed clear correlation between toxicity of fusion variants and their intracellular distribution. Only variants fused with EGFP or FLAG at their C-terminus exhibited strong cytotoxicity, while inverted fusion proteins or both EGFP-fused tVP3 variants exhibited much lower cytotoxicity or did not cause cell death. Association of toxic variants of the minor proteins (VP2-EGFP, VP3-EGFP) with cellular substructures examined by immunoelectron analysis, revealed their presence on membranes of swollen ER and damaged mitochondria. VP3-EGFP could be also seen readily associated with the nuclear membrane, often located between the inner and outer layer. Previous *in vitro* study showed that VP2 perforates the ER relevant membrane, whereas VP3 integrates into the membrane, but it is not sufficient for perforation [23]. However, our observations indicate that both minor proteins, VP2 and VP3, kill cells quickly, and both were found associated with damaged intracellular membranes, suggesting that perforation of intracellular membranes is the major cause of the observed toxicity induced by expression of either of two minor proteins.

We showed that the character of cell death caused by expression of VP2 or VP3 is induction of apoptosis. Apoptosis can be triggered by many different stimuli, including release of calcium from the ER or cytochrome C from mitochondria [183,184]. VP2 and VP3, with their ability to interact with and perforate cell membranes, may be thus considered as members of so-called viroporins. Viroporins usually possess at least one amphipathic α-helix and in some instances, a second hydrophobic domain [185]. VP2 of MPyV (and other polyomaviruses) possesses three and VP3 two hydrophobic domains [23]. The third domain forms at the C-terminus an amphipathic α-helix. Despite the study of Reiny-Berger suggested that only the domain

in unique part of VP2 (domain 1) is able to perforate cell membranes, intracellular distribution and cytoxicity of VP3-EGFP and low toxicity of the tVP3 (lacking domain 2) suggested that domain 2 possesses similar activity as domain 1. On the other hand, domain 3 alone (only hydrophobic domain present in tVP3 – α-helix at C-terminus of VP2/3) was not sufficient for efficient membrane binding or apoptosis induction, in agreement with the results of Reiny-Berger et al [23]. These authors hypothesized that C-terminal part, which interacts with the central cavity of VP1 pentamers, was unlikely to contribute to membrane binding without global disassembly of the virus [23]. However, in our experiments, VP1 covering the domain 3 in pentamers was absent. We thus speculate that membrane interaction of the third hydrophobic domain requires specific conditions, such as acidic pH or other, which appear in a particular cell compartments.

What is the contribution of the minor capsid proteins for cell death in the end of virus replication cycle? Levels of apoptotic markers and cytotoxicity detected during replication of WT MPyV and virus mutated in VP2 and VP3 AUG start codons, revealed that the minor capsid proteins are not main inducers of apoptosis in the infection process and that they are even dispensable for cell death in the end of virus lytic cycle. It is in agreement with the fact that during infection, the most of the minor capsid proteins become integral parts of capsomeres or virions and are apparently prevented from cell interactions. Moreover, only about 10% of cells at late stage of MPyV replication cycle exhibit the apoptotic phenotype while most cells exhibit significant features of ongoing necrosis, indicating that necrosis, not apoptosis, is the major mechanism of cell burst ([60] and Zila V., Stokrova J. unpublished results).

Further effort of our investigation will focus on examination of interactions of the minor structural proteins in cells, contributions of individual hydrophobic domains to their membrane affinity and on possible functions of VP2 and VP3 in the early steps of polyomavirus infection, during virion entry, uncoating processes and/or import of viral DNA genome from ER into the cell nucleus.

7. CONCLUSIONS

First aim of the Ph.D. thesis was specification of involvement of cell cytoskeleton during the endocytic trafficking of MPyV from the plasma membrane to the ER. To achieve this, we first used confocal fluorescence microscopy of living cells to reveal direct association of transported virions with cytoskeletal networks. Further, we followed dynamics of MPyV intracellular trafficking in living cells. We performed infectivity assays to test the effect of dominant-negative forms of dynein, kinesin-1 or kinesin-2 motor on MPyV productive transport. We used confocal and electron microscopy approaches and treatment with cytoskeleton-disrupting drugs for monitoring of involvement of microtubular network and actin cytoskeleton in MPyV transport from the plasma membrane to endosomes and in subsequent virus delivery to the ER. Finally, we investigated whether virus transfer via recycling endosomes represents an alternative endocytic pathway along microtubules utilized by MPyV to reach the ER.

Our research showed:

- Endocytosed MPyV is transported bi-directionally along microtubules as well as propelled by dynamic actin assemblies.
- Dynamics of MPyV cytoplasmic transport reflects the characteristics of microtubular motor-driven transport with saltatory movements.
- Productive trafficking of MPyV does not require the function of kinesin-1 and kinesin-2, but depends on functional dynein-mediated transport along microtubules, required for translocation of the virions from peripheral compartments to late endosomes and ER.
- Effective virus transport from the plasma membrane to endosomes of classical endocytic pathways (early, late and recycling endosomes) is mediated along microtubules, whereas actin cytoskeleton represents rather a barrier for virus endocytic transport and was showed to be connected with accumulation of virions in caveolin-1-positive compartments.
- Transport of MPyV to recycling endosomes was found to be realized along microtubules and to be dispensable for virus infection.

Second aim of the thesis was characterization of the cytotoxic properties of the minor capsid proteins, VP2 and VP3, in the absence of other MPyV gene products. To achieve this, we prepared several plasmids for individual expression of VP2, VP3 and their EGFP fusion variants as well as EGFP fusion variants of the truncated VP3 (containing 103 amino acids of the C-terminus). We followed intracellular localization of VP2 and VP3 in mouse cells, cell death, and the presence of apoptosis markers during their transient expression as well as during the infection cycle of WT MPyV and mutated MPyV, lacking both minor capsid proteins.

Our research showed that:

- Properties of the minor capsid proteins fused with EGFP at their C-terminus were similar to those of WT VP2 and VP3.
- Substantial subpopulations of VP2-EGFP and VP3-EGFP were detected in the cytoplasm, co-localizing there with intracellular membranes.
- Transient production of VP2-EGFP and VP3-EGFP was highly cytotoxic.
- Immunoelectron microscopy revealed association of the minor capsid proteins with damaged membranes of ER, NE and mitochondria. Truncated VP3 protein carrying only C-terminal α-helix, exhibited reduced both, affinity for intracellular membranes and cytotoxicity.
- Biochemical studies proved both minor proteins to be a very potent inducer of apoptosis, dependent on caspase activation.
- Analysis of apoptotic markers and cell death kinetics in cells transfected with the WT MPyV genome and the genome mutated in both VP2 and VP3 translation start codons revealed that the minor proteins contribute only moderately to apoptotic processes during infection and both are dispensable for cell destruction at the end of the virus replication cycle.

8. LIST OF ABBREVIATIONS

AA	amino acids	**MHC**	major histocompatibility complex
Act D	actinomycin D	**MOI**	multiplicity of infection
BFA	brefeldin A	**MPyV**	mouse polyomavirus
BKV	BK virus	**mRNA**	messenger RNA
CA	constitutively active	**MT**	middle T antigen
CCD	charge-coupled device	**NE**	nuclear envelope
CT	C-terminus fragment only	**NLS**	nuclear localization sequence
C-terminus	carboxyl-terminus	**NPC**	nuclear pore coplex
DAPI	4‘, 6‘-diamidino-2-phenylindole	**N-terminus**	amino-terminus
DMEM	Dulbecco’s Modified Eagle’s Medium	**NeuNAc**	*N*-acetylneuraminic acid
DN	dominant-negative	**Ori**	origin of replication
EGFP	enhanced green fluorescent protein	**PARP**	poly(ADP-ribose) polymerase
ER	endoplasmic reticulum	**PBS**	phosphate buffered saline
ERAD	endoplasmic reticulum associated protein degradation	**PFU**	plaque-forming units
FACS	fluorescence-activated cell sorting	**PML-NB**	Promyelocytic leukemia nuclear body
FBS	fetal bovine serum	**pRb**	Retinoblastoma protein
HBV	hepatitis B virus	**p.i.**	post-infection
HL	headless mutant	**RT**	room temperature
JCV	JC virus	**RFP**	red fluorescence protein
kbp	kilo base pairs	**SA**	sialic acid
kDa	kilodaltons	**siRNA**	small interfering RNA
KHCct	C-terminal fragment of kinesin-1 heavy chain	**ST**	small T antigen
kV	kilovolts	**SV40**	simian virus 40
LDH	lactate dehydrogenase	**tVP3**	truncated VP3
LT	large T antigen	**VLPs**	virus-like particles
MCC	Merkel cell carcinoma	**WHO**	World Health Organization
MCV	Merkel cell polyomavirus	**WT**	wild-type

9. REFERENCES

1. Martin D, Gutkind JS (2008) Human tumor-associated viruses and new insights into the molecular mechanisms of cancer. Oncogene 27 Suppl 2: S31-42.
2. Cole CN (1996) *Polyomavirinae*: the viruses and their replication. In: Fields BN, Knipe, D. M., Howley, P. M., Chanock, R. M., Melnick, J. L., Monath, T. P., Roizman, B. and Straus, S. E., editor. Fields Virology 3rd Edition. Philadelphia, PA: Lippincott-Raven. pp. 1997–2025.
3. Ashok A, Atwood WJ (2006) Virus receptors and tropism. Adv Exp Med Biol 577: 60-72.
4. Dawe CJ, Freund R, Mandel G, Ballmer-Hofer K, Talmage DA, et al. (1987) Variations in polyoma virus genotype in relation to tumor induction in mice. Characterization of wild type strains with widely differing tumor profiles. Am J Pathol 127: 243-261.
5. Imperiale MJ (2000) The human polyomaviruses, BKV and JCV: molecular pathogenesis of acute disease and potential role in cancer. Virology 267: 1-7.
6. Padgett BL, Walker DL, ZuRhein GM, Eckroade RJ, Dessel BH (1971) Cultivation of papova-like virus from human brain with progressive multifocal leucoencephalopathy. Lancet 1: 1257-1260.
7. Binet I, Nickeleit V, Hirsch HH, Prince O, Dalquen P, et al. (1999) Polyomavirus disease under new immunosuppressive drugs: a cause of renal graft dysfunction and graft loss. Transplantation 67: 918-922.
8. Hashida Y, Gaffney PC, Yunis EJ (1976) Acute hemorrhagic cystitis of childhood and papovavirus-like particles. J Pediatr 89: 85-87.
9. Nickeleit V, Singh HK, Mihatsch MJ (2003) Polyomavirus nephropathy: morphology, pathophysiology, and clinical management. Curr Opin Nephrol Hypertens 12: 599-605.
10. Sariyer IK, Akan I, Del Valle L, Khalili K, Safak M (2004) Tumor induction by simian and human polyomaviruses. Cancer Therapy Vol 2: 85-98.
11. Vilchez RA, Butel JS (2004) Emergent human pathogen simian virus 40 and its role in cancer. Clin Microbiol Rev 17: 495-508, table of contents.
12. Feng H, Shuda M, Chang Y, Moore PS (2008) Clonal integration of a polyomavirus in human Merkel cell carcinoma. Science 319: 1096-1100.
13. zur Hausen H (2012) Red meat consumption and cancer: reasons to suspect involvement of bovine infectious factors in colorectal cancer. Int J Cancer 130: 2475-2483.
14. Ashok A, Atwood WJ (2003) Contrasting roles of endosomal pH and the cytoskeleton in infection of human glial cells by JC virus and simian virus 40. J Virol 77: 1347-1356.
15. Engel S, Heger T, Mancini R, Herzog F, Kartenbeck J, et al. (2011) Role of endosomes in simian virus 40 entry and infection. J Virol 85: 4198-4211.
16. Gilbert J, Benjamin T (2004) Uptake pathway of polyomavirus via ganglioside GD1a. J Virol 78: 12259-12267.
17. Gilbert JM, Benjamin TL (2000) Early steps of polyomavirus entry into cells. J Virol 74: 8582-8588.
18. Liebl D, Difato F, Hornikova L, Mannova P, Stokrova J, et al. (2006) Mouse polyomavirus enters early endosomes, requires their acidic pH for productive infection, and meets transferrin cargo in Rab11-positive endosomes. J Virol 80: 4610-4622.
19. Mannova P, Forstova J (2003) Mouse polyomavirus utilizes recycling endosomes for a traffic pathway independent of COPI vesicle transport. J Virol 77: 1672-1681.
20. Pelkmans L, Kartenbeck J, Helenius A (2001) Caveolar endocytosis of simian virus 40 reveals a new two-step vesicular-transport pathway to the ER. Nat Cell Biol 3: 473-483.
21. Richterova Z, Liebl D, Horak M, Palkova Z, Stokrova J, et al. (2001) Caveolae are involved in the trafficking of mouse polyomavirus virions and artificial VP1 pseudocapsids toward cell nuclei. J Virol 75: 10880-10891.
22. Mannova P, Liebl D, Krauzewicz N, Fejtova A, Stokrova J, et al. (2002) Analysis of mouse polyomavirus mutants with lesions in the minor capsid proteins. J Gen Virol 83: 2309-2319.

23. Rainey-Barger EK, Magnuson B, Tsai B (2007) A chaperone-activated nonenveloped virus perforates the physiologically relevant endoplasmic reticulum membrane. J Virol 81: 12996-13004.
24. Gross L (1953) A filterable agent, recovered from Ak leukemic extracts, causing salivary gland carcinomas in C3H mice. Proc Soc Exp Biol Med 83: 414-421.
25. Sweet BH, Hilleman MR (1960) The vacuolating virus, S.V. 40. Proc Soc Exp Biol Med 105: 420-427.
26. Gardner SD, Field AM, Coleman DV, Hulme B (1971) New human papovavirus (B.K.) isolated from urine after renal transplantation. Lancet 1: 1253-1257.
27. Ewers H, Smith AE, Sbalzarini IF, Lilie H, Koumoutsakos P, et al. (2005) Single-particle tracking of murine polyoma virus-like particles on live cells and artificial membranes. Proc Natl Acad Sci U S A 102: 15110-15115.
28. Chen L, Fluck M (2001) Kinetic analysis of the steps of the polyomavirus lytic cycle. J Virol 75: 8368-8379.
29. Nemethova M, Smutny M, Wintersberger E (2004) Transactivation of E2F-regulated genes by polyomavirus large T antigen: evidence for a two-step mechanism. Mol Cell Biol 24: 10986-10994.
30. Lowe SW, Jacks T, Housman DE, Ruley HE (1994) Abrogation of oncogene-associated apoptosis allows transformation of p53-deficient cells. Proc Natl Acad Sci U S A 91: 2026-2030.
31. Gottlieb KA, Villarreal LP (2001) Natural biology of polyomavirus middle T antigen. Microbiol Mol Biol Rev 65: 288-318 ; second and third pages, table of contents.
32. Cahan LD, Singh R, Paulson JC (1983) Sialyloligosaccharide receptors of binding variants of polyoma virus. Virology 130: 281-289.
33. Fanning E, Zhao K (2009) SV40 DNA replication: from the A gene to a nanomachine. Virology 384: 352-359.
34. Cheng J, DeCaprio JA, Fluck MM, Schaffhausen BS (2009) Cellular transformation by Simian Virus 40 and Murine Polyoma Virus T antigens. Semin Cancer Biol 19: 218-228.
35. Cole CN, Tornow J, Clark R, Tjian R (1986) Properties of the simian virus 40 (SV40) large T antigens encoded by SV40 mutants with deletions in gene A. J Virol 57: 539-546.
36. Stahl H, Droge P, Knippers R (1986) DNA helicase activity of SV40 large tumor antigen. EMBO J 5: 1939-1944.
37. Marton A, Marko B, Delbecchi L, Bourgaux P (1995) Topoisomerase activity associated with polyoma virus large tumor antigen. Biochim Biophys Acta 1262: 59-63.
38. Howes SH, Bockus BJ, Schaffhausen BS (1996) Genetic analysis of polyomavirus large T nuclear localization: nuclear localization is required for productive association with pRb family members. J Virol 70: 3581-3588.
39. Schmitt MK, Mann K (1987) Glycosylation of simian virus 40 T antigen and localization of glycosylated T antigen in the nuclear matrix. Virology 156: 268-281.
40. Klockmann U, Deppert W (1983) Acylated simian virus 40 large T-antigen: a new subclass associated with a detergent-resistant lamina of the plasma membrane. EMBO J 2: 1151-1157.
41. Mellor A, Smith AE (1978) Characterization of the amino-terminal tryptic peptide of simian virus 40 small-t and large-T antigens. J Virol 28: 992-996.
42. Peden KW, Pipas JM (1992) Simian virus 40 mutants with amino-acid substitutions near the amino terminus of large T antigen. Virus Genes 6: 107-118.
43. Whalen KA, de Jesus R, Kean JA, Schaffhausen BS (2005) Genetic analysis of the polyomavirus DnaJ domain. J Virol 79: 9982-9990.
44. Gerits N, Moens U (2012) Agnoprotein of mammalian polyomaviruses. Virology 432: 316-326.
45. Chang D, Haynes JI, 2nd, Brady JN, Consigli RA (1992) Identification of a nuclear localization sequence in the polyomavirus capsid protein VP2. Virology 191: 978-983.
46. Moreland RB, Garcea RL (1991) Characterization of a nuclear localization sequence in the polyomavirus capsid protein VP1. Virology 185: 513-518.

47. Forstova J, Krauzewicz N, Wallace S, Street AJ, Dilworth SM, et al. (1993) Cooperation of structural proteins during late events in the life cycle of polyomavirus. J Virol 67: 1405-1413.
48. Lin W, Hata T, Kasamatsu H (1984) Subcellular distribution of viral structural proteins during simian virus 40 infection. J Virol 50: 363-371.
49. Stamatos NM, Chakrabarti S, Moss B, Hare JD (1987) Expression of polyomavirus virion proteins by a vaccinia virus vector: association of VP1 and VP2 with the nuclear framework. J Virol 61: 516-525.
50. Garcea RL, Benjamin TL (1983) Isolation and characterization of polyoma nucleoprotein complexes. Virology 130: 65-75.
51. Yuen LK, Consigli RA (1985) Identification and protein analysis of polyomavirus assembly intermediates from infected primary mouse embryo cells. Virology 144: 127-138.
52. Salunke DM, Caspar DL, Garcea RL (1986) Self-assembly of purified polyomavirus capsid protein VP1. Cell 46: 895-904.
53. Dalyot-Herman N, Ben-nun-Shaul O, Gordon-Shaag A, Oppenheim A (1996) The simian virus 40 packaging signal ses is composed of redundant DNA elements which are partly interchangeable. J Mol Biol 259: 69-80.
54. Oppenheim A, Sandalon Z, Peleg A, Shaul O, Nicolis S, et al. (1992) A cis-acting DNA signal for encapsidation of simian virus 40. J Virol 66: 5320-5328.
55. Spanielova H, Fraiberk M, Suchanova J, Soukup J, Forstova J (2014) The encapsidation of polyomavirus is not defined by a sequence-specific encapsidation signal. Virology 450-451: 122-131.
56. Campbell KS, Mullane KP, Aksoy IA, Stubdal H, Zalvide J, et al. (1997) DnaJ/hsp40 chaperone domain of SV40 large T antigen promotes efficient viral DNA replication. Genes Dev 11: 1098-1110.
57. Francke B, Eckhart W (1973) Polyoma gene function required for viral DNA synthesis. Virology 55: 127-135.
58. Chromy LR, Pipas JM, Garcea RL (2003) Chaperone-mediated in vitro assembly of Polyomavirus capsids. Proc Natl Acad Sci U S A 100: 10477-10482.
59. Tjian R (1978) The binding site on SV40 DNA for a T antigen-related protein. Cell 13: 165-179.
60. An K, Fattaey HK, Paulsen AQ, Consigli RA (2000) Murine polyomavirus infection of 3T6 mouse cells shows evidence of predominant necrosis as well as limited apoptosis. Virus Res 67: 81-90.
61. Daniels R, Sadowicz D, Hebert DN (2007) A very late viral protein triggers the lytic release of SV40. PLoS Pathog 3: e98.
62. Sanjuan N, Porras A, Otero J (2003) Microtubule-dependent intracellular transport of murine polyomavirus. Virology 313: 105-116.
63. Knipe DM, Howley PM, Griffin DE, R.A. L, Martin MA, et al. (2001) Fields Virology, 4th Edition. Philadelphia Lippincott Williams & Wilkins. 3280 p.
64. Butel JS, Lednicky JA (1999) Cell and molecular biology of simian virus 40: implications for human infections and disease. J Natl Cancer Inst 91: 119-134.
65. Wirth JJ, Chen L, Fluck MM (2000) Systemic polyomavirus genome increase and dissemination of capsid-defective genomes in mammary gland tumor-bearing mice. J Virol 74: 6975-6983.
66. Erickson KD, Bouchet-Marquis C, Heiser K, Szomolanyi-Tsuda E, Mishra R, et al. (2012) Virion assembly factories in the nucleus of polyomavirus-infected cells. PLoS Pathog 8: e1002630.
67. Liddington RC, Yan Y, Moulai J, Sahli R, Benjamin TL, et al. (1991) Structure of simian virus 40 at 3.8-A resolution. Nature 354: 278-284.
68. Stehle T, Gamblin SJ, Yan Y, Harrison SC (1996) The structure of simian virus 40 refined at 3.1 A resolution. Structure 4: 165-182.
69. Stehle T, Yan Y, Benjamin TL, Harrison SC (1994) Structure of murine polyomavirus complexed with an oligosaccharide receptor fragment. Nature 369: 160-163.

70. Barouch DH, Harrison SC (1994) Interactions among the major and minor coat proteins of polyomavirus. J Virol 68: 3982-3989.
71. Chen XS, Stehle T, Harrison SC (1998) Interaction of polyomavirus internal protein VP2 with the major capsid protein VP1 and implications for participation of VP2 in viral entry. EMBO J 17: 3233-3240.
72. Cremisi C, Pignatti PF, Yaniv M (1976) Random location and absence of movement of the nucleosomes on SV 40 nucleoprotein complex isolated from infected cells. Biochem Biophys Res Commun 73: 548-554.
73. Griffith J, Dieckmann M, Berg P (1975) Electron microscope localization of a protein bound near the origin of simian virus 40 DNA replication. J Virol 15: 167-172.
74. Christiansen G, Landers T, Griffith J, Berg P (1977) Characterization of components released by alkali disruption of simian virus 40. J Virol 21: 1079-1084.
75. Soussi T (1986) DNA-binding properties of the major structural protein of simian virus 40. J Virol 59: 740-742.
76. Moreland RB, Montross L, Garcea RL (1991) Characterization of the DNA-binding properties of the polyomavirus capsid protein VP1. J Virol 65: 1168-1176.
77. Chang D, Cai X, Consigli RA (1993) Characterization of the DNA binding properties of polyomavirus capsid protein. J Virol 67: 6327-6331.
78. Clever J, Dean DA, Kasamatsu H (1993) Identification of a DNA binding domain in simian virus 40 capsid proteins Vp2 and Vp3. J Biol Chem 268: 20877-20883.
79. Schowalter RM, Buck CB (2013) The Merkel cell polyomavirus minor capsid protein. PLoS Pathog 9: e1003558.
80. Yan Y, Stehle T, Liddington RC, Zhao H, Harrison SC (1996) Structure determination of simian virus 40 and murine polyomavirus by a combination of 30-fold and 5-fold electron-density averaging. Structure 4: 157-164.
81. Qian M, Cai D, Verhey KJ, Tsai B (2009) A lipid receptor sorts polyomavirus from the endolysosome to the endoplasmic reticulum to cause infection. PLoS Pathog 5: e1000465.
82. Qian M, Tsai B (2010) Lipids and proteins act in opposing manners to regulate polyomavirus infection. J Virol 84: 9840-9852.
83. Fried H, Cahan LD, Paulson JC (1981) Polyoma virus recognizes specific sialyligosaccharide receptors on host cells. Virology 109: 188-192.
84. Stehle T, Harrison SC (1996) Crystal structures of murine polyomavirus in complex with straight-chain and branched-chain sialyloligosaccharide receptor fragments. Structure 4: 183-194.
85. Komagome R, Sawa H, Suzuki T, Suzuki Y, Tanaka S, et al. (2002) Oligosaccharides as receptors for JC virus. J Virol 76: 12992-13000.
86. Low JA, Magnuson B, Tsai B, Imperiale MJ (2006) Identification of gangliosides GD1b and GT1b as receptors for BK virus. J Virol 80: 1361-1366.
87. Tsai B, Gilbert JM, Stehle T, Lencer W, Benjamin TL, et al. (2003) Gangliosides are receptors for murine polyoma virus and SV40. EMBO J 22: 4346-4355.
88. Erickson KD, Garcea RL, Tsai B (2009) Ganglioside GT1b is a putative host cell receptor for the Merkel cell polyomavirus. J Virol 83: 10275-10279.
89. Elphick GF, Querbes W, Jordan JA, Gee GV, Eash S, et al. (2004) The human polyomavirus, JCV, uses serotonin receptors to infect cells. Science 306: 1380-1383.
90. Ichikawa S, Nakajo N, Sakiyama H, Hirabayashi Y (1994) A mouse B16 melanoma mutant deficient in glycolipids. Proc Natl Acad Sci U S A 91: 2703-2707.
91. Stergiou L, Bauer M, Mair W, Bausch-Fluck D, Drayman N, et al. (2013) Integrin-mediated signaling induced by simian virus 40 leads to transient uncoupling of cortical actin and the plasma membrane. PLoS One 8: e55799.
92. Caruso M, Belloni L, Sthandier O, Amati P, Garcia MI (2003) Alpha4beta1 integrin acts as a cell receptor for murine polyomavirus at the postattachment level. J Virol 77: 3913-3921.

93. Caruso M, Busanello A, Sthandier O, Cavaldesi M, Gentile M, et al. (2007) Mutation in the VP1-LDV motif of the murine polyomavirus affects viral infectivity and conditions virus tissue tropism in vivo. J Mol Biol 367: 54-64.
94. Breau WC, Atwood WJ, Norkin LC (1992) Class I major histocompatibility proteins are an essential component of the simian virus 40 receptor. J Virol 66: 2037-2045.
95. Atwood WJ, Norkin LC (1989) Class I major histocompatibility proteins as cell surface receptors for simian virus 40. J Virol 63: 4474-4477.
96. Dugan AS, Eash S, Atwood WJ (2005) An N-linked glycoprotein with alpha(2,3)-linked sialic acid is a receptor for BK virus. J Virol 79: 14442-14445.
97. Dugan AS, Gasparovic ML, Atwood WJ (2008) Direct correlation between sialic acid binding and infection of cells by two human polyomaviruses (JC virus and BK virus). J Virol 82: 2560-2564.
98. Liu CK, Wei G, Atwood WJ (1998) Infection of glial cells by the human polyomavirus JC is mediated by an N-linked glycoprotein containing terminal alpha(2-6)-linked sialic acids. J Virol 72: 4643-4649.
99. Taube S, Jiang M, Wobus CE (2010) Glycosphingolipids as receptors for non-enveloped viruses. Viruses 2: 1011-1049.
100. Kartenbeck J, Stukenbrok H, Helenius A (1989) Endocytosis of simian virus 40 into the endoplasmic reticulum. J Cell Biol 109: 2721-2729.
101. Mackay RL, Consigli RA (1976) Early events in polyoma virus infection: attachment, penetration, and nuclear entry. J Virol 19: 620-636.
102. Pho MT, Ashok A, Atwood WJ (2000) JC virus enters human glial cells by clathrin-dependent receptor-mediated endocytosis. J Virol 74: 2288-2292.
103. Harder T, Simons K (1997) Caveolae, DIGs, and the dynamics of sphingolipid-cholesterol microdomains. Current Opinion in Cell Biology 9: 534-542.
104. Simons K, Ikonen E (1997) Functional rafts in cell membranes. Nature 387: 569-572.
105. Eash S, Querbes W, Atwood WJ (2004) Infection of vero cells by BK virus is dependent on caveolae. J Virol 78: 11583-11590.
106. Pelkmans L, Puntener D, Helenius A (2002) Local actin polymerization and dynamin recruitment in SV40-induced internalization of caveolae. Science 296: 535-539.
107. Henley JR, Krueger EW, Oswald BJ, McNiven MA (1998) Dynamin-mediated internalization of caveolae. J Cell Biol 141: 85-99.
108. Oh P, McIntosh DP, Schnitzer JE (1998) Dynamin at the neck of caveolae mediates their budding to form transport vesicles by GTP-driven fission from the plasma membrane of endothelium. J Cell Biol 141: 101-114.
109. Damm EM, Pelkmans L, Kartenbeck J, Mezzacasa A, Kurzchalia T, et al. (2005) Clathrin- and caveolin-1-independent endocytosis: entry of simian virus 40 into cells devoid of caveolae. J Cell Biol 168: 477-488.
110. Ewers H, Romer W, Smith AE, Bacia K, Dmitrieff S, et al. (2010) GM1 structure determines SV40-induced membrane invagination and infection. Nat Cell Biol 12: 11-18; sup pp 11-12.
111. Dangoria NS, Breau WC, Anderson HA, Cishek DM, Norkin LC (1996) Extracellular simian virus 40 induces an ERK/MAP kinase-independent signalling pathway that activates primary response genes and promotes virus entry. J Gen Virol 77 (Pt 9): 2173-2182.
112. Richards AA, Stang E, Pepperkok R, Parton RG (2002) Inhibitors of COP-mediated transport and cholera toxin action inhibit simian virus 40 infection. Mol Biol Cell 13: 1750-1764.
113. Gilbert JM, Goldberg IG, Benjamin TL (2003) Cell penetration and trafficking of polyomavirus. J Virol 77: 2615-2622.
114. Krauzewicz N, Stokrova J, Jenkins C, Elliott M, Higgins CF, et al. (2000) Virus-like gene transfer into cells mediated by polyoma virus pseudocapsids. Gene Ther 7: 2122-2131.
115. Hossain DM, Mohanty S, Ray P, Das T, Sa G (2012) Tumor gangliosides and T cells: a deadly encounter. Front Biosci (Schol Ed) 4: 502-519.

116. Vazquez-Calvo A, Saiz JC, McCullough KC, Sobrino F, Martin-Acebes MA (2012) Acid-dependent viral entry. Virus Res 167: 125-137.
117. Gilbert J, Ou W, Silver J, Benjamin T (2006) Downregulation of protein disulfide isomerase inhibits infection by the mouse polyomavirus. J Virol 80: 10868-10870.
118. Magnuson B, Rainey EK, Benjamin T, Baryshev M, Mkrtchian S, et al. (2005) ERp29 triggers a conformational change in polyomavirus to stimulate membrane binding. Mol Cell 20: 289-300.
119. Schelhaas M, Malmstrom J, Pelkmans L, Haugstetter J, Ellgaard L, et al. (2007) Simian Virus 40 depends on ER protein folding and quality control factors for entry into host cells. Cell 131: 516-529.
120. Walczak CP, Tsai B (2011) A PDI family network acts distinctly and coordinately with ERp29 to facilitate polyomavirus infection. J Virol 85: 2386-2396.
121. Jiang M, Abend JR, Tsai B, Imperiale MJ (2009) Early events during BK virus entry and disassembly. J Virol 83: 1350-1358.
122. Querbes W, O'Hara BA, Williams G, Atwood WJ (2006) Invasion of host cells by JC virus identities a novel role for caveolae in endosomal sorting of noncaveolar ligands. Journal of Virology 80: 9402-9413.
123. Hayer A, Stoeber M, Ritz D, Engel S, Meyer HH, et al. (2010) Caveolin-1 is ubiquitinated and targeted to intralumenal vesicles in endolysosomes for degradation. J Cell Biol 191: 615-629.
124. Norkin LC, Anderson HA, Wolfrom SA, Oppenheim A (2002) Caveolar endocytosis of simian virus 40 is followed by brefeldin A-sensitive transport to the endoplasmic reticulum, where the virus disassembles. J Virol 76: 5156-5166.
125. Norkin LC, Kuksin D (2005) The caveolae-mediated sv40 entry pathway bypasses the golgi complex en route to the endoplasmic reticulum. Virol J 2: 38.
126. Sandvig K, van Deurs B (2002) Transport of protein toxins into cells: pathways used by ricin, cholera toxin and Shiga toxin. FEBS Lett 529: 49-53.
127. Lippincott-Schwartz J, Yuan L, Tipper C, Amherdt M, Orci L, et al. (1991) Brefeldin A's effects on endosomes, lysosomes, and the TGN suggest a general mechanism for regulating organelle structure and membrane traffic. Cell 67: 601-616.
128. Tooze J, Hollinshead M (1992) In AtT20 and HeLa cells brefeldin A induces the fusion of tubular endosomes and changes their distribution and some of their endocytic properties. J Cell Biol 118: 813-830.
129. Aniento F, Emans N, Griffiths G, Gruenberg J (1993) Cytoplasmic dynein-dependent vesicular transport from early to late endosomes. J Cell Biol 123: 1373-1387.
130. Bayer N, Schober D, Prchla E, Murphy RF, Blaas D, et al. (1998) Effect of bafilomycin A1 and nocodazole on endocytic transport in HeLa cells: implications for viral uncoating and infection. J Virol 72: 9645-9655.
131. Baravalle G, Schober D, Huber M, Bayer N, Murphy RF, et al. (2005) Transferrin recycling and dextran transport to lysosomes is differentially affected by bafilomycin, nocodazole, and low temperature. Cell Tissue Res 320: 99-113.
132. Driskell OJ, Mironov A, Allan VJ, Woodman PG (2007) Dynein is required for receptor sorting and the morphogenesis of early endosomes. Nat Cell Biol 9: 113-120.
133. Eash S, Atwood WJ (2005) Involvement of cytoskeletal components in BK virus infectious entry. J Virol 79: 11734-11741.
134. Moriyama T, Sorokin A (2008) Intracellular trafficking pathway of BK Virus in human renal proximal tubular epithelial cells. Virology 371: 336-349.
135. Shimura H, Umeno Y, Kimura G (1987) Effects of inhibitors of the cytoplasmic structures and functions on the early phase of infection of cultured cells with simian virus 40. Virology 158: 34-43.
136. Huotari J, Helenius A (2011) Endosome maturation. EMBO J 30: 3481-3500.
137. Kobiler O, Drayman N, Butin-Israeli V, Oppenheim A (2012) Virus strategies for passing the nuclear envelope barrier. Nucleus 3: 526-539.

138. Rabe B, Delaleau M, Bischof A, Foss M, Sominskaya I, et al. (2009) Nuclear entry of hepatitis B virus capsids involves disintegration to protein dimers followed by nuclear reassociation to capsids. PLoS Pathog 5: e1000563.
139. Cohen S, Marr AK, Garcin P, Pante N (2011) Nuclear envelope disruption involving host caspases plays a role in the parvovirus replication cycle. J Virol 85: 4863-4874.
140. Cohen S, Pante N (2005) Pushing the envelope: microinjection of Minute virus of mice into Xenopus oocytes causes damage to the nuclear envelope. J Gen Virol 86: 3243-3252.
141. Lombardo E, Ramirez JC, Garcia J, Almendral JM (2002) Complementary roles of multiple nuclear targeting signals in the capsid proteins of the parvovirus minute virus of mice during assembly and onset of infection. J Virol 76: 7049-7059.
142. Lilley BN, Gilbert JM, Ploegh HL, Benjamin TL (2006) Murine polyomavirus requires the endoplasmic reticulum protein Derlin-2 to initiate infection. J Virol 80: 8739-8744.
143. Goodwin EC, Lipovsky A, Inoue T, Magaldi TG, Edwards AP, et al. (2011) BiP and multiple DNAJ molecular chaperones in the endoplasmic reticulum are required for efficient simian virus 40 infection. MBio 2: e00101-00111.
144. Inoue T, Tsai B (2011) A large and intact viral particle penetrates the endoplasmic reticulum membrane to reach the cytosol. PLoS Pathog 7: e1002037.
145. Nakanishi A, Itoh N, Li PP, Handa H, Liddington RC, et al. (2007) Minor capsid proteins of simian virus 40 are dispensable for nucleocapsid assembly and cell entry but are required for nuclear entry of the viral genome. J Virol 81: 3778-3785.
146. Nakanishi A, Nakamura A, Liddington R, Kasamatsu H (2006) Identification of amino acid residues within simian virus 40 capsid proteins Vp1, Vp2, and Vp3 that are required for their interaction and for viral infection. J Virol 80: 8891-8898.
147. Daniels R, Rusan NM, Wadsworth P, Hebert DN (2006) SV40 VP2 and VP3 insertion into ER membranes is controlled by the capsid protein VP1: implications for DNA translocation out of the ER. Mol Cell 24: 955-966.
148. Dohner K, Wolfstein A, Prank U, Echeverri C, Dujardin D, et al. (2002) Function of dynein and dynactin in herpes simplex virus capsid transport. Mol Biol Cell 13: 2795-2809.
149. Wozniak MJ, Allan VJ (2006) Cargo selection by specific kinesin light chain 1 isoforms. EMBO J 25: 5457-5468.
150. Wozniak MJ, Bola B, Brownhill K, Yang YC, Levakova V, et al. (2009) Role of kinesin-1 and cytoplasmic dynein in endoplasmic reticulum movement in VERO cells. J Cell Sci 122: 1979-1989.
151. Brown CL, Maier KC, Stauber T, Ginkel LM, Wordeman L, et al. (2005) Kinesin-2 is a motor for late endosomes and lysosomes. Traffic 6: 1114-1124.
152. Ginkel LM, Wordeman L (2000) Expression and partial characterization of kinesin-related proteins in differentiating and adult skeletal muscle. Mol Biol Cell 11: 4143-4158.
153. Sonnichsen B, De Renzis S, Nielsen E, Rietdorf J, Zerial M (2000) Distinct membrane domains on endosomes in the recycling pathway visualized by multicolor imaging of Rab4, Rab5, and Rab11. J Cell Biol 149: 901-914.
154. Bucci C, Thomsen P, Nicoziani P, McCarthy J, van Deurs B (2000) Rab7: a key to lysosome biogenesis. Mol Biol Cell 11: 467-480.
155. Li G, Stahl PD (1993) Structure-function relationship of the small GTPase rab5. J Biol Chem 268: 24475-24480.
156. Krauzewicz N, Streuli CH, Stuart-Smith N, Jones MD, Wallace S, et al. (1990) Myristylated polyomavirus VP2: role in the life cycle of the virus. J Virol 64: 4414-4420.
157. Huerfano S, Zila V, Boura E, Spanielova H, Stokrova J, et al. (2010) Minor capsid proteins of mouse polyomavirus are inducers of apoptosis when produced individually but are only moderate contributors to cell death during the late phase of viral infection. FEBS J 277: 1270-1283.

158. Türler H, Beard P (1985) Simian virus 40 and polyoma virus: growth, titration, transformation and purification of viral components. In: Mahy B, editor. Virology: a practical approach. Oxford, Washington DC: IRL Press. pp. 169-192.
159. Brankatschk B, Pons V, Parton RG, Gruenberg J (2011) Role of SNX16 in the dynamics of tubulo-cisternal membrane domains of late endosomes. PLoS One 6: e21771.
160. Zhou AY, Ichaso N, Adamarek A, Zila V, Forstova J, et al. (2011) Polyomavirus middle T-antigen is a transmembrane protein that binds signaling proteins in discrete subcellular membrane sites. J Virol 85: 3046-3054.
161. Zila V, Difato F, Klimova L, Huerfano S, Forstova J (2014) Involvement of microtubular network and its motors in productive endocytic trafficking of mouse polyomavirus. PLoS One 9: e96922.
162. Benesch S, Lommel S, Steffen A, Stradal TE, Scaplehorn N, et al. (2002) Phosphatidylinositol 4,5-biphosphate (PIP2)-induced vesicle movement depends on N-WASP and involves Nck, WIP, and Grb2. J Biol Chem 277: 37771-37776.
163. Orth JD, Krueger EW, Cao H, McNiven MA (2002) The large GTPase dynamin regulates actin comet formation and movement in living cells. Proc Natl Acad Sci U S A 99: 167-172.
164. Welsch T, Endlich N, Gokce G, Doroshenko E, Simpson JC, et al. (2005) Association of CD2AP with dynamic actin on vesicles in podocytes. Am J Physiol Renal Physiol 289: F1134-1143.
165. Block SM, Goldstein LS, Schnapp BJ (1990) Bead movement by single kinesin molecules studied with optical tweezers. Nature 348: 348-352.
166. Echeverri CJ, Paschal BM, Vaughan KT, Vallee RB (1996) Molecular characterization of the 50-kD subunit of dynactin reveals function for the complex in chromosome alignment and spindle organization during mitosis. J Cell Biol 132: 617-633.
167. Burkhardt JK, Echeverri CJ, Nilsson T, Vallee RB (1997) Overexpression of the dynamitin (p50) subunit of the dynactin complex disrupts dynein-dependent maintenance of membrane organelle distribution. J Cell Biol 139: 469-484.
168. Presley JF, Cole NB, Schroer TA, Hirschberg K, Zaal KJ, et al. (1997) ER-to-Golgi transport visualized in living cells. Nature 389: 81-85.
169. Coy DL, Hancock WO, Wagenbach M, Howard J (1999) Kinesin's tail domain is an inhibitory regulator of the motor domain. Nat Cell Biol 1: 288-292.
170. Botos E, Klumperman J, Oorschot V, Igyarto B, Magyar A, et al. (2008) Caveolin-1 is transported to multi-vesicular bodies after albumin-induced endocytosis of caveolae in HepG2 cells. J Cell Mol Med 12: 1632-1639.
171. Kiss AL, Botos E (2009) Ocadaic acid retains caveolae in multicaveolar clusters. Pathol Oncol Res 15: 479-486.
172. Ren M, Xu G, Zeng J, De Lemos-Chiarandini C, Adesnik M, et al. (1998) Hydrolysis of GTP on rab11 is required for the direct delivery of transferrin from the pericentriolar recycling compartment to the cell surface but not from sorting endosomes. Proc Natl Acad Sci U S A 95: 6187-6192.
173. Holtta-Vuori M, Tanhuanpaa K, Mobius W, Somerharju P, Ikonen E (2002) Modulation of cellular cholesterol transport and homeostasis by Rab11. Mol Biol Cell 13: 3107-3122.
174. Kerr JF, Wyllie AH, Currie AR (1972) Apoptosis: a basic biological phenomenon with wide-ranging implications in tissue kinetics. Br J Cancer 26: 239-257.
175. Lakadamyali M, Rust MJ, Babcock HP, Zhuang X (2003) Visualizing infection of individual influenza viruses. Proc Natl Acad Sci U S A 100: 9280-9285.
176. Loubery S, Wilhelm C, Hurbain I, Neveu S, Louvard D, et al. (2008) Different microtubule motors move early and late endocytic compartments. Traffic 9: 492-509.
177. Echarri A, Muriel O, Pavon DM, Azegrouz H, Escolar F, et al. (2012) Caveolar domain organization and trafficking is regulated by Abl kinases and mDia1. J Cell Sci 125: 3097-3113.
178. Pelkmans L, Burli T, Zerial M, Helenius A (2004) Caveolin-stabilized membrane domains as multifunctional transport and sorting devices in endocytic membrane traffic. Cell 118: 767-780.

179. Mundy DI, Li WP, Luby-Phelps K, Anderson RG (2012) Caveolin targeting to late endosome/lysosomal membranes is induced by perturbations of lysosomal pH and cholesterol content. Mol Biol Cell 23: 864-880.
180. Horgan CP, Hanscom SR, Jolly RS, Futter CE, McCaffrey MW (2010) Rab11-FIP3 links the Rab11 GTPase and cytoplasmic dynein to mediate transport to the endosomal-recycling compartment. J Cell Sci 123: 181-191.
181. Streuli CH, Griffin BE (1987) Myristic acid is coupled to a structural protein of polyoma virus and SV40. Nature 326: 619-622.
182. Palmer E, Freeman T (2004) Investigation into the use of C- and N-terminal GFP fusion proteins for subcellular localization studies using reverse transfection microarrays. Comp Funct Genomics 5: 342-353.
183. Boehning D, Patterson RL, Sedaghat L, Glebova NO, Kurosaki T, et al. (2003) Cytochrome c binds to inositol (1,4,5) trisphosphate receptors, amplifying calcium-dependent apoptosis. Nat Cell Biol 5: 1051-1061.
184. Mattson MP, Chan SL (2003) Calcium orchestrates apoptosis. Nat Cell Biol 5: 1041-1043.
185. Gonzalez ME, Carrasco L (2003) Viroporins. FEBS Lett 552: 28-34.

10. ATTACHMENTS

ATTACHMENT #1 – Zila et al., 2014

OPEN ACCESS Freely available online

PLOS ONE

Involvement of Microtubular Network and Its Motors in Productive Endocytic Trafficking of Mouse Polyomavirus

Vojtech Zila, Francesco Difato[¤a], Lucie Klimova[¤b], Sandra Huerfano, Jitka Forstova*

Department of Genetics and Microbiology, Faculty of Science, Charles University in Prague, Prague, Czech Republic

Abstract

Infection of non-enveloped polyomaviruses depends on an intact microtubular network. Here we focus on mouse polyomavirus (MPyV). We show that the dynamics of MPyV cytoplasmic transport reflects the characteristics of microtubular motor-driven transport with bi-directional saltatory movements. In cells treated with microtubule-disrupting agents, localization of MPyV was significantly perturbed, the virus was retained at the cell periphery, mostly within membrane structures resembling multicaveolar complexes, and at later times post-infection, only a fraction of the virus was found in Rab7-positive endosomes and multivesicular bodies. Inhibition of cytoplasmic dynein-based motility by overexpression of dynamitin affected perinuclear translocation of the virus, delivery of virions to the ER and substantially reduced the numbers of infected cells, while overexpression of dominant-negative form of kinesin-1 or kinesin-2 had no significant impact on virus localization and infectivity. We also found that transport along microtubules was important for MPyV-containing endosome sequential acquisition of Rab5, Rab7 and Rab11 GTPases. However, in contrast to dominant-negative mutant of Rab7 (T22N), overexpression of dominant-negative mutant Rab11 (S25N) did not affect the virus infectivity. Altogether, our study revealed that MPyV cytoplasmic trafficking leading to productive infection bypasses recycling endosomes, does not require the function of kinesin-1 and kinesin-2, but depends on functional dynein-mediated transport along microtubules for translocation of the virions from peripheral, often caveolin-positive compartments to late endosomes and ER – a prerequisite for efficient delivery of the viral genome to the nucleus.

Citation: Zila V, Difato F, Klimova L, Huerfano S, Forstova J (2014) Involvement of Microtubular Network and Its Motors in Productive Endocytic Trafficking of Mouse Polyomavirus. PLoS ONE 9(5): e96922. doi:10.1371/journal.pone.0096922

Editor: Sara Salinas, CNRS, France

Received December 20, 2013; **Accepted** April 14, 2014; **Published** May 8, 2014

Funding: This study was supported by the Grant Agency of the Czech Republic (Project P302/13-26115S), by the Ministry of Education, Youth and Sports of the Czech Republic (Project SVV-2014-260081), by the Charles University in Prague (Project UNCE 204013) and by the project BIOCEV – Biotechnology and Biomedicine Centre of the Academy of Sciences and Charles University (CZ.1.05/1.1.00/02.0109), from the European Regional Development Fund. The funders had no role in study design, data collection and analysis, decision to publish, or preparation of the manuscript.

Competing Interests: The authors have declared that no competing interests exist.

* E-mail: jitkaf@natur.cuni.cz

¤a Current address: Department of Neuroscience and Brain Technologies, Istituto Italiano di Tecnologia, Genoa, Italy
¤b Current address: Department of Transcriptional Regulation, Institute of Molecular Genetics, Academy of Sciences of the Czech Republic, Prague, Czech Republic

Introduction

Mouse polyomavirus (MPyV) is a tumor virus belonging to the *Polyomaviridae* family, whose members are small non-enveloped DNA viruses replicating in the cell nucleus. MPyV enter cells by clathrin- and caveolae-independent endocytosis [1–3], through the interaction of the major viral capsid protein, VP1, with ganglioside receptors, GD1a or GT1b [4] that associate with lipid rafts [5,6]. Efficient uptake of MPyV also requires remodeling of the actin cytoskeleton [2,5,7]. Virions are internalized into smooth endocytic vesicles [3,6,8], often positive for caveolin-1 [5,6], and subsequently fuse with larger endosomes [3,5,6,9]. Like other polyomaviruses, MPyV virions do not escape the endosomal system until they reach the lumen of smooth endoplasmic reticulum (ER) [5,6,9,10], where lumenal enzymes facilitate virus capsid disassembly and uncoating of viral genomes prior to their import into the nucleus [11–13]. Regardless of the multiplicity of infection, only a few virions are able to deliver their genomic DNA into the cell nucleus [10]. Currently, two possible ways for viral genome delivery to the cell nucleus have been proposed: either partially disassembled virions translocate from ER to the cytosol and then are imported into the nucleus via nuclear pore complexes or, alternatively, they penetrate directly from ER to the nucleoplasm through the nuclear envelope (reviewed in [14]).

Infection of MPyV is dependent on an intact microtubular network and microtubule depolymerizing drugs such as nocodazole or colcemid block virus infectivity [2,5,15,16]. The virus infectious pathway to ER is directed from the plasma membrane by the ganglioside receptor [9,17] and requires acidic environment of the endosomes [3,9]. Previous reports pointed to the importance of virus transfer via early and late endosomal compartments as overexpression of dominant-negative mutant of Rab5 [3,9] or Rab7 GTPase [9] inhibited MPyV infection. On the other hand, caveolin-1, accompanying the internalization and trafficking of the subpopulation of MPyV virions towards the nucleus, is not required for virus infectivity [3]. Our previous studies reported the virus presence in perinuclear area of cells co-localizing there with Rab11 GTPase and with transferrin, markers of recycling endosomes [3,10], suggesting the possibility that transfer of MPyV via mildly acidic early endosomes and later via recycling endosomes represents an alternative endocytic pathway along microtubules that virions can use for genome delivery into the host cell nucleus.

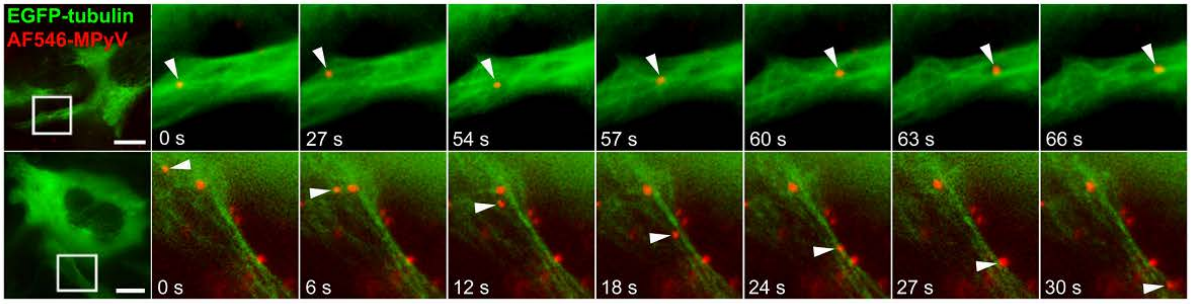

Figure 1. Tracking of MPyV in living cells expressing EGFP-fused tubulin. 3T6 cells expressing EGFP-tubulin (green) were infected with Alexa Fluor 546-labeled MPyV (red) (MOI of 10^2 to 10^3 virus particles per cell) at 37°C and scanned with $\Delta T = 3$ s. Virions were transported to both directions: to the nuclear periphery (upper panel) and to the cell periphery (lower panel). Selected frames from two different cells at 1 h p.i. are shown in detail (see Movie S1). Arrowheads point to MPyV virions. Bars, 10 µm. Cells were examined with an Olympus IX81 CellR microscope equipped with an MT20 illumination system.
doi:10.1371/journal.pone.0096922.g001

Intact microtubules are also essential for other polyomaviruses, including simian virus 40 (SV40), or human polyomaviruses BK virus (BKV) or JC virus (JCV) [18–24]. Although in some cells the trafficking of SV40 occurs in vesicles propelled by actin polymerization, functional microtubule-dependent transport was found to be essential for delivery of SV40 virions from acidic late endosomes to ER [23,25]. Similarly, involvement of microtubules in virus transport from acidic endosomes to the ER has been proposed for BKV [24]. It has been shown that microtubules mediate trafficking of MPyV from 'caveolin-1-positive environment' to the ER [5]. Authors of this study suggested that caveolin-1-rich compartments may represent so-called "caveosomes". However, since the caveosomes defined as caveolin-1-positive, pH-neutral organelles were recently identified as modified late endosomes or lysosomes [23,26], the involvement of microtubular network in endocytic trafficking of MPyV to early and premature late endosomes is not clear.

The requirement of intact microtubules for MPyV infection implies that specific microtubule-associated motor(s) play a key role in the intracellular trafficking of the virus, but these kinetic aspects of the MPyV infection pathway still remain to be determined. Microtubule-associated motors are essential for the function and spatio-temporal organization of the endosomal system. Opposing forces provided by dynein and kinesins are responsible for the oscillatory motion of endosomes along microtubules and are required for endosome trafficking towards the nucleus, plasma membrane or vesicular transport between other membrane compartments (reviewed in [27]). In contrast to JCV- and BKV-infected cells, where inhibition of dynein has an insignificant effect on virus infectivity [18,20], SV40 relies on functional dynein for infection at least in HeLa cells [23]. The possible role of kinesin-1 motor, which together with dynein is utilized by some other viruses for transport to the proximity of the nucleus (reviewed in [28]), or kinesin-2 motor, which together with dynein and kinesin-1 has been shown to be important for the motility of early and late endosomes (reviewed in [29]), has not yet been investigated for any polyomavirus.

In this study, we used confocal fluorescence microscopy of living cells to examine the dynamics of MPyV cytoplasmic trafficking. Further, we performed infectivity assays to test the effect of dominant-negative forms of dynein, kinesin-1 or kinesin-2 motor on MPyV productive transport and we used confocal and electron microscopy approaches to monitoring the involvement of microtubular network in transport of MPyV from the plasma membrane to classical endosomes and in subsequent virus delivery to the ER. Finally, we investigated whether virus transfer via recycling endosomes represents an alternative endocytic pathway along microtubules utilized by MPyV to reach the cell nucleus.

Results

MPyV Trafficking along Microtubular Tracks

We prepared a stable cell line of mouse 3T6 fibroblasts expressing α-tubulin fused with enhanced green fluorescent protein (EGFP) to follow the direct involvement of microtubules during MPyV trafficking in live cells. Cells expressing EGFP-tubulin were infected with fluorescently labeled MPyV and transport of virions along microtubules was followed at early stages (up to 2 h) post-infection (p.i.) by time-lapse fluorescence microscopy. We observed virus transport along microtubules soon after virus addition (20–30 min p.i.). Virions were moved along microtubules in a bi-directional manner, being transported into the cell interior but also back to the cell periphery (Figure 1, Movie S1). Although the virus cargo was transported in both directions (often along an identical microtubule), the virus fluorescent signal was found accumulated around the nucleus at later times post-infection (from ~3 h p.i.) (Movie S2). This observation indicates that MPyV transport to the vicinity of the nucleus is prevalent during a longer time span of trafficking.

Dynamics of MPyV Cytoplasmic Transport by Single Particle Tracking

To describe the dynamics of the MPyV trafficking, we performed single particle tracking analysis and mapped transport trajectories of fluorescently labeled virions in living 3T6 cells. In order to monitor the virus intracellular movement from infection start until the time when the virus appears in the proximity of the nucleus, we followed trafficking of virions from 30 min to 3 h p.i. As a control we performed the internalization assay, which showed that a considerable amount of virions (~50%) was already internalized after 30 min of infection and that the major part of the virus was internalized at 60 min p.i. (Figure S1). The presence of virions attached to the cell surface was taken into consideration during the virus tracking experiments (see Materials and Methods). Virus trajectories revealed complex patterns. They were not clearly oriented from the cell surface towards the nucleus, but instead, they displayed the characteristics of Brownian motion with fast random switching in velocities and direction of

movement (Figure 2A). The dynamics of virion transport was mostly saltatory – the fast forward movements were interrupted by short back-step movements or pausing at intervals (average pause duration of 40±6.5 s). Our measurements of movement velocities corresponded to approximately three main characteristic rates (trajectories and graphs in Figure 2B,C,D): i) slow movement (in a limited space) at rates up to 0.3 μm/s, ii) faster movement of virions with frequent velocity rate around 0.6 μm/s, and iii) fast, long-distance movement with peaks reaching rates of 1.2 μm/s – speed typical of motor-driven transport on microtubular tracks [30].

Following movements of more than 200 single virions in about 40 distinct cells, we computed the frequency of velocity rates. The most prevalent were slow movements (<0.2 μm/s) (Figure 2E), which can be assigned to pausing of virus-loaded vesicles on microtubule tracks before another motor was recruited (or activated), or to actin-driven motility of virus-carrying endosomes as the velocity of vesicles/endosomes propelled by actin polymerization reaches rates around 0.2 μm/s [31–33]. The association of slowly moved MPyV-loaded endosomes with assemblies of dynamic actin recruited at their membranes was confirmed in living EGFP-actin-expressing cells (Figure S2, Movie S3). During such a "stationary phase", we detected movement only in a limited range (0.5–1 μm). In contrast, fast, long-distance movements (up to 1.5 μm/s) were rare, with a distinct peak at 0.6 μm/s (Figure 2E). Our measurements of fast movements (≥0.6 μm/s) revealed that the average length of a single continuous movement was 2.5 μm (Figure 2F). Such values could correspond to recruitment of a single microtubular motor molecule on the transported vesicle and fit well with the processivity of individual kinesin or dynein molecule-mediated transport producing movements of approximately 1.5 μm before the motor dissociates from the microtubule [34]. We observed that events of faster (> 0.6 μm/s) long-range transport occurred exclusively for short time intervals and the time span of the movements was characterized by peaks at 3.3 and 7.2 s (Figure 2G). These data indicate that in the case of MPyV, the run length of the vesicle carrying the virus cargo-motor complex reflected an inherent microtubular motor processivity.

Dynein Motor is Essential for MPyV Infection and Virus Trafficking to the ER

The observation of the bi-directionality and dynamics of long-distance movements of single MPyV virions suggested the possible involvement of plus end-oriented kinesins and minus end-oriented dynein during virus endocytic trafficking towards the nucleus. We therefore investigated the role of dynein, kinesin-1 and kinesin-2 motor in productive trafficking of MPyV. The importance of the dynein motor for MPyV infection was tested by infectivity assays in 3T6 cells transiently overexpressing EGFP-fused dynamitin, as overexpression of dynamitin causes disassembly of the dynein-dynactin complex and thus inhibits dynein motor function [35–37]. The efficiency of infection of these cells was compared with that of control, mock-transfected cells and cells expressing EGFP alone. Compared to controls, overexpression of EGFP-dynamitin dramatically reduced the number of infected cells (more than 70% decrease) (Figure 3A). When confocal fluorescence microscopy was performed later (5 h) post-infection in dynamitin-EGFP expressing cells, substantial amounts of virions were still detected at the cell periphery (Figure 3B, right panel), while in mock-transfected cells, the virus was accumulated predominantly in perinuclear area (Figure 3B, left panel). To investigate the importance of kinesin-1 and kinesin-2 motor for MPyV infection, we performed infectivity assays in cells expressing their dominant-negative constructs. The function of kinesin-1 was inhibited by overexpression of the C-terminal domain of kinesin-1 heavy chain fused with red fluorescent protein (RFP-KHCct), as the expression of C-terminal segment inhibits kinesin-1-driven microtubule activity by binding to the kinesin motor domain [38–40]. The kinesin-2 motor was inhibited by overexpression of EGFP-fused dominant-negative subunits of kinesin-2, motorless KIF3A subunit (EGFP-KIF3A-HL), or C-terminus of KAP3 subunit (EGFP-KAP3-CT) [41,42]. For control, we infected mock-transfected cells, cells expressing RFP-fused form of kinesin-1 light chain (RFP-DTC) as negative control for kinesin-1 [39,40], and cells expressing EGFP alone as a control for EGFP-fused kinesin-2 constructs. Production of dominant-negative kinesin-1 or kinesin-2 did not reduce the virus infectivity. Moreover, a slight increase in the number of infected cells was detected when compared to controls (Figure 3C). Confocal microscopy of cells producing dominant-negative kinesin-1 or kinesin-2 performed at 5 h p.i. did not reveal any significant difference in virus localization when compared to mock-transfected cells (Figure 3D). Together, these results indicate that transport mediated by the dynein motor is critical for MPyV infection and its perinuclear sorting, whereas the function of kinesin-1 or kinesin-2 is dispensable.

As we observed reduced MPyV infectivity in dynamitin-overexpressing cells, we next investigated the involvement of the dynein motor in delivery of MPyV virions to the ER. For this, we infected dynamitin-EGFP-expressing cells and fixed them 5 h p.i. In the cells we followed and quantified co-localization of individual MPyV virions with the BiP (GRP78) protein as a marker of ER and compared it with that in control, mock-transfected cells. Co-localization of the VP1 signal of MPyV virions with the fluorescent signal of BiP protein was quantified from confocal images such as those shown in Figure 4A, as explained in Materials and Methods. The quantification revealed that inhibition of the dynein motor function by overexpression of dynamitin significantly reduced virus co-localization with BiP (by 40–50%) when compared to that in control cells (Figure 4B). We thus conclude that the dynein motor function is essential for the delivery of MPyV to ER.

Microtubules are Important for Trafficking of MPyV to Endosomes

Investigation of SV40 trafficking showed that transport of the virus to early and premature late endosomes is independent of intact microtubules and that microtubules are required later for maturation of SV40-carrying late endosomes and subsequent virus delivery to the ER [23]. However, the above-described effect of overexpression of dynamitin-EGFP on MPyV intracellular localization suggests that dynein-mediated transport is required soon after virus internalization for virus trafficking from the plasma membrane to endosomes. To dissect the involvement of microtubules or actin cytoskeleton in the presence of MPyV in individual endocytic compartments, we infected 3T6 cells (non-transfected or expressing EGFP-fused marker of interest) in the absence or presence of compounds selectively affecting the structure and dynamics of microtubules (nocodazole) or actin cytoskeleton (latrunculin A) and fixed them 5 h p.i. In the cells we followed and quantified tendencies in co-localization of individual MPyV virions with endocytic markers previously shown to be involved in trafficking of MPyV towards the nucleus: caveolin-1 for caveolar or other compartments functionally connected to lipid rafts, EGFP-Rab5 GTPase for early endosomes, EGFP-Rab7 GTPase for late endosomes, EGFP-Rab11 GTPase for recycling endosomes, and BiP protein as ER marker.

In non-treated control cells at 5 h p.i., virions co-localized with all of the tested markers (Figure 5A–E). Quantification of co-

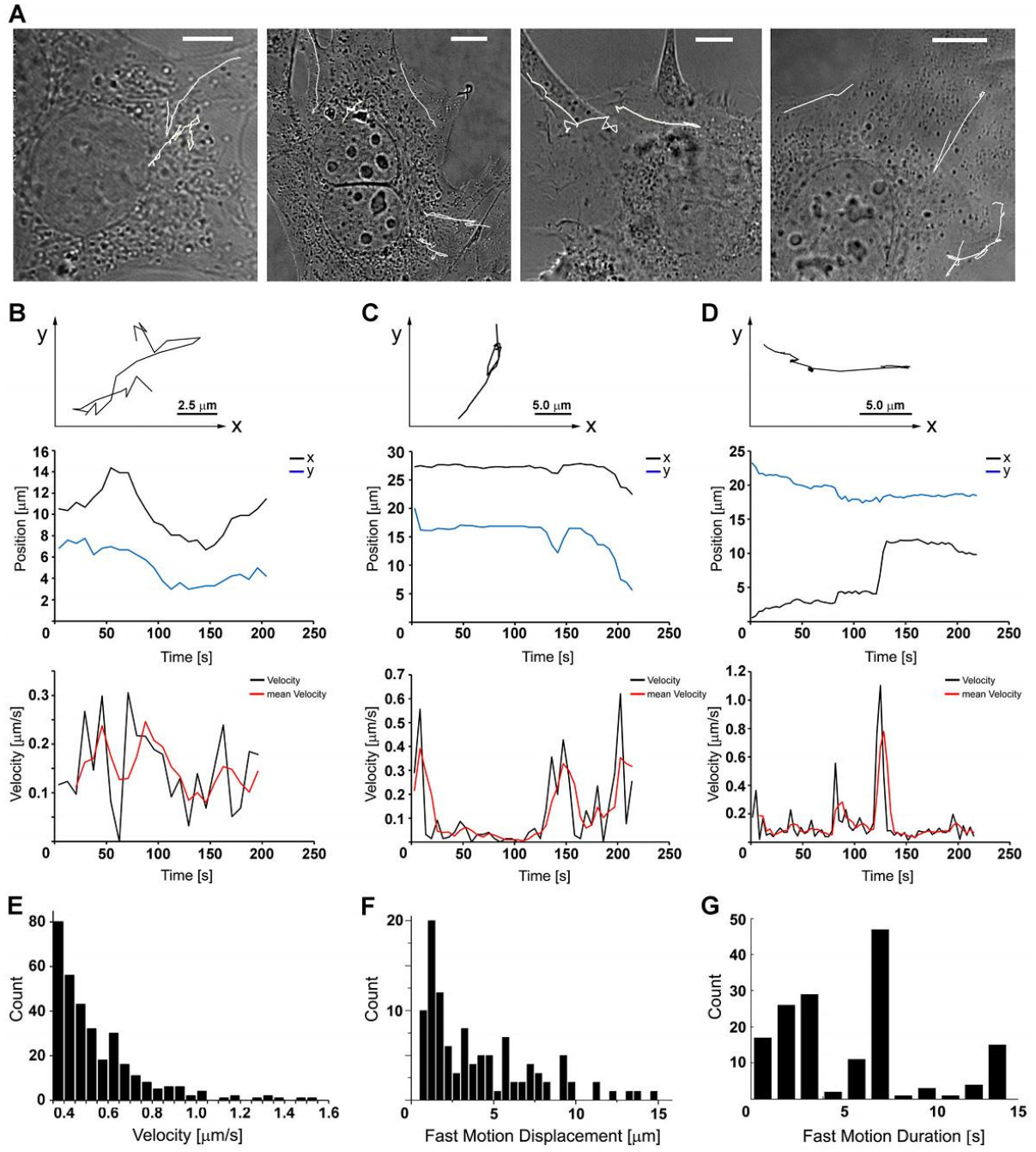

Figure 2. Single particle tracking analysis of MPyV transport. 3T6 cells were infected with Alexa Fluor 546-labeled MPyV (MOI of 10^2 to 10^3 virus particles per cell) at 37°C and scanned with $\Delta T = 6$ s. (A) Complex trajectories marked in white tracking curves in four selected cells shown in transmission light. Bars, 5 μm. (B–D) Dynamics of three independent single particle trackings (upper graphs) representing three main types of virion transport velocities with single particle position tracking in x-y coordinates (middle graphs) and course of movement velocities (lower graphs) measured at time intervals of 6 s (mean velocity was averaged from each three following time steps). (E) Frequency of virion transport velocity rates, counted from more than 200 different tracking experiments in 3T6 cells, with a distinct peak at 0.6 μm/s (x-coordinate was cropped to cut off the high frequency of short-range movements at rates <0.3 μm/s). (F) Histogram of fast movement distances counted from 109 single fast movements and sampled into 0.5 μm step intervals, with a maximum at 1.5 μm and the average distance of 2.5 μm. (G) Time span frequency of fast (≥0.6 μm/s) movements with maximum counts at 3.3 and 7.2 s.
doi:10.1371/journal.pone.0096922.g002

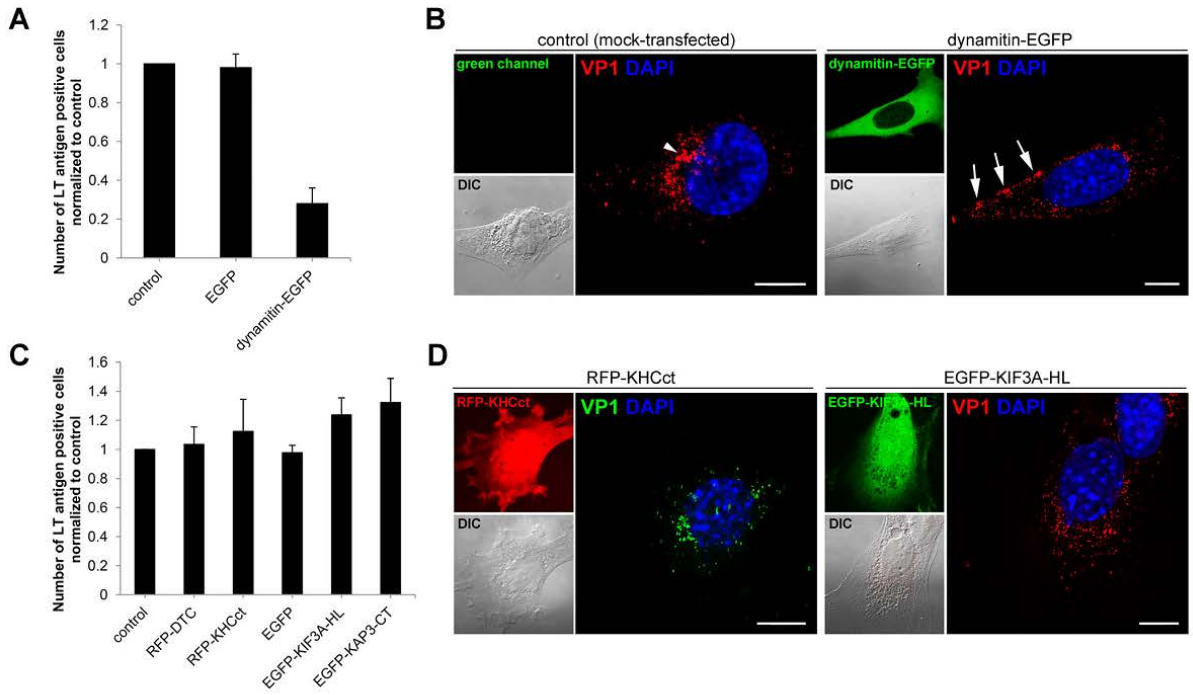

Figure 3. Role of microtubular motors in MPyV productive trafficking. (A and C) 3T6 cells were transfected with: (A) plasmid DNA for transient expression of EGFP (pEGFP-N1) or dynamitin-EGFP (inhibiting the dynein motor function) or (C) plasmid DNA for transient expression of RFP-DTC protein (pRFP-DTC), RFP-fused C-terminal fragment of kinesin-1 (pRFP-KHCct; inhibiting kinesin-1 motor function), EGFP (pEGFP-N1) or EGFP-fused dominant-negative subunits of kinesin-2 (pEGFP-KIF3A-HL or pEGFP-KAP3-CT). Cells expressing constructs were infected with MPyV, incubated until 24 h p.i., fixed and immunostained for MPyV LT antigen. The efficiency of infection was determined by levels (%) of LT antigen-positive cells normalized to that obtained in control, mock-transfected cells. During the experiment, more than 500 cells were counted for each sample. Data in the graphs represent mean values ± s.d. from three independent experiments. (B and D) Control, mock-transfected cells, or cells expressing dynamitin-EGFP, RFP-KHCct or EGFP-KIF3A-HL, infected with MPyV (MOI of 10^3 virus particles per cell), fixed 5 h p.i. and immunostained for MPyV VP1 capsid protein. DNA in nuclei was stained with DAPI (blue). Confocal sections of representative cells with corresponding signal in green or red channel and differential interference contrast (DIC) images are presented (the virus localization during EGFP-KIF3A-CT expression is not presented as it was similar to that in cells expressing the -HL form of kinesin-2). Arrowhead point to the virus at nuclear periphery. Arrows point to the virions at cell periphery. Bars, 10 μm.
doi:10.1371/journal.pone.0096922.g003

localization in control cells (Figure 5F, light grey bars) revealed that the highest percentage of virions co-localized with caveolin-1 (40.3±2.6%), but a substantial amount also co-localized with EGFP-Rab7 (26.5±2.9%) and small virus populations co-localized with EGFP-Rab11 (14.9±0.9%) and BiP (13.1±2.7%). Only residual co-localization of MPyV with early endosomal marker EGFP-Rab5 (5.9±1.6%) was detected at 5 h p.i. In the presence of microtubule-disrupting drug nocodazole (Figure 5F, dark grey bars), virus co-localization with caveolin-1 increased by 20% (to 48.4±2.9%), and a minor fraction of virions also co-localized with EGFP-Rab7 GTPase (13.2±2.5%). Only sporadic virions (~2%) co-localized with other tested markers (EGFP-Rab5, EGFP-Rab11, BiP). In contrast, in cells with actin cytoskeleton disrupted by latrunculin A (Figure 5F, black bars), MPyV co-localization with caveolin-1 dropped by ~50% (to 22.8±2.0%), while its co-localization with EGFP-Rab5 (8.0±2.4%), EGFP-Rab7 (40.1±4.1%), EGFP-Rab11 (20.1±2.7%) and BiP (18.3±5.2%) increased by 30–50% when compared to that in untreated cells. As the presence of the virions in early endosomes was sporadic even in control cells at 5 h p.i., we performed co-localization analysis earlier, at 1.5 h p.i., when a higher population of virions could be expected to co-localize with Rab5 GTPase. In untreated cells at that time p.i., a minor virus population co-localized with EGFP-Rab5 (12.2±2.2%). Virus co-localization with EGFP-Rab5 was markedly reduced in the presence of nocodazole (to 4.5±1.1%), and substantially increased (by 60%) in the presence of latrunculin A (to 19.5±3.6%) (Figure 5G).

These data demonstrate that disruption of microtubules by nocodazole significantly perturbed the virus presence in endosomes positive for Rab5, Rab7 and Rab11 GTPases and in the ER. The presence of latrunculin A apparently enhanced the efficiency of microtubule-mediated transport, and thus a higher percentage of virions co-localized with Rab5 and later post-infection with Rab7, Rab11 and BiP when compared to control untreated cells. We thus conclude that dynein-mediated transport along microtubules is important already for trafficking of MPyV from the plasma membrane to endosomes of classical endocytic pathways, while the actin meshwork rather represents a barrier that slows down the rate of virus endocytic transport and is connected with accumulation of the virions in caveolin-1-positive compartments.

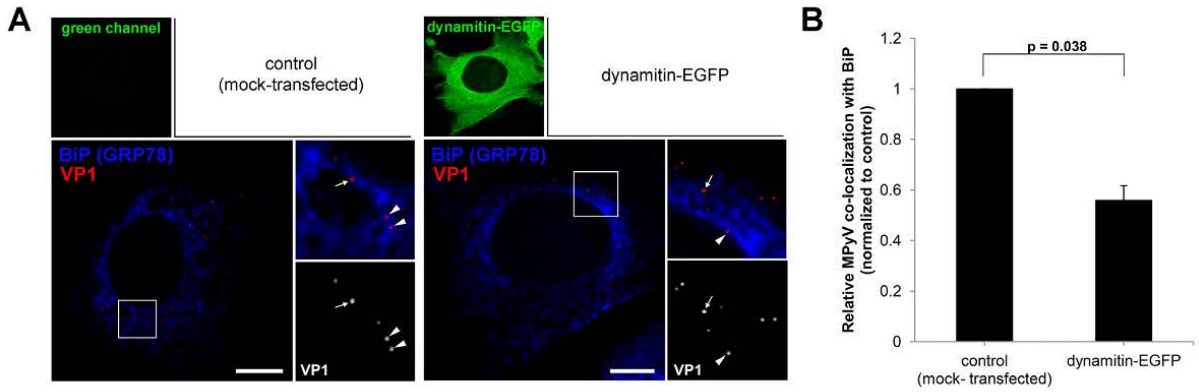

Figure 4. Dynein motor is required for trafficking of MPyV to the ER. 3T6 cells were transfected with plasmid DNA for expression of dynamitin-EGFP, infected with MPyV (MOI of 5×10^2 virus particles per cell) and fixed 5 h p.i. Cells were immunostained for MPyV VP1 capsid protein (red) and BiP (GRP78) marker of ER (blue). (A) Confocal sections of representative control (mock-transfected) cells and dynamitin-EGFP expressing cells at 5 h p.i. with enlarged details. Arrowheads point to selected MPyV virions co-localized with BiP protein. Arrows point to selected MPyV that did not co-localize with BiP protein. Bars, 10 μm. (B) Quantification of co-localization of MPyV virions with BiP at 5 h p.i. The percentage of co-localizing virions was calculated from images such as shown in panel A and levels (%) of co-localizing virions in dynamitin-expressing cells were normalized to that in control. During the experiment, more than 600 virions in at least 10 different cells were evaluated for each sample. Data in the graph represent mean values ± s.d. from three independent experiments; Student's t-test was used.
doi:10.1371/journal.pone.0096922.g004

In the Absence of Microtubules, MPyV is Accumulated in Multicaveolar-like Clusters

In the above analysis, only a minor subpopulation of the virus appeared in Rab7-positive endosomes of nocodazole-treated cells, while the amount of virions located within structures positive for caveolin-1 increased by 20% in comparison to the non-treated cells (Figure 6A,B, quantified in Figure 5F). To identify caveolin-1-positive compartments where MPyV virions appear in the absence of microtubules, we processed nocodazole-treated cells later (5 h) post-infection for immunogold labeling of caveolin-1 on thawed cryosections of the cells. Immunoelectron microscopy revealed that most virions were located at the cell periphery in tightly-fitting endocytic vesicles (~60 nm in diameter), often also positive for caveolin-1. Virus-carrying vesicles were found connected to flask-shape caveolae-like empty structures (70–100 nm in diameter), but also to other virus-carrying vesicles, creating caveolin-1-positive membrane clusters of irregular shape (Figure 6C) whose morphology resembled multicaveolar complexes [43,44]. Apart from these structures, only individual virions were found in late endosomal multivesicular bodies (MVBs), occasionally also positive for caveolin-1, and in caveolin-1-free endosomes (Figure 6D). These endosomal structures probably represented early or pre-mature late endosomes, since maturation of endosomes and their fusion with lysosomes is dependent on intact microtubular network and dynein motor function [45–48]. In contrast to nocodazole-treated cells, in non-treated cells at 5 h p.i. the accumulation of MPyV in caveolin-1-positive clusters was not apparent. Virions were found accumulated within multilamellar bodies or within MVBs also stained for caveolin-1 (Figure 7). This suggests that a high percentage of MPyV virions co-localizing with caveolin-1 in untreated cells (Figure 5F) is largely made up of virus within late endosomal structures. Together, these data demonstrate that in a situation when microtubular transport is not available for MPyV, most virions persist at the cell periphery within endocytic vesicles or within multicaveolar-like clusters.

The resemblance of caveolin-1-positive clusters of MPyV-carrying vesicles in nocodazole-treated cells to multicaveolar membrane structures prompted us to test whether the presence of the drug affected the way of virus internalization, since previous studies provided evidence that internalization of MPyV is caveolae-independent [1–3,6,8]. To explore that, we first performed live-cell labeling of infected untreated or nocodazole-treated cells at 15 or 90 min p.i. with anti-MPyV VP1 primary antibody, to visualize non-internalized virions (see Materials and Methods). For both, untreated or nocodazole-treated cells, immunostaining at 15 min p.i. revealed abundant presence of MPyV virions attached to the cell surface, whereas at 90 min p.i., only residual presence of virus attached at the surface of cells was detected (Figure 8A). This observation suggests that virus uptake was not prevented by nocodazole. Further, we followed the way of MPyV internalization in the presence of nocodazole by immunoelectron microscopy. We found that virions are internalized independently of caveolar invaginations into tightly-fitting endocytic vesicles (Figure 8B, panels a and b) and that the presence of caveolin-1 on virus-carrying vesicles is caused by virus uptake via caveolin-1-rich domains at the plasma membrane (Figure 8B, panel c). These results indicate that the way of MPyV internalization is not affected by nocodazole. In addition, we tested the impact of temporary absence of a functional microtubular network on virus infectivity. We pre-treated (1 h prior to infection) and infected cells with MPyV in the presence of nocodazole. We found that more than 70% inhibition of MPyV infection in the cells kept with the drug until 7 h p.i. could be efficiently restored by the drug washout and by prolonged time of incubation (for additional 24 h) before cell fixation and screening (Figure 8C). Such reversibility supports our microscopic observations indicating that nocodazole does not affect MPyV entry and also points to the effective productive transport of virions when their accessibility to microtubules was recovered.

Together, these data indicate that in a situation when microtubular transport is not available, most of MPyV virions persist at the cell periphery within endocytic vesicles or within multicaveolar-like clusters, where they are inaccessible for surface labeling with antibody. Our results also suggest that the presence of virions in these structures does not affect their ability to infect

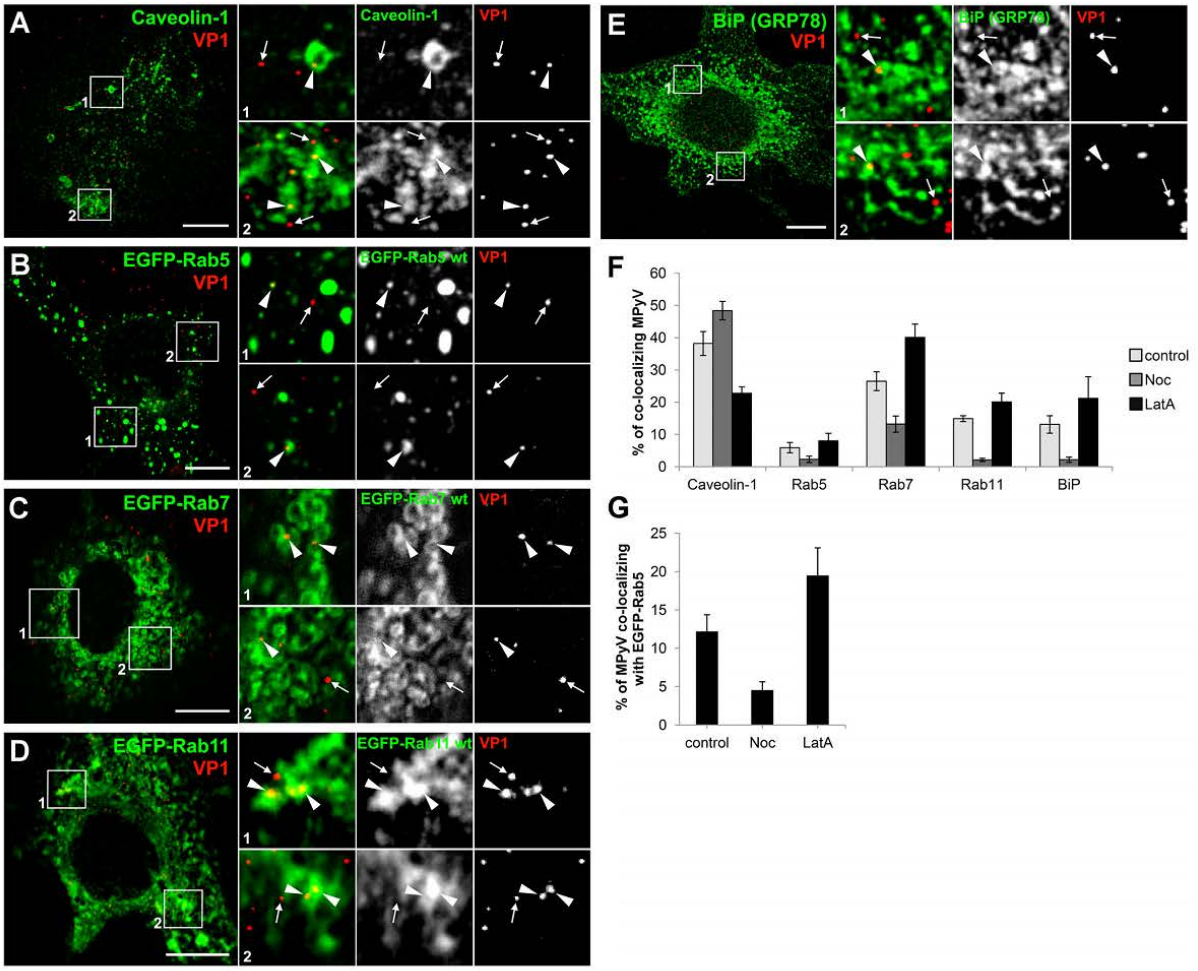

Figure 5. Effect of cytoskeleton-disrupting drugs on subcellular localization of MPyV. Non-transfected 3T6 cells (A and E) or cells transiently expressing EGFP-tagged marker of interest (B–D) were infected with MPyV (MOI of 5×10^2 virus particles per cell) and fixed 5 h p.i. Cells were immunostained for MPyV VP1 capsid protein (red) and for a second marker of interest (caveolin-1, BiP) if not fused with EGFP (green). Confocal sections of cells with enlarged details are shown. Arrowheads point to selected MPyV virions co-localized with the marker of interest. Arrows point to selected MPyV that did not co-localize with the marker of interest. Bars, 10 μm. (F) Quantification of co-localization of MPyV virions with indicated markers at 5 h p.i. in non-treated cells (control) or cells pre-treated (1 h) and infected in the presence of nocodazole (Noc) or latrunculin A (LatA). (G) Quantification of co-localization of MPyV virions with EGFP-Rab5 at 1.5 h p.i., in control, Noc- or LatA-treated cells. The percentage of co-localizing virions was calculated from images such as those showed in A–E. During the experiment, more than 600 virions in at least 10 different cells were evaluated for each sample. Data in the graph represent mean values ± s.d. from three independent experiments.
doi:10.1371/journal.pone.0096922.g005

cells and that with accessibility to microtubular network the virions continue in their trafficking to the endosomes and further to ER.

Recycling Endosomes are not Required for MPyV Infection

In previous reports we showed that substantial amounts MPyV VP1 capsid protein appeared in Rab11-positive recycling endosomes of 3T6 cells [3,10]. To investigate whether recycling endosomes participate in MPyV productive trafficking, we followed the virus infectivity in 3T6 cells transiently expressing EGFP-fused wild-type, dominant-negative or constitutively active mutant of Rab11 GTPase. As an additional control, we tested the virus infectivity during transient expression of analogous mutants of Rab7 GTPase, used previously to prove the dependence of MPyV infection on late endosomes in NIH 3T3 cells [9]. Our infection assays revealed that neither expression of EGFP-fused wild-type nor any mutant version of Rab11 GTPase affected the virus infectivity (Figure 9A). On the other hand, the expression of dominant-negative EGFP-Rab7 substantially reduced virus infectivity in comparison to the wild-type or constitutively active Rab7 version (Figure 9B). These data indicate that virus transport to the Rab11-positive recycling compartments is dispensable for MPyV. The functional expression of Rab11 GTPase constructs was confirmed by the intracellular distribution of fluorescently tagged transferrin. In accordance with observations of others [49,50], in the cells expressing the wild-type or constitutively active version of Rab11, most of the transferrin was accumulated in EGFP-Rab11-positive structures concentrated in the juxtanuclear region corresponding to the pericentriolar recycling compartment,

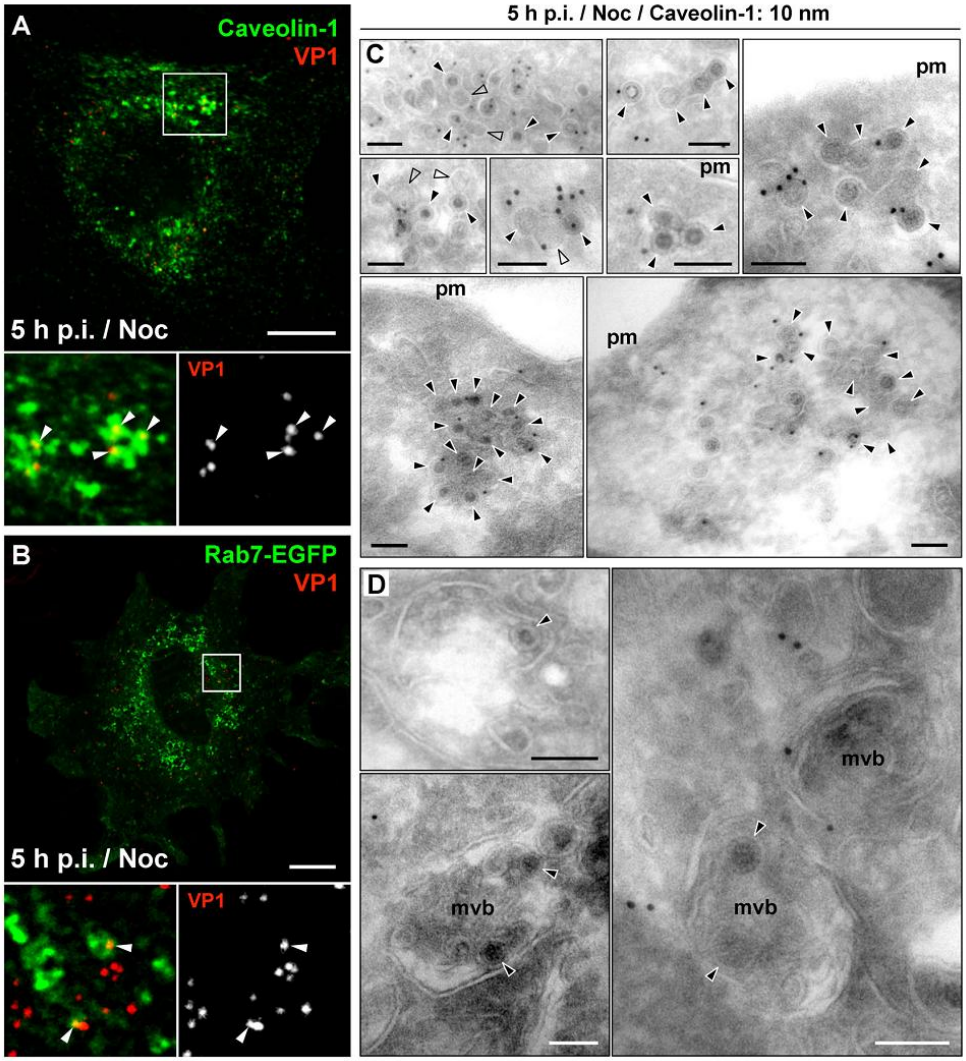

Figure 6. Localization of MPyV in nocodazole-treated cells. 3T6 cells were pre-treated (1 h) with nocodazole, infected with MPyV in the presence of the drug and fixed 5 h p.i. (A) Cells immunostained for MPyV VP1 (red) and caveolin-1 (green). (B) Cells expressing EGFP-fused Rab7 GTPase (green) immunostained for VP1 protein (red). Confocal sections of cells are shown. Arrowheads point to selected MPyV virions co-localizing with indicated marker. Bars, 10 μm. (C and D) Immunolabeling of thawed cryosections of cells with anti-caveolin-1 antibody, followed by immunolabeling with secondary antibody conjugated with 10 nm gold particles (seen as darkly stained dots). Arrowheads point to selected virions. Empty arrowheads point to flask-shape "empty" caveolar structures. Bars, 100 nm. Pm, plasma membrane; MVBs, multivesicular bodies.
doi:10.1371/journal.pone.0096922.g006

whereas in cells expressing the dominant-negative form, EGFP-Rab11 was dispersed in the cytoplasm or created thin tubular perinuclear elements, but the presence of transferrin in these structures was diminished (Figure S3).

Discussion

In this study, we focused on the dynamics of intracellular transport of MPyV virions towards the nucleus and addressed the relevance of virus movements along microtubules for its productive infection. Here, we present evidence that dynein mediates all the critical steps of MPyV trafficking, including efficient virus transport from the plasma membrane to endosomes of classical endocytic pathways, maturation of MPyV-carrying endosomes, and subsequent virus delivery to the ER. In addition, we show that microtubule-dependent virus transport to recycling endosomes is not required for MPyV infection.

Previous studies that focused on the role of microtubular network in trafficking of polyomaviruses reported that perturbation of the dynein motor function did not lead to significant inhibition of JCV, SV40 or BKV infection [18,20]. However, in accordance with our results, Engel et al [23] recently published RNA interference screening that revealed the dependence of SV40 infection on dynein motor in HeLa cells. The reason why some polyomaviruses do not require the dynein motor in some cell types is not clear. Ashok and Atwood [18] suggested that for transport in glial cells, JCV and SV40 require a different member of the dynein family whose function is independent of dynactin complex, or that

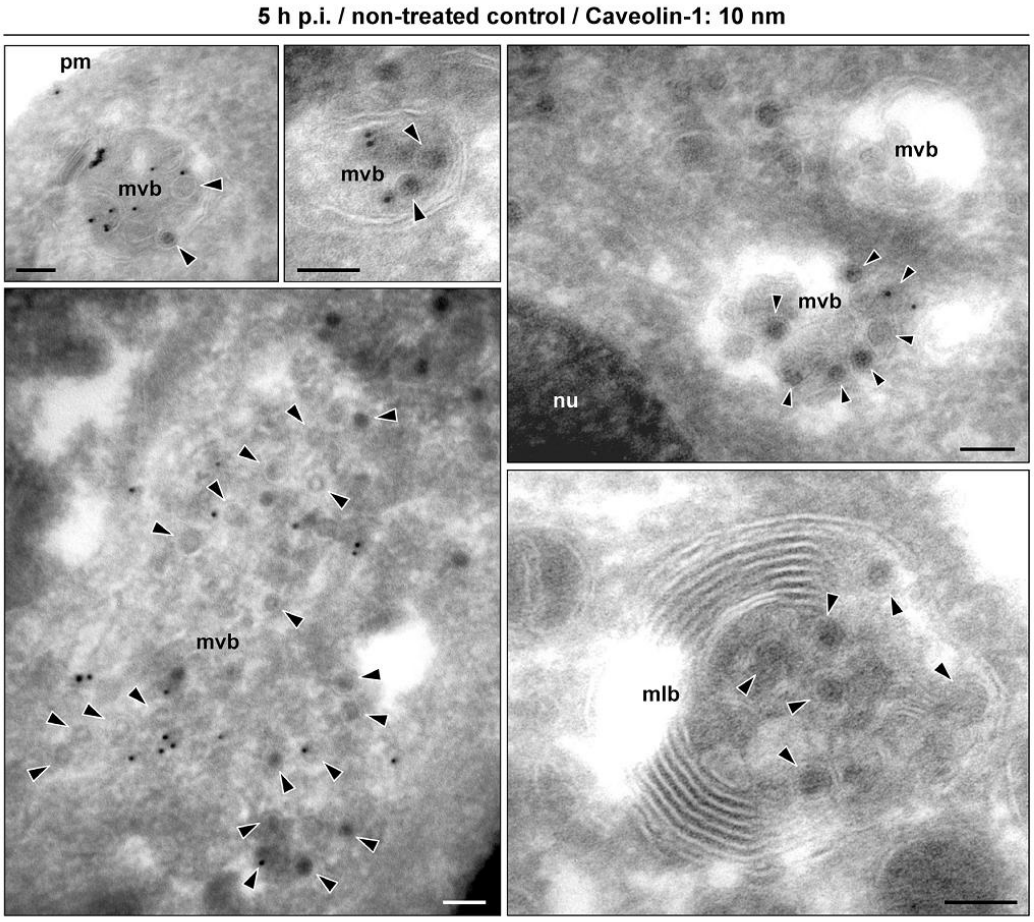

Figure 7. Immuno-electron microscopy of 3T6 cells at 5 h post-infection with MPyV. Thawed cryosections were immunolabeled with anti-caveolin-1 antibody followed by incubation with secondary antibody conjugated with 10 nm gold particles. Arrowheads point to selected virions. Bars, 100 nm. Pm, plasma membrane; MVBs, multivesicular bodies; MLB, multilamellar body; Nu, nucleus.
doi:10.1371/journal.pone.0096922.g007

the viral proteins can interact directly with microtubules for transport. The latter possibility can be ruled out in the case of MPyV, as the dynamics of long-distance movement of MPyV virions reflected microtubular motor processivity. Plus end-oriented movements of MPyV along microtubules mediated by kinesin-1 or kinesin-2 are apparently not required for virus productive trafficking. It has been found that kinesin-2 is required for normal steady-state localization of late endosomes [41]. However, despite the abnormal subcellular distribution of these compartments, authors of this study have shown that the uptake and trafficking of molecules through the conventional endocytic pathway was unaffected by inhibition of kinesin-2. Our results imply that this might also be true for trafficking of cargo via early endosomes whose motility requires kinesin-1 as well [51], since transfer via early endosomes is also important for MPyV [3,9].

The requirement of minus end-oriented dynein motor observed for MPyV trafficking underlies the polyomavirus strategy how to reach the nucleus. Polyomaviruses do not target the nucleus directly via nuclear pore complexes but, still enclosed in vesicles or endosomes, they have first to reach the ER for uncoating the viral genomes [11–13,52]. This strategy is in contrast with the one used by some enveloped viruses, e.g. HIV or Herpes viruses, which use bi-directional transport to reach the vicinity of the nucleus where they replicate. These viruses use dynein to reach the MTOC (microtubule organizing centre) and they can use kinesin-1 for their further transport from MTOC to the proximity of a nuclear envelope. However, capsids of these viruses, unlike those of polyomaviruses, travel usually naked in the cytosol, interacting directly with both, dynein and kinesin-1 motors (reviewed in [28]).

The results presented in this study indicate that utilization of the microtubular network and dynein motor by MPyV is different from that observed for SV40. We found that overexpression of dynamitin affected MPyV transport from the plasma membrane and reduced its presence in ER. Disruption of microtubules by nocodazole perturbed the presence of MPyV in classical endosomes, and only a small virus population was detected in premature late endosomes. Engel et al [23] observed no difference in the efficiency of SV40 trafficking to Rab5- or Rab7-positive endosomes in nocodazole-treated and non-treated cells. Nocodazole only blocked maturation of SV40-containing endosomes and subsequent transport of virions to ER. This group reported previously that vesicles carrying SV40 virions recruit actin in the form of actin comet tails and use it for their transport from the plasma membrane [25], suggesting that SV40 rather utilizes actin

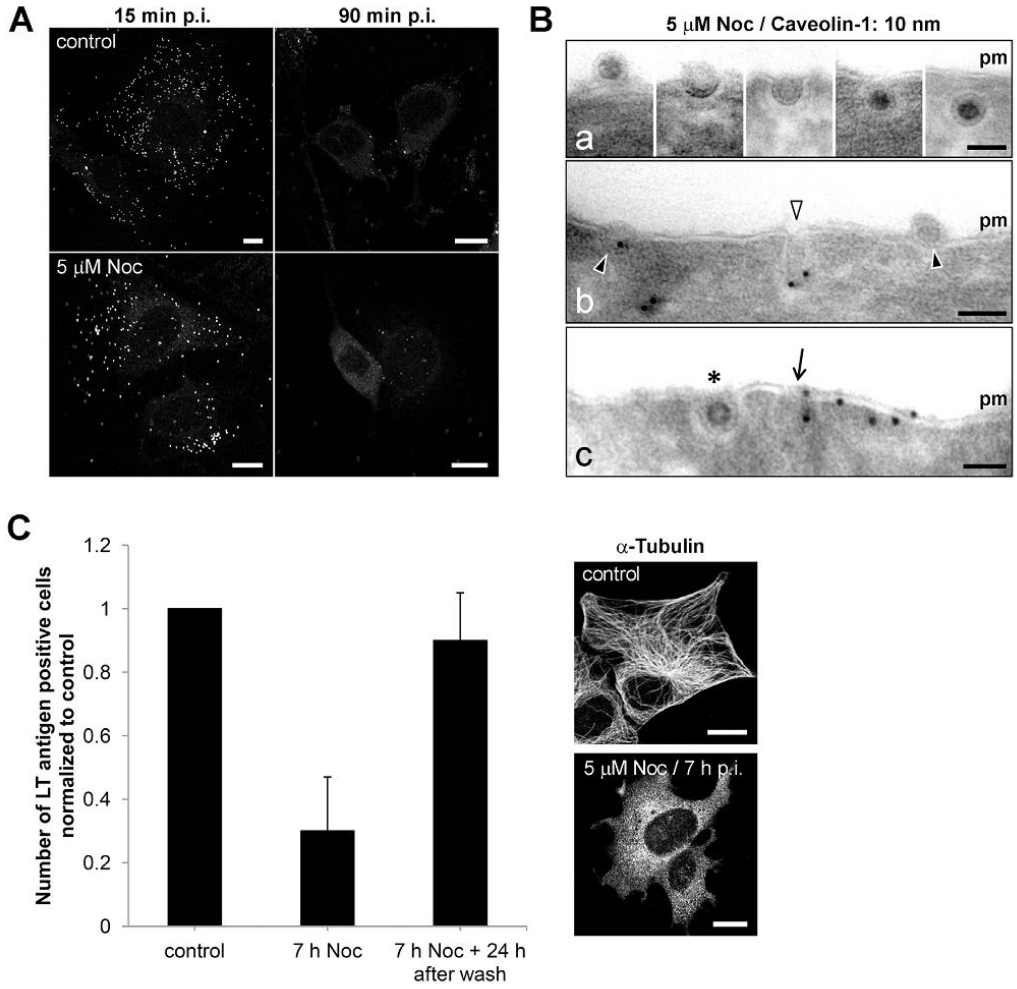

Figure 8. Internalization and infectivity of MPyV in nocodazole-treated cells. (A) 3T6 cells were pre-treated in culture medium alone or in medium supplemented with nocodazole for 1 h at 37°C and incubated with MPyV (MOI of 5×10^2 virus particles/cell) for 15 or 90 min at 37°C, also in the presence or absence of the drug. After that, immunofluorescence analysis was performed using an anti-MPyV VP1 antibody added to live cells, followed by fixation. Confocal sections of representative cells are shown. Bars, 10 μm. (B) Immunolabeling of thawed cryosections of cells pre-treated and infected with MPyV in the presence of nocodazole. Cells were immunolabeled with anti-caveolin-1 antibody, followed by immunolabeling with secondary antibody conjugated with 10 nm gold particles (seen as darkly stained dots). Arrowheads point to selected virions. Empty arrowhead points to caveolar invagination. Asterisk indicates virion internalizing to an invagination lacking caveolin-1. Arrow points to virion internalizing via a region at the plasma membrane enriched for caveolin-1. Pm, plasma membrane. Bars, 50 nm. (C) 3T6 cells were pre-treated (1 h) with nocodazole and infected with MPyV. The drug was washed out at 7 h p.i. and cells were further incubated until 24 h p.i. (middle bar) or for additional 24 h after washing (right bar). As a control, cells were infected in the absence of the drug and fixed 24 h p.i. Cells were immunostained for MPyV LT antigen and the efficiency of infection was determined by the levels (%) of LT antigen-positive cells, normalized to that in control. During the experiment, at least 500 cells of each sample were counted. Data in the graph represent mean values ± s.d. from three independent experiments. Immunofluorescent staining of microtubules (anti-α-tubulin antibody; panel on the right) shows the morphology of microtubular network at the time of washing (7 h p.i.) in control or nocodazole-treated cells. Bars, 10 μm.
doi:10.1371/journal.pone.0096922.g008

dynamics than the dynein motor to reach early and premature late endosomes. Although we have observed the involvement of actin dynamics in MPyV movement in 3T6 cells (Figure S2, Movie S3), disruption of actin microfilaments by latrunculin A did not prevent MPyV trafficking to classical endosomes. Moreover, it enhanced its efficiency. Correspondingly, virus infectivity in the presence of latrunculin A was higher than that in non-treated 3T6 cells (our unpublished results). Previous reports observing that treatment with actin-disrupting compounds increased MPyV infectivity in other naturally permissive cell lines are in agreement [2,15].

Exploring localization of MPyV in the absence of functional microtubular transport in more detail revealed virus retention at the periphery of cells, within endocytic vesicles often connected to flask-shape caveolae-like empty structures, or within membrane clusters heavily labeled for caveolin-1. The morphology of virion-containing clusters strikingly resembled multicaveolar complexes described previously [43,44]. These studies provided evidence that stimulation of caveolar endocytosis induces clustering of caveolae into multicaveolar complexes, mostly connected to the plasma membrane. However, we observed that upon nocodazole treat-

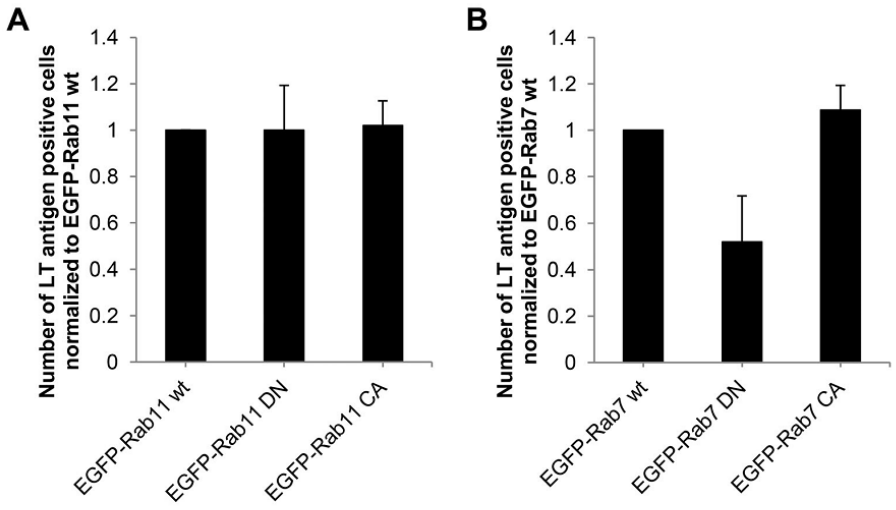

Figure 9. Rab11 GTPase is not required for MPyV infection. 3T6 cells were transfected with plasmid DNA for transient expression of (A) wild-type EGFP-Rab11 (wt), dominant-negative EGFP-Rab11 (DN) or constitutively active EGFP-Rab11 (CA), or (B) wild-type EGFP-Rab7 (wt), dominant-negative EGFP-Rab7 (DN) or constitutively active EGFP-Rab7 (CA). After 24 h, cells were infected with MPyV, incubated until 24 h p.i., fixed and immunostained for MPyV LT antigen. The efficiency of infection was determined by the levels (%) of LT antigen-positive cells from that expressing EGFP-fused version of the Rab11 or Rab7 GTPase normalized to that obtained in cells expressing its wild-type version. During the experiment, more than 500 cells were counted for each sample or control. Data in the graph represent mean values ± s.d. from three independent experiments.
doi:10.1371/journal.pone.0096922.g009

ment, MPyV virions entered the cells independently of caveolae, similarly as described for untreated cells [3,6,8]. The presence of caveolin-1 on some virus-carrying vesicles is apparently caused by internalization of the virions via caveolin-rich domains at the plasma membrane (Figure 8B, panel c). Recently, formation of multicaveolar complexes was shown to occur along actin microfilaments from individual caveolar domains physically linked to the microfilament structure [53]. This supports our observation that the virus presence in caveolin-1-positive compartments was reduced by disruption of actin microfilaments (Figure 5F). We thus hypothesize that during internalization of MPyV via caveolin-rich domains at the plasma membrane, invaginating virions might be, due to the presence of caveolins, organized along actin microfilaments similarly to caveolar domains. Such virus internalizing invaginations might thus create their interconnections or connections with "empty" caveolae in their proximity. As no apparent difference in the detection of virions at the plasma membrane of nocodazole-treated or non-treated cells was observed 90 min p.i., we speculate that these clusters are intracellular or connected to the cell surface by very narrow invaginations. Interestingly, SV40 was detected by electron microscopy in similar membrane clusters, presented as structures of caveosomes [21]. Since caveosomes were later identified as late endosomes or lysosomes modified by overexpression of caveolin-1 [23,26], we have to point out the presence of MPyV in structures whose morphology corresponds to the previous definition of caveosomes, but which by nature are not late endosomal compartments.

What is the fate of the virus in multicaveolar-like clusters? Trafficking of internalized caveolae into Rab11-positive endosomes has been reported [54]. We found transport of MPyV to Rab11-positive endosomes to be dependent on intact microtubules (Figure 5F), consistent with the finding that Rab11 together with the dynein motor mediate transport to the endosomal-recycling compartments [55]. For the virus, this apparently represents non-productive transport, as the expression of dominant-negative or constitutively active Rab11 GTPase did not affect MPyV infection. The appearance of MPyV in these compartments may thus be connected with recycling of the virus material back to the plasma membrane, as slow sorting of the VP1 signal from the perinuclear region to the cell periphery was observed in the interval 6–24 h p.i. (our unpublished results). However, the almost complete reversibility of inhibition of virus infection by nocodazole after its washout suggests that microtubules and dynein motor mediate the link for MPyV between multicaveolar-like structures and acidic endosomes. Several studies have reported caveolin-1 or caveolae trafficking into early endosomes [56] and, under specific conditions, also into MVBs and endolysosomal compartments [26,43,57] (reviewed in [58,59]). Nevertheless, our results bring evidence that the presence of MPyV in multicaveolar-like complexes is dispensable for virus infection and rather decreases and/or delays productive trafficking of the MPyV virions.

Materials and Methods

Ethics Statement

De novo cell lines were established with approval by the Institutional Review Board of Faculty of Science, Charles University in Prague (approval number: 2012/06).

Cell Line Cultivation and Transfection

Swiss albino mouse fibroblasts 3T6 (American Type Culture Collection, ATCC # CCL-96) were grown at 37°C and 5% CO_2 in complete Dulbecco's Modified Eagle's Medium (DMEM) (Sigma-Aldrich, St Louis, MO, USA) supplemented with 10% fetal bovine serum (FBS) (Sigma-Aldrich) and GlutaMAX-I (Gibco, Life Technologies). All transfections were performed by electroporation using Amaxa kits (Lonza, Basel, Switzerland) according to the manufacturer's instructions.

DNA Constructs and Stable Cell Lines

For stable expression of EGFP-tagged α-tubulin or β-actin, cells were transfected with pEGFP-human α-Tub vector (Clontech, cat. 6117–1) or with pEGFP-human β-actin vector (Clontech, cat. 6116-1), respectively. Cell lines were established by sub-cloning and maintained upon G418 (Sigma-Aldrich) selection antibiotic in DMEM culture medium supplemented with 10% FBS and 4mM GlutaMAX-I. Plasmid for expression of dynamitin-EGFP (pDynamitin-EGFP-N1) was kindly provided by Beate Sodeik (MHH Institute of Virology, Hannover, Germany) [60]. Plasmid for expression of RFP-tagged dominant-negative kinesin-1: C-terminal fragment of kinesin-1 heavy chain (pRFP-KHCct) with control vector (pRFP-DTC) were kindly provided by Victoria J. Allan (University of Manchester, Manchester, United Kingdom) [39,40]. Plasmids for expression of EGFP-fused dominant-negative subunits of kinesin-2: motorless KIF3A subunit (pEGFP-KIF3A-HL) and C-terminus of KAP3 accessory subunit (pEGFP-KAP3-CT) were kindly provided by Trina A. Schroer (The John Hopkins University, Baltimore, MD, USA) [41,42]. Plasmids for expression of EGFP-fused wild-type [61], dominant-negative (S25N) and constitutively active (Q70L) Rab11 mutant were kindly provided by Marino Zerial (Max Planck Institute, Dresden, Germany). Plasmids for expression of EGFP-fused wild-type, dominant-negative (T22N) and constitutively active (Q67L) Rab7 mutant were kindly provided by Cecilia Bucci (The University of Salento, Lecce, Italy) [62]. Vector for expression of EGFP-fused wild-type version of Rab5 was kindly provided by Philip D. Stahl (Washington University School of Medicine) [63]. For the infection assays evaluating the efficiency of MPyV infection, vector pEGFP-N1 (Clontech) was used as a control.

Virus

The A3 strain of MPyV (large-plaque strain) was isolated from infected WME (whole mouse embryo) cells according to Türler and Beard [64] and purified to homogeneity by CsCl and sucrose gradient ultracentrifugation. The quality of preparation was confirmed by Coomassie blue-stained sodium dodecyl sulfate-acrylamide gel electrophoresis and electron microscopy (negative staining). For microscopy of living cells, virions were labeled with the red fluorescent marker Alexa Fluor 546 carboxylic acid succinimidyl ester (Molecular Probes, Life Technologies) according to the manufacturer's protocol as described in Liebl et al [3]. Viral titers were determined by plaque assays and particle numbers by hemagluttination assays. For infections, MPyV was used at the indicated multiplicities of infection (MOIs).

Virus Tracking

For live microscopy, cells were grown in glass-bottom dishes (MatTek, Ashland, MA, USA) in phenol red-free DMEM culture medium supplemented with 10% FBS. Glass-bottom dishes were then mounted into a CO_2-supplemented chamber, maintained at 37°C. To avoid rapid temperature changes and microtubule depolymerization at 4°C, all procedures were performed at 37°C with pre-warmed media and solutions. The fluorescently labeled virus was diluted in serum-free culture medium and added to cells at MOI of 10^2 to 10^3 particles per cell. Unbound virus was gently washed away after 20 min and complete culture medium was added. Cytoplasmic transport was monitored by time-lapse live imaging using a Leica TCS SP2 AOBS confocal microscope equipped with an Argon laser (458, 476, 488, 496, 514 nm; 10 mW) and a HeNe laser (543, 594 nm; 1 mW). Cells were examined with a 1.2 N.A. water immersion objective (60x). To minimize the possibility of tracking of not yet internalized virions attached to the cell surface, a complete z-scanning of the cell starting from the apical until the basal cell membrane was performed. After this step, the objective focus was fixed on the middle plane of the cell, and only virions moving in the internal area of the cell corresponding to the cytosol were tracked. According to the specific signal to noise ratio and EGFP level of expression, we applied different sampling frequencies ($\Delta T = 3$–6 s). Sequential scanning between channels was used to separate fluorescence emission from different fluorochromes and to completely eliminate bleed through channels. EGFP-tubulin-expressing cells were alternatively examined with an Olympus IX81 CellR microscope equipped with an MT20 illumination system and a 63× oil-immersion objective, using Tx Red and GFP filter cube set. Video sequences and images were processed by Image J software (NIH, Bethesda, MD, USA) and Adobe Photoshop (Adobe Systems, San Jose CA, USA), respectively. Velocities and trajectories were calculated by 'particle tracking' plug-ins for Image J software (NIH) and data were processed with Excel software (Microsoft Corporation).

Immunofluorescence Staining

For fixed-cell staining, cells were fixed with 4% formaldehyde in PBS (20 min) and permeabilized with 0.5% Triton X-100 in PBS (5 min). Alternatively, to follow the virus localization in EGFP-Rab7-positive compartments, we fixed cells with 4% formaldehyde plus 0.05% glutaraldehyde in PBS (60 min) as combined fixative was shown to sufficiently preserve the fragile structures of late endosomes for immunofluorescence analysis [62,65]. After washing in PBS, cells were incubated with 0.25% bovine serum albumin and 0.25% porcine skin gelatin in PBS. Immunostaining with primary and secondary antibody was carried out for 1 h and 30 min, respectively, with extensive washing in PBS after each incubation. The following primary antibodies were used: rat monoclonal anti-MPyV large T (LT) antigen (kindly provided by B. E. Griffin, Imperial College of Science, Technology and Medicine at St. Mary's, London, United Kingdom), mouse monoclonal anti-MPyV VP1 (prepared in our laboratory), rabbit polyclonal anti-MPyV VP1 (prepared in our laboratory), rabbit polyclonal anti-caveolin-1 (Santa Cruz, CA, USA), rabbit polyclonal anti-BiP (Abcam, Cambridge, UK), mouse monoclonal anti-α-tubulin (Exbio, Prague, Czech Republic) and rabbit polyclonal anti-GFP (Abcam). The following secondary antibodies were used: donkey anti-rat, donkey anti-mouse and goat anti-rabbit conjugated with Alexa Fluor 488; goat anti-rat conjugated with Alexa Fluor 546; Cy3-conjugated goat anti-mouse antibody (all purchased from Molecular Probes); and donkey anti-rabbit conjugated with CF633 fluorescent dye (Biotinum, CA, USA). DNA was stained with DAPI (4′, 6′-diamidino-2-phenylindole). For testing the EGFP-fused versions of Rab11 GTPase, transferrin tagged with Alexa Fluor 647 (Molecular Probes) was used.

Live-cell labeling was performed as described in Zhou et al [66]. At indicated times (15 or 90 min) post-infection, cells were washed three times with complete Dulbecco's PBS (DPBS) at 37°C and incubated with mouse monoclonal anti-MPyV VP1 antibody for 20 min at 37°C. The cells were then washed three times with DPBS (37°C) and fixed with 4% formaldehyde in PBS (10 min). Fixed but not permeabilized cells were washed in PBS and incubated with Cy3-conjugated anti-mouse secondary antibody as described above.

Internalization Assay

Cells grown on 13-mm glass coverslips in 24-well plates were incubated with MPyV labeled with Alexa Fluor 546 dye, diluted in serum-free culture medium and added to cells at MOI of 10^3 particles per cell. After 20 min (at 37°C), cells were washed to

remove unbound virus and complete DMEM medium (37°C) was added. Cells were incubated until indicated time points p.i. and fixed with 4% formaldehyde in PBS (20 min). The detection of non-internalized virions was accomplished by surface labeling of non-permabilized cells, washed in PBS and incubated with anti-MPyV VP1 antibody, followed by incubation with secondary antibody conjugated to green dye Alexa Fluor 488. The percentages of internalized virions were determined from the maximum-intensity projections of Z-stacks of confocal optical sections of the examined cells.

Infectivity Assays

To determine MPyV infectivity during the expression of fluorescently tagged versions of the proteins or fluorescent proteins alone, cells were transfected with protein encoding plasmid DNA and seeded on 13-mm glass coverslips in 24-well plates. Cells were allowed to grow for 24 or 48 h (two days for expression of kinesin-2 subunits, as they turn out slowly [41]), washed and incubated with MPyV diluted in serum-free medium at MOI of 0.3 PFU/cell, for 1 h at 37°C. The infection start was measured from virus addition to cells. After virus adsorption, cells were washed to remove the unbound virus and incubated in DMEM with 10% FBS until 24 h p.i. and fixed. Fixed cells were immunostained with antibody against MPyV early LT antigen. The efficiency of infection was determined from the percentage of LT-positive cells from that expressing the fluorescently tagged protein of interest, normalized to that obtained in control cells.

To determine the reversibility of MPyV infection after nocodazole treatment, cells were pre-treated in medium with 5 μM nocodazole (Calbiochem, Merck) for 1 h at 37°C and in the presence of drug infected with MPyV as above (the functional disruption of microtubules by nocodazole was confirmed by immunostaining with anti-α-tubulin antibody). At 7 h p.i., the drug was washed out and the cells were incubated until 24 h p.i., or in parallel samples, cells were incubated for additional 24 h prior to fixation and immunostaining to prove the reversibility of the inhibition effect. Fixed cells were immunostained for the MPyV LT antigen and the cell nuclei were visualized by DAPI. The efficiency of infection was determined from the percentage of cells positive for LT antigen normalized to that obtained in cells infected in the absence of drug and fixed 24 h p.i.

For assay quantification, coverslips were observed with an Olympus BX-60 fluorescence microscope equipped with a COHU CCD camera and images of optical fields were taken using Lucia software (Laboratory Imaging, Prague, Czech Republic). Cells were counted using the 'cell counter' plug-in for Image J software (NIH).

Quantification of Co-localization

Cells transfected with plasmid DNA for expression of the EGFP-fused protein of interest, mock-transfected or non-transfected cells were seeded on 13-mm coverslips in 24-well plates and left to grow for 16–24 h. Cells at 10–20% of confluency were used. For co-localization analysis in the presence of cytoskeleton drugs, cells were pre-incubated in culture medium alone (control) or medium containing 5 μM nocodazole or 0.1 μM latrunculin A (Calbiochem, Merck) for 1 h (at 37°C) prior to infection (the functional disruption of microtubules or microfilaments by the drugs was confirmed in parallel samples by immunostaining with anti-α-tubulin antibody or with rhodamine-conjugated phalloidin, respectively). Cells were infected with MPyV diluted in serum-free culture medium (with or without the drug) at MOI $\sim 5\times10^2$ virus particles/cell, allowing quantification of individual virions (counted approximately from 30 to 120 virions per cell). The infection start was measured from virus addition to cells. After 1 h at 37°C, the inoculum was removed, cells were washed three times to remove unbound virions, and complete DMEM medium +10% FBS (with or without drug) was added. Cells were incubated until indicated time p.i., fixed, and immunostained for MPyV VP1 capsid protein and the second marker of interest if not fused to EGFP. The cells were examined with a Leica TCS SP2 AOBS confocal microscope using a ×63 1.4 N.A. oil immersion objective. For each examined cell, Z-sections were taken and co-localization of individual virions was determined in individual sections using the 'colocalization highlighter' plug-in for Image J software (NIH). The intensity ratio of co-localized pixels was set at 50%. The obtained image with co-localizing pixels was merged with the image with MPyV VP1 signal and co-localized and non-colocalized virions were counted.

Immunoelectron Microscopy of Cryosections

Cells grown on Petri dishes were pre-treated (1 h/37°C) in culture medium alone or medium containing 5 μM nocodazole and in the absence or presence of the drug were infected with MPyV at MOI of 5×10^3 virus particles per cell for 1 h (rocking). Cells were washed and complete DMEM with 10% FBS (37°C) with or without nocodazole was added. Cells were fixed 5 h p.i. with 4% formaldehyde plus 0.05% glutaraldehyde solution in 0.1M Sörensen buffer (Na_2HPO_4/NaH_2PO_4, pH 7.2). Fixed cells were gently scraped from the plate with a rubber policeman and embedded in 10% gelatin in PBS. Gelatin-embedded samples were cut into 1-mm^3 blocks and infiltrated with 2.3M sucrose overnight at 4°C. Infiltrated blocks were mounted onto aluminum pins, frozen in liquid nitrogen and then sectioned at −120°C with a Leica EM FC7 microtome. Ultrathin cryosections were transferred in a drop of 2.3M sucrose, 2% methylcellulose onto formwar-carbon-coated nickel grids and immunolabeled with rabbit polyclonal antibody against caveolin-1 (BD Transduction Laboratories, BD Biosciences), followed by incubation with goat anti-rabbit antibody conjugated to 10 nm gold particles (British Biocell Int.). After labeling, the sections were contrasted and embedded in a mixture of 3% aqueous uranyl acetate and 2% methylcellulose. The samples were observed with a JEM-1011 JEOL electron microscope equipped with a side mounted 2k×2k CCD Camera (Veleta, Olympus SIS).

Supporting Information

Figure S1 Internalization assay. 3T6 cells were incubated with MPyV labeled with red fluorescent dye Alexa Fluor 546 (AF546-MPyV) diluted in serum-free medium (MOI of 10^3 virus particles/cell) for 20 min at 37°C. After virus adsorption, cells were washed and incubated in complete DMEM medium (37°C) until indicated times p.i. The extracellular and intracellular AF546-MPyV virions (red) were distinguished by surface immunolabeling of fixed but not permeabilized cells with anti-MPyV VP1 antibody, followed by incubation with secondary antibody conjugated to green dye Alexa Fluor 488. (A and B) Visualization of AF546-MPyV virions (red) in permeabilized (A) and non-permeabilized (B) cells by immunostaining with anti-VP1 antibody (green). Confocal sections of cells fixed 60 min p.i. with enlarged details are shown. In panel B, arrows point to selected extracellular virions. (C) Quantification of the amount of internalized AF546-MPyV virions at 20, 30, 60 and 120 min p.i. The percentages of internalized virus were calculated from images such as shown in panel B. More than 1100 virions were evaluated for each time point. Data in the graph represent mean values ± s.d. for 10 different cells.

(TIF)

Figure S2 Movement of MPyV-carrying endosomes associated with dynamic actin assemblies. 3T6 cells stably expressing EGFP-fused β-actin (green) were infected with Alexa Fluor 546-labeled MPyV (red) (MOI of 10^2 to 10^3 virus particles per cell) at 37°C and scanned with $\Delta T = 4$ s. Selected frames of cell at 45 min p.i. with corresponding transmission light images illustrate short-distance movement of virus-carrying endosomes associated with dynamic assemblies of EGFP-actin (see Movie S3). White arrowheads point to MPyV virions. Arrows point to endosome-associated actin assemblies. Black arrowheads indicate MPyV-containing endosomes. Bars, 5 μm. Cells were examined using a Leica TCS SP2 AOBS confocal microscope.
(TIF)

Figure S3 Intracellular distribution of fluorescently tagged transferrin during expression of Rab11 GTPase mutants. 3T6 cells expressing EGFP-fused wt, DN or CA version of Rab11 were incubated for 5 min (pulse) at 37°C with 25 μg/ml Alexa Fluor 647-transferrin. Cells were further incubated for 30 min (chase) at 37°C in serum-containing medium, fixed and processed for fluorescence microscopy. Confocal sections showing representative distribution of transferrin in the cells are presented. Arrows point to places of concentrated transferrin. Arrowheads point to tubular perinuclear elements of Rab11 DN. Bars, 10 μm.
(TIF)

Movie S1 Bi-directional transport of MPyV virions along microtubules. 3T6 cells expressing EGFP-tubulin (green) were infected with fluorescently labeled MPyV (red) at 37°C and analyzed by time-lapse fluorescence microscopy. Virions were transported in both directions: towards the nucleus (left) and to the cell periphery (right). Images were taken with intervals of 3 seconds. Video sequences were obtained using an Olympus IX81 CellR microscope.
(AVI)

Movie S2 MPyV virions accumulate in perinuclear space later post-infection (3 h p.i.). 3T6 cells expressing EGFP-tubulin (green) were infected with fluorescently labeled MPyV (AF594-MPyV; red) with MOI of 10^3 virus particles per cell at 37°C and analyzed by time-lapse confocal microscopy. Images were taken with intervals of 6 seconds. Bar, 10 μm. Video sequence was obtained using a Leica TCS SP2 AOBS confocal microscope.
(AVI)

Movie S3 Movement of MPyV associated with dynamic actin. 3T6 cells expressing EGFP-actin (green) were infected with fluorescently labeled MPyV (red) at 37°C and analyzed by time-lapse confocal microscopy. Video sequence with fluorescent signals (left) and corresponding sequence from transmission light (right) are shown. Images were taken with intervals of 4 seconds. Video sequences were obtained using a Leica TCS SP2 AOBS confocal microscope.
(AVI)

Acknowledgments

We are grateful to Dr. David Liebl and Dr. Jiří Janáček for help with tracking measurements and to Šárka Takáčová for assistance in preparation of the manuscript. We wish to thank Drs. Victoria J. Allan, Cecilia Bucci, Trina A. Schroer, Beate Sodeik, Philip D. Stahl and Marino Zerial for providing valuable expression plasmids.

Author Contributions

Conceived and designed the experiments: VZ FD LK SH JF. Performed the experiments: VZ FD LK SH. Analyzed the data: VZ FD LK SH JF. Wrote the paper: VZ JF SH.

References

1. Gilbert JM, Benjamin TL (2000) Early steps of polyomavirus entry into cells. J Virol 74: 8582–8588.
2. Gilbert JM, Goldberg IG, Benjamin TL (2003) Cell penetration and trafficking of polyomavirus. J Virol 77: 2615–2622.
3. Liebl D, Difato F, Hornikova L, Mannova P, Stokrova J, et al. (2006) Mouse polyomavirus enters early endosomes, requires their acidic pH for productive infection, and meets transferrin cargo in Rab11-positive endosomes. J Virol 80: 4610–4622.
4. Tsai B, Gilbert JM, Stehle T, Lencer W, Benjamin TL, et al. (2003) Gangliosides are receptors for murine polyoma virus and SV40. EMBO J 22: 4346–4355.
5. Gilbert J, Benjamin T (2004) Uptake pathway of polyomavirus via ganglioside GD1a. J Virol 78: 12259–12267.
6. Richterova Z, Liebl D, Horak M, Palkova Z, Stokrova J, et al. (2001) Caveolae are involved in the trafficking of mouse polyomavirus virions and artificial VP1 pseudocapsids toward cell nuclei. J Virol 75: 10880–10891.
7. Ewers H, Smith AE, Sbalzarini IF, Lilie H, Koumoutsakos P, et al. (2005) Single-particle tracking of murine polyoma virus-like particles on live cells and artificial membranes. Proc Natl Acad Sci U S A 102: 15110–15115.
8. Mackay RL, Consigli RA (1976) Early events in polyoma virus infection: attachment, penetration, and nuclear entry. J Virol 19: 620–636.
9. Qian M, Cai D, Verhey KJ, Tsai B (2009) A lipid receptor sorts polyomavirus from the endolysosome to the endoplasmic reticulum to cause infection. PLoS Pathog 5: e1000465.
10. Mannova P, Forstova J (2003) Mouse polyomavirus utilizes recycling endosomes for a traffic pathway independent of COPI vesicle transport. J Virol 77: 1672–1681.
11. Gilbert J, Ou W, Silver J, Benjamin T (2006) Downregulation of protein disulfide isomerase inhibits infection by the mouse polyomavirus. J Virol 80: 10868–10870.
12. Magnuson B, Rainey EK, Benjamin T, Baryshev M, Mkrtchian S, et al. (2005) ERp29 triggers a conformational change in polyomavirus to stimulate membrane binding. Mol Cell 20: 289–300.
13. Walczak CP, Tsai B (2011) A PDI family network acts distinctly and coordinately with ERp29 to facilitate polyomavirus infection. J Virol 85: 2386–2396.
14. Kobiler O, Drayman N, Butin-Israeli V, Oppenheim A (2012) Virus strategies for passing the nuclear envelope barrier. Nucleus 3: 526–539.
15. Krauzewicz N, Stokrova J, Jenkins C, Elliott M, Higgins CF, et al. (2000) Virus-like gene transfer into cells mediated by polyoma virus pseudocapsids. Gene Ther 7: 2122–2131.
16. Sanjuan N, Porras A, Otero J (2003) Microtubule-dependent intracellular transport of murine polyomavirus. Virology 313: 105–116.
17. Qian M, Tsai B (2010) Lipids and proteins act in opposing manners to regulate polyomavirus infection. J Virol 84: 9840–9852.
18. Ashok A, Atwood WJ (2003) Contrasting roles of endosomal pH and the cytoskeleton in infection of human glial cells by JC virus and simian virus 40. J Virol 77: 1347–1356.
19. Eash S, Atwood WJ (2005) Involvement of cytoskeletal components in BK virus infectious entry. J Virol 79: 11734–11741.
20. Moriyama T, Sorokin A (2008) Intracellular trafficking pathway of BK Virus in human renal proximal tubular epithelial cells. Virology 371: 336–349.
21. Pelkmans L, Kartenbeck J, Helenius A (2001) Caveolar endocytosis of simian virus 40 reveals a new two-step vesicular-transport pathway to the ER. Nat Cell Biol 3: 473–483.
22. Shimura H, Umeno Y, Kimura G (1987) Effects of inhibitors of the cytoplasmic structures and functions on the early phase of infection of cultured cells with simian virus 40. Virology 158: 34–43.
23. Engel S, Heger T, Mancini R, Herzog F, Kartenbeck J, et al. (2011) Role of endosomes in simian virus 40 entry and infection. J Virol 85: 4198–4211.
24. Jiang M, Abend JR, Tsai B, Imperiale MJ (2009) Early events during BK virus entry and disassembly. J Virol 83: 1350–1358.
25. Pelkmans L, Puntener D, Helenius A (2002) Local actin polymerization and dynamin recruitment in SV40-induced internalization of caveolae. Science 296: 535–539.
26. Hayer A, Stoeber M, Ritz D, Engel S, Meyer HH, et al. (2010) Caveolin-1 is ubiquitinated and targeted to intralumenal vesicles in endolysosomes for degradation. J Cell Biol 191: 615–629.
27. Huotari J, Helenius A (2011) Endosome maturation. EMBO J 30: 3481–3500.
28. Dodding MP, Way M (2011) Coupling viruses to dynein and kinesin-1. EMBO J 30: 3527–3539.

29. Hunt SD, Stephens DJ (2011) The role of motor proteins in endosomal sorting. Biochem Soc Trans 39: 1179–1184.
30. Presley JF, Smith C, Hirschberg K, Miller C, Cole NB, et al. (1998) Golgi membrane dynamics. Mol Biol Cell 9: 1617–1626.
31. Benesch S, Lommel S, Steffen A, Stradal TE, Scaplehorn N, et al. (2002) Phosphatidylinositol 4,5-biphosphate (PIP2)-induced vesicle movement depends on N-WASP and involves Nck, WIP, and Grb2. J Biol Chem 277: 37771–37776.
32. Orth JD, Krueger EW, Cao H, McNiven MA (2002) The large GTPase dynamin regulates actin comet formation and movement in living cells. Proc Natl Acad Sci U S A 99: 167–172.
33. Welsch T, Endlich N, Gokce G, Doroshenko E, Simpson JC, et al. (2005) Association of CD2AP with dynamic actin on vesicles in podocytes. Am J Physiol Renal Physiol 289: F1134–1143.
34. Block SM, Goldstein LS, Schnapp BJ (1990) Bead movement by single kinesin molecules studied with optical tweezers. Nature 348: 348–352.
35. Echeverri CJ, Paschal BM, Vaughan KT, Vallee RB (1996) Molecular characterization of the 50-kD subunit of dynactin reveals function for the complex in chromosome alignment and spindle organization during mitosis. J Cell Biol 132: 617–633.
36. Burkhardt JK, Echeverri CJ, Nilsson T, Vallee RB (1997) Overexpression of the dynamitin (p50) subunit of the dynactin complex disrupts dynein-dependent maintenance of membrane organelle distribution. J Cell Biol 139: 469–484.
37. Presley JF, Cole NB, Schroer TA, Hirschberg K, Zaal KJ, et al. (1997) ER-to-Golgi transport visualized in living cells. Nature 389: 81–85.
38. Coy DL, Hancock WO, Wagenbach M, Howard J (1999) Kinesin's tail domain is an inhibitory regulator of the motor domain. Nat Cell Biol 1: 288–292.
39. Wozniak MJ, Allan VJ (2006) Cargo selection by specific kinesin light chain 1 isoforms. EMBO J 25: 5457–5468.
40. Wozniak MJ, Bola B, Brownhill K, Yang YC, Levakova V, et al. (2009) Role of kinesin-1 and cytoplasmic dynein in endoplasmic reticulum movement in VERO cells. J Cell Sci 122: 1979–1989.
41. Brown CL, Maier KC, Stauber T, Ginkel LM, Wordeman L, et al. (2005) Kinesin-2 is a motor for late endosomes and lysosomes. Traffic 6: 1114–1124.
42. Ginkel LM, Wordeman L (2000) Expression and partial characterization of kinesin-related proteins in differentiating and adult skeletal muscle. Mol Biol Cell 11: 4143–4158.
43. Botos E, Klumperman J, Oorschot V, Igyarto B, Magyar A, et al. (2008) Caveolin-1 is transported to multi-vesicular bodies after albumin-induced endocytosis of caveolae in HepG2 cells. J Cell Mol Med 12: 1632–1639.
44. Kiss AL, Botos E (2009) Ocadaic acid retains caveolae in multicaveolar clusters. Pathol Oncol Res 15: 479–486.
45. Aniento F, Emans N, Griffiths G, Gruenberg J (1993) Cytoplasmic dynein-dependent vesicular transport from early to late endosomes. J Cell Biol 123: 1373–1387.
46. Bayer N, Schober D, Prchla E, Murphy RF, Blaas D, et al. (1998) Effect of bafilomycin A1 and nocodazole on endocytic transport in HeLa cells: implications for viral uncoating and infection. J Virol 72: 9645–9655.
47. Baravalle G, Schober D, Huber M, Bayer N, Murphy RF, et al. (2005) Transferrin recycling and dextran transport to lysosomes is differentially affected by bafilomycin, nocodazole, and low temperature. Cell Tissue Res 320: 99–113.
48. Driskell OJ, Mironov A, Allan VJ, Woodman PG (2007) Dynein is required for receptor sorting and the morphogenesis of early endosomes. Nat Cell Biol 9: 113–120.
49. Ren M, Xu G, Zeng J, De Lemos-Chiarandini C, Adesnik M, et al. (1998) Hydrolysis of GTP on rab11 is required for the direct delivery of transferrin from the pericentriolar recycling compartment to the cell surface but not from sorting endosomes. Proc Natl Acad Sci U S A 95: 6187–6192.
50. Holtta-Vuori M, Tanhuanpaa K, Mobius W, Somerharju P, Ikonen E (2002) Modulation of cellular cholesterol transport and homeostasis by Rab11. Mol Biol Cell 13: 3107–3122.
51. Loubery S, Wilhelm C, Hurbain I, Neveu S, Louvard D, et al. (2008) Different microtubule motors move early and late endocytic compartments. Traffic 9: 492–509.
52. Schelhaas M, Malmstrom J, Pelkmans L, Haugstetter J, Ellgaard L, et al. (2007) Simian Virus 40 depends on ER protein folding and quality control factors for entry into host cells. Cell 131: 516–529.
53. Echarri A, Muriel O, Pavon DM, Azegrouz H, Escolar F, et al. (2012) Caveolar domain organization and trafficking is regulated by Abl kinases and mDia1. J Cell Sci 125: 3097–3113.
54. Muriel O, Echarri A, Hellriegel C, Pavon DM, Beccari L, et al. (2011) Phosphorylated filamin A regulates actin-linked caveolae dynamics. J Cell Sci 124: 2763–2776.
55. Horgan CP, Hanscom SR, Jolly RS, Futter CE, McCaffrey MW (2010) Rab11-FIP3 links the Rab11 GTPase and cytoplasmic dynein to mediate transport to the endosomal-recycling compartment. J Cell Sci 123: 181–191.
56. Pelkmans L, Burli T, Zerial M, Helenius A (2004) Caveolin-stabilized membrane domains as multifunctional transport and sorting devices in endocytic membrane traffic. Cell 118: 767–780.
57. Mundy DI, Li WP, Luby-Phelps K, Anderson RG (2012) Caveolin targeting to late endosome/lysosomal membranes is induced by perturbations of lysosomal pH and cholesterol content. Mol Biol Cell 23: 864–880.
58. Kiss AL (2012) Caveolae and the regulation of endocytosis. Adv Exp Med Biol 729: 14–28.
59. Parton RG, del Pozo MA (2013) Caveolae as plasma membrane sensors, protectors and organizers. Nat Rev Mol Cell Biol 14: 98–112.
60. Dohner K, Wolfstein A, Prank U, Echeverri C, Dujardin D, et al. (2002) Function of dynein and dynactin in herpes simplex virus capsid transport. Mol Biol Cell 13: 2795–2809.
61. Sonnichsen B, De Renzis S, Nielsen E, Rietdorf J, Zerial M (2000) Distinct membrane domains on endosomes in the recycling pathway visualized by multicolor imaging of Rab4, Rab5, and Rab11. J Cell Biol 149: 901–914.
62. Bucci C, Thomsen P, Nicoziani P, McCarthy J, van Deurs B (2000) Rab7: a key to lysosome biogenesis. Mol Biol Cell 11: 467–480.
63. Li G, Stahl PD (1993) Structure-function relationship of the small GTPase rab5. J Biol Chem 268: 24475–24480.
64. Türler H, Beard P (1985) Simian virus 40 and polyoma virus: growth, titration, transformation and purification of viral components. In: Mahy B, editor. Virology: a practical approach. Oxford, Washington DC: IRL Press. 169–192.
65. Brankatschk B, Pons V, Parton RG, Gruenberg J (2011) Role of SNX16 in the dynamics of tubulo-cisternal membrane domains of late endosomes. PLoS One 6: e21771.
66. Zhou AY, Ichaso N, Adamarek A, Zila V, Forstova J, et al. (2011) Polyomavirus middle T-antigen is a transmembrane protein that binds signaling proteins in discrete subcellular membrane sites. J Virol 85: 3046–3054.

ATTACHMENT #1 – Zila et al., 2014; Supporting Figure S1

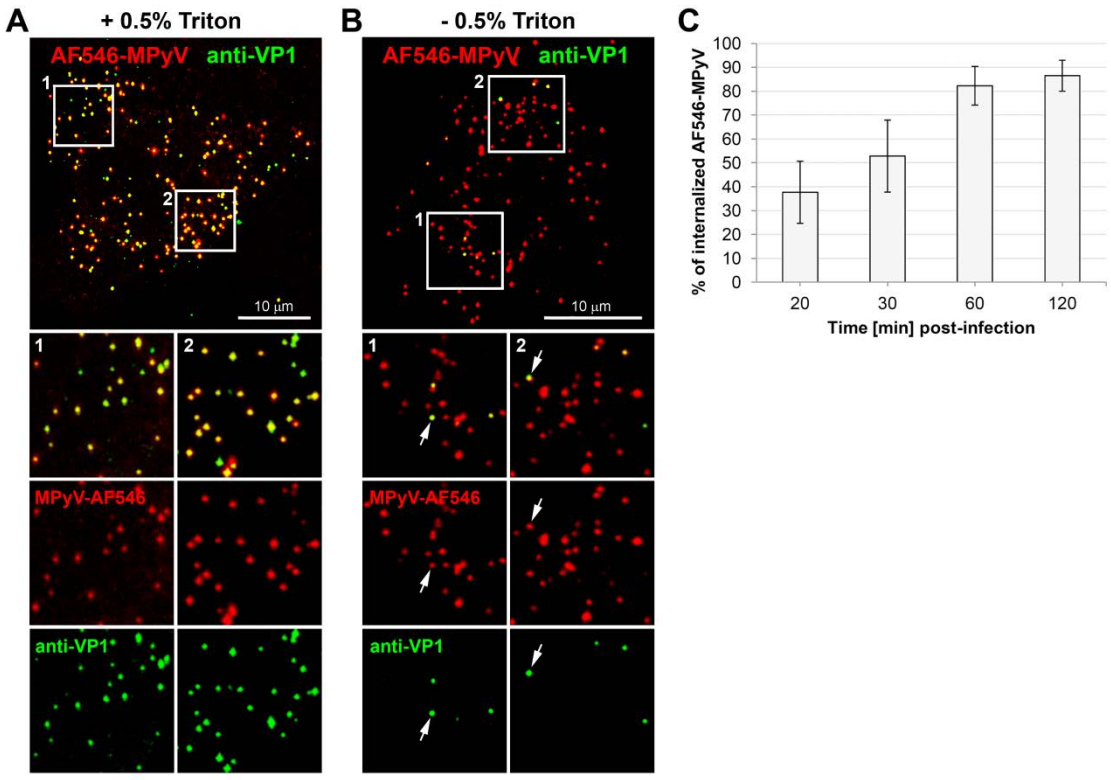

(figure legend in article)

ATTACHMENT #1 – Zila et al., 2014; Supporting Figure S2

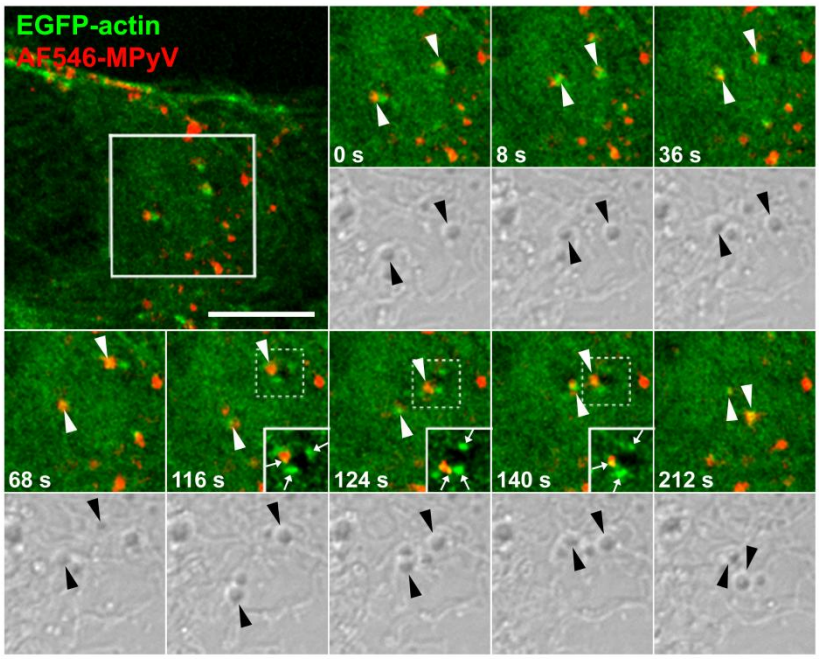

(figure legend in article)

ATTACHMENT #1 – Zila et al., 2014; Supporting Figure S3

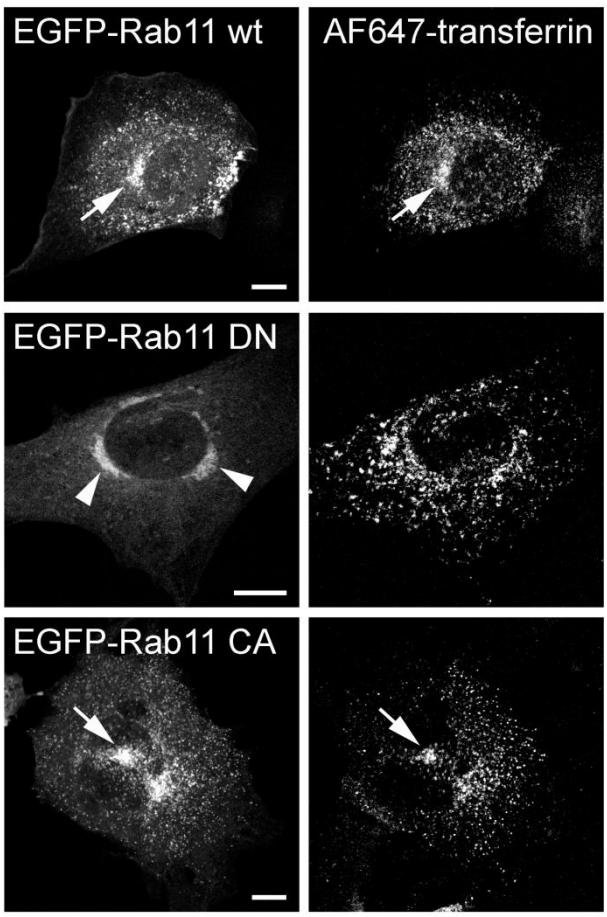

(figure legend in article)

ATTACHMENT #1 – Zila et al., 2014; Supporting Movies

Movie S1, download link:

http://www.plosone.org/article/fetchSingleRepresentation.action?uri=info:doi/10.1371/journal.pone.0096922.s004

(AVI)

Movie S2, download link:

http://www.plosone.org/article/fetchSingleRepresentation.action?uri=info:doi/10.1371/journal.pone.0096922.s005

(AVI)

Movie S3, download link:

http://www.plosone.org/article/fetchSingleRepresentation.action?uri=info:doi/10.1371/journal.pone.0096922.s006

(AVI)

(legends in article)

ATTACHMENT #2 – Huerfano et al., 2010

the FEBS Journal

Minor capsid proteins of mouse polyomavirus are inducers of apoptosis when produced individually but are only moderate contributors to cell death during the late phase of viral infection

Sandra Huerfano, Vojtěch Žíla, Evžen Bouřa, Hana Španielová, Jitka Štokrová and Jitka Forstová

Department of Genetics and Microbiology, Faculty of Science, Charles University, Prague, Czech Republic

Keywords
apoptosis; minor proteins; mouse polyomavirus; VP2; VP3

Correspondence
J. Forstová, Department of Genetics and Microbiology, Charles University in Prague, Viničná 5, 128 44 Prague 2, Czech Republic
Fax: +420 2 21951729
Tel: +420 2 21951730
E-mail: jitkaf@natur.cuni.cz

(Received 4 November 2009, revised 15 December 2009, accepted 22 December 2009)

doi:10.1111/j.1742-4658.2010.07558.x

Minor structural proteins of mouse polyomavirus (MPyV) are essential for virus infection. To study their properties and possible contributions to cell death induction, fusion variants of these proteins, created by linking enhanced green fluorescent protein (EGFP) to their C- or N-termini, were prepared and tested in the absence of other MPyV gene products, namely the tumor antigens and the major capsid protein, VP1. The minor proteins linked to EGFP at their C-terminus (VP2–EGFP, VP3–EGFP) were found to display properties similar to their nonfused, wild-type versions: they killed mouse 3T3 cells quickly when expressed individually. Carrying nuclear localization signals at their common C-terminus, the minor capsid proteins were detected in the nucleus. However, a substantial subpopulation of both VP2 and VP3 proteins, as well as of the fusion proteins VP2–EGFP and VP3–EGFP, was detected in the cytoplasm, co-localizing with intracellular membranes. Truncated VP3 protein, composed of 103 C-terminal amino acids, exhibited reduced affinity for intracellular membranes and cytotoxicity. Biochemical studies proved each of the minor proteins to be a very potent inducer of apoptosis, which was dependent on caspase activation. Immunoelectron microscopy showed the minor proteins to be associated with damaged membranes of the endoplasmic reticulum, nuclear envelope and mitochondria as soon as 5 h post-transfection. Analysis of apoptotic markers and cell death kinetics in cells transfected with the wild-type MPyV genome and the genome mutated in both VP2 and VP3 translation start codons revealed that the minor proteins contribute moderately to apoptotic processes in the late phase of infection and both are dispensable for cell destruction at the end of the virus replication cycle.

Structured digital abstract

- MINT-7386399, MINT-7386463, MINT-7386515: *VP3* (uniprotkb:P03096-2) and *GRP94* (uniprotkb:P08113) *colocalize* (MI:0403) by *fluorescence microscopy* (MI:0416)
- MINT-7386328, MINT-7386434, MINT-7386493: *VP2* (uniprotkb:P03096-1) and *GRP94* (uniprotkb:P08113) *colocalize* (MI:0403) by *fluorescence microscopy* (MI:0416)
- MINT-7386294, MINT-7386413, MINT-7386482: *VP2* (uniprotkb:P03096-1) and *Lamin-B* (uniprotkb:P14733) *colocalize* (MI:0403) by *fluorescence microscopy* (MI:0416)
- MINT-7386354, MINT-7386450, MINT-7386504: *VP3* (uniprotkb:P12908-2) and *Lamin-B* (uniprotkb:P14733) *colocalize* (MI:0403) by *fluorescence microscopy* (MI:0416)

Abbreviations
CMV, cytomegalovirus; EGFP, enhanced green fluorescent protein; ER, endoplasmic reticulum; FACS, fluorescence-activated cell sorting; LDH, lactate dehydrogenase; MPyV, mouse polyomavirus; PARP, poly(ADP-ribose) polymerase; SV40, simian virus 40; tVP3, truncated VP3; Z-VAD-FMK, carbobenzoxy-valyl-alanyl-aspartyl-[*O*-methyl]-fluoromethylketone.

Introduction

Mouse polyomavirus (MPyV) is a nonenveloped dsDNA virus belonging to the *Polyomaviridae* family. The capsid is formed by three structural proteins: a major protein (VP1) and two minor proteins (VP2 and VP3). VP1 is organized into 60 hexavalent and 12 pentavalent pentamers. The minor proteins are translated from the same open reading frame, and the shorter of the two – VP3 (23 kDa) – is identical to the C-terminal part of the longer VP2 protein (35 kDa). Minor proteins are not exposed on the surface of MPyV capsids. Their common C-termini interact with the central cavity of VP1 pentamers, while their N-termini are oriented towards the nucleocore, itself composed of a circular dsDNA genome, cellular histones (except H1) and VP1. The central cavity of each pentamer contains one molecule of either VP2 or VP3 [1].

VP1 protein is responsible for the interaction of MPyV virions with the ganglioside GD1a and GT1b receptors [2]. Its N-terminus contains basic amino acids involved in nonspecific DNA-binding activities and targeting VP1 to the cell nucleus. Both MPyV minor proteins possess a nuclear localization signal at their C-terminus; however, they do not bind DNA [3–5]. Minor capsid proteins of primate and human polyomaviruses [simian virus 40 (SV40), BK virus, JC virus] have additional amino acids in their C-terminus that are responsible for nonspecific DNA-binding activity [6]. The VP2 of all known polyomaviruses is myristylated at its N-terminal glycine [7]. VP2 and VP3 are presumed to be transported to the nucleus (where virion assembly occurs) in complexes with VP1 pentamers [8,9].

The functions of the MPyV minor proteins are as yet, however, poorly defined. It has been shown that mutated virions lacking either VP2 or VP3 lose infectivity, indicative of defects in the early stages of infection [10]. Similarly for SV40, it has been reported that mutated virions, lacking VP2 and VP3, are poorly or noninfectious as a result of the failure to deliver viral DNA into the cell nucleus [11,12]. Recent *in vitro* studies [13,14] have shown that minor proteins of polyomaviruses are able to bind, insert into and even perforate membranes of the endoplasmic reticulum (ER). Rainey-Barger *et al.* [14] analyzed the hydrophobic character of amino acid sequences of VP2 and VP3 proteins and defined three transmembrane domains for VP2 that were predicted by the Membrane Protein Explorer 3.0 program: domain 1 comprised residues 69–101 at the N-terminus of the unique part of VP2; domain 2 comprised residues 126–165 in the common VP2 and VP3 sequences; and domain 3 comprised residues 287–305 at the common VP2/VP3 C-terminus. The authors suggested VP2-specific domain 1 to be responsible for the perforation of membranes and domain 2 to be involved in membrane binding, while it was thought that domain 3, which is part of the sequence interacting with the central cavity of VP1 pentamers, was unlikely to be exposed and to contribute to membrane binding without global disassembly of the virus. According to the authors, these interactions may play a role in the delivery of polyomavirus genomes to the cell nucleus, as well as in the release of virus progeny from infected cells. In the late phase of SV40 infection, production of a late protein, VP4 (125 amino acids from the C-terminus of VP3), which triggers the lytic release of virus progeny, was recently described [15].

The MPyV infection cycle is completed within a 36–48 h interval. Cytopathic effects can be observed at times which coincide with the production of high levels of the structural proteins. Studies on the mechanism of the cytotoxic effect of MPyV infection show predominant necrosis (40–46% cells) and moderate apoptosis (5–10% cells) after two cycles of infection (72 h). Recombinant MPyV capsid-like particles composed of all three structural proteins were unable to induce cell death [16].

To study the properties of MPyV minor capsid proteins, and the extent and character of cytotoxicity induced by them, we prepared several plasmids for individual production of VP2, VP3 and their enhanced green fluorescent protein (EGFP) fusion variants, as well as EGFP fusion variants of the truncated VP3 (containing 103 amino acids of the C-terminus). We followed minor protein localization in mouse cells, cell death and the presence of apoptosis markers during their transient expression as well as during the infection cycle of wild-type (wt) MPyV and mutated MPyV, lacking both minor proteins.

Results

Individual expression of the minor capsid proteins (VP2 or VP3)

Attempts to transiently express individual MPyV structural proteins VP2 or VP3 in the permissive cells NIH 3T3 from expression plasmids with cytomegalovirus (CMV), SV40 or *Drosophila hsp70* promoters resulted, in each case, in unsatisfactorily low numbers of positive cells (< 1% of transfected cells). The few cells that expressed VP2 or VP3 between 8 and 18 h post-transfection exhibited remarkable morphology

alterations, or were dead. Therefore, for further studies of cellular responses to the minor structural proteins, VP2 and VP3, as well as VP3 truncated at its N-terminus, were transiently produced as fusion proteins with EGFP (which was attached to either their C-terminus or their N-terminus). Truncated VP3 (tVP3) corresponds to the region in the C-terminus of VP2 (216–319 amino acids) that includes only the third hydrophobic domain (described by Rainey-Barger *et al.* [14]).

The addition of EGFP sequences to either the N-terminus or the C-terminus of the minor proteins improved the efficiency of transfection/expression markedly (it oscillated between 50 and 70%). The production of the fused proteins was confirmed (4 h post-transfection) by western blot analysis using an anti-VP2/3 MPyV IgG (Fig. S1A) and an anti-GFP IgG (results not shown). Fused proteins recognized by both antibodies migrated with expected sizes. Confocal microscopy of cells expressing VP2–EGFP or VP3–EGFP revealed that VP2/VP3-specific antibody and anti-GFP IgG displayed similar patterns of product distribution, suggesting that both antibodies detected the fused proteins (Fig. S1B).

Intracellular localization of the wt minor proteins and their fusion variants

Distribution of the fused minor capsid proteins was followed through the analysis of confocal microscopy images of cells stained with a common anti-VP2 and -VP3 IgG, and an antibody against ER markers (GRP 94 or GRP 78) or against lamin B. Figure 1 shows characteristic differences in the cellular distribution of all VP2 or VP3 fusion variants, as well as sections of cells producing wt VP2 or VP3, for comparison. Wild-type VP2 and VP3 exhibited, besides nuclear localization, evident affinity for the nuclear envelope and the ER. Similar findings were observed with the minor proteins fused with EGFP at their C-terminus (VP3–EGFP and VP2–EGFP). By contrast, the minor structural proteins fused with EGFP at their N-terminus (EGFP–VP2 and EGFP–VP3) as well as both fusion variants of tVP3, had substantially lower affinity, or no affinity at all, to these membranes. As a control, VP2 and VP3, fused at their C-terminus with the 8-amino acid-long FLAG sequence (VP2–FLAG and VP3–FLAG), were examined (Fig. S2A). They proved comparable in location to the data obtained with wt VP2 and VP3 and the fusion variants VP2–EGFP and VP3–EGFP.

To further examine the membrane localization of the cytoplasmic fractions of fusion proteins, the mutual location of membranes stained by 1,6-diphenylhexatriene and EGFP fusion proteins was followed in living cells. Only VP2–EGFP and VP3–EGFP exhibited strong co-localization with intracellular membranes, in agreement with results obtained with fixed cells (Fig. 2). The cytoplasmic subpopulation of both fusion variants of tVP3 did not co-localize with membranes convincingly (Fig. 2, bottom panel).

We used immuno-electron microscopy to follow the association of VP2–EGFP and VP3–EGFP with cellular substructures. Cells expressing EGFP only were used as a control. EM pictures of cells at early time-points post-transfection, but before cell death, were obtained (5 h), showing the presence of VP2–EGFP and VP3–EGFP on the membranes of a swollen ER and also on damaged mitochondria. VP3–EGFP was seen to be associated with the nuclear membrane, often located between the inner and outer layers (Fig. 3).

Both VP2 and VP3 induce fast cell death

We followed the toxicity of the fused EGFP variants of VP2, VP3 and tVP3 during their transient expression by measuring the lactate dehydrogenase (LDH) concentration (LDH was released from dead cells) in the medium at the indicated time-points post-transfection (Fig. 4). Cytotoxicity was detected as early as 7 h post-transfection. VP2–EGFP and VP3–EGFP were highly toxic. As a control, cytotoxicity of VP2–FLAG and VP3–FLAG was measured and found to be of comparable intensity to that of VP2–EGFP and VP3–EGFP (Fig. S2B). By contrast, the inverted fusion proteins EGFP–VP2 and EGFP–VP3 exhibited much lower cytotoxicity during the time-period followed. Truncated VP3 fused with EGFP did not cause cell death during the period tested (24 h post-transfection; Fig. 4). These results indicate that transient expression of the minor structural proteins in permissive cells induces cell death; however, the cytotoxicity caused by their expression decreases when minor proteins are fused with EGFP at their N-terminus. Also, deletion of half of the VP3 sequences (including hydrophobic domain 2) from its N-terminus suppressed (at least during the period evaluated) its ability to kill cells.

Taken together, the intracellular localization and toxicity results suggest that (a) VP2 or VP3 fused with EGFP at their C-terminus (VP2–EGFP, VP3–EGFP) possesses properties similar to those of natural VP2 or VP3 and(b) truncation of the N-terminal part of VP3 (cutting off the hydrophobic domain 2) decreases its toxicity as well as its affinity to membranes.

ATTACHMENT #2 – Huerfano et al., 2010

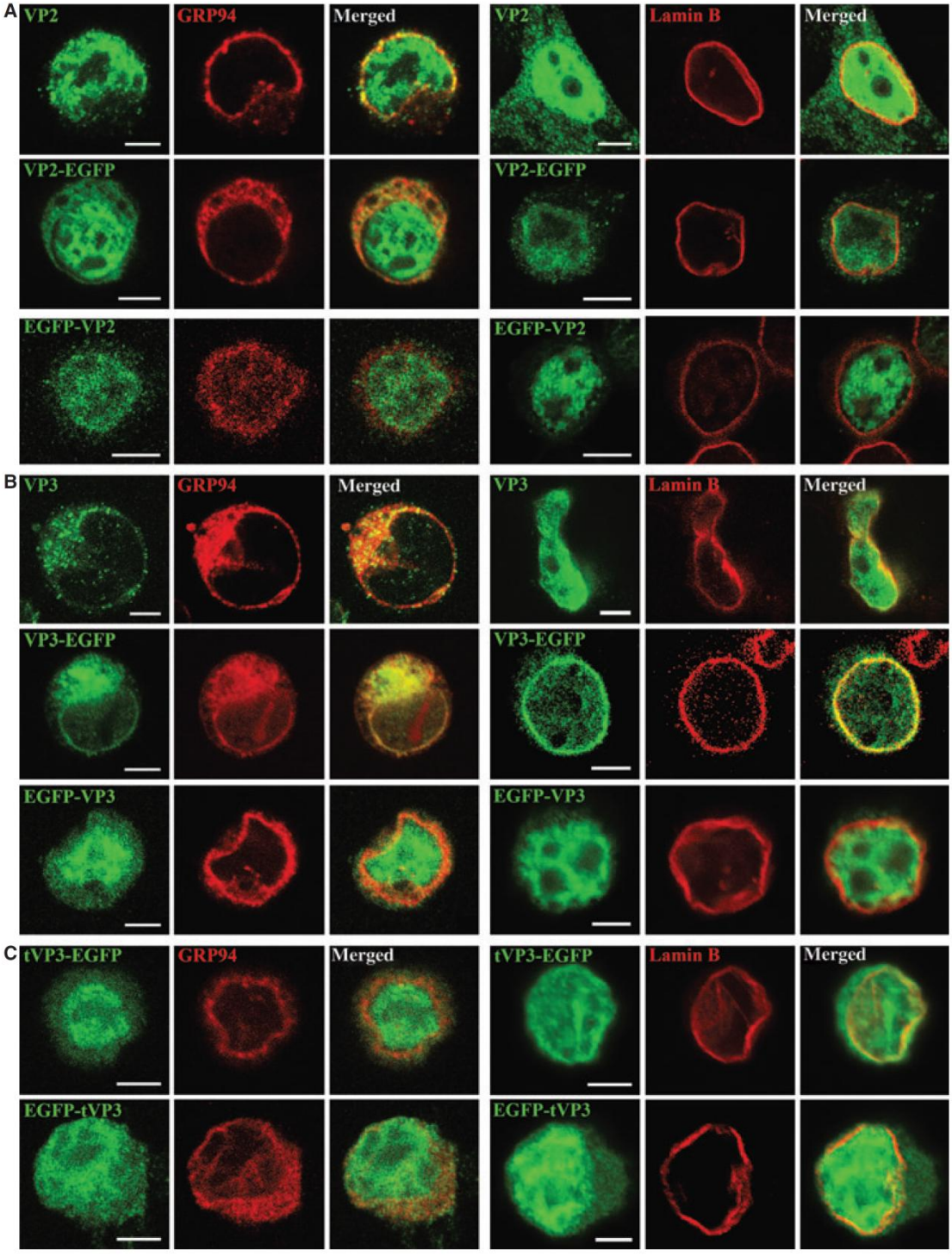

Fig. 1. Localization of VP2, VP3 and their fusion variants in transfected 3T3 cells. Selected confocal microscopy sections of 3T3 cells, 4 h post-transfection, are presented. Cells were stained with antibody against the GRP 94 ER marker, or with lamin B (red). Minor structural proteins were stained with anti-VP2/3 IgG (green), and EGFP fused variants were enhanced with anti-VP2/3 IgG (green). (A) VP2 and its EGFP variants. (B) VP3 and its EGFP variants. (C) EGFP variants of tVP3. Bars, 5 μm.

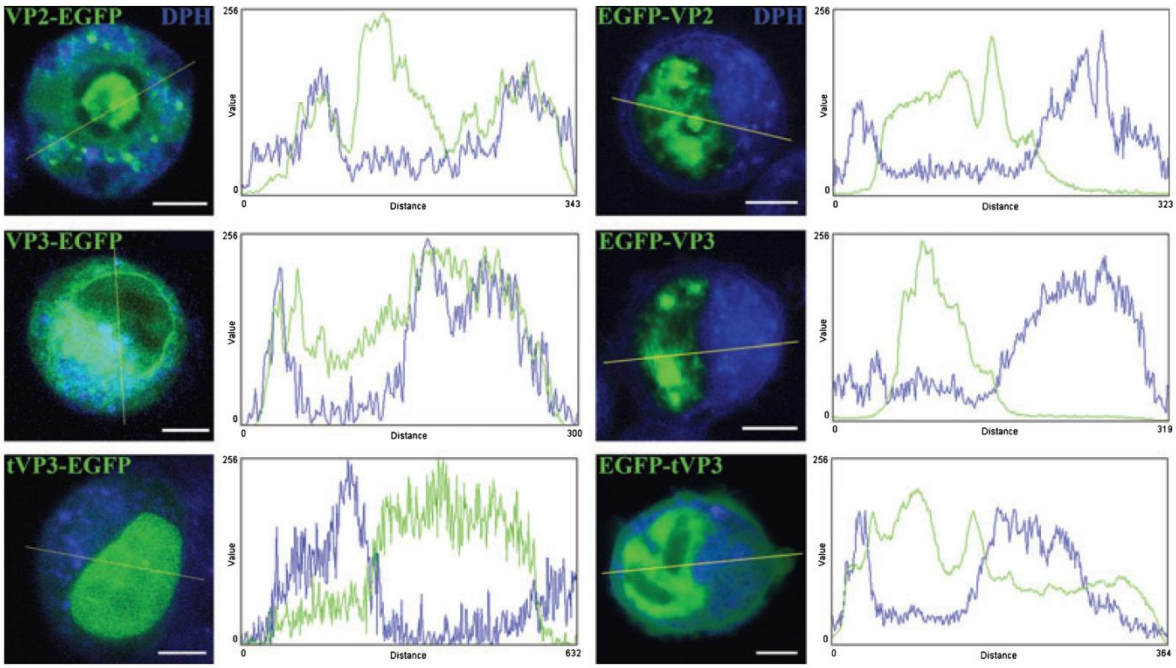

Fig. 2. Localization of EGFP fused variants of VP2, VP3 or tVP3 in living 3T3 cells. Selected confocal microscopy sections of living cells were observed 4–5 h post-transfection. Membranes were stained with 1,6-diphenylhexatriene (DPH, blue), EGFP fusion variants of the minor structural proteins are shown in green. Presented profiles of signal intensities were measured across selected lines of shown cell sections. Bars 5 μm.

Both VP2 and VP3 are potent inducers of apoptosis

We further examined the character of cell death induced by VP2 or VP3 proteins. To assess the contribution of apoptosis to toxicity, we evaluated the cleavage of both effector caspase 3 and one of its substrates, poly(ADP-ribose) polymerase (PARP), by western blotting (Fig. 5A). Cleavage of caspase 3, indicating activation as well as cleavage of PARP, as soon as 5 h post-transfection, was detected in cells transfected with all plasmids encoding VP2, VP3 or tVP3, fused with EGFP either at the C-terminus or the N-terminus. By contrast, expression of EGFP alone induced neither caspase 3 nor PARP cleavage. Because of differences in the cytotoxicity of the fused products (Fig. 4), we quantified caspase 3 activity in cells tranfected with individual constructions. The results presented in Fig. 5B show remarkably high activity in the lysates of cells producing VP2–EGFP and VP3–EGFP proteins 4 h post-transfection (the activity was comparable to the values obtained for lysates of cells treated with 2 μM actinomycin D). Markedly lower activity was detected in cells producing EGFP–VP2, EGFP–VP3, or either fusions of tVP3. No activation of caspase 3 was observed in nontransfected control cells or in cells transfected with the EGFP expression plasmid.

Cells producing all fusion variants of VP2 and VP3 proteins were further tested (5 h post-transfection) for exposure of phosphatidylserine in the outer leaflet of the plasma membrane by staining with annexin V conjugated to the fluorescent Cy3 dye, followed by quantification using fluorescence-activated cell sorting (FACS) analysis (Fig. 5C). A significant subpopulation of cells producing VP2–EGFP (23.9%) or VP3–EGFP (23.0%) exhibited annexin V binding. By contrast, no significant population (between 1 and 6% only) was found in cells producing EGFP–VP2, EGFP–VP3, EGFP–tVP3 or tVP3–EGFP.

These results show that the levels of cytotoxicity of individual VP2 and VP3 variants correlate with their ability to induce apoptosis. The highly toxic variants of VP2 and VP3 proved to be very potent inducers of apoptosis. The low toxicity of tVP3, observed during the first 24 h post-transfection, suggests that domain 2 of the minor capsid proteins may be important for the potentiation of apoptosis.

ATTACHMENT #2 – Huerfano et al., 2010

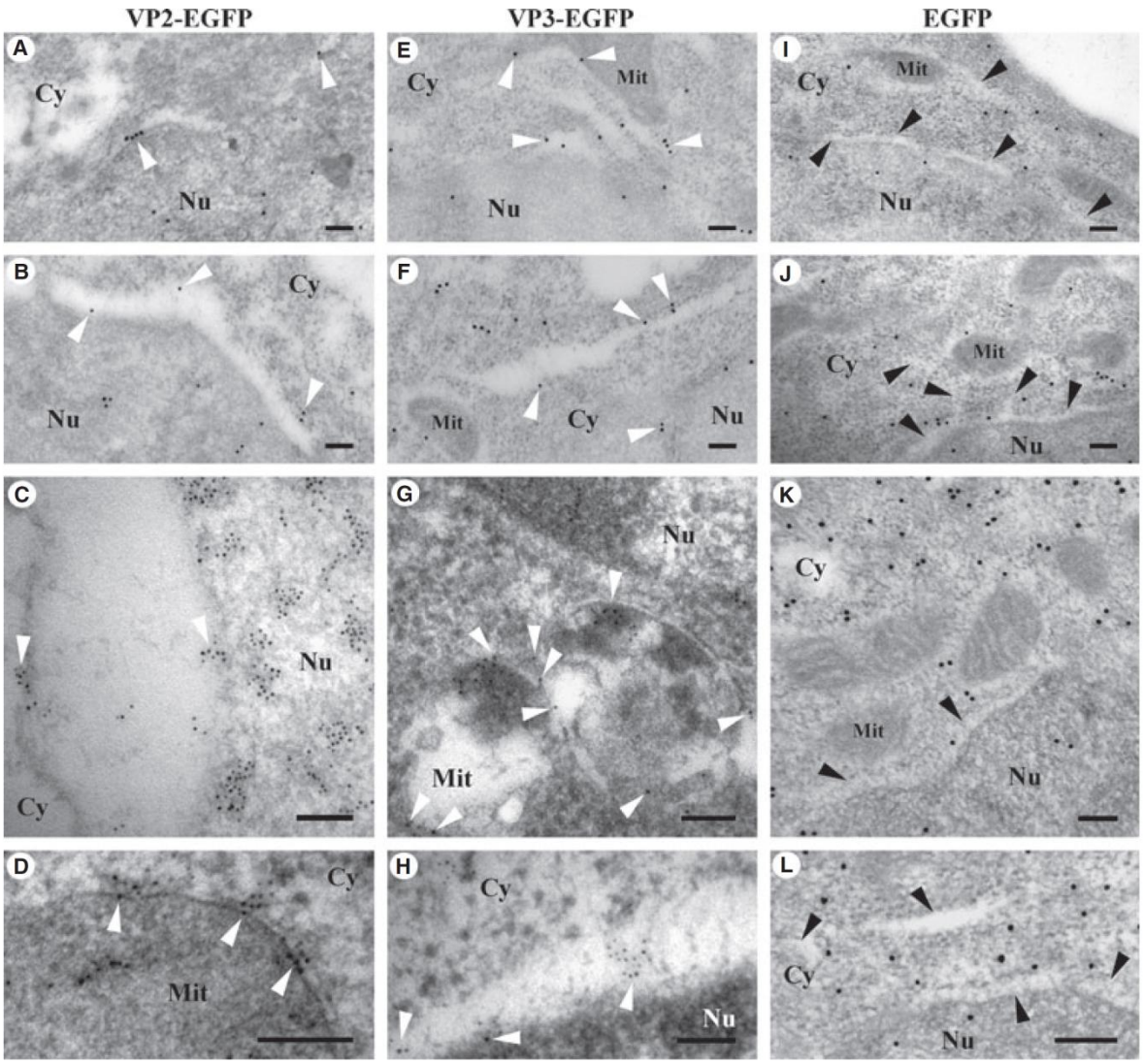

Fig. 3. Immuno-electron microscopy on ultrathin sections of 3T3 cells expressing VP2–EGFP, VP3–EGFP or EGFP only. Cells were fixed 5 h post-transfection. Fused minor capsid proteins were detected by incubation of cell sections with anti-GFP IgG followed by incubation with the secondary antibody conjugated with 10-nm gold particles (A, B, E, F, I–L) or 5-nm gold particles (C, D, G, H). Selected gold particles are indicated by white arrowheads. Black arrowheads indicate ER cisternae on sections of cells expressing EGFP only. Bars 100 nm. Cy, cytoplasm; Mit, mitochondria; Nu, nucleus.

To further characterize the induction of apoptosis caused by transient expression of VP2–EGFP and VP3–EGFP, and to determine the role of the mitochondrial pathway in apoptosis, cleavage of caspase 9 was investigated. Figure 5D shows caspase 9 cleavage (resulting in the appearance of a large, 35kDa, active fragment) in cells expressing VP2–EGFP or VP3–EGFP at early time-points post-transfection (4 h). Additionally, morphology of cells was analysed (5 h post-transfection) by transmission electron microscopy. Cells with the typical caspase-dependent apoptotic condensed chromatin features (Fig. S3) were observed among the floating cells collected from the medium (agreeing with loss of adherence, a known feature of apoptotic cells).

The results obtained from all the experiments described above, the subcellular localiztion of VP2–EGFP and VP3–EGFP 5 h post-transfection (Fig. 3) and the fact that apoptosis is induced quickly (as soon as production of the proteins could be detected) (Fig. 5), suggest that the main actions of VP2 or VP3

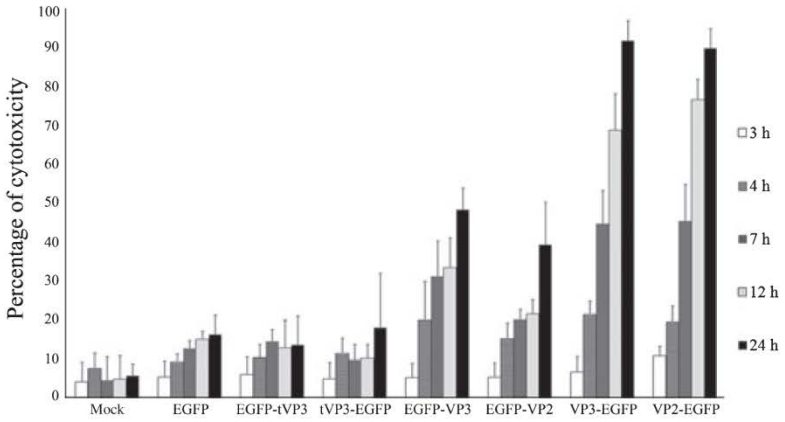

Fig. 4. Cytotoxicity of VP2 or VP3 fusion proteins. Cytotoxicity of individual protein variants transiently expressed in 3T3 cells was followed by measuring LDH leakage from transfected cells into the medium at the indicated time-points post-transfection. Values are presented relative to that of LDH release obtained by treatment of cells with 9% Triton X-100 (=100%). Data represent mean values measuring duplicates of three independent experiments. Mock-transfected cells were used as a negative control.

leading to apoptosis might be their interaction with the ER and/or with other intracellular membranes causing their damage.

Cell death induced by VP2 and VP3 is dependent on the activation of caspases

To dissect whether the cell death induced by VP2 or VP3 is caspase-dependent, we treated transfected 3T3 cells with the cell-permeable pancaspase inhibitor, carbobenzoxy-valyl-alanyl-aspartyl-[*O*-methyl]-fluoromethylketone (Z-VAD-FMK). The percentage of toxicity was determined at selected time-points post-transfection (Fig. 6A). A remarkable decrease or prevention of cell death by the pancaspase inhibitor was observed in cells transfected with VP2 or VP3 fused with EGFP at their C-terminus (VP2–EGFP, VP3–EGFP). The blocking of cleavage of the caspase was confirmed by measuring caspase 3 activity (Fig. 6B). From the results, we can conclude that MPyV minor structural proteins (when expressed individually) induce programmed death that is dependent on the activities of caspase.

VP2 and VP3 contribute to apoptosis induced during MPyV infection

To test whether the minor proteins function as inducers of apoptosis also during infection, we prepared the MPyV genome mutated in ATG codons of both VP2 and VP3. We and others have previously shown [10–12] that the virus lacking either VP2 or VP3 was practically noninfectious; therefore, the VP2, VP3 minus mutant could be used only for analysis of the first replication cycle after transfection of its genome.

To determine the appropriate times for measuring apoptotic markers, we first established the kinetics of apoptosis during the infection cycle of mouse 3T6 fibroblasts with the wt virus. The apoptotic markers caspase 3 and PARP were tested. The activity of caspase 3 was first detected at 18 h postinfection and increased remarkably during the interval between 36 and 48 h after infection (Fig. S4A). Additionally, strong PARP processing was detected 36 h postinfection (Fig. S4B). These results revealed a strong increase of apoptotic markers in the late phase of the first lytic cycle.

Furthermore, we followed the apoptotic markers and cytotoxicity induced in 3T6 cells transfected with either the wt genome or the mutated MPyV genome. Initially, we established the conditions allowing the same efficiency of transfection for both (measured by counting large T-antigen positive cells 12 h post-transfection; data not shown). Induction of apoptotic markers, phosphatidylserine exposure, caspase 3 activation and PARP processing were measured in the late stages of the first replication cycle (34–40 h). The apoptotic population, measured following annexin V staining, was similar for cells transfected with wt (28%) and mutant (24%) forms (Fig. 7A). Also, although the activity of caspase 3, as well as PARP processing by caspase 3, were significantly higher in the cells transfected with the wt genome (Fig. 7B,C), substantial levels of both markers were present in cells transfected with the mutant genome. This suggests that VP2 and VP3 (albeit strong inducers of apoptosis in the absence of VP1 and other viral components) have only a moderate contribution to apoptosis induction during the virus infection cycle. The cytotoxicity was detected by quantification of LDH release into the medium and was followed during the first viral cycle from 12 to 48 h post-transfection (Fig. 7D). This experiment showed that the replication of both wt and mutant virus (lacking VP2 and VP3) results in cell destruction within 48 h post-transfection, suggesting that the minor proteins are dispensable for cell death.

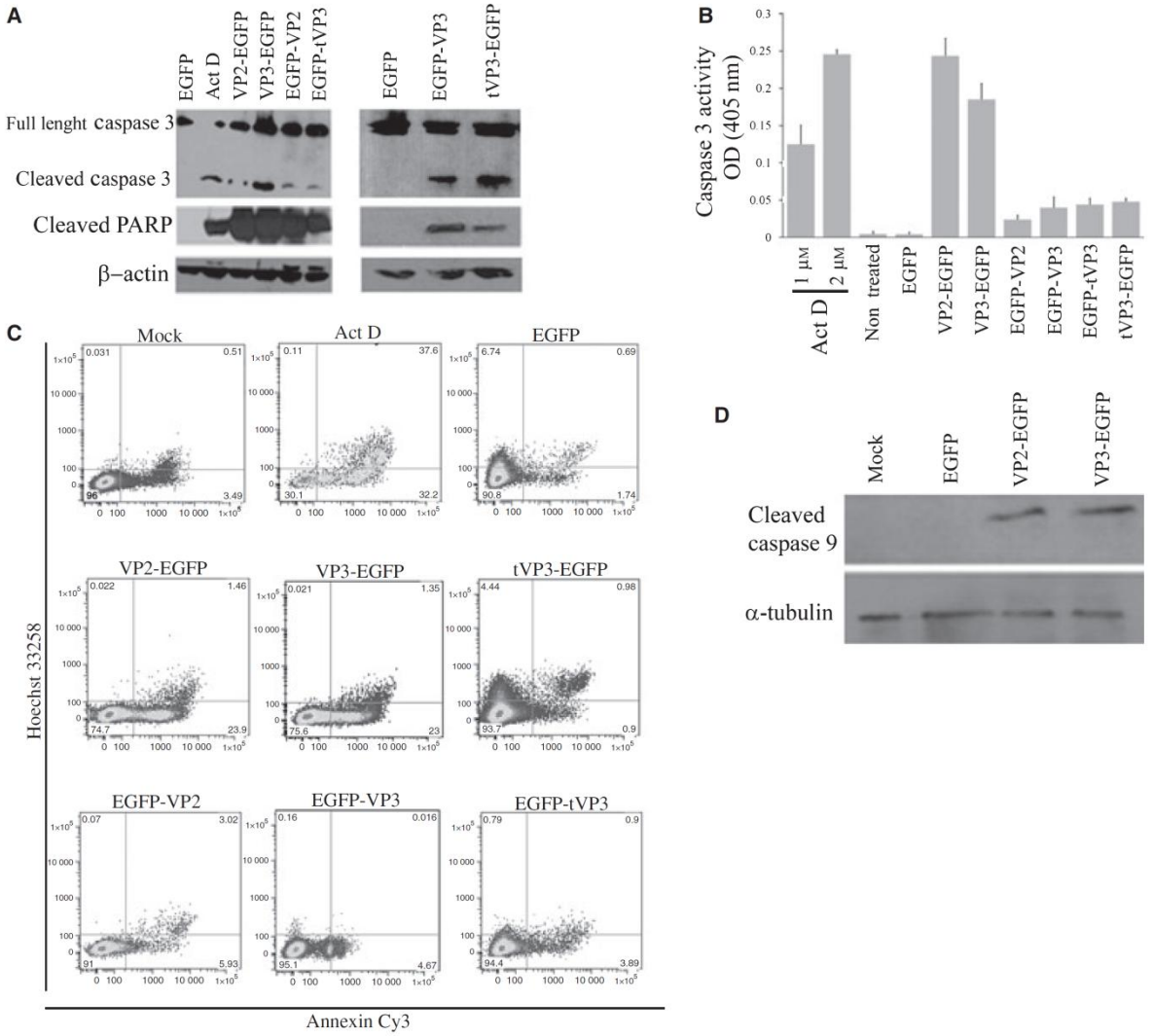

Fig. 5. Detection of apoptosis in cells expressing EGFP-fused MPyV structural minor capsid proteins. Lysates of 3T3 cells transfected with plasmids encoding either individual EGFP fused variants of the minor proteins or EGFP only, mock-transfected cells, cells treated with actinomycin D (ActD), or untreated cells. (A) Cleavage of caspase 3 and of PARP in lysates of cells collected 5 h post-transfection. Western blot analysis using anti-caspase 3 (recognizing full and cleaved forms), or anti-cleaved PARP IgGs. An antibody against β-actin was used as a control for loaded samples. (B) Measurements of caspase 3 activities in cell lysates (4 h post-transfection) carried out using the CaspACE assay system, Colorimetric. (C) Early exposure of phosphatidylserine detected by FACS analysis. Annexin-positive cells expressing all fusion variants of the minor proteins, EGFP only, or mock-transfected cells analysed at peak time (5 h post-transfection). For transfected cells, only the EGFP-positive population is presented. For mock-infected cells and actinomycin D-induced cells, the whole cell population is presented. (D) Cleavage of caspase 9 was detected by immunoblotting of cell lysates transfected with VP2–EGFP or VP3–EGFP (4 h post-transfection) using an antibody directed against cleaved caspase 9. Anti-α-tubulin IgG was used as a control of sample loadings.

Discussion

In the present work, the cytotoxic properties of the minor structural proteins (VP2 and VP3) of the MPyV were studied in the absence of other virus components as well as during the late phase of virus infection. The role of the minor structural proteins in the replication cycle still remains obscure. Our previous analysis of MPyV mutated in the minor structural proteins VP2 or VP3 [10] suggested possible function(s) of the minor proteins in the early steps of the MPyV replication cycle, during virus entry, trafficking and/or uncoating

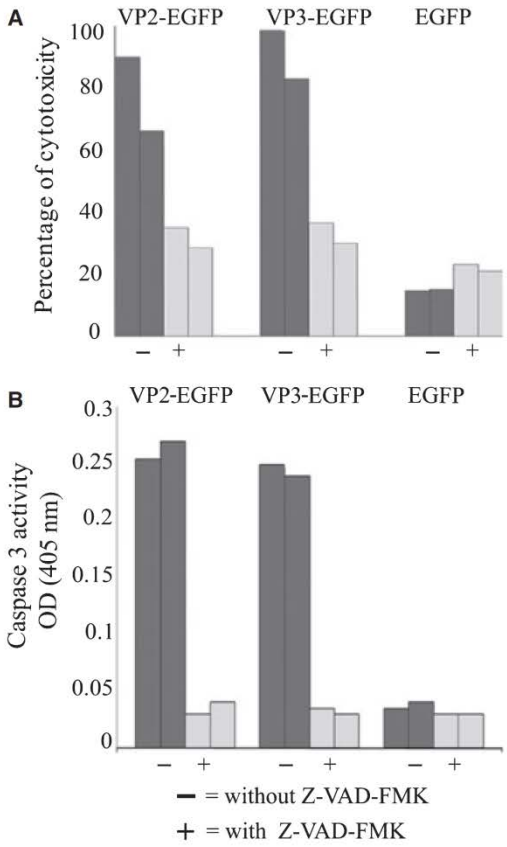

Fig. 6. Influence of caspase inhibition on cell death. (A) Measurement of cell toxicity by LDH release into medium after treatment of 3T3 cells expressing fused VP2 and VP3 minor proteins, EGFP alone, or mock-transfected cells, treated with the pancaspase inhibitor Z-VAD-FMK. (B) Measurement of caspase 3 activity in cells expressing fused minor proteins (4 h post-transfection), EGFP alone, or mock-transfected cells after treatment with Z-VAD-FMK. Values of two independent experiments are presented.

and delivery of the virus genomes into the cell nucleus. The ability of VP2 and VP3 of SV40 and MPyV to interact with membranes has been demonstrated recently *in vitro* and suggests that the minor protein might help the partially uncoated virus to escape from ER on its way to the nucleus [14]. We were interested in whether the minor proteins will exhibit affinity to intracellular membranes inside the host cell when produced uncovered by VP1. We demonstrated that each of the two minor structural proteins (VP2 and VP3) of MPyV, when expressed in the absence of VP1 structural protein, is a potent inducer of cell apoptosis. Our results suggest that the induction of apoptosis is related to the ability of the minor proteins to interact with intracellular membranes. The polyomavirus replication cycle ends by cell destruction. Several viruses are known to promote necrotic or apoptotic processes for effective release of viral progeny from the infected cells. However, we found that during infection, the contribution of the minor proteins to cell destruction via apoptosis is only moderate, suggesting that toxicity of the minor proteins is controlled during the infectious cycle and that other viral components and/or cell responses are involved in cell death during the late phase of viral infection.

Various attempts to express VP2 or VP3 of MPyV individually, using transfection by vectors with different promoters, have not proved successful, ending in very inefficient expression. The use of histone deacetylase inhibitors to suppress possible gene-silencing activities also did not increase the number of VP2- or VP3-positive cells (data not shown). The reasons for the low expression of sequences encoding minor proteins are unknown, but they may be attributed to tight regulation at several levels, such as pre-mRNA processing, nuclear export or translation [17,18]. Nevertheless, we were able to substantially increase expression of the minor proteins by fusing them with sequences encoding tag sequences, such as EGFP or FLAG.

During MPyV infection, newly synthesized structural proteins form complexes (5VP1–1VP2, or 5VP1–1VP3) in the cytoplasm, which are then transported into the cell nucleus [8,9,19]. In the absence of VP1, we found that a substantial amount of VP2 or VP3 in the cytoplasm was co-localized with intracellular membranes, similar to the observation with fusion variants where EGFP was connected to their C-termini (VP2–EGFP, VP3–EGFP). Surprisingly, thus, although VP2 contains the entire VP3 sequence, possesses another transmembrane domain in its unique region [14] and is myristylated at its N-terminal glycine, it does not seem to have a higher affinity for intracellular membranes than VP3. The proteins with EGFP in the opposite orientation (EGFP–VP2, EGFP–VP3) were targeted preferentially into the cell nucleus, and had markedly lower affinity to intracellular membranes. In agreement with our results, previous studies have shown that minor proteins were not targeted efficiently into the nucleus in insect cells or in African Green monkey kidney cells when VP1 was not co-expressed [8,9].

C-terminal tagging of proteins with EGFP is, in general, preferable to N-terminal tagging, in that the corresponding proteins are usually targeted correctly within the cell and resemble their wt counterparts [20]. Formation of a stable tertiary structure is a cooperative process, functioning at the level of protein domains (50–300 amino acid residues). An average domain can complete folding with the help of chaperones only when its entire sequence has emerged from

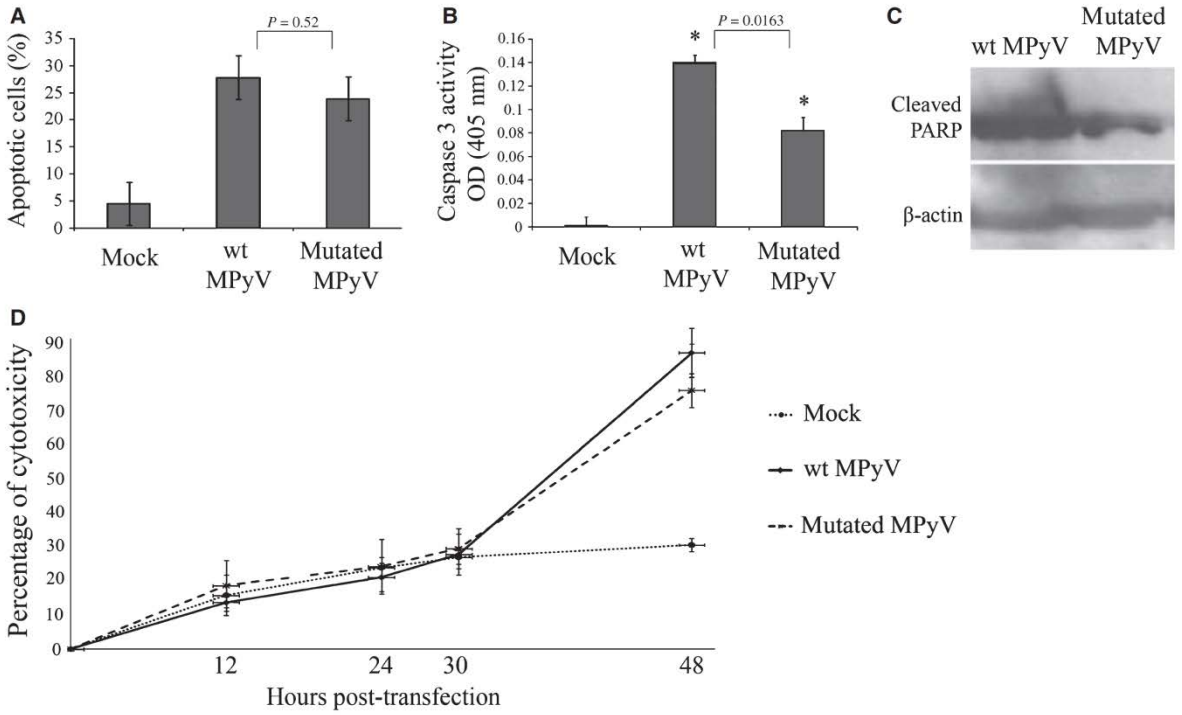

Fig. 7. Detection of apoptotic markers and cell destruction during the first replication cycle in cells transfected with wt MPyV genome or with MPyV genome mutated in the ATG start codons for translation of VP2 and VP3. (A) Exposure of phosphatidylserine was detected by FACS analysis. Annexin V-positive cells 34 h post-transfection. The columns represent the mean values of three experiments. (B) Caspase 3 activity measured 40h post-transfection using the CaspACE assay system, Colorimetric. The columns represent the mean values of three independent experiments. (C) PARP cleavage (analysed by western blot analysis using antibody specific for cleaved PARP) tested in cell lysates 40 h post-transfection. (D) Cytotoxicity, indicated by a burst of mouse 3T6 fibroblasts transfected with wt or mutated MPyV genomes, was followed by LDH release. Values of LDH release are presented relative to those obtained by treatment of cells with Triton X-100 (= 100%). Data represent the mean of three independent experiments. Mock-transfected cell lysates were used as a negative control.

the ribosome. EGFP is 238 amino acids long, and, when tagged to the N-terminus, will fold first. Its influence is thus probably greater than when tagged to the C-terminus of a protein [20,21]. This is in line with other studies [22,23].

In vitro studies have shown that VP2 binds to, integrates into and perforates the ER membrane, whereas VP3 integrates into the ER membrane, but is not sufficient for perforation [14]. However, we observed that both VP2 and VP3 kill cells comparably fast and efficiently and are associated not only with a damaged ER, but also with mitochondrial and other intracellular membranes.

The observed association of VP2 and VP3 with damaged membranes suggests that this is probably the major cause of the toxicity of both proteins produced without other virus components. Apoptosis can be triggered by many different stimuli, including the release of calcium from the ER or of cytochrome *c* from mitochondria [24,25].

VP2 and VP3, with their ability to interact with and perforate cell membranes, may be considered members of the growing group of so-called viroporins. Viroporins usually possess at least one amphipathic α-helix, and, in some instances, a second hydrophobic domain [26]. As described before [14], VP2 of MPyV (and other polyomaviruses) possesses three, and VP3 two, hydrophobic domains. The third domain at the C-terminus of both proteins forms an amphipathic α-helix.

In this study, we observed that the third domain present in tVP3 (in the context of sequences of tVP3 flanking it from its N-terminus) is not sufficient for efficient membrane binding or apoptosis induction. This suggests that both the second and third domains (present in both VP2 and VP3) are needed for viriopo-rin-like behaviour. It is also possible that membrane interaction of the third hydrophobic domain of the MPyV minor capsid antigens requires acidic pH or other special conditions present in a particular cell compartment and is utilized during the transport of

MPyV virions from the cell surface to the nucleus. These hypotheses are now being tested.

Recently, viroporins of RNA viruses (such as 6K protein of Sindbis virus, E protein of mouse hepatitis virus, M2 protein from influenza A, 2B and 3A proteins of poliovirus, or p7 and NS4A of hepatitis C virus) were shown to induce caspase-dependent apoptosis when produced individually in hamster cells [27].

We found increasing levels of apoptotic markers during the late stages of MPyV infection. However, comparison of the levels of apoptotic markers and cytotoxicity during the replication of wt MPyV, and replication of the virus mutated in *VP2* and *VP3* gene AUG start codons, suggests that the minor capsid proteins are not the sole or even the main inducers of apoptosis in the infection process and are dispensable for cell death. During infection, most of the minor capsid proteins become integral parts of capsomeres or virions apparently prevented from cell interactions. Our preliminary experiments showed that production of MPyV VP2 and VP3 together with VP1 dramatically decreased the cytotoxicity induced by the minor proteins (results not shown).

In the late phase of SV40 infection, VP4 protein (a shorter form of VP3 that contains only the third, C-terminal hydrophobic domain) is produced. It has been reported as a trigger of lytic processes for release of the virus progeny [15]. Accordingly, Gordon-Shaag *et al.* [28] showed that 35 C-terminal amino acids of VP3 of SV40 bind PARP and stimulate its enzymatic activity, thus leading cells to necrosis. The *VP3* gene of MPyV contains three internal AUG codons. Although not yet observed, we cannot exclude that a shorter form of VP3, contributing to the induction of apoptotic markers and/or cell death, is produced by both wt and mutated MPyV in the late infection. However, the cytotoxicity of fusion variants of tVP3 (which is of comparable length to that of SV40 VP4 and contains the amphiphatic α-helix) is low. In addition, 27 of 35 amino acids, present in the C-terminus of SV40 VP3 and reported to bind to and stimulate PARP [28], are not present in VP3 of the MPyV.

Regulation of cell death during infection can be a complex process of several viral functions as well as functions associated with cell defence mechanisms. Cellular responses to the late transcription, allowing dsRNA formation [29] as well as virus genome replication, can contribute to induction of the apoptotic processes.

Further experiments will be needed to test interactions of the minor structural proteins in cells, contributions of individual hydrophobic domains to their membrane affinity and to reveal possible functions of VP2 and VP3 in the early steps of polyomavirus infection, during virion entry and/or during uncoating processes.

Experimental procedures

Cell lines and transfections

Mouse fibroblasts (NIH 3T3 and NIH 3T6) were grown at 37 °C in a humidified incubator with a 5% CO_2 atmosphere, using Dulbecco's modified Eagle's medium (Sigma-Aldrich, St Louis, MO, USA) supplemented with 10% fetal bovine serum and 4 mM L-glutamine. Transfections were performed using kits (Amaxa, Lonza, Basel, Switzerland) according to the manufacturer's instructions.

Cell infection

MPyV (strain A3) was propagated and isolated according to Türler & Beard [30]. For analysis of kinetics of apoptosis, 3T6 cells (70% confluence) were infected the virus at a multiplicity of infection of 1 plaque-forming unit per cell. Viral adsorption was carried out for 30 min on ice. Dulbecco's modified Eagle's medium plus serum was then added and the cells were further incubated for indicated intervals at 37 °C.

DNA constructs

Sequences of *VP2* or *VP3* genes from MPyV strain A3 were cloned into pSVL (Pharmacia, Uppsala, Sweden) under the control of SV40 late regulatory sequences by insertion into an *Xba*I cloning site, or into a *Bgl*II site of pLNHX (Clontech, Mountain View, CA, USA) under the *Drosophila hsp70* promoter. In addition, *VP3* gene was cloned into pEGFP-C2 (Clontech) under the CMV IE promoter by substitution of *EGFP* gene, or by replacing the CMV IE promoter and *EGFP* gene with the *VP3* gene under control of the MPyV late promoter.

Proteins fused to the EGFP tag were prepared by insertion of sequences of MPyV minor proteins VP2, VP3 or truncated VP3 (tVP3, with a deletion of the first 101 amino acids at the N-terminus) into the vectors pEGFP–C2 and pEGFP–N1 (Clontech). Sequences encoding VP2 and VP3 were amplified by PCR using the pMJG plasmid, which contains the entire genome of MPyV (strain A3) as a template [31]. Plasmids for production of VP2 or VP3, fused at the N-terminus of EGFP (VP2–EGFP, VP3–EGFP), were prepared by the insertion of amplified sequences into the *Hin*dIII and *Bgl*II sites of pEGFP–N1. Amplified sequences encoding tVP3 were inserted into the pEGFP–N1 plasmid using *Bgl*II and *Sal*I cloning sites. Amplified sequences encoding VP2 or VP3 fused at their N-terminus with EGFP (EGFP–VP2, EGFP–VP3) were inserted into the *Bgl*II and

*Eco*RI sites of pEGFP–C2, and coding sequences for tVP3 were inserted into the *Sac*I and *Bam*HI sites of pEGFP–C2.

Proteins fused to the FLAG tag were prepared by insertion of the VP2 and VP3 coding sequences into the plasmid pCMV–FLAG 5a (Sigma-Aldrich). Sequences encoding VP2 and VP3 were prepared by PCR, using pMJG as a template. The plasmid for production of VP2 was prepared by insertion of amplified sequences into the *Hin*dIII and *Bgl*II sites, and the plasmid for production of VP3 was prepared by insertion of amplified sequences into *Bgl*II and *Kpn*I cloning sites.

Preparation of wt and mutant viral genomes

pMJG plasmid [31], which contains the entire genome of MPyV strain A3 (opened and inserted into the bacterial plasmid in the unique *Eco*RI site), was used as a source of wt MPyV genome. Plasmid pMJMA was used as a source of the MPyV genome, carrying the MPyV genome mutated at the ATG start codon for VP2 and VP3 translation. This plasmid was constructed using the plasmids previously described [31]: pMJA has a deletion in the *VP3* start codon and pMJM has a mutation in the *VP2* start codon. pMJMA was prepared from pMJM by exchanging the wt *VP3* gene with the mutated *VP3* gene cleaved from pMJA. To ensure replication of wt MPyV and mutated virus (lacking both minor structural proteins), genomes were excised from plasmids with *Eco*RI and circularised as described [10]. Ligation mixtures were used for the transfection of 3T6 cells.

Antibodies

The primary antibodies used were: rabbit polyclonal anti-caspase 3 IgG, mouse monoclonal anti-cleaved PARP IgG (Asp214), rabbit polyclonal anti-cleaved caspase 9 IgG (Cell Signalling); mouse monoclonal anti-α-tubulin IgG (Exbio, Vestec, Czech Republic); rabbit polyclonal anti-β-actin IgG (Cell Signaling, Danvers, MA, USA); rabbit polyclonal anti-GFP IgG (Sigma-Aldrich); goat polyclonal anti-lamin B IgG (Santa Cruz, CA, USA); rabbit polyclonal anti-GRP 78 IgG (Alexis, Enzo Life Sciences, Farmingdale, NY, USA); rat monoclonal anti-GRP94 IgG (Abcam); rat monoclonal IgG against the MPyV common region of early T-antigens; mouse monoclonal anti-MPyV VP1 IgG, and mouse monoclonal IgG against the common region of VP2 and VP3 [8]. Secondary antibodies included goat anti-rabbit and goat anti-mouse IgGs conjugated with peroxidase (Pierce), donkey anti-mouse IgG conjugated with Alexa Fluor 488 and goat anti-rat, goat anti-rabbit and donkey anti-goat IgGs conjugated with Alexa Fluor 546 (all from Molecular Probes). Goat anti-rabbit IgG conjugated with 5- or 10-nm-diameter gold particles was from GE Healthcare (Waukesha, WI, USA).

Western blot analysis

Attached cells, as well as floating cells, were harvested at the indicated time-points post-transfection, washed with phosphate-buffered saline ($NaCl/P_i$), then resuspended in ice-cold cell lysis buffer (10 mM Tris/HCl, pH 7.4, 1 mM EDTA, 150 mM NaCl, 1% Nonidet P-40, 1% sodium deoxycholate, 0.1% SDS) supplemented with protease inhibitor cocktail [Complete Mini EDTA free (Roche, Indianapolis, IN, USA)]. Cell lysis was carried out by incubating the cells for 20 min on ice. Cell debris was removed by centrifugation. The concentration of proteins was determined using a standard Bradford protein assay. Cellular proteins (40 μg) were applied to SDS/PAGE, blotted onto nitrocellulose-NC45 or poly(vinylidene difluoride) membranes, immunostained with antibodies and developed using an enhanced chemiluminescence reagent (Pierce, Rockford, IL, USA).

Immunofluorescent staining and live imaging

Cells were fixed and immunostained as described in Richterová *et al.* [32]. For live imaging, membranes of transfected cells were labelled by incubation with 1,6-diphenylhexatriene (10 μM in growth medium) for 30 min at 37 °C. Cells were then placed into a heated (37 °C), CO_2-supplemented, chamber and live images were taken. Confocal microscopy was performed using a Leica SP2 AOBS confocal microscope. Cell section images were analysed, using the IMAGE J program (NIH, Bethesda, MD, USA), to determine the distribution and intensities of markers.

Evaluation of cytotoxicity

The release of LDH occurring upon cell lysis at different time-points post-transfection of mouse fibroblasts was quantified using a CytoTox 96 cytotoxicity assay kit (Promega, Madison, WI, USA), according to the manufacturer's instructions.

Flow cytometry analysis

Externalization of phosphatidylserine was assessed using an Annexin V-Cy3 Apoptosis Detection Kit (Abcam, Cambridge, UK), and dead cells were detected by exclusion using Hoechst 33258 (Molecular Probes, Invitrogen, Carlsbad, CA, USA). Briefly, floating and adherent cells ($\sim 2 \times 10^5$ cells) were collected and processed according to instructions provided by the manufacturer. Then, samples were incubated (for 15 min at room temperature) in the dark and analysed using a flow cytometer (LSRII cytometer; BD Biosciences, San Jose, CA, USA). Data were processed using FLOWJO software (Treestar, San Carlos, CA, USA).

Quantification of caspase 3 activity and the caspase inhibition assay

At indicated time-points, cell lysates were prepared and tested for cleavage of amino acid DEVD sequences by caspase 3 using the CaspACE assay system, Colorimetric (Promega), according to the manufacturer's instructions. Caspases were inhibited by addition of the pancaspase inhibitor, Z-VAD-FMK (Promega) to the cell medium 2 h post-transfection. The final concentration of the inhibitor was 50 μM. Cells were incubated in the presence of the inhibitor, and caspase 3 activity and cell death were measured at the time-points indicated. Incubation of cells with actinomycin D (18–24 h; 1, 2 or 4 μM) was used as a positive control of apoptosis induction.

Electron microscopy

Ultrastructural analysis was performed according to Richterová *et al.* [32].

Immuno-electron microscopy

Cells were fixed with 3% paraformaldehyde and 0.1% glutaraldehyde in 0.2 M Hepes buffer, pH 7.5. Pelleted cells were washed twice in Sörensen buffer, pH 7.4, dehydrated in a series of increasing ethanol concentrations and embedded in LR-White resin (Polysciences, Inc., Warrington, PA, USA). Ultrathin sections on nickel grids were immunolabelled. Nonspecific binding was blocked with 10% normal goat serum in NaCl/P_i containing 1% BSA, followed by incubation of cells with rabbit anti-GFP IgG diluted in NaCl/P_i containing 0.5% BSA and 0.1% fish gelatine (pH 7.4). After washing in NaCl/P_i containing 0.1% BSA, sections were incubated with the secondary antibody conjugated to 5- or 10-nm-diameter gold particles that were diluted in NaCl/P_i containing 0.5% BSA and 0.1% fish gelatine (pH 8.2). Sections were washed in NaCl/P_i containing 0.1% BSA, then contrasted by staining with uranyl acetate. The samples were examined using a JEOL JEM 1200 EX electron microscope operating at 60 kV.

Acknowledgements

This work was supported by projects 1M0508, MSM0021620858 and LC545 from the Ministry of Education, Youth and Sports of the Czech Republic and by project no. 156307 from the Grant Agency of the Charles University in Prague. We thank Dr Z. Kečkešová and Mgr. L. Klímová for constructing the pLNHX and pEGFPdel-VP3 control plasmids, respectively and Dr J. Frič and Dr Z. Mělková for help with FACS analysis. We thank Prof. Beverly E. Griffin for critically reading the manuscript.

References

1 Rayment I, Baker TS, Caspar DLD & Murakami WT (1982) Polyoma virus capsid structure at 22.5 Å resolution. *Nature* **295**, 110–115.
2 Tsai B, Gilbert JM, Stehle T, Lencer W, Benjamin TL & Rapoport TA (2003) Gangliosides are receptors for murine polyoma virus and SV40. *EMBO J* **22**, 4346–4355.
3 Chang D, Haynes JI, Brady JN & Consigli RA (1992) Identification of a nuclear localization sequence in the polyomavirus capsid protein VP2. *Virology* **191**, 978–983.
4 Chang D, Haynes JI, Brady JN & Consigli RA (1993) Identification of amino acid sequences in the polyomavirus capsid proteins that serve as nuclear localization signals. *Trans Kans Acad Sci* **96**, 35–39.
5 Moreland RB & Garcea RL (1991) Characterization of a nuclear localization sequence in the polyomavirus capsid protein VP1. *Virology* **185**, 513–518.
6 Clever J, Dean DA & Kasamatsu H (1993) Identification of a DNA binding domain in simian virus 40 capsid proteins Vp2 and Vp3. *J Biol Chem* **268**, 20877–20883.
7 Streuli CH & Griffin BE (1987) Myristic acid is coupled to a structural protein of polyoma virus and SV40. *Nature (London)* **326**, 619–621.
8 Forstová J, Krauzewicz N, Wallace S, Street AJ, Dilworth SM, Beard S & Griffin BE (1993) Cooperation of structural proteins during late events in the life cycle of polyomavirus. *J Virol* **67**, 1405–1413.
9 Stamatos NM, Chakrabarti S, Moss B & Hare JD (1987) Expression of polyomavirus virion proteins by vaccinia virus vector: association of VP1 and VP2 with the nuclear framework. *J Virol* **61**, 516–525.
10 Mannová P, Liebl D, Krauzewicz N, Fejtová A, Štokrová J, Palková Z, Griffin BE & Forstová J (2002) Analysis of mouse polyomavirus mutants with lesions in the minor capsid proteins. *J Gen Virol* **83**, 2309–2319.
11 Nakanishi A, Nakamura A, Liddington R & Kasamatsu H (2006) Identification of amino acid residues within simian virus 40 capsid proteins VP1, VP2 and VP3 that are required for their interaction and for viral infection. *J Virol* **80**, 8891–8898.
12 Nakanishi A, Itoh N, Li PP, Handa H, Liddington RC & Kasamatsu H (2007) Minor capsid protein of simian virus 40 are dispensable for nucleocapsid assembly and cell entry but are required for nuclear entry of the viral genome. *J Virol* **81**, 3778–3785.
13 Daniels R, Rusan NM, Wadsworth P & Hebert DN (2006) SV40 VP2 and VP3 insertion into ER membranes is controlled by the capsid proteins VP1: implications for DNA translocation out of the ER. *Mol Cell* **24**, 955–966.

14 Rainey-Barger EK, Magnuson B & Tsai B (2007) A chaperone-activated nonenveloped virus perforates the physiologically relevant endoplasmid reticulum membrane. *J Virol* **81**, 12996–13004.
15 Daniels R, Sadowicz D & Hebert DN (2007) A very late viral protein triggers the lytic release of SV40. *PLoS Pathog* **3**, 928–937.
16 An K, Fattaey HK, Paulsen AQ & Consigli RA (2000) Murine polyomavirus infection of 3T6 mouse cells shows evidence of predominant necrosis as well as limited apoptosis. *Virus Res* **67**, 81–90.
17 Acheson NH (1981) Efficiency of processing of viral RNA during the early and late phases of productive infection by polyoma virus. *J Virol* **37**, 628–635.
18 Barrett NL, Li X & Carmichael GG (1995) The sequence and context of the 5′ splice site govern the nuclear stability of polyomavirus late RNAs. *Nucleic Acids Res* **23**, 4812–4817.
19 Cai X, Chang D, Rottinghaus S & Consigli RA (1994) Expression and purification of recombinant polyomavirus VP2 protein and its interactions with polyomavirus proteins. *J Virol* **68**, 7609–7613.
20 Palmer E & Freeman T (2004) Investigation into the use of C- and N-terminal GFP fusion proteins for subcellular localization studies using reverse transfection microarrays. *Comp Funct Genomics* **5**, 342–353.
21 Hartl F & Hayer-Hartl M (2002) Molecular chaperones in the cytosol: from nascent chain to folded protein. *Science* **295**, 1852–1858.
22 Huh W, Falvo J, Gerke L, Carroll A, Howson R, Weissman J & O'Shea E (2003) Global analysis of protein localization in budding yeast. *Nature* **425**, 686–691.
23 Weimann S, Weil B, Wellenreuther R, Gassenhuber J, Glassl S, Ansorge W, Böcher M, Blöcker H, Bauersachs S, Blum H *et al.* (2001) Toward a catalog of human genes and proteins: sequencing and analysis of 500 novel complete protein coding human cDNAs. *Genome Res* **11**, 422–435.
24 Boehning D, Patterson RL, Sedaghat L, Glebova NO, Kurosaki T & Snyder SH (2003) Cytochrome C binds to inositol (1,4,5) triphosphate receptors, amplifying calcium-dependent apoptosis. *Nat Cell Biol* **6**, 1051–1061.
25 Mattson MP & Chang SL (2003) Calcium orchestrates apoptosis. *Nat Cell Biol* **5**, 1041–1043.
26 Gonzales ME & Carrasco L (2003) Virioporins. *FEBS Lett* **552**, 28–34.
27 Madan V, Castelló A & Carrasco L (2008) Virioporins from RNA viruses induce caspase-dependent apoptosis. *Cell Microbiol* **10**, 437–451.
28 Gordon-Shaag A, Yosef Y, El-Latif MA & Oppenheim A (2003) The abundant nuclear enzyme PARP participates in the life cycle of simian virus 40 and is stimulated by minor capsid protein VP3. *J Virol* **77**, 4273–4282.
29 Gu R, Zhang Z, De Cerbo JN & Carmichael GG (2009) Gene regulation by sense-antisense overlap of polyadenylation singals. *RNA* **15**, 1154–1163.
30 Türler H & Beard P (1985) Simian virus 40 and polyoma virus: growth, titration, transformation and purification of viral components. In *Virology: a practical approach* (Mahy B Ed), pp 169–192. IRL Press, Oxford, Washington DC.
31 Krauzewicz N, Streuli CH, Stuart-Smith N, Jones MD, Wallace S & Griffin BE (1990) Myristylated polyomavirus VP2: role in the life cycle of the virus. *J Virol* **64**, 4414–4420.
32 Richterová Z, Liebl D, Horák M, Palková Z, Štokrová J, Hozák P & Forstová J (2001) Caveolae are involved in the trafficking of mouse polyomavirus virions and artificial VP1 pseudocapsids toward cell nuclei. *J Virol* **75**, 10880–10891.

Supporting information

The following supplementary material is available:
Fig. S1. Control of expression of MPyV minor capsid proteins fused with EGFP.
Fig. S2. Localisation and cytotoxicity of VP2 and VP3 fused with FLAG epitope in transfected 3T3 cells.
Fig. S3. Apoptotic morphology of cells producing MPyV minor capsid proteins, VP2 or VP3.
Fig. S4. Kinetics of apoptotic markers during MPyV infection.

This supplementary material can be found in the online version of this article.

Please note: As a service to our authors and readers, this journal provides supporting information supplied by the authors. Such materials are peer-reviewed and may be re-organized for online delivery, but are not copy-edited or typeset. Technical support issues arising from supporting information (other than missing files) should be addressed to the authors.

ATTACHMENT #2 – Huerfano et al., 2010; Supporting Figure S1

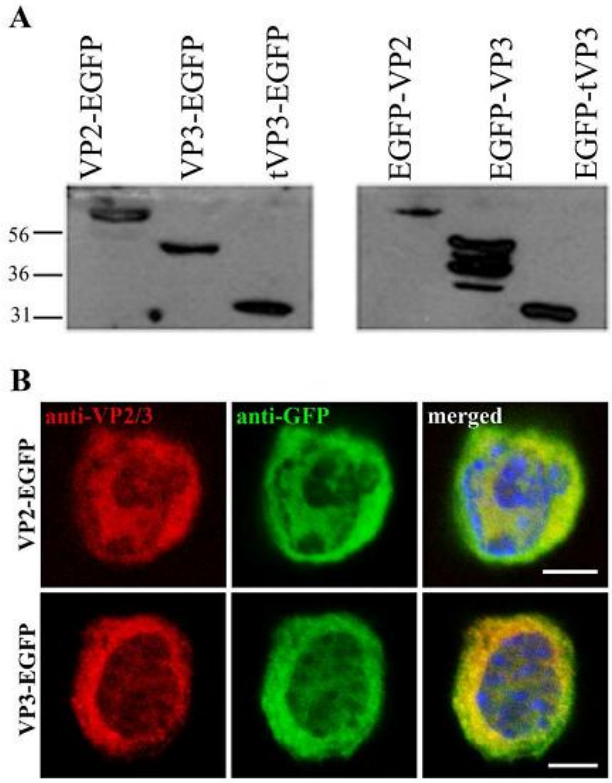

Fig. S1. Control of expression of MPyV minor capsid proteins fused with EGFP. **A**: Immunoblot of 3T3 cells transfected with plasmids for expression of the minor proteins VP2, VP3 and truncated VP3 (tVP3) fused with EGFP, detected by antibody against the common sequence of VP2 and VP3. Cells were lysed 4 h post-transfection and proteins separated on SDS PAGE. **B:** Confocal microscopy sections of cells expressing VP2-EGFP or VP3-EGFP, fixed 4 h post-transfection and immunostained with anti-VP2/3 antibody (red). The EGFP signal was enhanced by anti-GFP (green) antibody. Bars 5 μm.

ATTACHMENT #2 – Huerfano et al., 2010; Supporting Figure S2

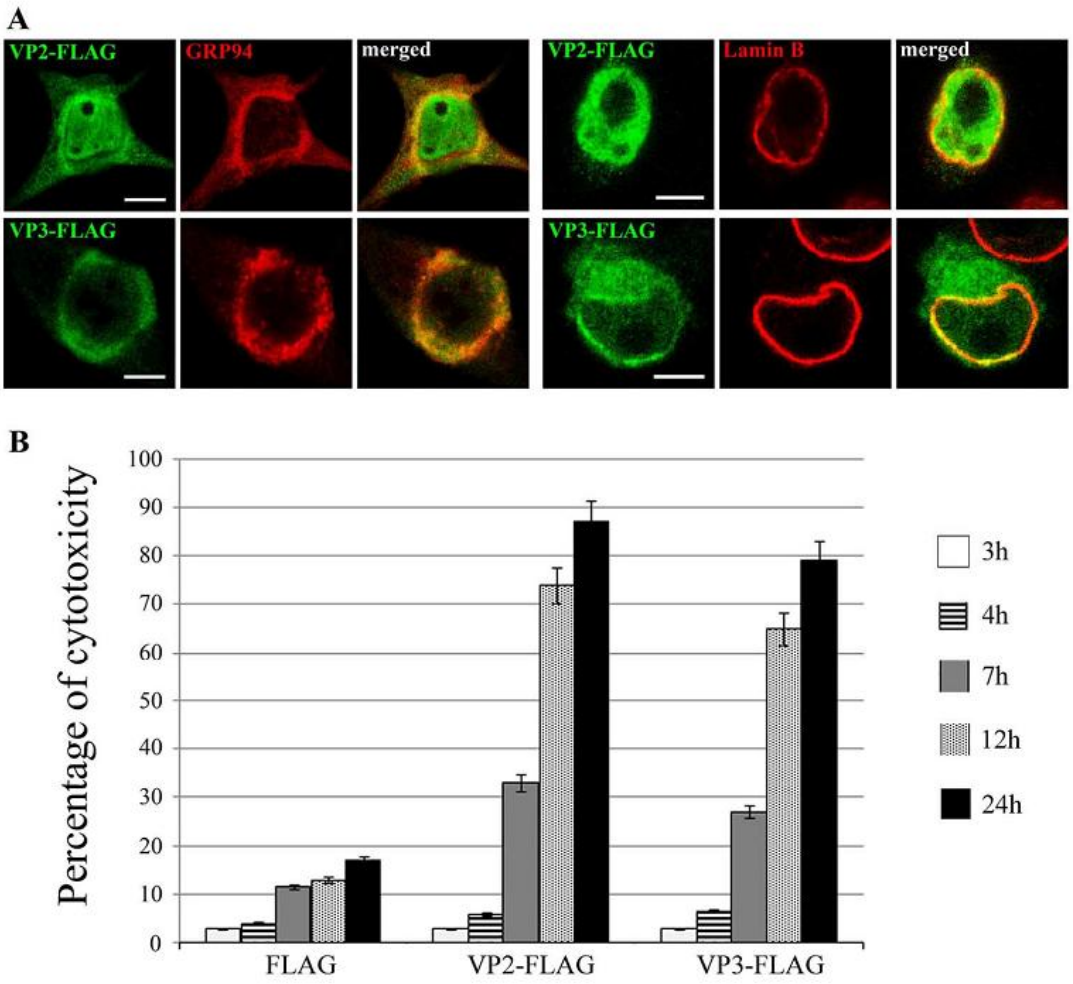

Fig. S2. Localisation and cytotoxicity of VP2 and VP3 fused with FLAG epitope in transfected 3T3 cells. **A:** Selected confocal microscopy sections of 3T3 cells 4 h post transfection are presented. Cells were fixed and stained by antibody against GRP 94 endoplasmic reticulum marker or lamin B (red) and anti-VP2/3 antibody (green). Bars 5 μm. **B:** Cytotoxicity of individual FLAG fused proteins produced in 3T3 cells was followed by measuring of LDH leakage from transfected cells into the medium at indicated times post-transfection. Values are related to that of LDH release obtained by treatment of cells with 9% Triton X-100 (=100%). Data represent mean values measuring duplicates of three independent experiments. FLAG only transfected cells were used as control.

ATTACHMENT #2 – Huerfano et al., 2010; Supporting Figure S3

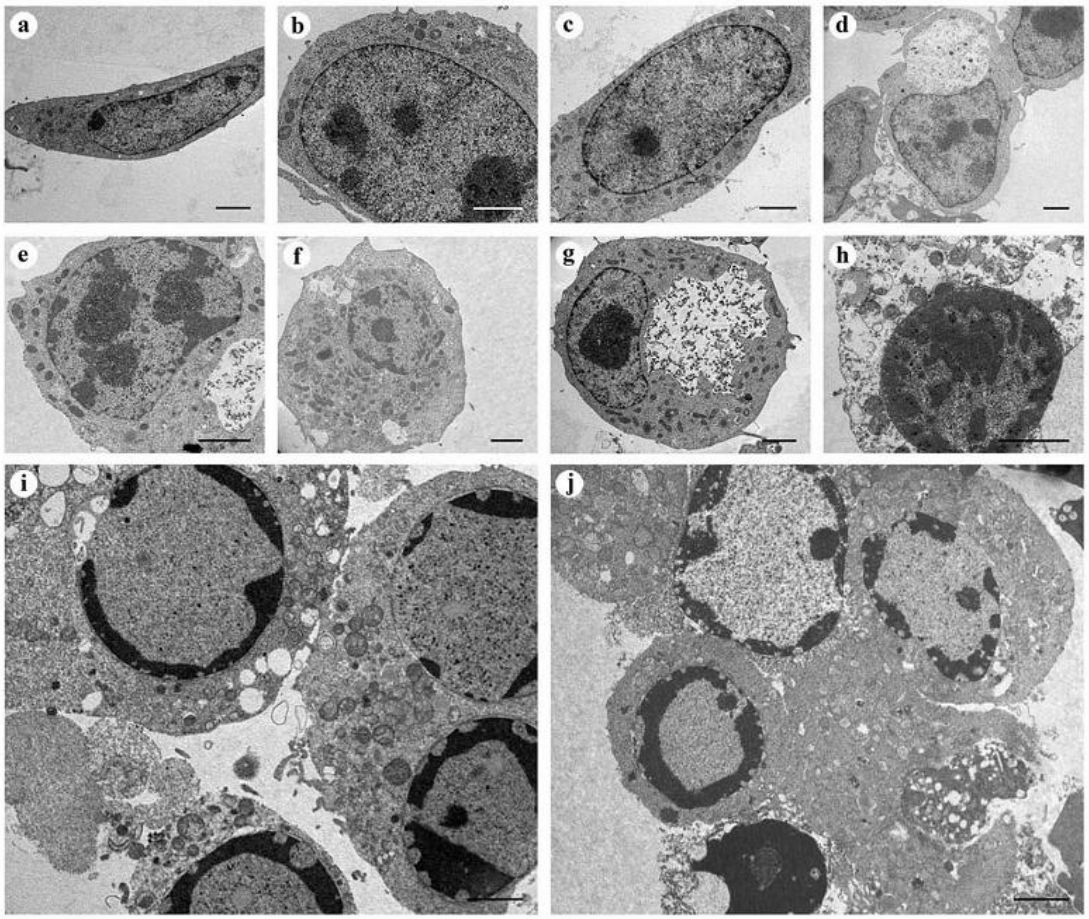

Fig. S3. Apoptotic morphology of cells producing MPyV minor capsid proteins, VP2 or VP3. Cells were fixed 5 h post transfection. Electron microscopy of ultrathin sections of control, non-transfected 3T3 cells (a,b) or cells producing EGFP only (c-h) or VP2-EGFP (i), or VP3-EGFP (j). Cells attached to the plate (a-d) or floating in the medium (e-j). Bars 2 μm.

ATTACHMENT #2 – Huerfano et al., 2010; Supporting Figure S4

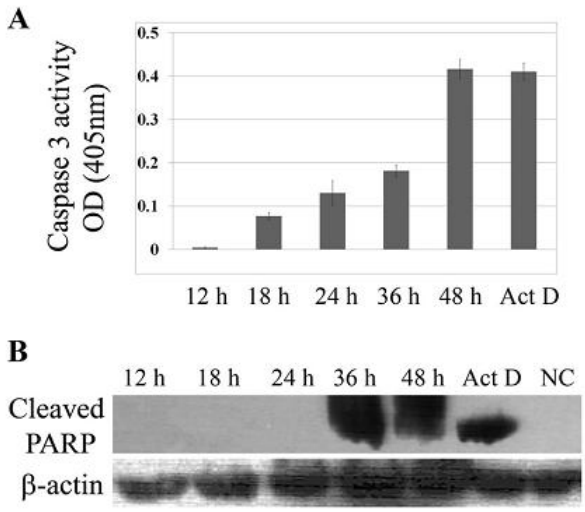

Fig. S4. Kinetics of apoptotic markers during MPyV infection. **A:** Caspase 3 activity detected by colorimetric assay. The data represent the mean of three independent experiments. **B:** Cell lysates collected at indicated times post infection immunobloted with the antibody against PARP cleavage fragment. NC - a negative control of lysates from non infected cells, Act D - actinomycin D treated cells. As a control of sample loadings, anti-β-actin antibody was used.